COMPUTERISED GRAFT MONITORING

Nizamettin AYDIN

A thesis submitted to the University of Leicester
for the degree of Doctor of Philosophy

Division of Medical Physics,
Faculty of Medicine,
University of Leicester
1994

This thesis is lovingly dedicated to my wife, who was extremely supportive during my study, and to my children.

CONTENTS

ABSTRACT
ACKNOWLEDGEMENT
STATEMENT OF ORIGINALITY

CHAPTER 1 - **Introduction**
1.1 Definition of the problem 1-1
1.2 Causes of the graft failures 1-2
1.2.1 Grafts as arterial substitutes 1-3
1.2.2 Failures of arterial grafts 1-5
1.2.3 Medium and long term graft surveillance after operation 1-7
1.3 Current graft surveillance methods 1-8
1.4 Patient monitoring 1-10
1.4.1 History of patient monitoring 1-11
1.4.2 Patient monitoring and management 1-12
1.5 Introduction to the graft monitoring system 1-13
1.6 Conclusion 1-15

CHAPTER 2 - **Doppler instrumentation for velocity measurement**
2.1 Introduction 2-1
2.2 Physical principle of Doppler ultrasound 2-1
2.3 Detection of Doppler ultrasound signals 2-2
2.3.1 Ultrasonic transducers 2-4
2.3.2 Velocity detecting systems 2-4
2.3.3 Demodulation of Doppler frequency shifted signals 2-7
2.4 Summary 2-14

CHAPTER 3 - **Design and construction of a CW Doppler unit for IBM-PC compatible computers**
3.1 Introduction 3-1
3.2 A CW Doppler board for IBM-PC's 3-1
3.2.1 General design considerations 3-2
3.2.2 Oscillator design 3-4
3.2.3 Transmitter design 3-6
3.2.4 Demodulator design 3-7
3.2.5 PC interface 3-14
3.2.6 Audio amplifier 3-16
3.3 System performance 3-16

3.3.1 Performances of the signal generator and the demodulator 3-16
3.3.2 Frequency response of the system 3-17
3.3.3 Dynamic range and cross-talk rejection 3-18
3.4 Conclusion 3-20

CHAPTER 4 - **Processing of Doppler ultrasound signals for spectral analysis**
4.1 Introduction 4-1
4.2 Tools for digital signal processing 4-2
4.2.1 Understanding the complex Fourier transform 4-2
4.2.2 The Hilbert transform 4-5
4.2.3 Frequency translation and modulation 4-7
4.2.4 Digital filters 4-8
4.3 Digital implementations of directional Doppler detectors 4-10
4.3.1 The phasing-filter technique 4-10
4.3.2 The weaver receiver technique 4-14
4.3.3 The complex FFT 4-17
4.4 Conclusion 4-20

CHAPTER 5 - **Signal processing algorithms for producing directional time domain outputs**
5.1 Introduction 5-1
5.2 General definition of a quadrature Doppler signal 5-1
5.3 Time domain processing 5-2
5.3.1 Phasing filter technique 5-2
5.3.2 Extended Weaver receiver technique 5-6
5.4 Frequency domain processing 5-16
5.4.1 Frequency domain Hilbert transform method 5-16
5.4.2 Complex FFT method 5-18
5.4.3 Spectral translocation method 5-21
5.5 Simulation study 5-23
5.6 Results and Conclusion 5-25

CHAPTER 6 - **Implementation of the signal processing algorithms**
6.1 Introduction 6-1
6.2 Floating point DSP systems 6-1
6.2.1 A dedicated floating-point digital signal processor: DSP32C 6-3
6.3 Generation of the quadrature test signals 6-6
6.3.1 Using the spectral translocation method 6-8
6.3.2 Using the high-pass/low-pass filter combination 6-11
6.4 Implementations of time domain processing 6-12

6.4.1 Implementation of the phasing filter technique 6-12
6.4.2 Implementation of the Weaver receiver technique and the extended Weaver receiver technique 6-16
6.5 Implementations of frequency domain processing 6-21
6.5.1 Implementation of the Hilbert transform method 6-22
6.5.2 Implementation of the complex FFT 6-23
6.5.3 Implementation of the spectral translocation method 6-24
6.6 Summary and comments 6-27
6.6.1 Separation for spectral analysis (frequency domain output) 6-27
6.6.2 Separation for time domain output 6-30

CHAPTER 7 - **The extraction of maximum and mean frequency envelopes from sonograms and calculation of indices**

7.1 Introduction 7-1
7.2 The extraction of the mean frequency envelope 7-1
7.3 The extraction of the maximum frequency envelope 7-2
7.3.1 Description of the MF envelope detection methods 7-3
7.3.2 Real-time implementations and simulations of the algorithms 7-8
7.4 Calculation of frequency indices 7-12
7.4.1 Calculation of pulsatility index 7-12
7.4.2 Waveform identification for calculation of the PI 7-13
7.5 Conclusion 7-15

CHAPTER 8 - **Computerised graft monitoring system and preliminary results**

8.1 Introduction 8-1
8.2 Arrangement of the graft monitoring system 8-3
8.2.1 Software organisation 8-2
8.2.2 Operation of the graft monitoring system 8-6
8.3 Clinical study - preliminary results 8-9
8.3.1 Method 8-9
8.3.2 Results 8-10
8.3.3 Discussion 8-29
8.3.4 Some practical problems related to the graft monitoring system . 8-29

CHAPTER 9 - **Summary and conclusion**

9.1 Summary and conclusion 9-1
9.2 The future 9-3

APENDICES

Appendix A Review of monitoring methods A.1

Appendix B Interpretation of the complex Fourier transform B.1
Appendix C1 Quadrature test signal generation using the PFT C.1
C2 Quadrature test signal generation using the EWRT C.2
Appendix D Gain dependency in the geometric method D.1
Appendix E Graft monitoring software user manual E.1

REFERENCES

ABSTRACT

Many vascular disorders require surgical procedures to overcome failing blood supply. Deficient arteries are replaced by prosthetic or vein bypass grafts to recover normal blood flow. However some grafts fail after operation. Therefore graft surveillance programs are important to increase the patency rate of grafts. Although there are a number of methods for medium and long term graft surveillance, these are not suitable for monitoring grafts immediately after operation to detect early graft failures which account for 20% of the total.

This dissertation describes a computerised graft monitoring system which is suitable for continuous or intermittent monitoring of grafts immediately after surgery. The system comprises a floating point DSP board, an IBM compatible computer and a purpose built CW Doppler board. The Doppler board is designed to be installed in the computer. The possibility of implementation of DSP algorithms for obtaining directional information is extensively discussed. This study shows that digital techniques outperform their analogue counterparts. Therefore in this system, apart from the quadrature demodulation of the Doppler signals all processes are implemented digitally. Maximum frequency envelope detection algorithms are also discussed.

The results obtained from monitoring seven patients are presented and practical difficulties encountered during the monitoring process are highlighted.

ACKNOWLEDGEMENTS

This thesis would not be complete without the acknowledgement of several people who have contributed in various ways. Thanks are firstly due to my supervisor Prof. David H Evans who accepted me as his student and guided me during this study, and to the Turkish Ministry of Education who supported this work financially. I would like to express my gratitude to my friends Lingke Fan, Colin Tysoe, Raimes Moraes and Robin Willink for their long friendship and their contributions to my knowledge. I also thank Stefan Nydahl who helped me to collect patient data.

Many thanks to Naïm Dahnoun, Stephen Bentley, Harry Hall, Tim Hartshorne, Abigail Thrush, and Glen Bush. My thanks also to Troy Johnson, Vaughan Acton and David Heaton.

STATEMENT OF ORIGINALITY

The work presented in this thesis is original and unless otherwise stated in the text or by references has been performed by myself. Some of the material contained in this thesis have been published under the name of "Implementation of directional Doppler techniques using a digital signal processor" by Aydin and Evans (1994) and "Quadrature-to-directional format conversion of Doppler signals using digital methods" by Aydin *et al.* (1994). No part of this thesis has been submitted for another degree in this or any other university.

Nizamettin AYDIN

1. INTRODUCTION

1.1. DEFINITION OF THE PROBLEM

Vascular disorders which sometimes cause loss of limb or even death are common diseases found mostly in Western societies. They result in the reduction of the diameter and compliance of arteries leading to possible ischaemia or infarction. The most common reason for ischaemia is atherosclerosis which causes 95% of arterial occlusions (Hansteen *et al* 1974). The factors in the development of atherosclerosis include family history, tobacco smoking, diabetes mellitus, excessive consumption of animal fats and refined carbohydrates, hypertension and lack of physical exercise.

Since the medical treatment of established atherosclerosis is both unsatisfactory and controversial, surgical procedures to overcome failing blood supplies in certain specific sites are common. Deficient arteries are replaced by prosthetic or vein bypass grafts to recover normal blood flow. A successful graft will relieve the symptoms at the affected site and result in limb salvage. The early success of such bypasses is highly dependent on technique; their durability may be a function of many other factors, including the diameter and length of the graft, the inflow source, and the outflow capacity (run-off) (Leather *et al* 1988). Naturally, some grafts fail at intervals after the operation due to a variety of reasons. Early intervention can reverse a graft failure into a successfully functioning graft but requires an early detection of failed or failing grafts (Whittemore *et al* 1981). Therefore it is essential to follow-up grafts efficiently in the postoperative period. The majority of graft stenoses occur within the first six months after operation. The most dangerous lesions develop very soon after operation and progress rapidly (Fig. 1.1), so monitoring should be most intensive during the first few weeks after operation and become less frequent with time (Harris 1992).

Some work has been reported on graft monitoring immediately after operation (Dahnoun 1990, Thrush and Evans 1990, Brennan *et al* 1991a). These studies have shown that it may be possible to predict early graft failures by analysing Doppler ultrasound signals. The instrumentation need not to be very sophisticated, so a simple continuous wave Doppler system (Dahnoun *et al* 1990) and a Doppler signal processor based on modern DSP systems (Schlindwein *et al* 1988) are adequate to the task. It is a challenge for researchers to implement sophisticated analysis procedures on such simple systems. The work reported in this thesis is an attempt to combine several simple units into one compact system and bring benefits provided by technological achievements in electronics and computing into the clinical area.

To clarify the problem, the nature of graft failure should be understood. Therefore a brief clinical introduction is given in next section.

1.2. CAUSES OF GRAFT FAILURE

Although an arterial bypass graft can fail at any time depending on complications developed, graft failures have been defined in terms of postoperative intervals as early failure, intermediate failure and late failure. If a graft occludes within 30 days of operation, it is generally accepted as an early failure. Intermediate failure occurs between 1 and 12 months. Late failure of arterial grafts occurs after 12 months. Fig. 1.1 shows an example of the number of grafts that fail according to time after surgery. Different centres have different figures but the general trend of failure rates is more or less the same.

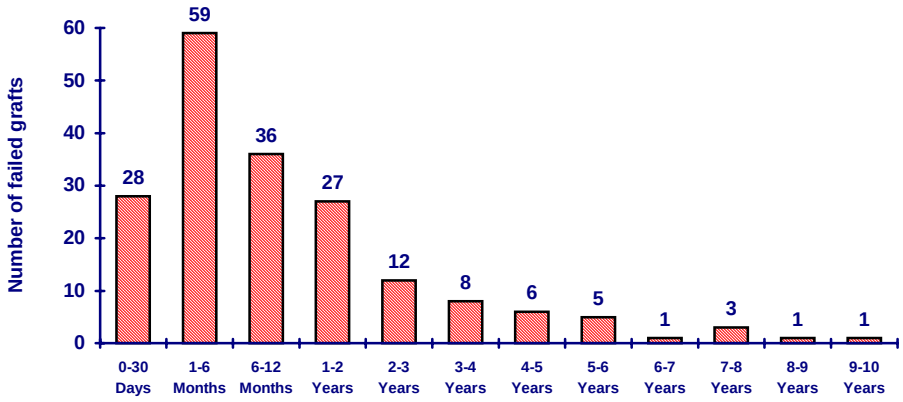

Figure 1.1 Frequency of graft failure and interval failure rate in follow-up period after femoropopliteal bypass graft procedures. (From Brewster *et al* 1983).

1.2.1. Grafts as arterial substitutes

An ideal graft must be readily available in a variety of sizes and lengths and suitable for use throughout the body. It must be durable in long term implantation in man, non reactive, and free of toxic or allergic side effects. Its handling characteristics must include elasticity, conformability, pliability, ease of suturing, and absence of fraying at cut ends or kinking at flexion points. Its luminal surface must be smooth, minimally traumatic to formed blood elements, resistant to infection, and non-thrombogenic (Kempczinski 1984).

None of the current prosthetic materials satisfy all these requirements. However some very satisfactory alternatives are available. Different grafts such as heterografts, veingrafts and prosthetic grafts have been used as arterial substitutes in arterial bypass operations. Although the suitability of homologous and heterologous artery and vein as arterial substitutes in dogs was demonstrated by Carrel (1906) early grafts were impervious non-biologic tubes which functioned as short term passive conduits and ultimately were subject to suture line disruption,

distal embolization and thrombosis. In 1948, Gross used the first arterial allograft. The first use of fabric arterial prosthesis was reported in 1952 by Edwards and Tapp. Polytetrafluoroethylene (Teflon, PTFE) was first used in 1957 (Edwards and Lyons 1958). Table 1.1 charts the introduction of various vascular grafts materials.

1906	Carrel	Homologous and heterologous artery and vein transplant in dogs
1906	Goyanes	First autologous vein transplant in man
1915	Tuffier	Paraffin-lined silver tubes
1942	Blakemore	Vitallium tubes
1947	Hufuagel	Polished methyl methacrylate tubes
1948	Gross	Arterial allografts
1949	Donovan	Polyethylene tubes
1952	Voorhees	Vinyon-N, first fabric prosthesis
1955	Egdahl	Siliconized rubber
1955	Edwards and Tapp	Crimped nylon
1957	Edwards	Teflon
1960	DeBakey	Dacron
1966	Rosenberg	Bovine heterograft
1968	Sparks	Dacron-supported autogenous fibrous tubes
1972	Soyer	Polytetrafluoroethylene (PTFE)
1975	Dardik	Human umbilical cord vein

Table 1.1 History of vascular grafts.

No graft currently available is suitable for every clinical application, and grafts must be selected on an individual basis for each case. Although autogenous artery is an ideal vascular replacement, its availability is limited.

Autogenous vein is usually available in longer segment and is the most widely used vascular replacement. Prosthetic grafts are used where a biologic graft is not available or suitable to replace large vessels such as the aorta or vena cava. The age of the patient must also be considered. Because grafts used in children must be capable of growth, an autogenous tissue should be used. Table 1.2 lists the vascular grafts used clinically and indicates the preferred and alternate choices for various applications.

1.2.2. Failures of arterial grafts

Early graft failure is caused by such technical defects as intimal flaps, anastomotic narrowing, twisting or kinking of the graft, or thrombus formation, embolization, coagulation disorders and inadequate runoff (Stept *et al* 1987). Technical problems occur more often in vein grafts. In prosthetic grafts, usually the only source of technical problem is the distal anastomosis.

Intermediate failures are mainly caused by evolving changes in the vein graft itself, with the important exception of true atherosclerotic lesions in the graft. These lesions include the sequelae of technical mishaps such as suture or clamp site stenosis, and the more universally occurring valve fibrosis and intimal hyperplasia, which is proliferation of smooth muscle and deposition of connective tissue in the intima of the graft.

Late failures are generally caused by progression of atherosclerotic disease in the native arterial segments proximal or distal to the graft (Whittemore *et al* 1981, Rutter and Wolfe 1992).

Clinical Application	Type of Graft							
	Biologic				*Prosthetic*			
	Autograft		Allograft	Heterograft	Fabric			Non-Textile
					Dacron		Teflon	PTFE
	Artery	Vein	HUCVAG	Bovine	Knitted	Woven	Woven	
Thoracic aorta or ruptured aneurysm						P	P	A
Infrarenal aorta					P	A	A	A
Aortovisceral	P	P	A		A			A
Femoropopliteal		P	A		A			A
Femorotibial		P	A					A
Axillofemoral					P			P
Femorofemoral					P			P
Extrathoracic bypass of arch vessel occlusion					P			P
Coronary artery	P	A						
Arteriovenous fistula			A	P	A			P
Carotid	P	P			A			A
Venous replacement		P			A			A

P, preferred; A, alternate

Table 1.2 Vascular grafts in use at present and their clinical application (adapted from Kempczinski 1984).

Fig. 1.2 shows the temporal distribution of the three most frequent failure modes for femoropopliteal vein graft resulting from the study performed by Whittemore *et al* (1981).

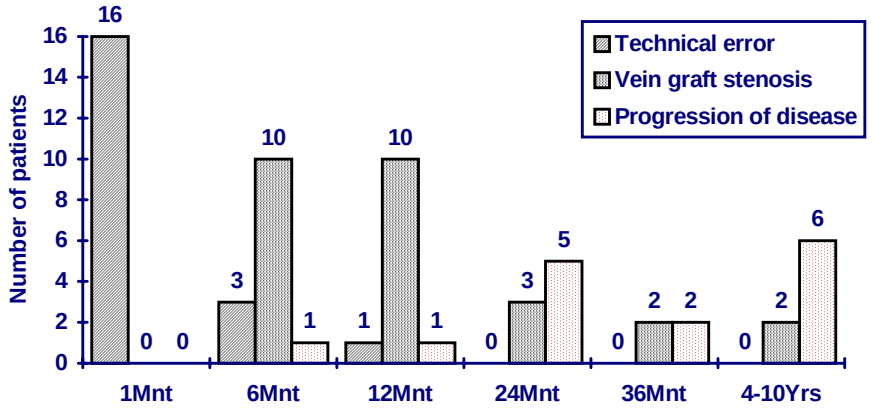

Figure 1.2 The temporal distribution of the three most frequent failure modes for femoropopliteal vein grafts. (From Whittemore *et al* 1981).

1.2.3. Medium and long term graft surveillance after operation

The main purpose of graft surveillance programmes is the maintenance of patency of a number of grafts which would otherwise fail. Durable long term improvement in patency rates of around 15 percent may be achieved by implementation of a systematic programme of graft surveillance and selective secondary intervention (Moody *et al* 1990). Although graft surveillance programs adopted by many centres have not been justified universally yet, many studies conclude that graft surveillance is justified (Berkowitz 1985, Moody *et al* 1990, Brennan *et al* 1991b, Wolfe *et al* 1991, Harris 1992). Since the cost of a graft surveillance program is also an important factor, simple, inexpensive and efficient methods are important. There are several techniques which can be used to assess graft patency, but not all these can detect tight localised stenosis.

1.3. CURRENT GRAFT SURVEILLANCE METHODS

A number of methods exist for following grafts after operation and the choice is to some extent determined by the resources available.

Angiography which remains the yardstick against which other methods are measured is the most widely used method. This is a technique for showing defects in blood vessels by means of x-rays. An iodine compound which casts a shadow is injected into the suspected artery or vein immediately before the film is exposed. This is an invasive method and not very convenient for studying grafts. However the introduction of digital subtraction angiography (DSA), has lessened this problem and image resolution has been greatly enhanced. Although DSA is a sensitive test it is expensive and time consuming. Because of the necessary infusion of contrast it is not suitable for repeated investigations.

Periodic graft examinations are now usually performed by using a combination of duplex scanning and Doppler ankle pressures. Ankle pressure indices (API) as an indicator for significant stenosis in femorodistal grafts or adjacent inflow and run-off arteries have extensively been investigated (Wolfe *et al* 1987, Bandyk *et al* 1988, Barnes *et al* 1989, Brennan *et al* 1991b). While resting API measurements are usually insensitive (Barnes *et al* 1989), postexercise measurements of API may provide more reliable evidence of graft stenosis (Brennan *et al* 1991b).

Ultrasound imaging is a non-invasive alternative to the angiography. Doppler flow analysis combined with real-time B-mode ultrasound imaging has proved to be a very powerful tool in assessing grafts postoperatively (Bandyk *et al* 1985). The ultrasound scan is used to identify the graft, after which the cursor may be accurately placed to measure the frequency change caused by the moving blood within the lumen. If the angle between the Doppler beam and the graft is measured then the velocity of the blood flow in the graft can be calculated. Color flow

technology is able to map the arterial system and both vascular anatomy and hemodynamics can be assessed. Detailed mapping of extracranial cerebral, abdominal, and peripheral arteries is possible with color Doppler imaging. Both conventional and color duplex systems provide real-time high resolution B-mode images. But while conventional systems rely on a grey-scale image to differentiate tissue types and vascular structures, color duplex systems simultaneously process the returned signals for this tissue information as well as Doppler flow information. After signal processing Doppler shifted data is displayed in a color display, which is superimposed on the grey-scale tissue information. By coding specific colors as to flow direction and the magnitude of the frequency shifted signal, a vascular road map is provided in real-time. This vascular map speeds up the process of vessel identification, and helps to differentiate sites with normal flow from those with disturbed flow, making it easier to localise areas of stenosis. However, it is not a quantitative technique. Objective data regarding stenosis is obtained from conventional grey-scale images and Doppler spectrum analysis. High resolution imaging allows a precise measure of the anatomic degree of restenosis, particularly in lateral cross-sectional views where percent area reduction can also be calculated. With the pulsed Doppler sample volume placed in the centre of the patent lumen, the entire region of interest can be scanned to acquire quantitative velocity data and evaluate hemodynamic disturbances associated with restenosis.

Magnetic resonance imaging (MRI) can be used to image blood vessels and measure the velocity of blood flow (Crooks and Kaufman 1984, Walker *et al* 1988). MRI is a method of imaging the soft tissues of the body taking advantage of inherent differences among tissues in how they respond to the presence of a magnetic field and to the introduction of energy in the form of radio-frequency waves. Clinical MRI examines only the hydrogen atoms (protons) within the tissue of interest. Detailed descriptions of the basic principles can be found in the literature (see for example Young 1984, Stark and Bradley 1988). The observation that blood moving from an area unaffected by the magnet and radio-frequency

waves could be easily distinguished as it passed into an area already activated made it possible to calculate the transit time of the blood. Development of this concept led to the imaging of flowing blood without visualisation of the tissues that were stationary. Since these images of flowing blood are similar to those obtained by the injection of intravenous contrast, the technique is termed *magnetic resonance angiography* (MRA). The potential advantage of MRA over conventional contrast angiography is the ability to obtain necessary diagnostic information without the risk of catheterization, contrast injection, and radiation.

Wyatt *et al* (1991) have proposed a non-invasive impedance analysis technique as an alternative to duplex scanning of femorodistal vein grafts. They claim that impedance analysis is superior to black and white duplex scanning in detecting the "at risk" femorodistal graft. In another study, it was shown that impedance analysis was as effective as color duplex for graft surveillance (Davies *et al* 1993). The technique involves computer assisted analysis of pulsatile pressure and flow signals utilising Fourier waveform analysis to predict mean limb impedance values for the thigh and calf respectively.

Although some of the methods introduced above are efficient in long and medium term graft surveillance none of them are suitable for continuous monitoring of grafts immediately after operation, the subject of this thesis.

1.4. PATIENT MONITORING

Monitoring means the analysis and interpretation of data coming from a system in order to recognise alarm conditions (Mora *et al* 1993). In clinical terms these alarm conditions (a significant change in a patient's condition) will generally be inferred from a change in one or several of the patient's physiological parameters over a period of time. In this case monitoring a patient's condition becomes a matter of

statistically monitoring the measure of the appropriate physiological parameters to determine when significant changes in those values occur (Lewis 1971). Many monitoring systems have been developed to monitor various physiological parameters such as blood pressure, heart rate, respiration rate, etc.

1.4.1. History of patient monitoring

The earliest written record relevant to the history of patient monitoring is contained in a papyrus. This document written in 1550 BC, shows that the ancient Egyptian physicians were familiar with the fact that the peripheral pulse could be correlated with the heart beat (Stewart 1970). In 1658, Galileo made an important contribution to the clinical measurement by discovering the principle of the pendulum which was used to measure the pulse rate (Graham 1956). The medical electronic age began in 1887 when Waller recorded the electrical activity of the human heart. MacKenzie, a general practitioner cardiologist, introduced graphical records of the pulse rate and blood pressure in 1925.

In 1945, the computer age started when the first electronic digital computer, ENIAC, based on the algebraic principles founded by Boole (1854) was constructed (Armytage 1961). From this point on, technologic developments accelerated the advances in monitoring equipment. Heart rate, blood pressure and respiratory rate were monitored (Geddes *et al* 1962). Computers were used to analyse data (Freimen and Steinberg 1964), and facilities for on-line computing were developed (Jensen *et al* 1966). The first computerised patient monitoring system was introduced by Warner *et al* (1968) and many studies were carried out using on-line digital or hybrid computing (Sheppard *et al* 1968, Osborn *et al* 1968, Lewis *et al* 1970, Raison 1970, Greer 1970, Taylor 1971, Kasai *et al* 1974, McClure *et al* 1975, Sheppard 1979). Developments in computer technology allowed the application of statistical methods for pattern recognition in monitoring systems (Lewis 1971,

Hope *et al* 1973, Hitchings *et al* 1974, Taylor 1975, Hill and Endresen 1978, Stoodley and Mirnia 1979, Allen 1983). The concept of intelligent monitoring systems has developed by the application of modern signal processing and pattern recognition methods such as artificial intelligence, expert systems, fuzzy logic, artificial neural networks, etc (Broman 1988, Papp *et al* 1988, Sztipanovits and Karsai 1988, Mora *et al* 1993, Siregar *et al* 1993, Sukuvaara *et al* 1993, Watt *et al* 1993).

1.4.2. Patient monitoring and management

If monitoring means to interpret incoming system data, management implies decision making about the required interventions on the system being monitored (Mora *et al* 1993). Fig. 1.3 represents a general monitoring and management process.

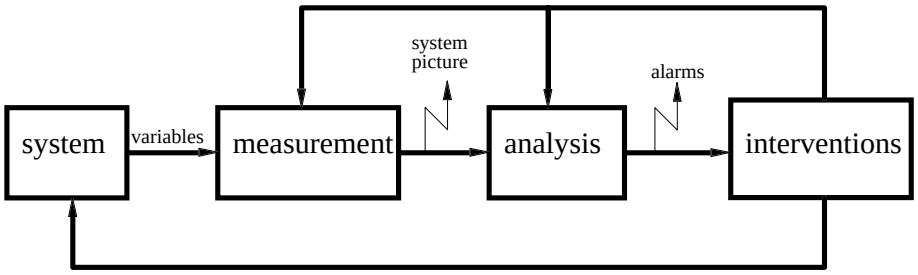

Figure 1.3 General diagram of monitoring and management process.

The system variables (physiological parameters) are measured. These measurements form a system picture. This is analysed using previous knowledge about the system. If there is an inconsistency between the analysis of the current and expected system picture alarm conditions are triggered and an intervention is requested. This intervention is directed to the system or any other blocks depending on the analysis results.

The elements of a monitoring system are patient, staff, therapeutic equipment and monitoring equipment. The aim of patient monitoring is to detect early or dangerous deterioration, with reliability and accuracy, and to give an appropriate warning or alarm. This alarm is activated when the measured variable strays outside limits that are set by the physician to indicate a change in the patient's condition. However, if these limits are set too finely this may result in a high incidence of false alarms that destroy the confidence of the nursing staff. On the other hand, alarm levels are frequently set so far apart to avoid this problem that the monitor may miss some important changes in the patient's condition. Problems with computerised patient monitoring are well reported (Maloney 1968, Crook 1970, Taylor 1971, McClure *et al* 1975, Taylor and Whamond 1975, Cullen and Teplick 1979). Since monitoring equipment is not intented to replace staff but to increase their skills, it is important to design reliable and more intelligent monitoring equipment. A review of statistical monitoring methods is given in Appendix A.

1.5. INTRODUCTION TO THE GRAFT MONITORING SYSTEM

Early attempts to develop a graft monitoring system employed only a CW Doppler unit and a tape recorder (Dahnoun 1990, Thrush and Evans 1990, Brennan *et al* 1991a). Raw Doppler signals (either quadrature or separated) were first recorded in the theatre or ward and then analysed later using a Doppler spectrum analyser (Schlindwein *et al* 1988).

A graft monitor should at least be able to perform these tasks on-line in the theatre or ward and minimise human interaction to derive desired parameters. It should also be flexible enough to be easily modified when necessary and operational cost should be minimum. Keeping these essential requirements in mind, a computerised graft monitor has been developed. The basic elements and a functional block

diagram of this monitoring system are illustrated in Fig. 1.4 and Fig. 1.5 respectively.

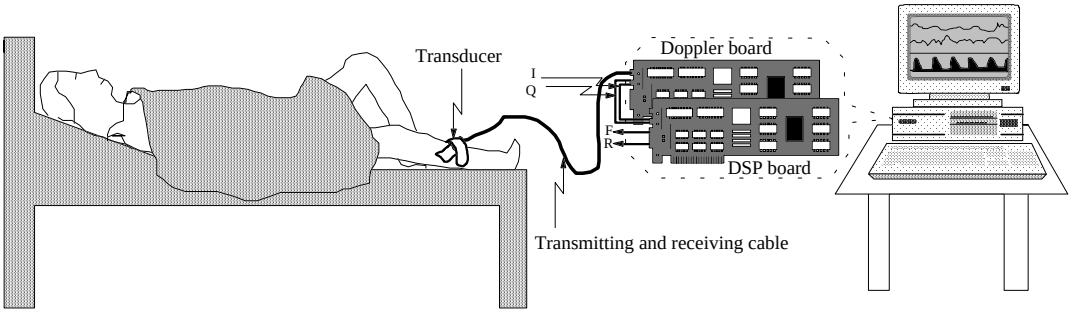

I: In-phase, Q: Quadrature-phase, F: Forward, R: Reverse Doppler signals.

Figure 1.4 Representative basic graft monitoring system.

The system is composed of three main units: an IBM-PC AT compatible personal computer (PC); a commercially available high performance floating point digital signal processor (DSP) board[1] and a purpose built continuous wave (CW) Doppler board. The related software implementations (DSP assembler and PC control) can also be taken as part of the whole system.

The following chapters will concentrate on the design of the hardware and the description and implementation of some digital signal processing (DSP) algorithms. After reviewing Doppler instrumentation in Chapter 2, the design and development of the CW Doppler unit for the IBM-compatible PC will be described. Digital signal pocessing algorithms for frequency domain display and time domain outputs will be discussed in Chapters 4 and 5 respectively and their implementations on a floating point DSP system will be given in Chapter 6. In Chapter 7, the extraction of some frequency parameters and waveform classification principles will be

[1]Loughborough Sound Images Limited,
The Technology Centre, Epinal Way, Loughborough,
Leics LE11 0QE, UK.

introduced. The operation of this computerised graft monitoring system will be summarised and some preliminary results will be presented in Chapter 8.

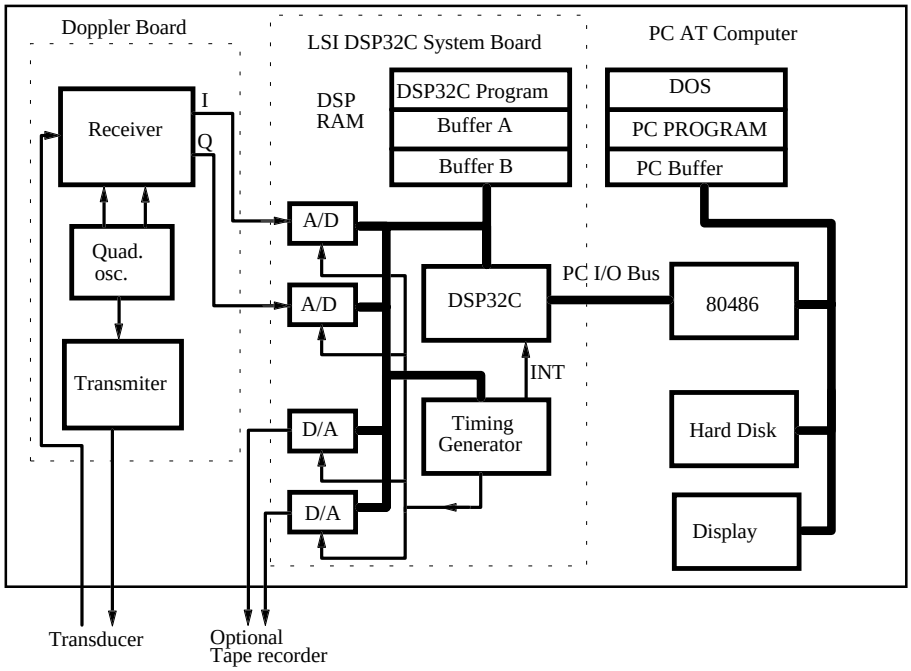

Figure 1.5 Functional block diagram of the graft monitoring system.

1.6. CONCLUSION

The nature of graft failures, the concept of patient monitoring and descriptions of some methods used in graft surveillance after operation have been briefly given and a computerised graft monitoring system has been introduced. Some graft surveillance methods are very efficient at identifying grafts at risk. Although angiography may be regarded as the gold standard for imaging vascular structure, it is invasive and does not provide functional information. Instead many centres are now using duplex scanners to visualise vascular structure and obtain functional information. It is also a non-invasive technique and so can be performed routinely. However costs of these techniques are high and they are not practical for continuous monitoring of grafts immediately after operation. Developments in

signal processing and computing technologies can enhance simple non-invasive flow measurement techniques based on Doppler ultrasound. While these developments have simplified the physical structure of the system being implemented, they provide a powerful engine to perform the most complicated computational tasks such as digitally processing and analysing Doppler ultrasound signals. These will be highlighted in the following chapters.

2. DOPPLER INSTRUMENTATION FOR VELOCITY MEASUREMENT

2.1. INTRODUCTION

The Doppler principle, which was first described in the nineteenth century, has many applications in astronomy, physics, communication and medicine. In medicine, it is mainly used for the study of blood flow. Use of Doppler ultrasound in medicine was first reported in 1959 by Satomura in Japan. Early Doppler units were continuous wave (CW), non-directional devices. In 1967, McLeod introduced the first directional Doppler ultrasound equipment. Two years later pulsed wave Doppler systems were developed (Wells 1969). The development in this area was rapid, and more complicated Doppler equipment such as multigate and infinite gate systems followed shortly (Baker 1970). In 1971, Doppler imaging was introduced by Mozersky et al. These developments have made Doppler systems both sophisticated and widely applicable. Real-time colour flow imaging (Namekawa *et al* 1982, Omoto *et al* 1984, Kasai *et al* 1985) is one of the latest development in this area.

As a result of these developments, Doppler techniques have been widely used in areas such as cardiology, obstetrics and in general circulation studies. Many different types of commercial equipment based on the Doppler ultrasound principle are widely available.

2.2. PHYSICAL PRINCIPLE OF DOPPLER ULTRASOUND

Doppler ultrasound is based on the fact that any moving object in the path of a sound beam will shift the frequency of the transmitted signal. It can be shown that

the difference between the transmitted frequency f_t and received frequency f_r is given by:

$$f_d = f_t - f_r = \frac{2vf_t \cos\theta}{c} \qquad 2.1$$

where v is the velocity of the target, θ the angle between the ultrasound beam and the direction of the target's motion, and c the velocity of sound in the medium. The velocity and the transmitted frequency are known and the angle between the ultrasound beam and the direction of the target's motion can be determined. In this case, the velocity of the target can be found from the expression:

$$v = \frac{f_d c}{2 f_t \cos\theta} \qquad 2.2$$

Since the reflectors in a moving (flowing) media have different velocities, the Doppler shift signal contains a spectrum of frequencies which are within the audio range (0-20 kHz). The moving media is usually blood flow in clinical applications and Doppler studies are concentrated on interpreting the Doppler shift frequency spectra.

Detection of the returned (scattered) Doppler ultrasound signals is only made possible by employing a suitable electronic system. This requires a signal conversion process which is performed by an ultrasonic transducer. The next section introduces the basic principles of processing ultrasound Doppler signals.

2.3. DETECTION OF DOPPLER ULTRASOUND SIGNALS

Detection of Doppler ultrasound signals is a technical problem rather than a clinical one. It can be taken as a measurement problem and a general ultrasound Doppler

signal measurement system can be modelled as in Fig. 2.1. This system can be divided into the three main parts: transduction, processing, interpretation and display.

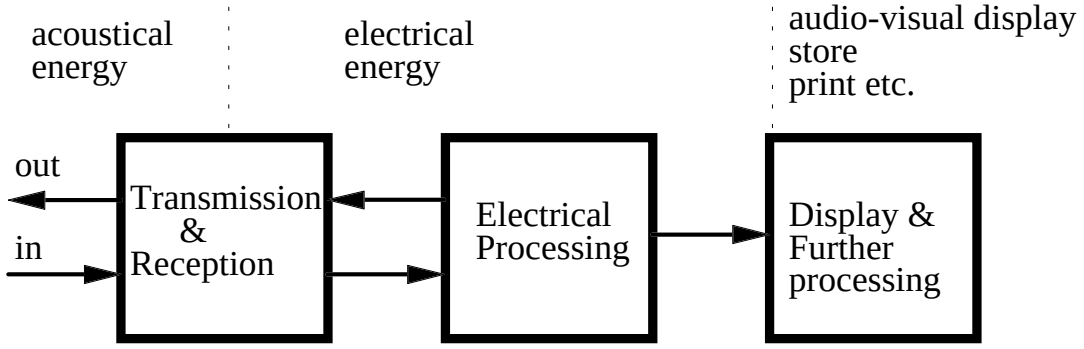

Figure 2.1 A general Doppler ultrasound signal measurement system.

The transduction stage performs the energy conversion from electrical to acoustic energy and vice-versa. In general terms, a transducer is any device that converts energy in one form to energy in another. However, in its applied usage, the term refers to rather specialised devices. The majority either convert electrical energy to mechanical displacement or convert some nonelectrical physical quantity, such as temperature, sound, or light, to an electrical signal. Electro-acoustical transducers are used in the ultrasound systems.

The processing stage prepares the signal for transmission and/or processes the signal already converted to the electrical form by the transducer for display or further analysis. An example of this stage is the Doppler signal demodulator which is an electronic system which extracts the Doppler shifted signals from the returned signal. The last stage is mainly for the presentation and/or further analysis of the processed signals.

2.3.1. Ultrasonic transducers

An ultrasonic transducer converts electrical energy into acoustic energy during transmission when its active element is excited by a voltage signal. Conversely, the acoustic energy of the returned signal is converted into electrical energy when acoustic pressure is applied to the transducer during reception. This phenomenon is known as the piezoelectric effect. Piezoelectric properties occur naturally in some crystalline materials and can be induced in other polycrystalline materials. Many applications of piezoelectricity use polycrystalline ceramics instead of natural crystals because of their versatility.

A simplified equivalent representation of an ultrasonic transducer is given in Fig 2.2. This is a four terminal network. In electrical circuit theory, it is well known that the maximum power transfer is achieved when the electrical impedances of the generator and the load are matched. The same consideration is also valid for the acoustical side of the transducer (mechanical impedance matching).

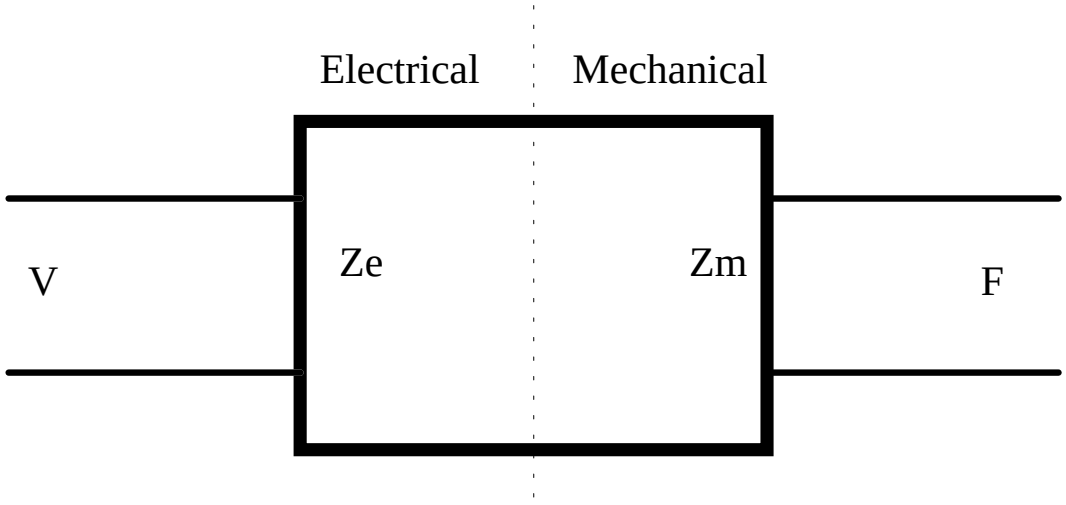

Figure 2.2 A simplified equivalent representation of an ultrasonic transducer.

2.3.2. Velocity detecting systems

The simplest Doppler units are stand-alone systems that produce an output signal related to the velocity of the targets in a single volume. Velocity detecting systems can be categorised as either continuous wave (CW) or pulsed wave (PW) Doppler systems.

2.3.2.1. Continuous wave Doppler systems

Continuous wave (CW) Doppler ultrasound is a widely used non invasive diagnostic technique to evaluate cardiovascular disorders. CW Doppler instruments detect blood flow velocity using the Doppler effect by means of continuous wave transmission of ultrasound into the tissues. The backscattered ultrasound signal is detected and amplified by the instrument as an audio frequency signal. Because the transmission is continuous, CW Doppler instruments have no depth resolution. However, CW methods are extremely simple and able to detect high velocities.

A block diagram of a CW Doppler system is depicted in Fig. 2.3. CW Doppler probes are constructed using two identical crystals. One insonates the moving media when excited by the oscillator, a radio frequency (rf) signal generator. The other detects back-scattered ultrasound signal and converts it into an electrical signal. This electrical signal is amplified by the rf amplifier if necessary, and the frequency-shifted audio signals are demodulated by means of the mixer. The mixer is an electronic device that basically multiplies two incoming signals and produces an output proportional to the amplitudes of the input signals. The output of the mixer has two main frequency bands; f_t+f_r and f_t-f_r . A low-pass filter, which forms the product detector with the mixer, filters out the frequency band containing high frequency signals. The remaining signals are the frequency shifted Doppler signals.

These are amplified by the audio amplifier and may be presented audibly via a speaker or processed for further interpretation.

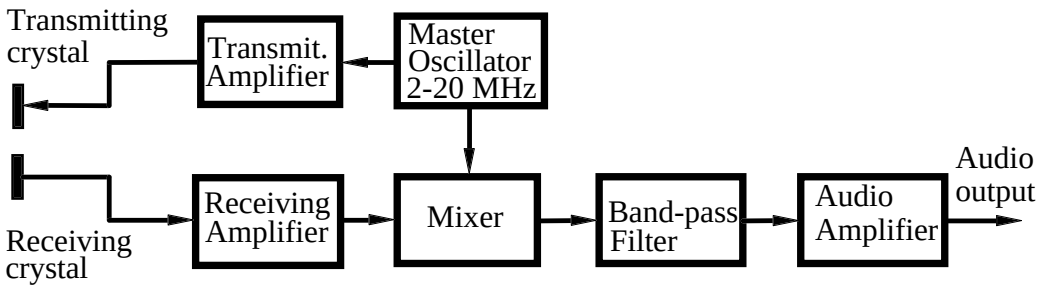

Figure 2.3 Block diagram of a non-directional continuous wave Doppler system.

2.3.2.2. Pulsed wave Doppler systems

CW Doppler systems do not provide information about the range at which movement is taking place. They are often unable to separate mixed signals and quantify velocities. These limitations of the CW Doppler systems can be overcome using pulsed wave (PW) Doppler systems which combine the spatial ability on which ultrasonic imaging is based with the ultrasound phase detection on which Doppler measurement is based.

A basic PW Doppler system is outlined in Fig. 2.4. PW Doppler systems use the same transducer for transmitting and receiving. During transmission, the transducer is excited by a pulse produced by gating the rf signal generated by the master oscillator. The gate is under the control of the pulse repetition frequency (PRF) generator. During reception, the transmitting gate is closed and the receiving gate opened. This occurs after an operator selected time delay which determines the depth from which the signals are gathered. This signal is demodulated by the mixer and sampled during the time the receiving gate is open. It is then filtered, amplified and sent for further processing.

Because it samples the data rather than gathering continuously, PW Doppler systems have a well known limitation: aliasing. The maximum Doppler shift frequency a PW Doppler system is able to detect unambiguously is half of the PRF. These systems are also more complex than the CW Doppler systems.

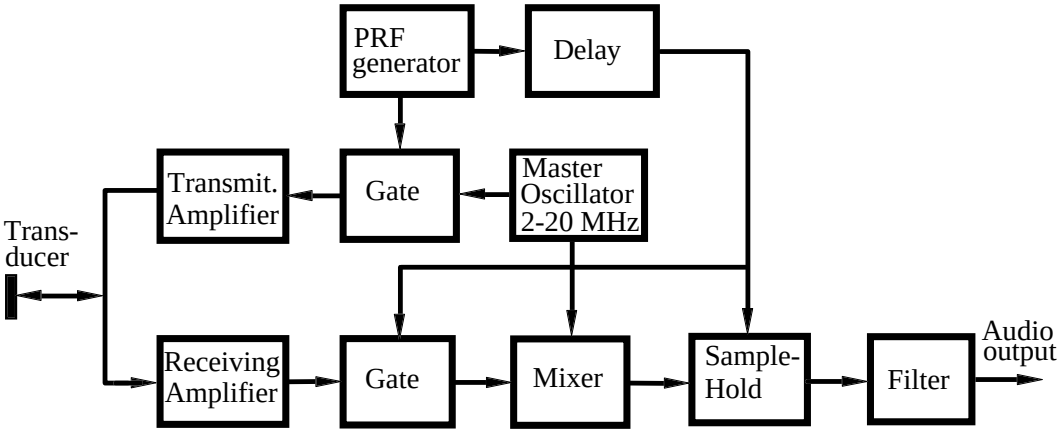

Figure 2.4 Block diagram of a non-directional pulsed wave Doppler system.

2.3.3. Demodulation of Doppler frequency shifted signals

One of the most important stages in a Doppler ultrasound system is demodulation of the Doppler frequency shifted signals which are generated in the transducer by the returning ultrasonic signals. Most of the demodulation techniques employed in communication systems are equally applicable to Doppler ultrasound systems. Since the theoretical bases of these methods can be found in many textbooks, the detailed theory will be avoided and the feasibility of the practical implementations emphasised.

The simplest form of the Doppler signal demodulators which does not preserve the directional information has been already described. These instruments only give the magnitude of the Doppler shift frequency. However, the directional information can be preserved in a number of ways (DeJong *et al* 1975, Cross and Light 1974,

Coghlan and Taylor 1976). In this section, some of these techniques will be briefly introduced.

2.3.2.1. Single side-band detection

The Doppler shift signal can be taken as a modulated signal having an upper side-band (USB) and a lower side-band (LSB) around a carrier signal. The USB is formed by the positive Doppler shift frequencies which correspond to one direction and the LSB is formed by the negative Doppler shift frequencies which correspond to the other direction. The USB and the LSB can be separated using a high-pass filter (HPF) which rejects the LSB and a low-pass filter (LPF) which rejects the USB. These signals are then demodulated and low-pass filtered to produce separate audio signals, one composed of forward flow and the other of reverse flow. The method is outlined in Fig. 2.5.

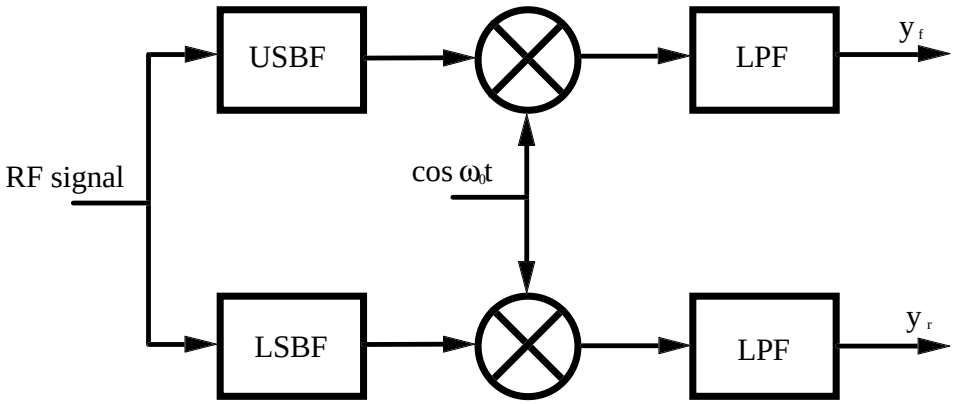

Figure 2.5 Single side-band detection of the Doppler shift signals. **USBF**, upper side-band filter; **LSBF**, lower side-band filter; **LPF**, low-pass filter

Since the USB and LSB signal frequencies are very close the side-band filters must be extremely sharp. This imposes a practical limitation on this method. Designing such filters using analogue signal processing components is difficult and their

performance is readily influenced by environmental changes such as temperature and ageing. However, this method can be easily implemented using very high speed digital signal processing components. In this case, the returned rf signal is digitised by a high speed A/D converter and then processed digitally. Although this will eliminate the problems associated with analogue signal processing, the price of the system will increase considerably.

2.3.2.2. Heterodyne detection

A block diagram of the system is shown in Fig. 2.6. Because it utilises only one demodulator the heterodyne detection system is a single channel system. The direction information is maintained by demodulating the returning ultrasound signal with a signal whose frequency is slightly less than the master oscillator frequency. This is derived by mixing the heterodyne frequency signal with the master oscillator signal and then filtering it to retain the lower side-band (LSB) of the mixer output. Again the LSB filter must be extremely sharp and stable.

After demodulation, the unwanted high frequency components are removed by a simple low-pass filter and the final output is a directional Doppler signal around the heterodyne frequency signal. The signals whose frequencies are greater than the heterodyne signal frequency form one direction, the signals whose frequencies are less than the heterodyne signal frequency form the other direction. The heterodyne signal frequency must be higher than the highest Doppler shift frequency and a sharp notch filter is necessary to remove the large clutter component that is generated at the heterodyne frequency. Since the system has only one output a single channel spectrum analyser is sufficient.

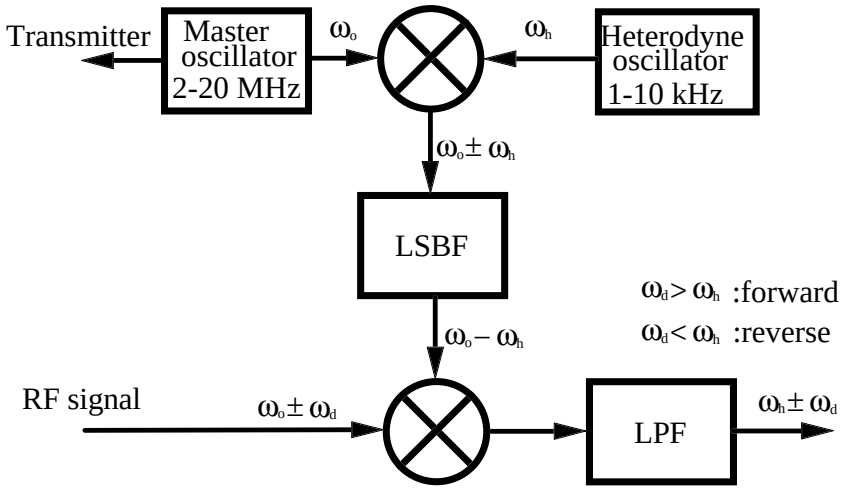

Figure 2.6 Heterodyne detection of the Doppler shift signals. **LSBF**, lower side-band filter; **LPF**, low-pass filter

2.3.2.3. Frequency translation and side-band filtering detection

The frequency translation and side-band filtering detection system, which is outlined in Fig. 2.7, combines single side-band detection and heterodyne detection. The incoming rf signal frequency is translated to a much lower frequency (2-20 kHz) signal by mixing it with a signal whose frequency is slightly higher or lower than the master oscillator (oscillator1). This process will produce an output in the same way as heterodyne detection. This frequency translated Doppler signal can then easily be decoded into the separated directional outputs by applying single side-band detection.

Although this system seems quite complicated, the implementation of it is extremely simple when digital signal processing techniques are used. If a direct digital synthesizer (DDS) is used in order to generate signal-1 and-2 (produced by the oscillator1 and the oscillator2 respectively) and the side-band separation is performed using a digital signal processor (DSP) the processing stage framed by dotted lines is unnecessary. If the system is implemented using analogue signal

processing components this stage is necessary to produce a pilot frequency signal whose frequency is equal to the difference between signal-1 and -2. This signal is then used to translate the separated Doppler signals to the base-band.

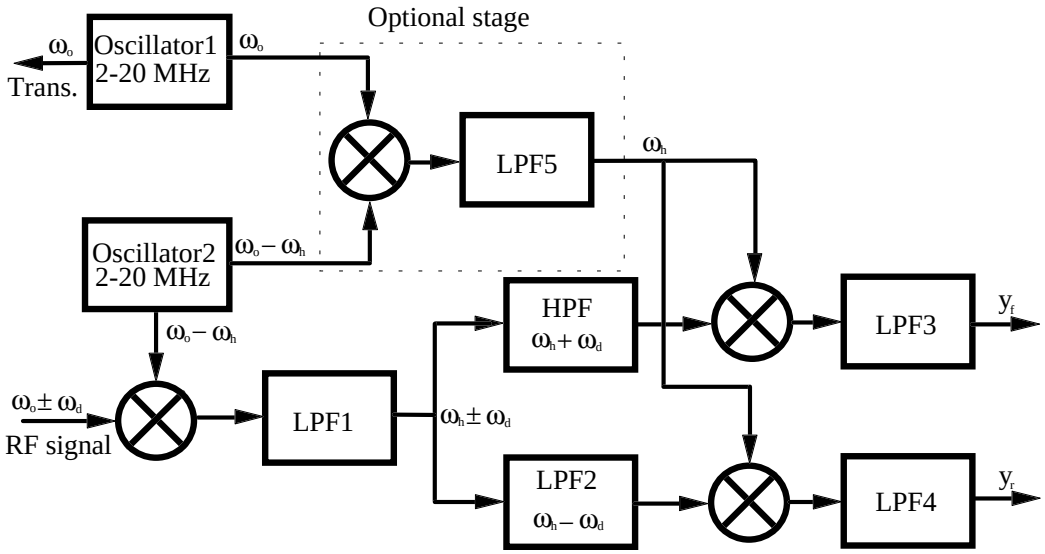

Figure 2.7 Frequency translation and side-band filtering detection of the Doppler shift signals. **HPF**, high-pass filter; **LPF**, low-pass filter

Employing the DDS and the DSP in this system removes most of the design difficulties encountered in the previous implementations of the heterodyne and single side-band detection systems. A DDS produces extremely stable and precise sinusoidal signals and is entirely programmable. Since the frequency difference between signal-1 and -2 can be controlled numerically, this can be predefined and it is unnecessary to recover it. Instead it is digitally generated during the digital signal processing. Large clutter signals can be easily removed using very sharp digital notch filters.

2.3.2.4. Quadrature phase detection

A block diagram of quadrature phase detection is shown in Fig 2.8. This is the most widely used detection method to preserve direction information.

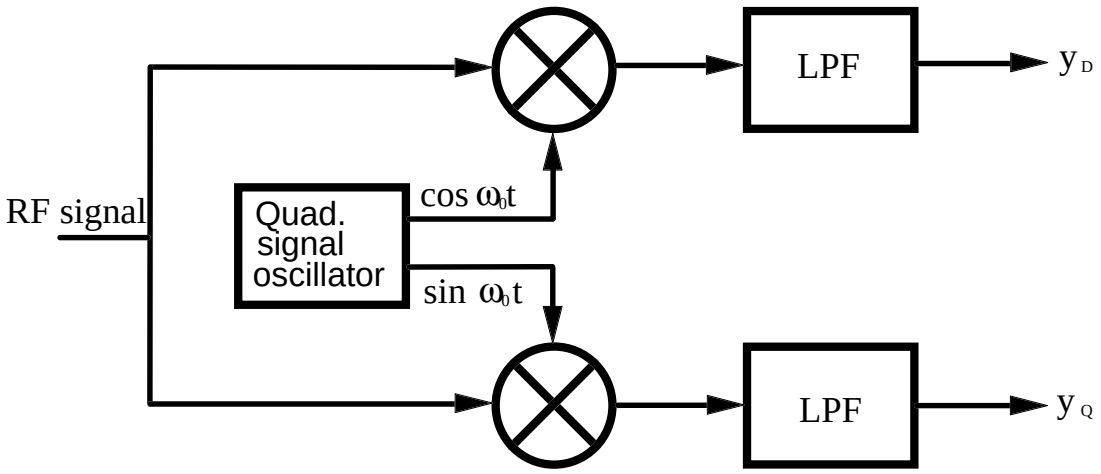

Figure 2.8 Quadrature phase detection of the Doppler shift signals.

The returning Doppler signal is demodulated using two reference signals having 90^0 of phase shift between them. The high frequency components are removed by low-pass filtering and the outputs are within the audio frequency range. This process produces a complex quadrature signal which is composed of the real and imaginary (or in-phase and quadrature-phase) components of the Doppler signal. The direction information is encoded into the phase relationship between these components. A number of methods to obtain totally separated directional Doppler signals from the quadrature Doppler signals are described in chapter 5.

One of the most important considerations in the design of quadrature phase detectors is the amplitude and phase balance of the quadrature carrier signals. Ideally, the amplitudes of these signals must be identical and the phase difference between them must be 90^0. Any gain and/or phase error in the carrier signals will appear at the quadrature outputs. This will lead to crosstalk artefact being generated in the directional outputs.

2.3.2.5. Detection by direct sampling

From the explanations of the Doppler demodulation systems given above we can conclude that all Doppler signal detection systems are based on modulation theory. Since a sampling process is considered as a modulation process, the returning signals can be directly sampled to recover the Doppler signals. A number of sampling strategies applied to Doppler ultrasound signals have been reported (Powers *et al* 1980, Halberg and Thiele 1986, Forsberg and Jorgensen 1988, Ahn *et al* 1988, Chang *et al* 1993).

The Nyquist sampling theorem states that the sampling frequency of a signal must be at least twice the maximum frequency component of this signal. Any input signal violating this condition will give rise to aliasing. The sampling which generates aliasing effects is termed undersampling. This is usually an unwanted feature. However, undersampling can be used in certain carefully chosen applications. The generalised sampling theorem says that a sampled input can be reconstructed from the sampled data if the input frequency components lie entirely between adjacent integral multiples of one-half the sample rate. This is illustrated in Fig. 2.9.

The returning ultrasound signal can be regarded as a double side-band (DSB) modulated narrow-band signal in which the USB represents one direction of the flow and the LSB other. In order to preserve the information contained in both side-bands quadrature sampling can be applied or the DSB signal can be slightly shifted providing that the shifted signal bandwidth is within half of the sampling rate.

Direct sampling requires a very high speed and accurate A/D conversion process. Alternatively, the A/D conversion can be preceded by a sample-hold (S/H) circuit. The S/H must have sufficient bandwidth and slewing capability to pass the input signal without introducing significant distortion (Forsberg and Jorgensen 1989, Kirsten and Fleming 1991).

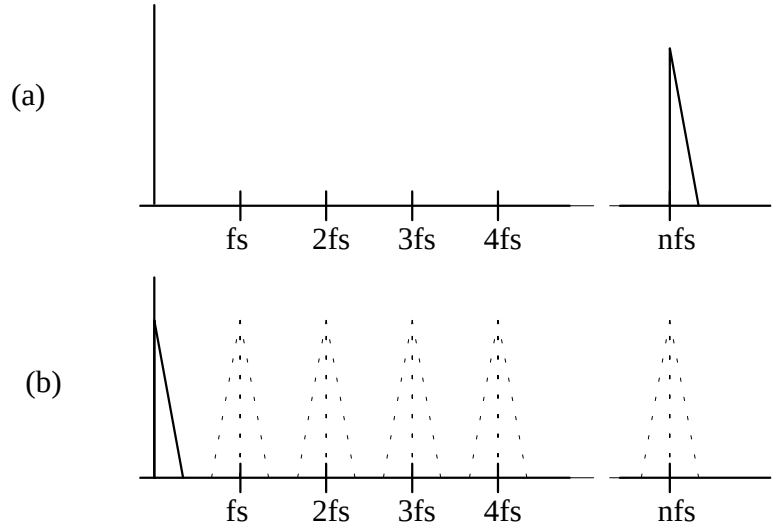

Figure 2.9 Effect of the undersampling. (a) before sampling; (b) after sampling

2.4. SUMMARY

In this chapter, the basic Doppler instrumentation has been introduced. Two basic methods (the CW and PW Doppler) are available for continuous or intermittent monitoring of arterial grafts.The CW Doppler system has been chosen for the monitoring instrument because of its simplicity, and the quadrature demodulation technique has been employed for preservation of directional information. The construction of this unit will be described in next chapter and derivation of the directional information using digital signal processing techniques will be explained in Chapters 4, 5 and 6.

3. DESIGN AND CONSTRUCTION OF A CW DOPPLER UNIT FOR IBM-PC COMPATIBLE COMPUTERS

3.1. INTRODUCTION

An arterial graft can fail after operation due to one of the reasons discussed in Chapter 1. Intermediate and late failures can be prevented by applying periodic graft surveillance programs as demonstrated by many studies (refer to Chapter 1). However these surveillance programs are not appropriate for detection of very early graft failures accounting for 20% of the total. Therefore the concept of graft monitoring, aiming to monitor blood flow changes in a graft just after operation and possibly to detect early failures has recently developed (Dahnoun 1990, Thrush and Evans 1990, Brennan *et al* 1991a). Since the efficiency of a monitor is highly influenced by the quality of the measured signal, perhaps the most important element of a graft monitoring system is a reliable Doppler unit. This chapter will describe the design and construction of a Doppler unit for IBM-PC compatible computers and highlight some practical considerations. The Doppler board is based on the quadrature detection method and the outputs are not separated. The directional channel separation is performed digitally in the DSP section and will be discussed in Chapters 4 and 5.

3.2. A CW DOPPLER BOARD FOR IBM-PC'S

The block diagram of the Doppler board is illustrated in Fig. 3.1. This is basically a CW Doppler unit based on the phase quadrature demodulation method. The operation of this method has been described in Chapter 2. The only difference is that this board is interfaced to the PC via a *PC interface unit* and installed in one of

the PC's expansion slots. In the following sections, design considerations and implementations of each stage are given.

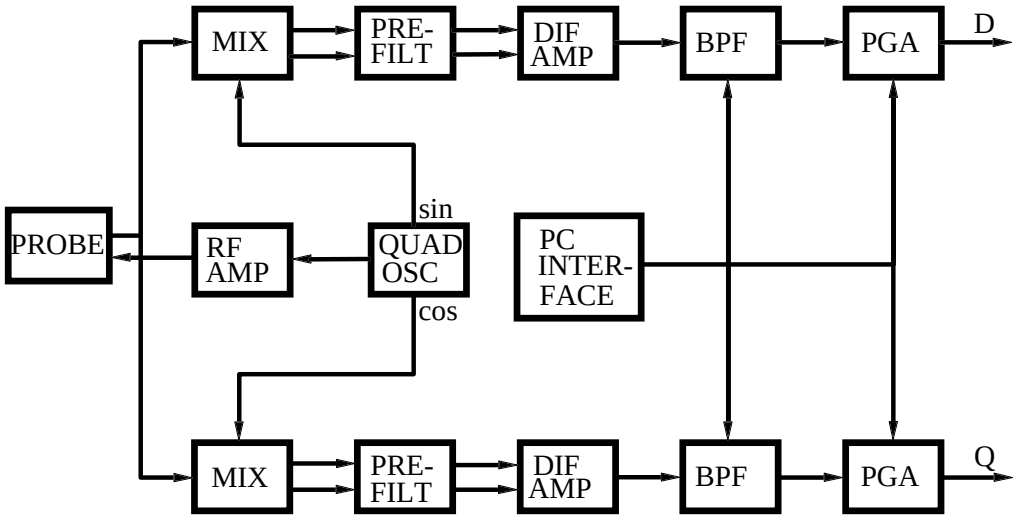

Figure 3.1 Block diagram of the Doppler unit. MIX: Mixer; DIF AMP: Differential amplifier; BPF: Band-pass filter; PGA: Programmable gain amplifier

The unit (Fig. 3.1) can be divided into four main blocks: Oscillator, transmitter, detector, and PC interface. The oscillator is formed by using a crystal controlled integrated circuit (IC). The transmitter uses two transistors to form a transformer coupled push-pull class B amplifier. The detector consists of two mixers, differential audio amplifiers, programmable filters, and programmable gain amplifiers (PGA).

3.2.1. General design considerations

In the design of such a system, there are numerous considerations depending on the application for which the system is intended. Perhaps the first consideration is the necessity of designing custom-built units. In most cases, commercially available Doppler units satisfy a wide range of applications. However, in some cases

researchers have no alternative but to design their own system. In our case we have chosen to develop our own Doppler unit to be installed in a PC. Although there are some Doppler systems sold with computers, they are not very flexible. Most computers offer expandability via expansion slots, so designing a Doppler unit which uses a computer as a host is a logical choice for a monitoring system which is required not to be bulky. However such a design needs extra attention to noise problems since the computer is full of switching circuits which are a major source of noise radiation. Another criteria which should be considered in the early design stage is the choice of design method. The CW Doppler has been preferred because of its simplicity, low cost and versatility. More complicated PW Doppler systems also tend to be noisier than the CW Doppler systems. Although it is not a primary consideration, power consumption of the Doppler unit should be kept as low as possible since a flowing current in a circuit can be regarded as an rf interference carrier. Programmability of the system should be possible through the host computer. For example, the insonation time should be under control of the computer for automated monitoring operation, and the filters and amplifiers should be programmable. Further features may be needed depending on the application. But a major consideration for all kinds of applications is noise elimination and/or reduction.

Every signal is corrupted by the superimposition of extra signal fluctuations which are unpredictable at any instant of time. These undesirable signals are called noise. The noise can generally be classified as transmitted noise, intrinsic noise, and interference noise.

The transmitted noise is received with the original signal and is indistinguishable from it. However statistical techniques such as averaging for repetitive signals and smoothing for non repetitive signals (in this case the signal must be oversampled) may help to reduce transmitted noise.

Intrinsic noise (such as thermally generated Johnson noise, shot noise, and popcorn noise) originates within the components (resistors, transistors, integrated circuits etc.) which constitute an electronic circuit. Using low noise components leads to an improved noise performance. Statistical techniques can also reduce this type of noise.

The major noise problem in an electronic circuit which designers must deal with is caused by interference type noise. This may be due to natural disturbances (lightning, cosmic rays etc.) or coupled in from other electrical apparatus in the system (for example, computers, radio transmitters, switch contacts, etc.). Process induced errors such as measurement, quantization, truncation and signal generation errors also corrupt the signal introducing extra noise power and loss of resolution.

Interference type noise is the form of noise that can be most easily influenced by the designer. Correct design strategies and proper shielding can eliminate or significantly reduce this type of noise. A clear definition and treatment of interference type noise is given by Rich (1982, 1983). General noise reduction techniques in electronic systems are discussed in detail by Ott (1988). Interference control in computers is well explained by Mardiguan (1984) and White *et al*. (1985). The design data supplied by manufacturers of electronic components are also valuable guides for designers. The effect of interference on Doppler equipment is discussed, and some solutions are proposed, by Follet (1991).

3.2.2. Oscillator design

Signal generation is one of the most important parts of the Doppler system. The stability of the oscillator will affect the system stability. Since the transducer is driven by the signal generated by the oscillator and the returned Doppler signal is demodulated using the quadrature signal derived from the oscillator, it is important

to make sure that the signal to noise ratio of the oscillator is high. In this design, a sine wave oscillator rather than a square wave type is employed to minimise the possibility of modulation with the signal harmonics radiated by the other switching circuits within the computer.

The oscillator is based on Motorola's crystal oscillator chip MC12061. This IC is designed for use with an external crystal to form a crystal controlled oscillator. In addition to the fundamental series mode crystal, two bypass capacitors are required (plus usual power supply pin bypass capacitors).

The circuit diagram of the oscillator is illustrated in Fig. 3.2. This is a general configuration to implement a sine wave oscillator giving an output between 600 mV and 800 mV depending on the load. Series mode crystals, whose equivalent series resistance is less than 155 ohm, should be used with the oscillator. If it is necessary or desirable to adjust the crystal frequency, a reactive element can be inserted in series with the crystal (an inductor to lower the frequency or a capacitor to raise it).

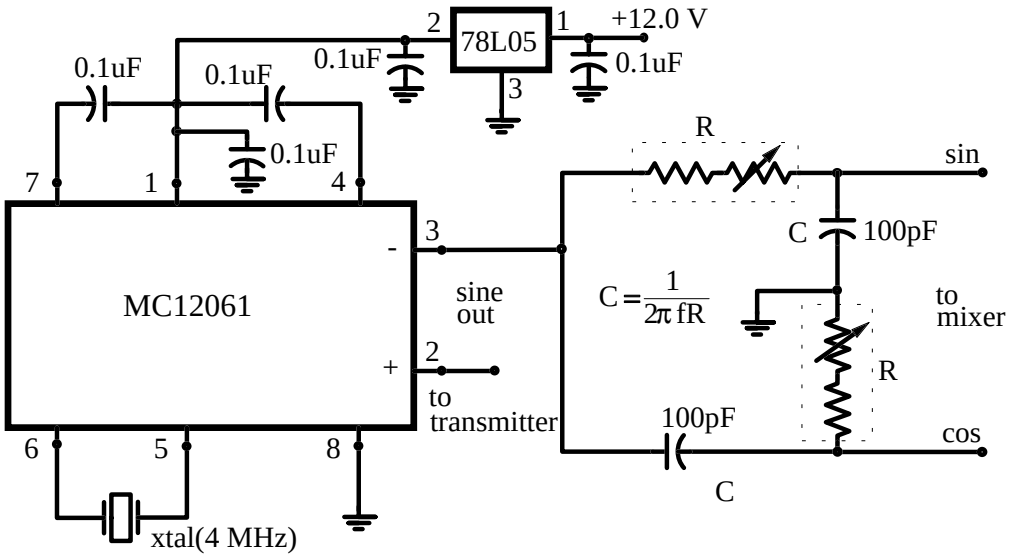

Note: All unused pins should be connected to ground

Figure 3.2 The circuit diagram of the oscillator.

This crystal oscillator has been chosen, because it is stable, flexible and easy to use. The output frequency can range from 2 MHz to 20 MHz, simply by changing the series mode crystal.

Since the Doppler unit is based on the quadrature detection system, it is necessary to produce a quadrature carrier signal. This is implemented using a phase-shift circuit, which is basically a combination of a low-pass and high-pass filters as shown in Fig. 3.2. At the cut-off frequency (4 MHz in our design) the high-pass filter provides $+45^0$ and the low-pass filter -45^0. The total phase difference is 90^0. This network works only over a narrow range of frequencies (bandwidths of 100 kHz) and is thus limited to fixed frequency applications. Using this kind of network above 10 MHz is not recommended. Some other rf quadrature phase shift networks (single frequency and wide band) have been described by Harrison (1978). A new approach to generating quadrature signals is to use a direct digital synthesiser(DDS) which produces digitized samples of a sine wave that drive a digital-to-analogue converter (DAC). The resulting sine wave has a fine frequency resolution and phase control, a broad bandwidth of operation, fast switching speed between output frequencies, and excellent phase noise performance. Although it is a quite expensive solution to the quadrature signal generation, the frequency and phase of the generated signal are entirely programmable.

3.2.3. Transmitter design

The circuit diagram of the transmitter is shown in Fig. 3.3. This is a class B push-pull amplifier. In class B push-pull operation, one transistor conducts while the other is cut-off. Thus the two transistors amplify alternate halves of the waveform, and their inputs are 180^0 out of phase. The main advantages of class B push-pull operation are low quiescent current and high efficiency at full output. This

amplifier is driven by the one of complementary outputs of the signal generator given in Fig. 3.2.

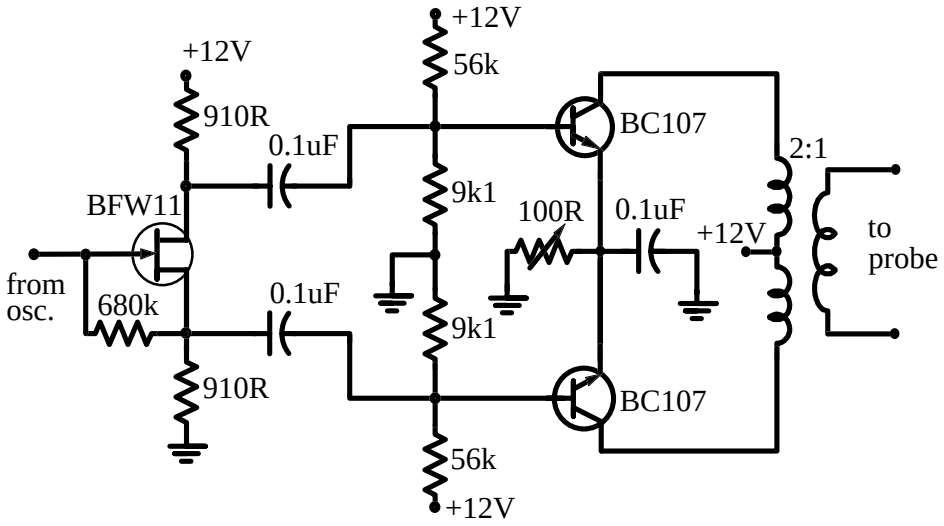

Figure 3.3 The circuit diagram of the transmitter.

The first stage of the amplifier (BFW11) behaves as a buffer and the phase splitter. The signals at the drain and source are 180^0 out of phase. The output and driver transformer turns ratio is 2:1 (22+22:11). A toroidal core was used to design the transformer. It also provides isolation between the transmitter and patient.

3.2.4. Demodulator design

The demodulator circuit illustrated in Fig. 3.4 is based on the MC1496 balanced modulator-demodulator chip. The chip is sensitive enough to detect reflected ultrasound signals without a preamplifier and exhibits a good dynamic range. The circuit performs as a single side-band product detector. The input signal is applied to the circuit through the transformer having a turns ratio of 1:1.5 (16:25). This also

serves as an isolation transformer between the receiver and the patient. The carrier signals are derived from the quadrature signal generator given in Fig 3.2.

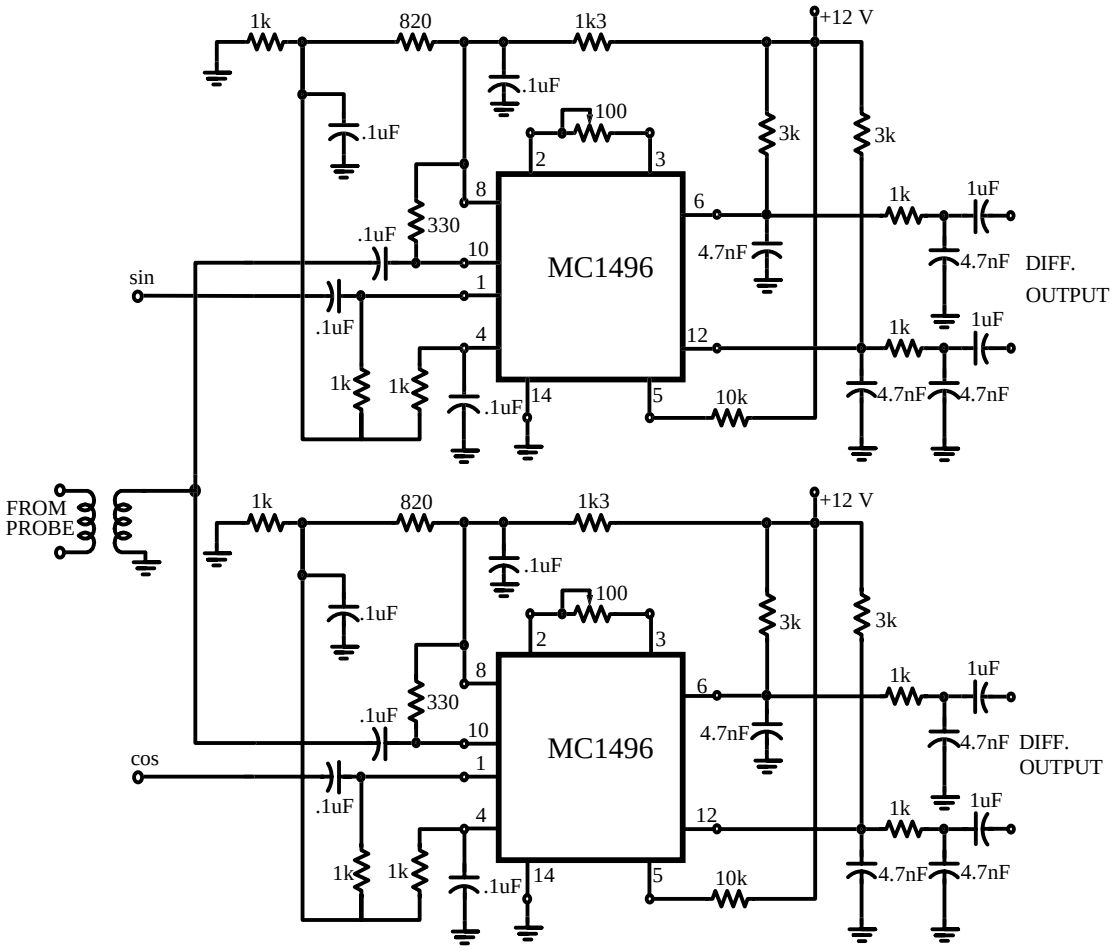

Figure 3.4 The circuit diagram of the demodulator.

The signal coming from the transducer and the carrier signal are mixed and the demodulated signal then filtered by a very simple prefilter which is formed by a resistor (1 kohm) and a capacitor (4.7 nF). The mixer output is differential (complimentary) and within the audio range. The differential mode was used to give rejection of common mode noise. A differential audio amplifier (SSM-2015) converts the differential output to a single ended signal. The circuit diagram for the differential audio amplifier is given in Fig. 3.5.

The SSM-2015 is an ultra low noise (1.3 nV/Hz$^{1/2}$) differential preamplifier. Gains from 10 to over 2000 can be selected with wide bandwidth and low distortion over the full gain range. The gain is set by an external resistor (R_G). The nominal gain of this circuit is given by:

$$G \cong \frac{R_1 + R_2}{R_G} + \frac{R_1 + R_2}{8k\Omega} + 1 \text{ or } G = \frac{20k\Omega}{R_G} + 3.5 \text{ for } R_1, R_2 = 10k\Omega.$$

The output of the SSM-2015 is an audio signal which is caused by the Doppler shift. However, it may also include low frequency signals caused by slowly moving tissues such as the arterial wall, and high frequency signals generated during demodulation. A band-pass filter (high-pass filter followed by a low-pass one) attenuates these unwanted low frequency and high frequency signals. The low-pass filter also serves as an anti-aliasing filter.

Since one of the processing stages where performance degradation happens is the filtering, special attention should be paid to the filtering stage. The filter characteristics of both channels must be identical to prevent any amplitude and phase mismatch, which both result in cross-talk between the forward and reverse channels. The channels must also exhibit good dynamic range. It is better if the cut-off frequency of the filters is programmable. Switched capacitor filters can be used to build programmable filters, but they tend to be noisy. First, a Sallen-Key type analogue band-pass filter with a fixed cut-off frequency was designed. However, as mentioned before it was difficult to match the in-phase and quadrature-phase filters. Instead, we preferred to use integrated continuous time filters which are factory trimmed and highly matched. Although the high-pass filter cut-off frequency was fixed, the low-pass filter cut-off frequency was entirely programmable.

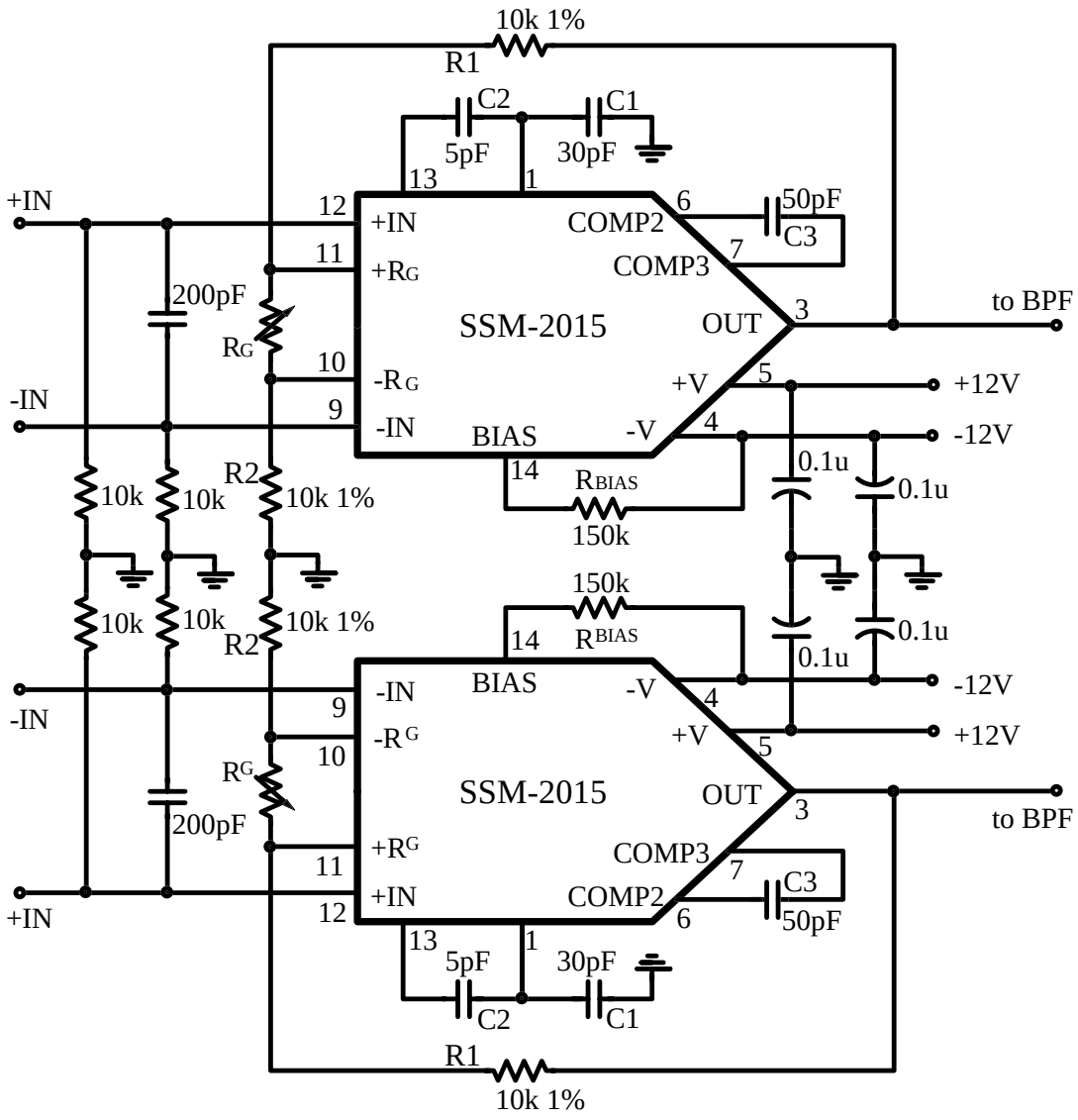

Figure 3.5 The circuit diagram of the two channel differential audio amplifier.

The high-pass filter utilises a single in-line hybrid resistor-tuneable filter (FLJ-UR4HB1) produced by *DATEL, inc.*[2]. This is a four pole high-pass Chebyshev type filter having a pass-band ripple of 0.28 $dB_{p\text{-}p}$. The cut-off frequency is set by only four resistors. The complete circuit diagram of this filter is shown in Fig. 3.6. The values of $\boldsymbol{R_1}$, $\boldsymbol{R_2}$, $\boldsymbol{R_3}$, and $\boldsymbol{R_4}$ can be obtained using the equations given below.

[2]DATEL, Inc. 11 Cabot Bouleward, Mansfield, MA 02048-1194

$R_1=0.726R$, $R_2=0.491R$, $R_3=0.386R$, $R_4=2.757R$.

where R can be calculated as;

$$R=\frac{15.9\times10^6}{f_c(Hz)}(\Omega)$$

In our design, f_c was set to be 150 Hz. So, the resistor values were calculated as

$$R=\frac{15.9\times10^6}{150}=106000\ \Omega$$

$R_1=0.726R=76956\ \Omega \approx 75\ k\Omega$,

$R_2=0.491R=52046\ \Omega \approx 51\ k\Omega$,

$R_3=0.386R=40916\ \Omega \approx 39\ k\Omega$,

$R_4=2.757R=292242\ \Omega \approx 270\ k\Omega$.

Note that the calculated resistor values are rounded to the closest standard commercially available resistor values. It is recommended to use metal film resistors of at least 1% tolerance for f_c setting. Metal film resistors are stable, accurate and low noise and are available with low temperature coefficients.

The low-pass section of the filtering stage is performed by the MAX270 filter chip. The MAX270 which is produced by *MAXIM INTEGRATED PRODUCTS*[3] is a digitally-programmed, dual, second-order, continuous-time, low-pass filter. This chip requires no external components and has a 96 dB dynamic range. The two filter sections are independently programmable and cut-off frequencies in the 1 kHz to 25 kHz range can be selected. The filter is programmed by writing appropriate data code into the latch which is internal to the chip. The code is calculated using the following equations and sent to the chip by the host computer.

[3]Maxim Integrated Products, 120 San Gabriel Drive, Sunnyvale, CA 94086.

$$f_c < 3.57\ kHz \qquad CODE = \mathbf{int}(87.5 - \frac{87.5}{f_c})$$

$$f_c > 3.57\ kHz \qquad CODE = \mathbf{int}(137.5 - \frac{262.5}{f_c})$$

where f_c is the cut off frequency, and **int** refers to integer value.

The arrangement of the 4th order low-pass filter is shown in Fig. 3.6. Here, two chips are used to implement the dual channel 4th order programmable low-pass filter.

The last stage in Fig. 3.6 is the programmable amplifier/attenuator formed by a programmable gain/loss circuit (PGLC) SC11310. The SC11310 PGLC is produced by *SIERRA SEMICONDUCTOR*[4]. The gain is adjustable from -25.5 to +25.5 dB in steps of 0.1 dB via parallel, serial or through interfaces (refer to data sheet). In this design the parallel interface was used. The control is performed using an eight bit binary word, which results in 256 steps of 0.1 dB each. Another bit selects between gain and loss. The gain can easily be modified through the computer keyboard.

[4]Sierra Semiconductor Corporation, 2075 North Capitol Avenue, San Jose CA 95132.

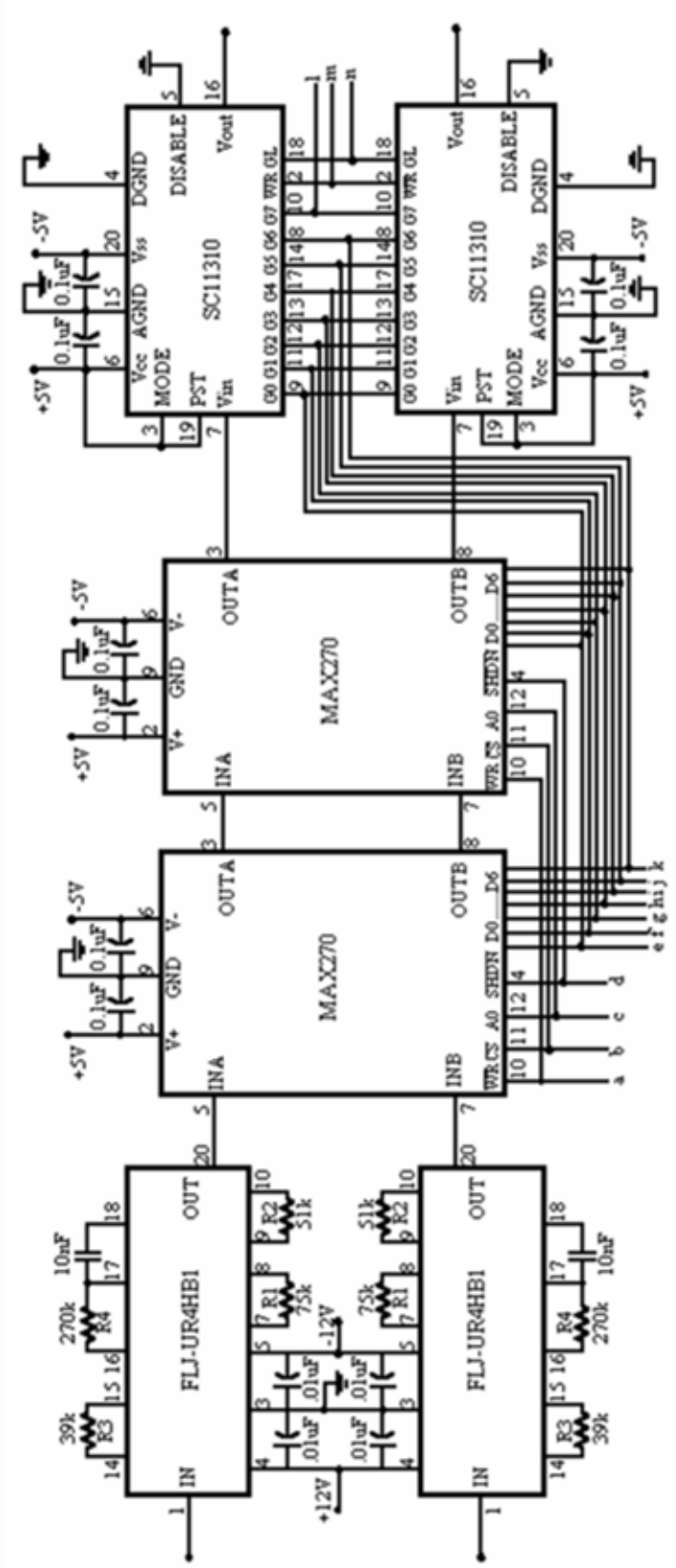

Figure 3.6 The circuit diagram of the programmable filter and amplifier stages.

3.2.5. PC interface

Since the computer controls the Doppler board, the PC interface is one of the most important parts of the circuit. The PC interface consists of industry standard logic integrated circuits (IC). However, a field programmable gate array (FPGA) chip can be used to implement a more integrated system.

The circuit diagram of the system is given in Fig. 3.7. The PC address bus and control lines are buffered by the octal buffer IC, 74LS244. The octal bus transceiver IC, 74LS245, buffers the data bus and permits the data to be read from or written to the computer. The combination of an eight bit bus comparator IC (74F521), two logic gate ICs (74F00 and 74F02) and a dip-switch performs I/O address selection. The 74HCT573 ICs are octal D-type transparent latches and they retain the latest control code for the Doppler board. The 16 bit data format being sent to the Doppler board is given in Table 3.1.

Bn	15	14	13	12	11	10	9	8	7	6	5	4	3	2	1	0
fil	X	X	H	/WR	/CS	A0	X	X	D6	D5	D4	D3	D2	D1	D0	on/off
amp	X	X	/WR	H	H	X	G/L	G7	G6	G5	G4	G3	G2	G1	G0	

fil: filter control, amp: amplifier control, Bn: bit no, X: don't care, H: logic high (one)

Table 3.1 16 bit PC data format to control the Doppler board..

Bn0 is used to switch the Doppler board on and off. A logic one switches it on and a logic zero off. Other control bits were arranged according to the programmable filter and amplifier data sheets. When writing to the filter, this must not change the amplifier settings and vice versa. These writing actions must also not effect the Doppler board's present state. This is ensured by the control software.

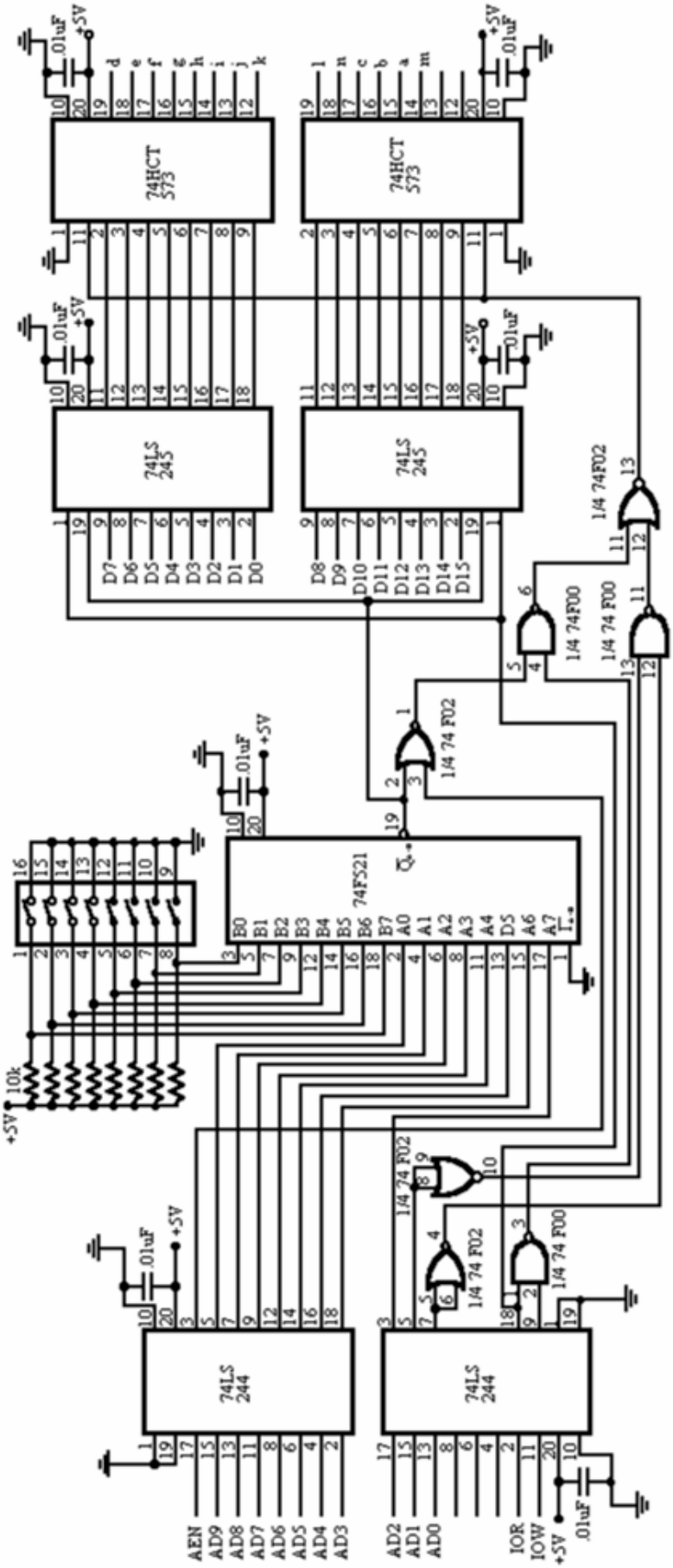

Figure 3.7 The circuit diagram of the PC interface.

3.2.6. Audio amplifier

The audio amplifier circuit which is shown in Fig. 3.8 is based on the LM386 low power audio amplifier IC and it is driven by one of the D/A outputs of the DSP board. Although this is not essential for the monitoring system the audio output will help the user to place the ultrasonic probe to the best location. The volume can be adjusted via a potentiometer and after securing the probe in the correct position it can be turned off.

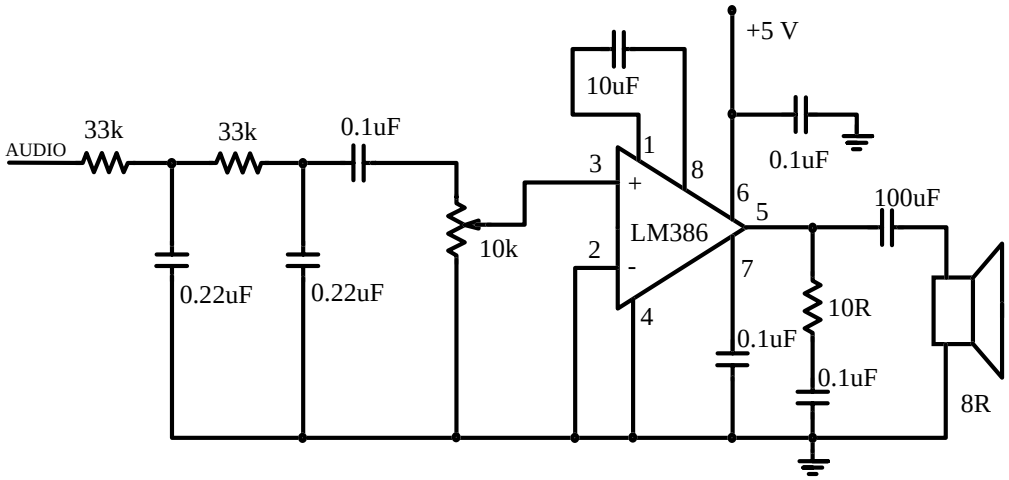

Figure 3.8 The circuit diagram of the audio amplifier.

3.3. SYSTEM PERFORMANCE

3.3.1. Performances of the signal generator and the demodulator

Fig 3.9 illustrates frequency spectrum of the sinusoidal signal produced by the signal oscillator which has been described in Section 3.2.2. This figure also illustrates the performance of the demodulator circuit described in Section 3.2.4. It was measured by down-converting the 4 MHz signal produced by the oscillator to a

4 kHz signal using the circuit illustrated in Fig. 3.4. This figure gives an idea about the dynamic range of the demodulator (≈90 dB) as well as the purity of the sinusoidal signal (≈70dB) produced by the circuit given in Fig. 3.2.

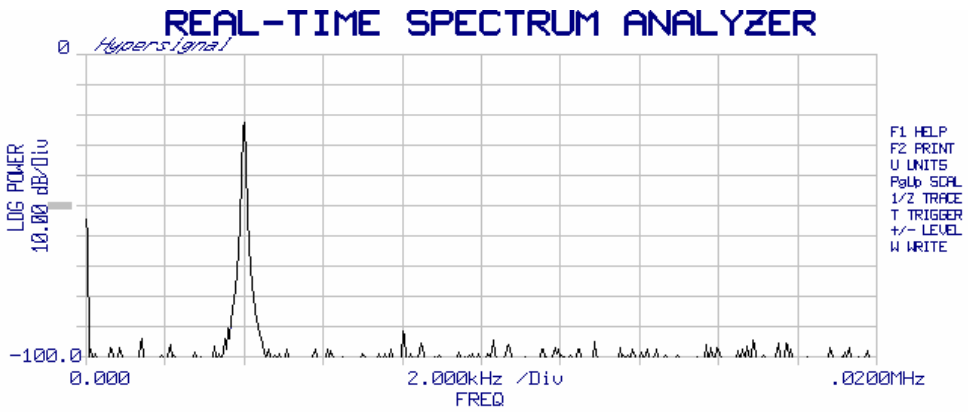

Figure 3.9 Frequency spectrum of the signal produced by the circuit given in Fig. 3.2.

3.3.2. Frequency response of the system

The frequency response of the Doppler system is shown in Fig. 3.10. It illustrates the frequency response of the wall-thump filter (the high-pass filter described above) as well as the frequency response of the low-pass filter. Fig. 3.11 gives the pass-band characteristic of the system.

These responses were measured by injecting a high frequency (4 MHz+Δf) sinusoidal signal into the system (to the mixer input). The results were obtained using a PC based audio spectrum analyser (Fig. 3.10) and a digital scope (Fig. 3.11). The ripple at the pass-band represents the Chebyshev filter characteristic. However this is negligible.

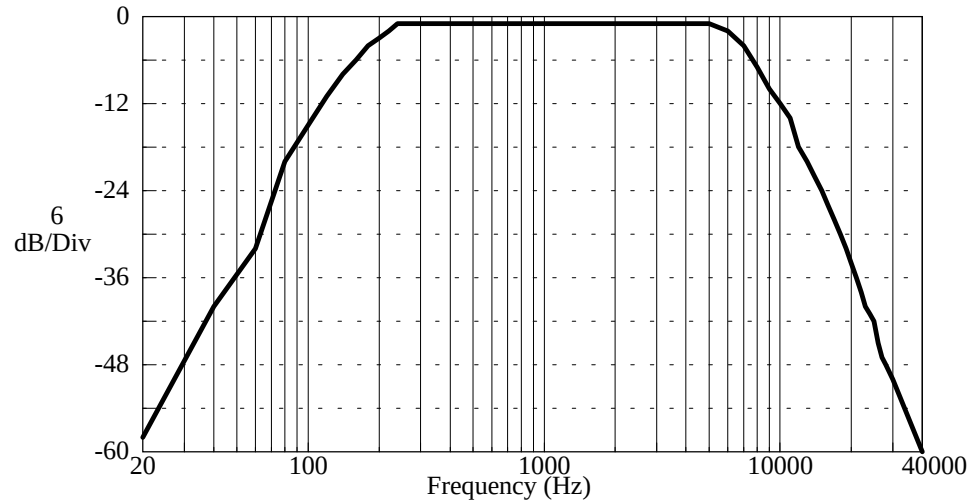

Figure 3.10 Frequency response of the Doppler system including the wall-thump filter (the hybrid high-pass filter described in the text) and the low-pass filter.

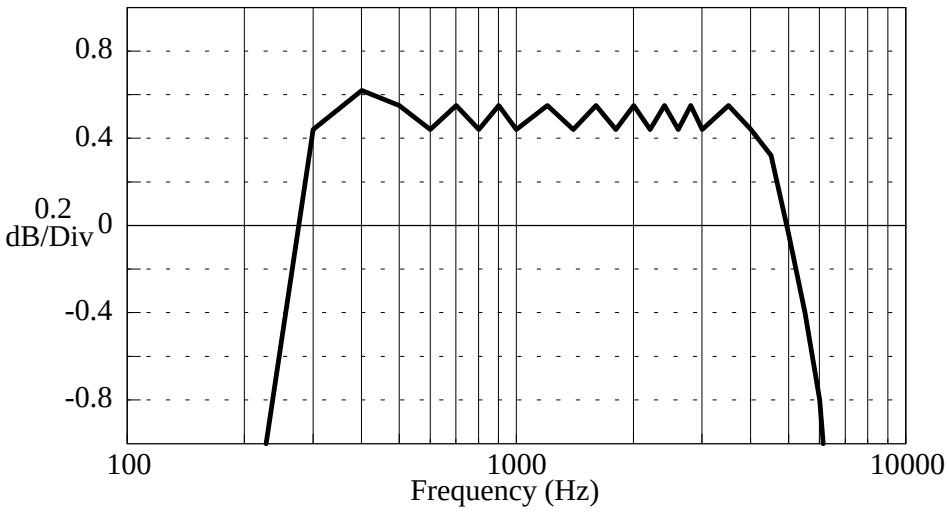

Figure 3.11 Pass-band characteristic of the system.

3.3.3. Dynamic range and cross-talk rejection

Dynamic range is a parameter which is often quoted for analogue signal conditioning and processing electronics. One used definition of the dynamic range is the signal-to-noise ratio (SNR), which is the ratio between the maximum output

level and the output noise with no input signal. It gives an indication of the range of signal levels which could be applied to the circuit without major degradation. As illustrated in Fig. 3.12, the measured SNR of the Doppler unit was about 50 dB. Here, 0 dB represents the maximum signal level which can be applied to the circuit without causing major degradation.

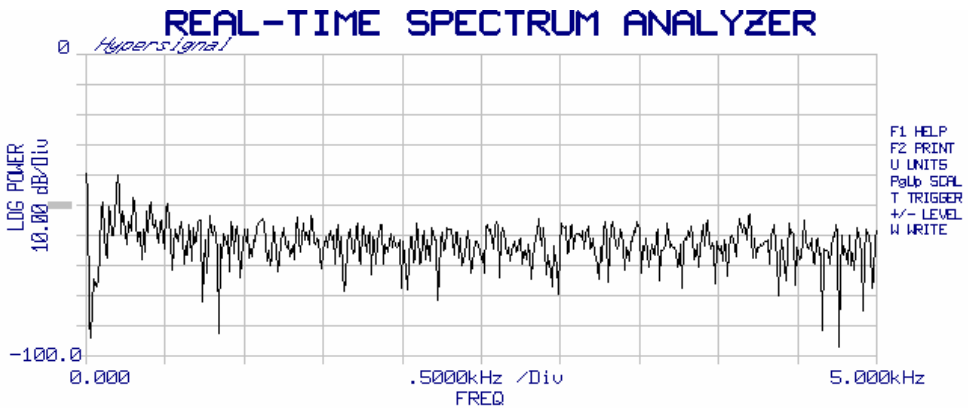

Figure 3.12 Output noise level of the Doppler unit with no input signal.

Cross-talk rejection level is another important indicator of a Doppler system based on the quadrature demodulation method. Cross-talk in such a system is a function of the amplitude and phase errors. Ideally, the in-phase and quadrature-phase signals produced by the demodulator must have the same amplitude and the phase between these two must be exactly 90 degrees. However this is impossible in practice.

The cross-talk rejection level of the Doppler unit was approximately -30 dB throughout the usable frequency range. The cross-talk level for a particular frequency (1 kHz) is illustrated in Fig. 3.13 (-30.16 dB). This was measured by generating a 4.001 MHz radio-frequency signal using a signal synthesizer (HP3325A). This interference signal was demodulated by the system, the quadrature data was captured by the DSP board and then the complex FFT was applied.

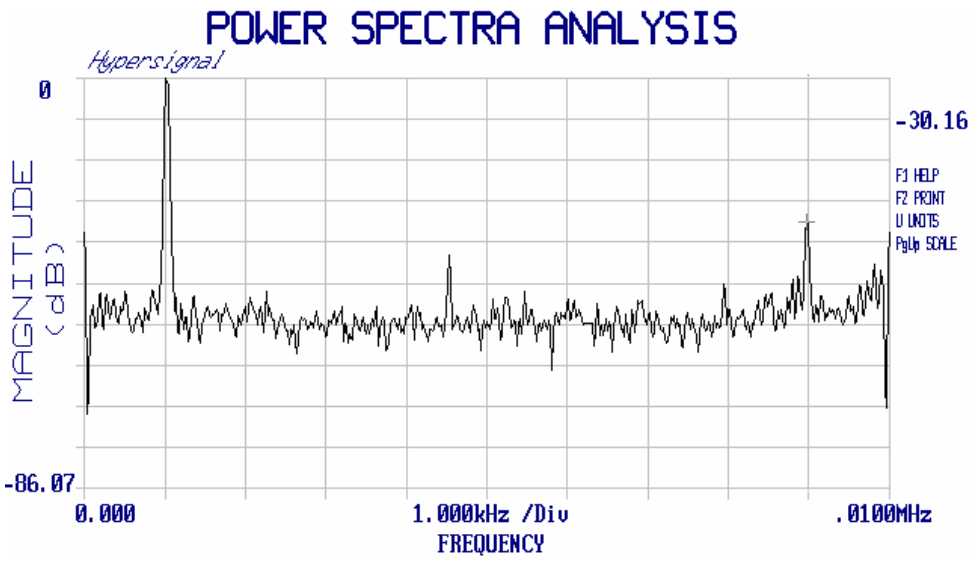

Figure 3.13 Cross-talk level at 1 kHz produced by the Doppler unit.

3.4. CONCLUSION

A CW Doppler unit based on the quadrature detection technique has been built for IBM compatible computers. This unit occupies one full length ISA expansion slot. A photograph of the prototype unit and the Doppler probe is shown in Fig. 3.14. It is interfaced to the DSP board as well as the PC. Fig. 3.15 shows the interior of the IBM-PC compatible computer with the Doppler unit and DSP board installed. In Figs. 3.14 and 3.15, it is shown that a part of the Doppler unit consisting of the transmitter and the receiver (quadrature demodulator) is enclosed by a metal case (shield). This is mainly to reduce the possible interference generated locally or introduced externally.

As a conclusion, the overall system performance is good enough to monitor blood flow in arterial grafts. However the performance of the system may be improved by bringing the digital signal processing techniques as close as possible to the ultrasonic transducer. Following chapters will deal with this issue in detail.

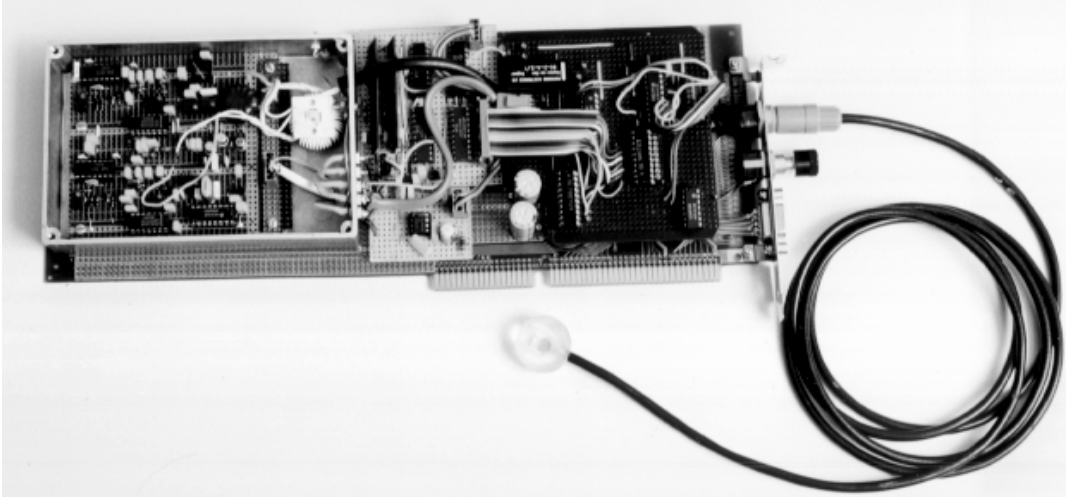

Figure 3.14 Photograph showing the prototype Doppler unit and purpose built Doppler probe.

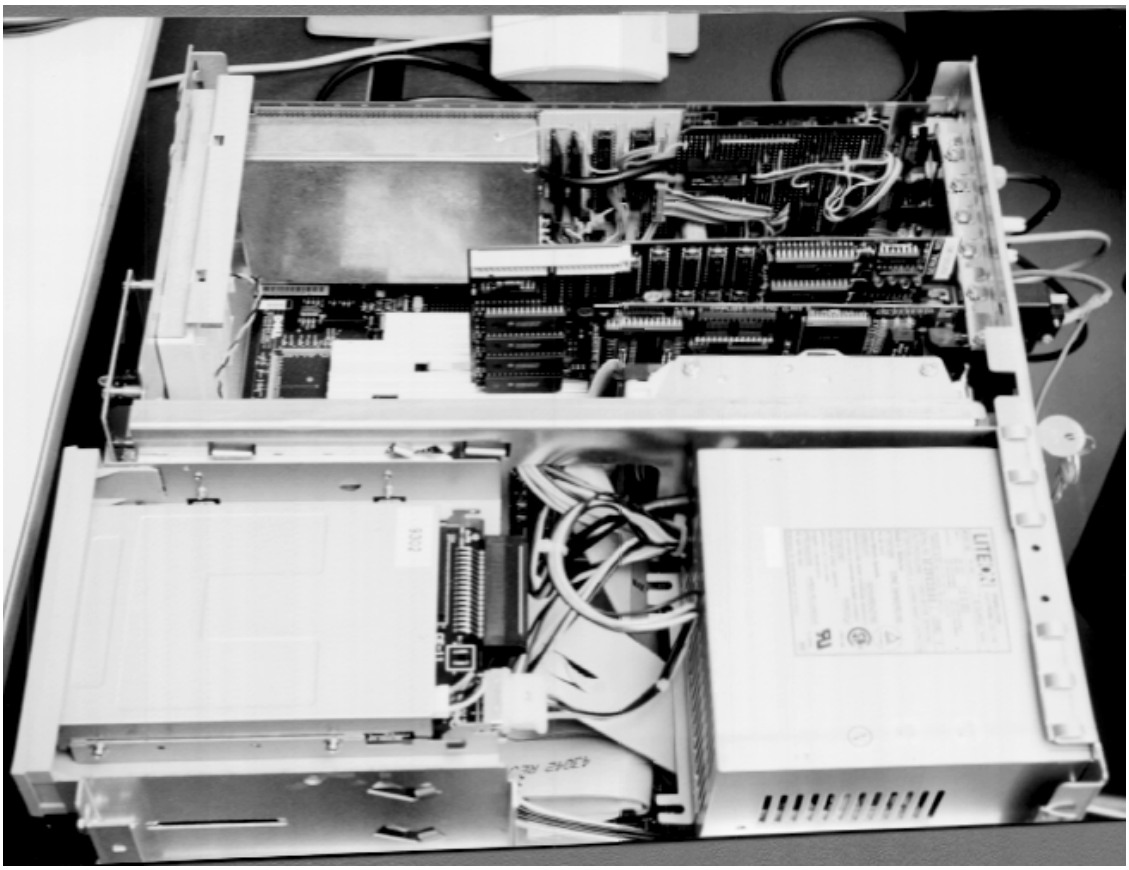

Figure 3.15 Photograph showing the interior of the IBM-PC compatible computer.

4. PROCESSING OF DOPPLER ULTRASOUND SIGNALS FOR SPECTRAL ANALYSIS

4.1. INTRODUCTION

The processing of Doppler ultrasound signals is performed in different stages. A general configuration of Doppler signal processors based on continuous wave (CW) and pulsed wave (PW) techniques has been given in Fig. 2.1. The term "processing" refers to all processes performed on the Doppler signals. Some of these have been briefly described in chapter 2 (transduction, demodulation etc.). In this chapter, after introducing some basic digital signal processing tools, methods for spectral analysis of Doppler signals will be discussed.

In recent years significant progress has been made in the analysis and design of discrete data and digital systems. These systems have gained popularity and importance because of the advances made in digital signal processors (DSP).

All processes performed in the continuous time domain can be classified as analogue processes. Most Doppler ultrasound systems are implemented using analogue signal processing components such as signal amplifiers, analogue mixers and filters. The advantage of an analogue system is that it operates in real time and is capable of a very high bandwidth. It is equivalent to having an infinite sampling frequency, so that the system is effective at all times. However, analogue systems are built by hard-wiring. The characteristics of the components used in the system are fixed, making it more difficult to make design changes, and component ageing and sensitivity to environmental changes can be quite severe. Analogue components are also more susceptible to noise problems.

The advantages offered by digital systems make them superior to analogue systems. For example, they are less sensitive to noise and less susceptible to ageing and environmental variations. They are therefore more reliable. DSPs allow more flexibility in programming so changing a design does not require an alteration of the hardware. Many different tasks can be implemented using the same system. For these reasons, newer designs are more digitally oriented.

Although many textbooks concerning digital signal processing exist, some general DSP tools relevant to this thesis are introduced here.

4.2. TOOLS FOR DIGITAL SIGNAL PROCESSING

Some of the common DSP tools used to implement our system will be summarised. These are the complex FFT, the Hilbert transform, modulation theory and digital filtering.

4.2.1. Understanding the complex Fourier transform

The Fourier transform pair is defined as

$$X(f) = \int_{-\infty}^{+\infty} x(t) e^{-j2\pi ft} dt, x(t) = \int_{-\infty}^{+\infty} X(f) e^{j2\pi ft} df \qquad 4.1$$

In general the Fourier transform is a complex quantity:

$$X(f) = R(f) + jI(f) = |X(f)| e^{j\theta(f)} \qquad 4.2$$

where $R(f)$ is the real part of the Fourier transform, $I(f)$ is the imaginary part, $|X(f)|$ is the amplitude or Fourier spectrum of $x(t)$ and is given by $\sqrt{R^2(f)+I^2(f)}$, $\theta(f)$ is the phase angle of the Fourier transform and given by $\tan^{-1}[I(f)/R(f)]$.

If $x(t)$ is a complex time function, i.e. $x(t)=x_r(t)+jx_i(t)$ where $x_r(t)$ and $x_i(t)$ are respectively the real part and imaginary part of the complex function $x(t)$, then the Fourier integral becomes

$$X(f)=\int_{-\infty}^{+\infty}[x_r(t)+jx_i(t)]e^{-j2\pi ft}dt=\int_{-\infty}^{+\infty}[x_r(t)\cos\omega t+x_i(t)\sin\omega t]dt$$
$$-j\int_{-\infty}^{+\infty}[x_r(t)\sin\omega t-x_i(t)\cos\omega t]dt=R(f)+jI(f) \qquad 4.3$$

The following table summarises some properties of the Fourier transform for various complex time functions.

Time domain ($x(t)$)	**Frequency domain ($X(f)$)**
Real	Real part even, imaginary part odd
Imaginary	Real part odd, imaginary part even
Real even, imaginary odd	Real
Real odd, imaginary even	Imaginary
Real and even	Real and even
Real and odd	Imaginary and odd
Imaginary and even	Imaginary and even
Imaginary and odd	Real and odd
Complex and even	Complex and even
Complex and odd	Complex and odd

Table 4.1 Properties of the Fourier transform for complex time functions.

The discrete Fourier transform (DFT) is a special case of the continuous Fourier transform. To determine the Fourier transform of a continuous time function by means of digital analysis techniques, it is necessary to sample this time function. An infinite number of samples are not suitable for machine computation. It is necessary to truncate the sampled function so that a finite number of samples are considered.

The discrete Fourier transform pair is given by

$$X(k) = \begin{cases} \sum_{n=0}^{N-1} x(n) e^{-j(2\pi/N)kn}, 0 \le k \le N-1 \\ 0, \quad otherwise \end{cases} \tag{4.4}$$

$$x(n) = \begin{cases} \frac{1}{N} \sum_{n=0}^{N-1} X(k) e^{j(2\pi/N)kn}, 0 \le n \le N-1 \\ 0, \quad otherwise \end{cases} \tag{4.5}$$

The DFT plays an important role in the analysis, design and implementation of digital signal processing algorithms and systems. The DFT in its original form is computationally inefficient. However, the development of efficient algorithms for computing the DFT led to widespread use of it in digital signal processing. These algorithms are known as fast Fourier transform (FFT) algorithms and many of them are well documented (for example, a collection of related papers can be found in Rabiner and Rader 1972). Most of them are also available as library routines supplied with modern DSP systems. A number of the FFT implementations, for example, are supplied as callable functions with AT&T DSP32C DSP chip. Nowadays, general purpose DSP devices are capable of implementing real-time FFT systems for processing of signals at frequencies up to several hundred kilohertz. For higher speeds (megahertz ranges), dedicated FFT processors are available to designers.

Some mathematical and simulation results are given in Appendix B for when the input signal is a complex quadrature time signal.

4.2.2. Hilbert transform

The Hilbert transform (HT) is another widely used frequency domain transform. It shifts the phase of positive frequency components by -90^0 and negative frequency components by $+90^0$. The HT of a given function $x(t)$ is defined by the convolution between this function and the impulse response of the HT ($1/\pi t$).

$$H[x(t)] = x(t) * \frac{1}{\pi t} = \frac{1}{\pi}\int_{-\infty}^{+\infty}\frac{x(\tau)}{t-\tau}d\tau \qquad 4.6$$

Since the Hilbert transformation is a convolution and does not change the domain, both $x(t)$ and $H[x(t)]$ are functions of time.

Specifically, if $X(f)$ is the Fourier transform of $x(t)$, its Hilbert transform is represented by $X_H(f)$, where

$$X_H(f) = H[X(f)] = H_H(f)X(f) = (-j\,\mathrm{sgn}\,f)X(f) \qquad 4.7$$

A $\pm 90^0$ phase shift is equivalent to multiplying by $e^{\pm j90^0} = \pm j$, so the transfer function of the HT $H_H(f)$ can be written as

$$H_H(f) = -j\,\mathrm{sgn}\,f = \begin{cases} -j, f > 0 \\ +j, f < 0 \end{cases} \qquad 4.8$$

The corresponding impulse response is

$$h_H(n) = \begin{cases} 0, n = 0 \\ \dfrac{2\sin^2(\pi n/2)}{\pi n}, n \neq 0 \end{cases} \qquad 4.9$$

The normalised impulse response of the HT is plotted in Fig. 4.1.

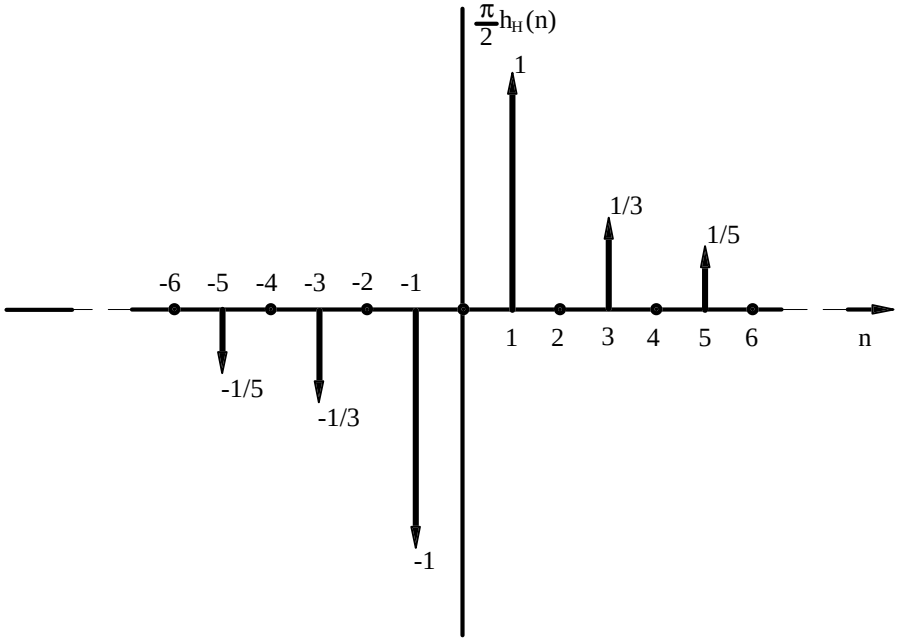

Figure 4.1 Normalised impulse response of an ideal Hilbert transform filter.

An ideal HT filter can be approximated using standard filter design techniques. If a FIR filter is to be used , only a finite number of samples of the impulse response suggested in Fig. 4.1 would be utilised.

4.2.3. Frequency translation and modulation

The *duality theorem* states that if ***x*(*t*)** and ***X*(*f*)** constitute a known transform pair, and if there exists a time function ***y*(*t*)** related to the function ***X*(*f*)** by ***y*(*t*)=*X*(*t*)** then ***F*[*y*(*t*)]=*x*(-*f*)** where ***x*(-*f*)** equals ***x*(*t*)** with ***t*=-*f***.

A dual of the well known time-delay theorem is

$$x(t)e^{j\omega_c t} \leftrightarrow X(f - f_c) \qquad 4.10$$

where $\omega_c = 2\pi f_c$.

Multiplying a time function by $e^{j\omega_c t}$ causes its spectrum to be translated in frequency by $+f_c$. This is called *frequency translation* or *complex modulation*. The process is illustrated graphically in Fig. 4.2 for the case when $x(t)$ has a band limited spectrum. From this translated spectrum, we can conclude that the significant components are concentrated around the frequency f_c and translation has doubled spectral width, i.e. the negative frequency portion of $X(f)$ appears at positive frequencies.

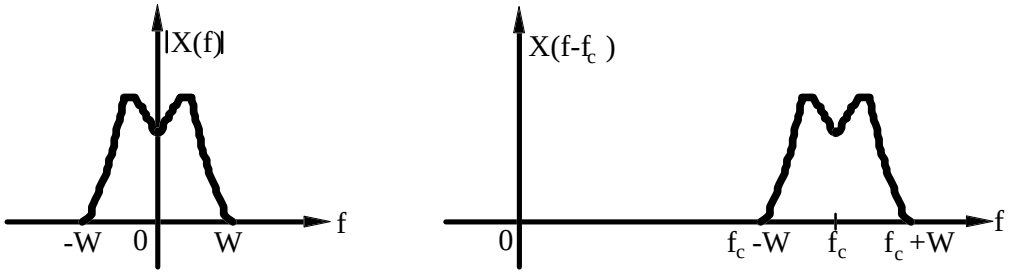

Figure 4.2 Frequency translation of a band limited signal.

$x(t)e^{j\omega_c t}$ is not a real time function and cannot occur as a communication signal. However, signals of the form $x(t)\cos(\omega_c t+\theta)$ are common and the related *modulation theorem* can be given as

$$x(t)\cos(\omega_c t + \theta) \leftrightarrow \frac{e^{j\theta}}{2} X(f - f_c) + \frac{e^{-j\theta}}{2} X(f + f_c) \qquad 4.11$$

So, multiplying a band limited signal by a sinusoidal signal translates its spectrum up and down in frequency by f_c.

4.2.4. Digital filters

Digital filtering is one of the most important DSP tools. Its main objective is to eliminate or remove unwanted signals and noise from the required signal. Compared to analogue filters digital filters offer sharper rolloffs, require no calibration, and have greater stability with time, temperature, and power supply variations. Adaptive filters can easily be created by simple software modifications.

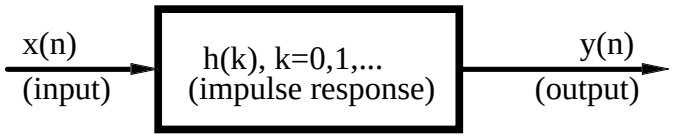

Figure 4.3 A representation of a digital filter.

Digital filter designs can be divided into two basic categories; non-recursive (finite impulse response, FIR) and recursive (infinite impulse response, IIR). Either type of filter can be represented by its impulse response sequence as in Fig. 4.3. The input and the output signals of the filter are related by the convolution sum, which is given by Eq. 4.12 for the IIR and in Eq. 4.13 for the FIR type filter.

$$y(n) = \sum_{k=0}^{\infty} h(k)x(n-k) = \sum_{k=0}^{N} a_k x(n-k) - \sum_{k=1}^{N} b_k y(n-k) \qquad 4.12$$

$$y(n) = \sum_{k=0}^{N-1} h(k)x(n-k) \qquad 4.13$$

where a_k and b_k are the coefficients of the IIR filter. While the output of an FIR filter is a function of past and present values of the input, the output of an IIR filter is a function of past outputs as well as past and present values of the input. Typical FIR and IIR digital filter topologies are shown in Fig. 4.4. These are the direct form realisations of the IIR and FIR type filters. However, there are other realisation

structures for FIR and IIR filters such as frequency sampling (FIR), fast convolution (FIR), cascade (IIR), parallel (IIR), and lattice (IIR or FIR).

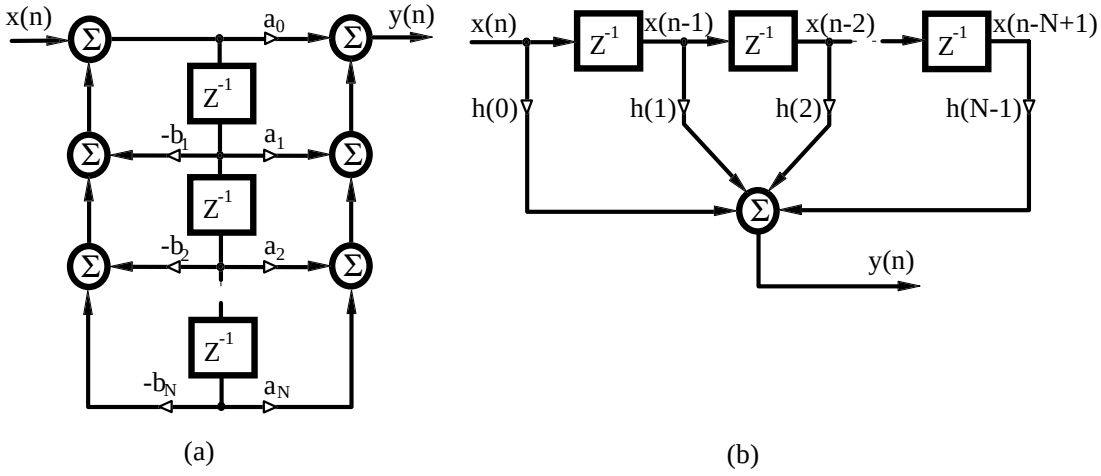

Figure 4.4 Block diagram representation of (a) a basic IIR filter and (b) FIR filter realisations.

If no phase distortion is desired in the system, it is best to use an FIR type filter design. If the most important requirements are sharp rolloff and high throughput then an IIR type filter design should be considered. Further discussions on digital filters can be found in the literature (see for example Oppenheim and Schafer, 1975; McClellan et al, 1973; Rabiner, 1973; Rabiner and Gold, 1975)

After this very brief introduction to some common DSP tools, the implementation of directional Doppler techniques using a digital signal processor for spectral analysis will be described.

4.3. DIGITAL IMPLEMENTATIONS OF DIRECTIONAL DOPPLER DETECTORS

In this section, three digital implementations which may be used to derive directional signals from phase quadrature Doppler systems for spectral analysis will

be described. The basic theory behind these approaches will also be presented without recourse to complicated mathematical expressions. These techniques are *the phasing-filter technique* (phase domain processing), *the Weaver receiver technique* (frequency domain processing), and *the complex FFT*. In order to clarify this approach, DSP simulations have been implemented and the results illustrated graphically.

4.3.1. The phasing-filter technique (PFT)

A block diagram of this technique is shown in Fig. 4.5. The system is based on a wide-band digital Hilbert transform (HT) which produces a $\mathbf{90^0}$ phase shift in the input signal. The ideal frequency response and corresponding ideal impulse response of the HT are given by Eq. 4.8 and Eq. 4.9 respectively. This ideal response can be approximated by using finite impulse response (FIR) or infinite impulse response (IIR) filters (Ansari 1987). The main properties of the HT are well documented (see for example Schwartz *et al* 1966). In our application an FIR filter was implemented using the FIR filter design option of the **Hypersignal**[5] DSP software. The software implements the Parks-McClellan design algorithm.

The delay filter (DF) is an all-pass filter which introduces a delay which is exactly the same as that introduced by the HT filter. It was also implemented using a basic Parks-McClellan design. The pass-band area stretches from dc (zero) up to half the sampling rate, which means that the filter is all pass-band, with no transition bands. Once again the Hypersignal package was used to implement this filter.

[5]Hyperception, Inc.
9550 Skillman LB125, Dallas, TX 75243

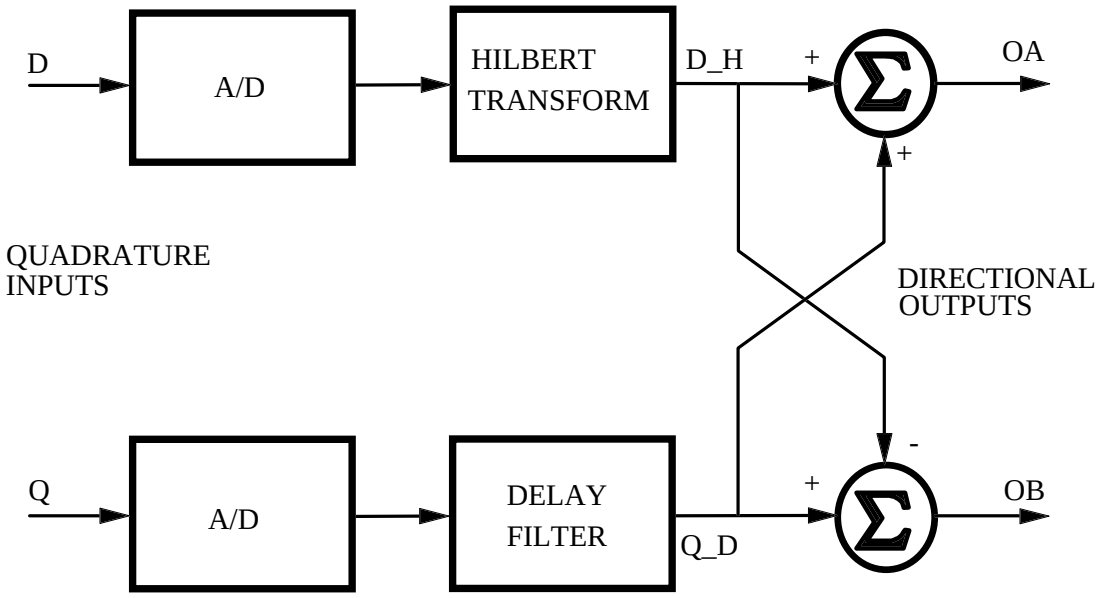

Figure 4.5 The phasing-filter technique (PFT) for use with quadrature phase detected signals.

Consider a perfect quadrature detection system having ideal quadrature outputs

$$D=A\cos\omega_a t+B\sin\omega_b t \text{ and } Q=A\sin\omega_a t+B\cos\omega_b t, \qquad 4.14$$

where ω_a represents the signal frequency due to flow in one direction and ω_b represents the signal frequency due to flow in the other. If these signals are applied to the system shown in Fig. 4.5, separated outputs are obtained. From the properties of the HT, the output of the HT filter is

$$D\_H=A\sin\omega_a t-B\cos\omega_b t, \qquad 4.15$$

which is the Hilbert transform of the in-phase component of the input signal. The output of DF is

$$Q\_D=A\sin\omega_a t+B\cos\omega_b t, \qquad 4.16$$

which is the delayed version of the quadrature component of the input signal. Note that in Eq. 4.15 and Eq. 4.16 the equal time delays between input and output have been ignored.

After addition and subtraction, the results are

$$OA = Q\_D + D\_H = 2A\sin\omega_a t, \quad (4.17)$$

$$OB = Q\_D - D\_H = 2B\cos\omega_b t. \quad (4.18)$$

In order to confirm these results a simulation has been implemented using a commercially available signal processing software package (Hypersignal DSP software). Two complex waveforms were created having a sampling frequency of 16 kHz and 512 data points to simulate 1 kHz forward and 2 kHz reverse signals. They were

$$D = 1000\cos(2\pi n 1000/16000) + 500\sin(2\pi n 2000/16000) \quad (4.19)$$

$$Q = 1000\sin(2\pi n 1000/16000) + 500\cos(2\pi n 2000/16000). \quad (4.20)$$

A digital phase shifter was implemented using a digital HT and DF. The signal processing algorithm was implemented using signal processing functions of the DSP software package. The results are displayed in both the time and frequency domains in Fig. 4.6. As can be seen from the figure, the digital filters introduce a time delay of approximately 6 ms. As the outputs are totally separated, two independent real FFTs are required to produce the frequency domain display. In Fig. 4.6, note that the spectra of two channels are displayed side by side as one display. A practical implementation of this algorithm is described in chapter 6.

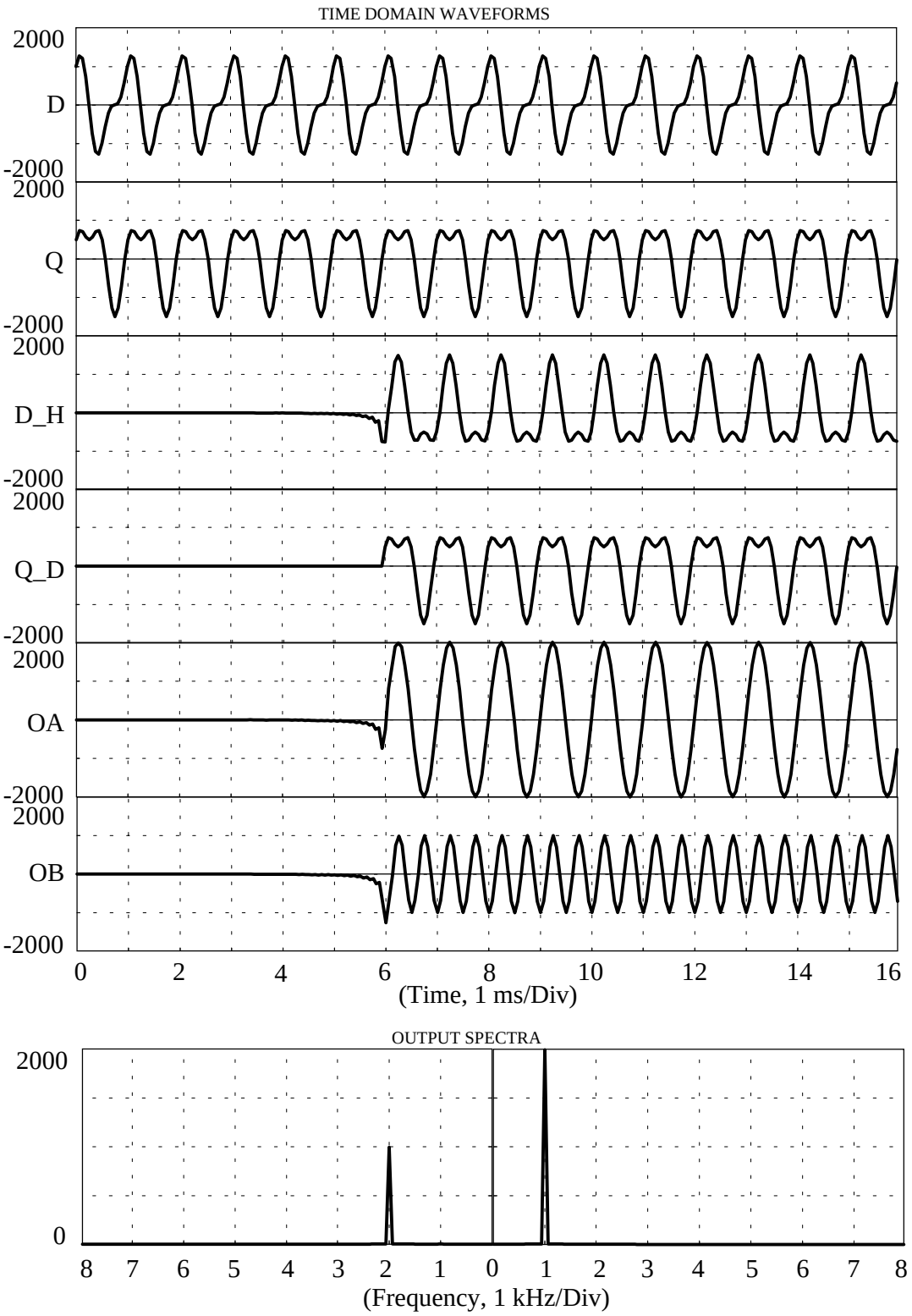

Figure 4.6 Time domain displays of each processing stages and output spectra for the PFT (simulation results). The labels on each trace correspond to the results labelled in Fig 4.5.

4.3.2. The weaver receiver technique (WRT)

This system, also known as the IQ demodulator, employs a digitally implemented quadrature mixer. Fig. 4.7 is a block diagram of the system. The internal signal oscillator generates a quadrature waveform, which determines the pilot frequency around which the directional outputs appear. The digital input quadrature signal is mixed with this pilot frequency and the outputs of the mixers added to give a directional output around the pilot frequency.

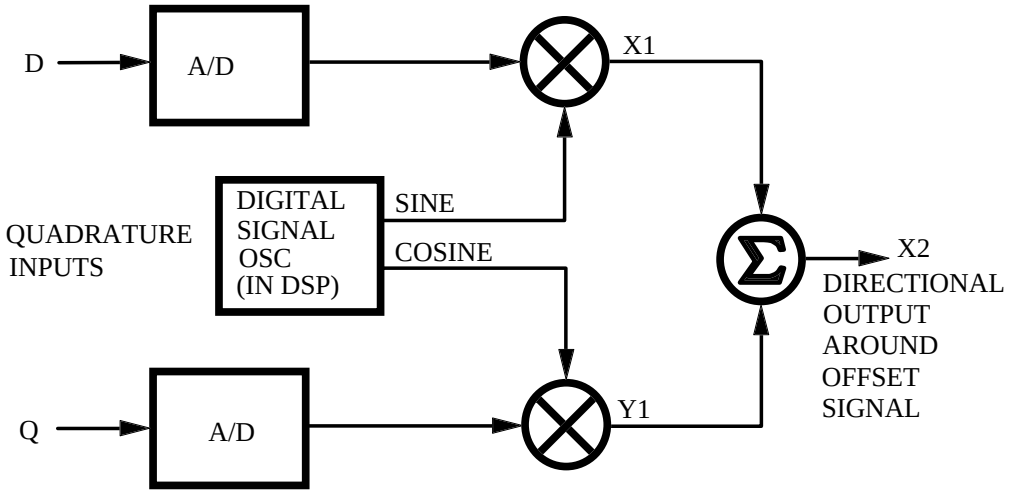

Figure 4.7 The Weaver receiver technique (WRT) for use with quadrature phase detected signals.

To explain this technique mathematically, let the quadrature pilot frequency signals be $p_i=\sin\omega_p t$, $p_q=\cos\omega_p t$. Again, consider the input signals to be perfect quadrature signals as defined by Eq. 4.14.

After mixing, the results are

$$X1 = D.\,p_i = \sin\omega_p t(A\cos\omega_a t + B\sin\omega_b t) \qquad 4.21$$
$$= \frac{A}{2}\sin(\omega_p - \omega_a)t + \frac{A}{2}\sin(\omega_p + \omega_a)t + \frac{B}{2}\cos(\omega_p - \omega_b)t - \frac{B}{2}\cos(\omega_p + \omega_b)t$$

$$\mathbf{1} = Q.\, p_q = \cos\omega_p t(A\sin\omega_a t + B\cos\omega_b t) \qquad 4.22$$
$$= -\frac{A}{2}\sin(\omega_p - \omega_a)t + \frac{A}{2}\sin(\omega_p + \omega_a)t + \frac{B}{2}\cos(\omega_p - \omega_b)t + \frac{B}{2}\cos(\omega_p + \omega_b)t$$

If we add $X\mathbf{1}$ (Eq. 4.21) and $Y\mathbf{1}$ (Eq. 4.22), the output is

$$X\,2 = X\,1 + Y\,1 = A\sin(\omega_p + \omega_a)t + B\cos(\omega_p - \omega_b)t. \qquad 4.23$$

This method has a single output, giving directional information around the pilot frequency signal which means that only one real FFT is needed to produce the output spectra.

To confirm the results obtained above, a simulation of the system has been implemented using signal processing functions of the DSP software package. The D and Q signals were created as for the PFT (Eq. 4.19 and Eq. 4.20).

A complex (quadrature) pilot frequency signal having the same sampling frequency and number of data points was created using the same DSP function. The frequency of the pilot signal was set at 4 kHz. The in-phase and quadrature-phase components of the pilot frequency signal were

$$p_i = \sin(2\pi n 4000/16000),\ p_q = \cos(2\pi n 4000/16000). \qquad 4.24$$

These signals were mixed with quadrature inputs and the outputs of the two mixers added. The result was an SSB modulated signal, or in other words an SSB frequency shifted signal. The waveforms at each processing stage and at the output are illustrated in Fig. 4.8. The spectrum of the output of the system shows clearly that the output is shifted by the 4 kHz pilot signal frequency giving one spectral line at 5 kHz (4+1) and another at 2 kHz (4-2). Note that the lower side-band is rejected for the 1 kHz signal and the upper side-band is rejected for the 2 kHz signal.

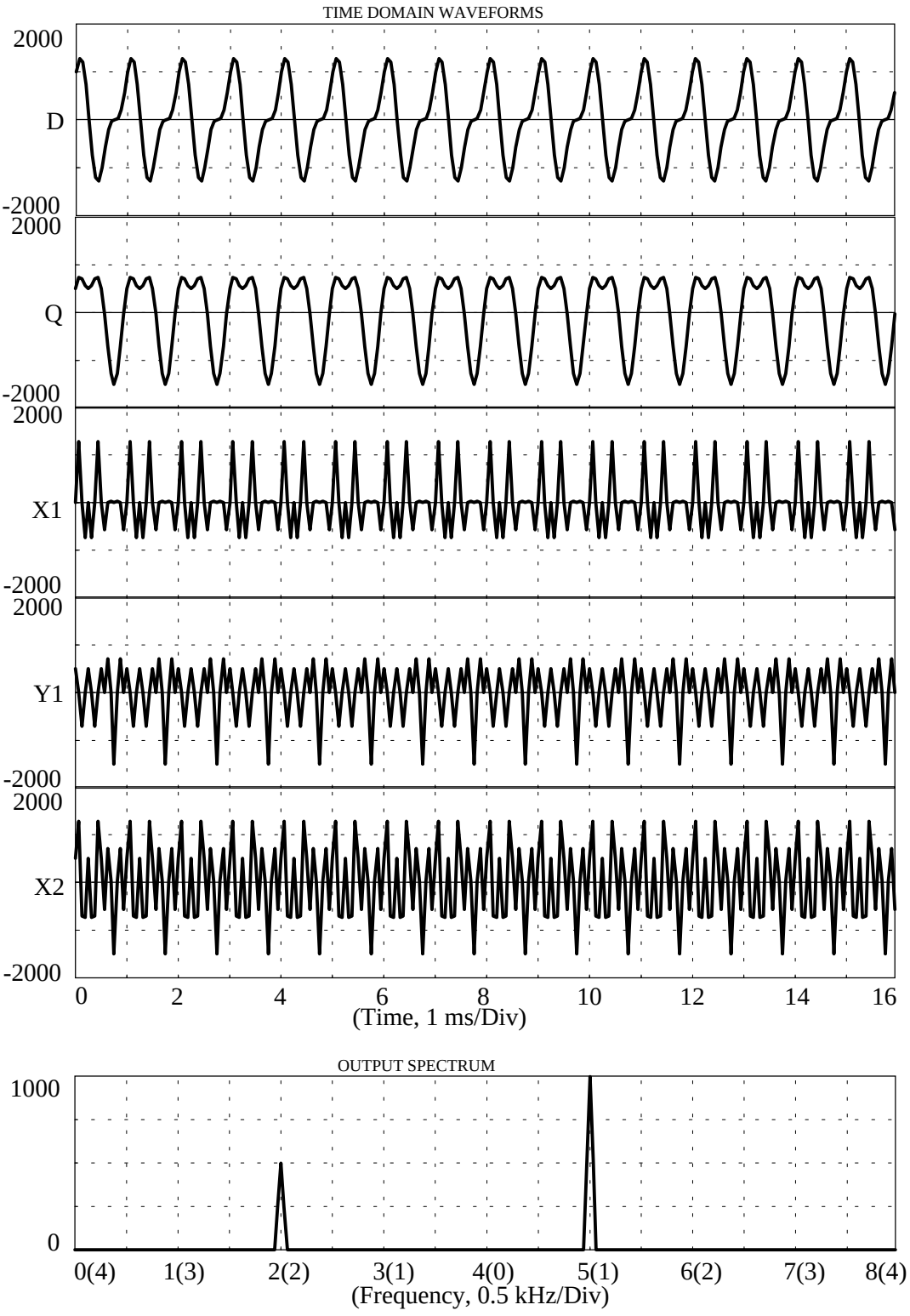

Figure 4.8 Time domain displays of each processing stages and the output spectrum for the WRT (simulation results). The labels on each trace correspond to the results labelled in Fig 4.7.

4.3.3. The complex FFT (CFFT)

The complex FFT is a straightforward technique for deriving directional data as no extra signal processing is required to produce frequency domain information. A block diagram of the system is shown in Fig. 4.9. Quadrature input signals ***D*** and ***Q*** are taken as the real and imaginary parts of a complex time signal. Because of the properties of the complex Fourier transform (Brigham 1974), if the complex input time signal is in quadrature (i.e., the phase difference between the real and imaginary parts is 90^0), the output is directional and the output spectrum is dual sided. That is to say, the positive part of the spectrum gives one direction, the negative part of the spectrum gives other direction.

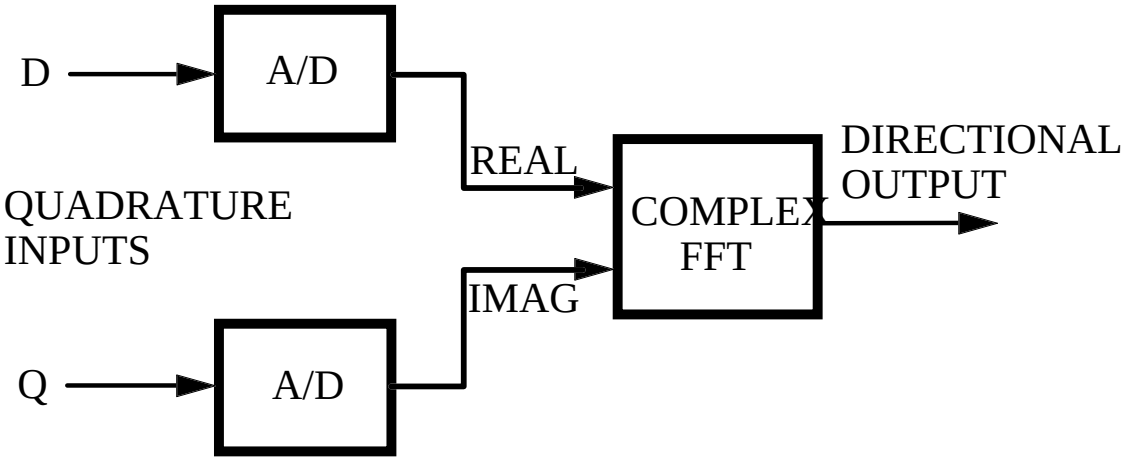

Figure 4.9 Block diagram of the complex FFT (CFFT) for use with quadrature phase detected signal.

The complex Fourier transform has some very useful properties which allow the detection of the direction of blood flow when it is applied to quadrature signals, let us consider a complex time signal. If its real part is even and its imaginary part odd,

then the complex Fourier transform is real. If its real part is odd and its imaginary part even, then the complex Fourier transform is imaginary.

In order to clarify these properties, let a complex time signal including both cases be

$$x(t)=x_a(t)+x_b(t)=x_r(t)+jx_i(t) \quad (4.25)$$

$$x_a(t)=(A\cos 2\pi f_a t+jA\sin 2\pi f_a t) \quad (4.26)$$

$$x_b(t)=(B\sin 2\pi f_b t+jB\cos 2\pi f_b t) \quad (4.27)$$

where $x_a(t)$ represents the first case and $x_b(t)$ represents the second case. Hence,

$$x(t)=(A\cos 2\pi f_a t+B\sin 2\pi f_b t)+j(A\sin 2\pi f_a t+B\cos 2\pi f_b t) \quad (4.28)$$

The Fourier transform of this complex time function is

$$\begin{aligned} X(f) &= \int_{-\infty}^{+\infty} x(t)e^{-j2\pi ft}dt = \int_{-\infty}^{+\infty}(x_r(t)+jx_i(t))e^{-j2\pi ft}dt \quad (4.29)\\ &= \int_{-\infty}^{+\infty} A\cos 2\pi f_a t e^{-j2\pi ft}dt + \int_{-\infty}^{+\infty} B\sin 2\pi f_b t e^{-j2\pi ft}dt \\ &+ j\int_{-\infty}^{+\infty} A\sin 2\pi f_a t e^{-j2\pi ft}dt + j\int_{-\infty}^{+\infty} B\cos 2\pi f_b t e^{-j2\pi ft}dt \\ &= \frac{A}{2}\delta(f-f_a)+\frac{A}{2}\delta(f+f_a)-j\frac{B}{2}\delta(f-f_b)+j\frac{B}{2}\delta(f+f_b) \\ &+ \frac{A}{2}\delta(f-f_a)-\frac{A}{2}\delta(f+f_a)+j\frac{B}{2}\delta(f-f_b)+j\frac{B}{2}\delta(f+f_b) \end{aligned}$$

$$X(f)=A\delta(f-f_a)+jB\delta(f+f_b) \quad (4.30)$$

This result (Eq. 4.30) substantiates the statement made about the complex Fourier transform of complex quadrature signals above.

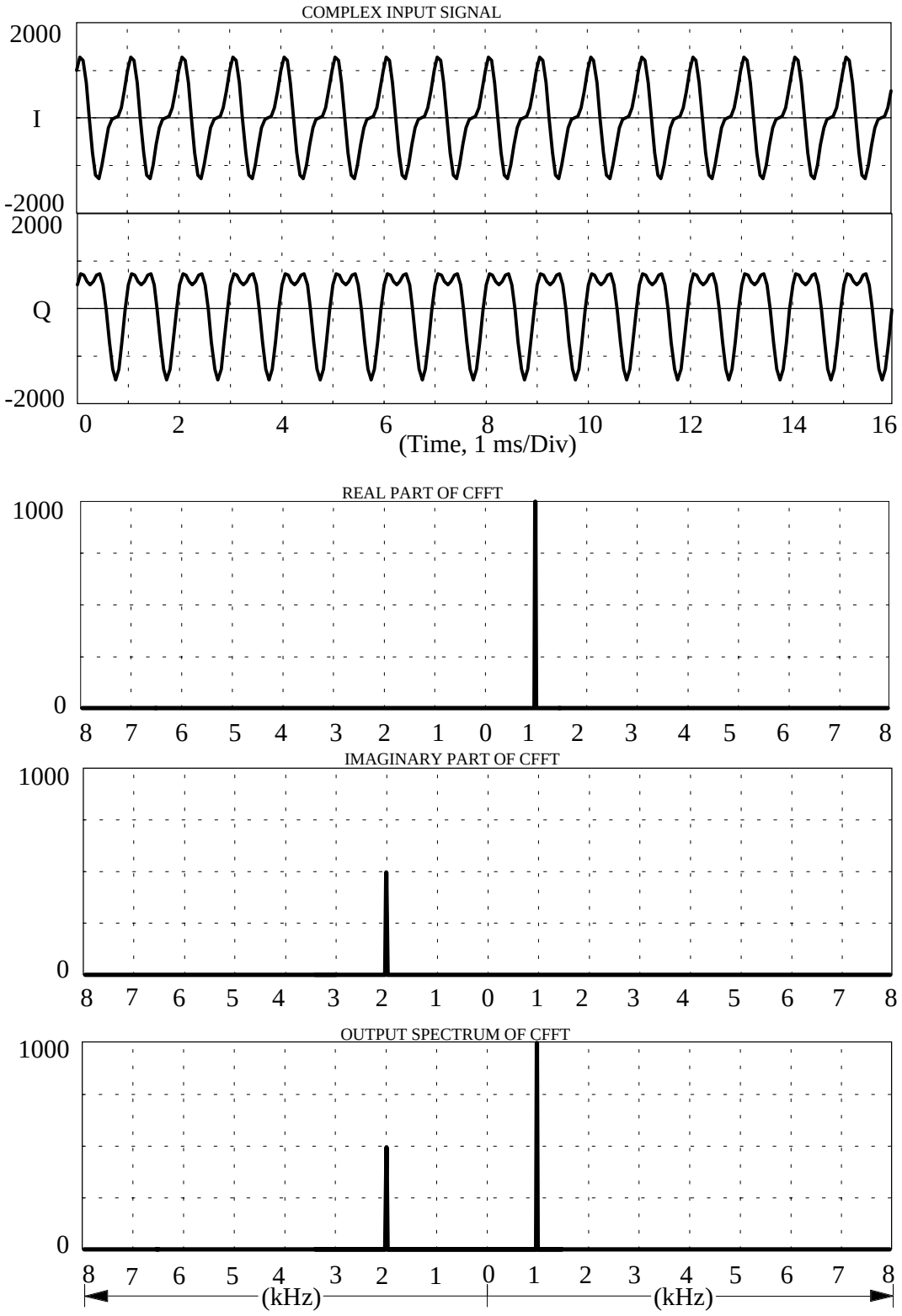

Figure 4.10 The real part, imaginary part and output spectrum of the complex FFT simulation when the input is a complex quadrature signal.

In order to verify this result graphically, a complex time signal including both cases which satisfy the properties of the complex Fourier transform stated above was created. This is

$$X=D+jQ=\{1000\cos(2\pi n1000/16000)+500\sin(2\pi n2000/16000)\} + j\{1000\sin(2\pi n1000/16000)+500\cos(2\pi n2000/16000)\}. \quad 4.31$$

The complex FFT was implemented using the FFT function of the DSP software package. The results obtained from this process are illustrated in Fig. 4.10. The output of the complex FFT of the 1 kHz signal is real, illustrating the first property above, the output of the complex FFT of the 2 kHz signal is imaginary, illustrating the second property.

The resultant output spectrum is dual sided and directional. Unlike the other two methods, the separation in this method is purely in the frequency domain.

4.4. CONCLUSION

Some basic digital signal processing tools have been summarised and three different algorithms to obtain forward and reverse flow signals for spectral analysis have been described. The simulation results have demonstrated excellent performances of these algorithms. Practical implementations of these algorithms using a floating point DSP chip and results which were consistent with simulation results will be discussed in chapter 6.

5. SIGNAL PROCESSING ALGORITHMS FOR PRODUCING DIRECTIONAL TIME DOMAIN OUTPUTS

5.1. INTRODUCTION

Since most Doppler ultrasound systems employ the quadrature detection method, obtaining directional time domain outputs requires some decoding processes which have traditionally been implemented using analogue techniques (Coghlan and Taylor 1976). It is known that the results obtained using digital techniques are better than those obtained by analogue ones (Aydin and Evans 1994). Wide spread use of audio tape recorders to store the Doppler shifted ultrasound signals shows the importance of time domain separation. Recording quadrature Doppler signals onto audio tape is not possible because neither analogue (Smallwood 1985) nor digital tape recorders (Bush and Evans 1993) are capable of preserving the precise phase and amplitude relationships of the quadrature pair to permit subsequent separation of the forward and reverse signals.

In this chapter, the theoretical background of digital quadrature to directional format conversion will be introduced and several algorithms performing time domain directional signal separation described. In general these algorithms can be divided into two main processing groups namely time domain processing and frequency domain processing. In order to generalise these algorithms, a discrete Doppler quadrature signal pair must be defined.

5.2. GENERAL DEFINITION OF A QUADRATURE DOPPLER SIGNAL

A general definition of a discrete quadrature Doppler signal equation can be given by Eq. 5.1.

$$\begin{cases} D(n) = s_f(n) + H[s_r(n)] \\ Q(n) = H[s_f(n)] + s_r(n) \end{cases} \qquad 5.1$$

***D*(*n*)** and ***Q*(*n*),** each containing information concerning forward channel and reverse channel signals (**$s_f(n)$** and **$s_r(n)$** and their Hilbert transforms **$H[s_f(n)]$** and **$H[s_r(n)]$**), are real signals.

Unless otherwise stated the discrete form of the signal definition is used and the Doppler signal pair is band limited to $f_s / 2$, where f_s is the sampling frequency of the system.

Some signal processing functions such as filtering introduce a certain amount of time delay. Because they have no significant effect on the results, all delays introduced by the digital filters have been ignored.

5.3. TIME DOMAIN PROCESSING

Two main types of time domain processing will be presented: the phasing filter technique (PFT), which is based on the Hilbert transform (HT) implemented using a convolution, and the extended Weaver receiver technique (EWRT), which is based on the quadrature modulation and frequency translation principles.

5.3.1. Phasing-Filter Technique (PFT)

The name "phasing-filter technique" is used because the algorithms for this technique are based on phasing processes. This process is simply to introduce a 90^0 phase shift into the in-phase and/or quadrature-phase components of the quadrature

Doppler signal. This is done by a wide-band digital Hilbert transform filter. The Hilbert transform is the name given to an operator which, when applied to a band limited signal, generates the exact quadrature of the waveform.

5.3.1.1. Asymmetrical implementation of the PFT.

The algorithm shown in Fig. 5.1 utilises a time domain Hilbert transform filter and a delay filter. The latter introduces a time delay that equals the time delay introduced by the HT filter.

If the signal defined by Eq. 5.1 is applied to the system illustrated in Fig. 5.1, the following results are obtained:

Ignoring the time delays introduced by the digital filters, the Hilbert transform of $\boldsymbol{D(n)}$ is

$$\boldsymbol{H[D(n)] = H[s_f(n) + H[s_r(n)]] = H[s_f(n)] - s_r(n)}. \qquad 5.2$$

After addition and subtraction of $\boldsymbol{Q(n)}$ (Eq. 5.1) and $\boldsymbol{H[D(n)]}$ (Eq. 5.2) the separated outputs will be

$$\begin{cases} y_f(n) = Q(n) + H[D(n)] = H[s_f(n)] + s_r(n) + H[s_f(n)] - s_r(n) \\ y_r(n) = Q(n) - H[D(n)] = H[s_f(n)] + s_r(n) - H[s_f(n)] + s_r(n) \end{cases} \qquad 5.3a$$

$$\begin{cases} y_f(n) = 2H[s_f(n)] \\ y_r(n) = 2s_r(n) \end{cases} \qquad 5.3b$$

where the outputs are totally separated. Note that the output $\boldsymbol{y_f(n)}$ contains the $\mathbf{90^0}$ phase shifted forward signals.

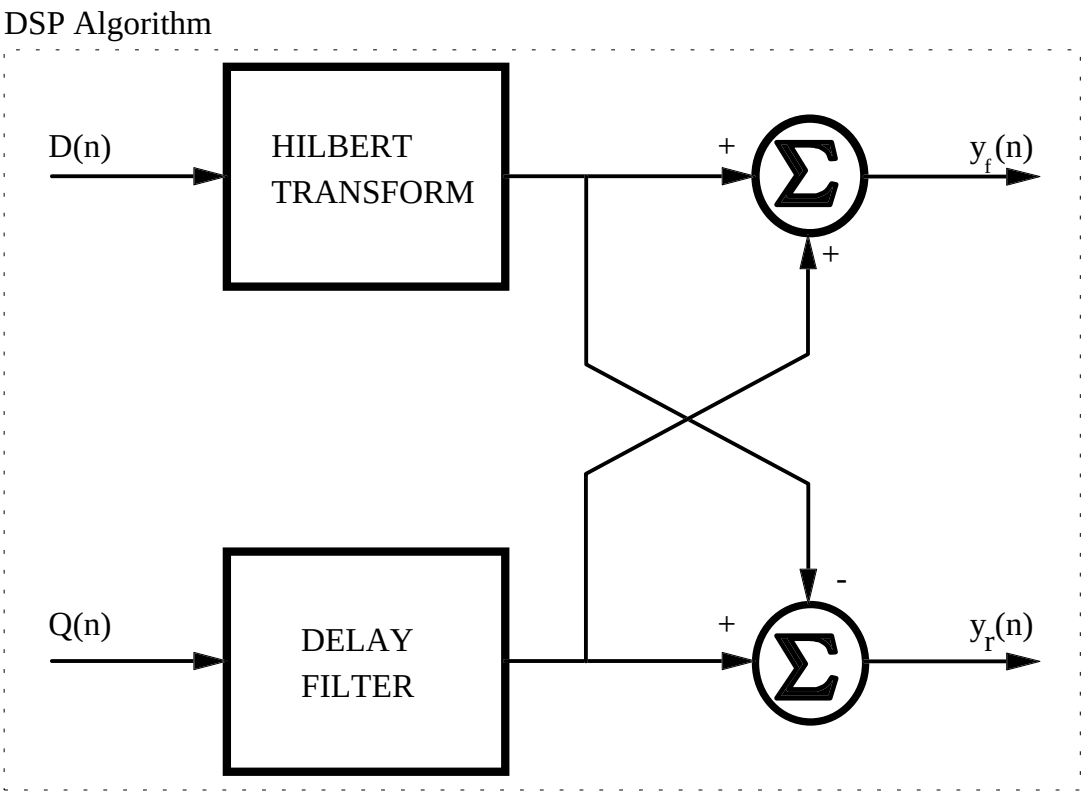

Figure 5.1 Asymmetrical implementation of the PFT algorithm using single filter FIR Hilbert transform.

5.3.1.2. Symmetrical implementation of the PFT.

This algorithm can be implemented by applying the Hilbert transform to both the in-phase and quadrature-phase signals, as depicted in Fig. 5.2. In the FIR type implementation of the HT filter the output is in quadrature with the delayed input signal. The required compensating delay corresponding to the HT filter delay is given by **(*N*-1)/2** samples where ***N*** is order of the HT filter.

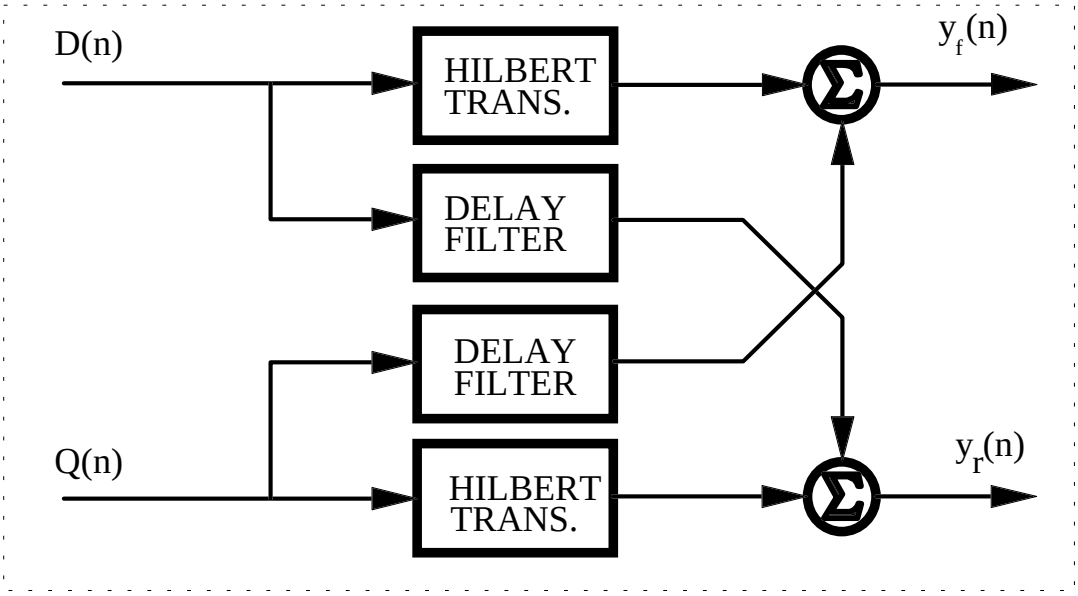

Figure 5.2 Symmetrical implementation of the PFT algorithm using single filter FIR Hilbert transform.

As in Eq. 5.2, the HT of ***Q*(*n*)** is

$$\boldsymbol{H[Q(n)] = H[H[s_f(n)] + s_r(n)] = -s_f(n) + H[s_r(n)]}. \qquad 5.4$$

Referring to Fig. 5.2 and equations 5.1 and 5.4, the sums of ***D*(*n*)** and ***H*[*Q*(*n*)],** and ***Q*(*n*)** and ***H*[*D*(*n*)]** are given by:

$$\begin{cases} y_f(n) = Q(n) + H[D(n)] = 2H[s_f(n)] \\ y_r(n) = D(n) + H[Q(n)] = 2H[s_r(n)] \end{cases} \qquad 5.5$$

where outputs are totally separated and $\mathbf{90^0}$ phase shifted.

By implementing subtraction instead of addition, the unshifted separated time domain outputs can be obtained.

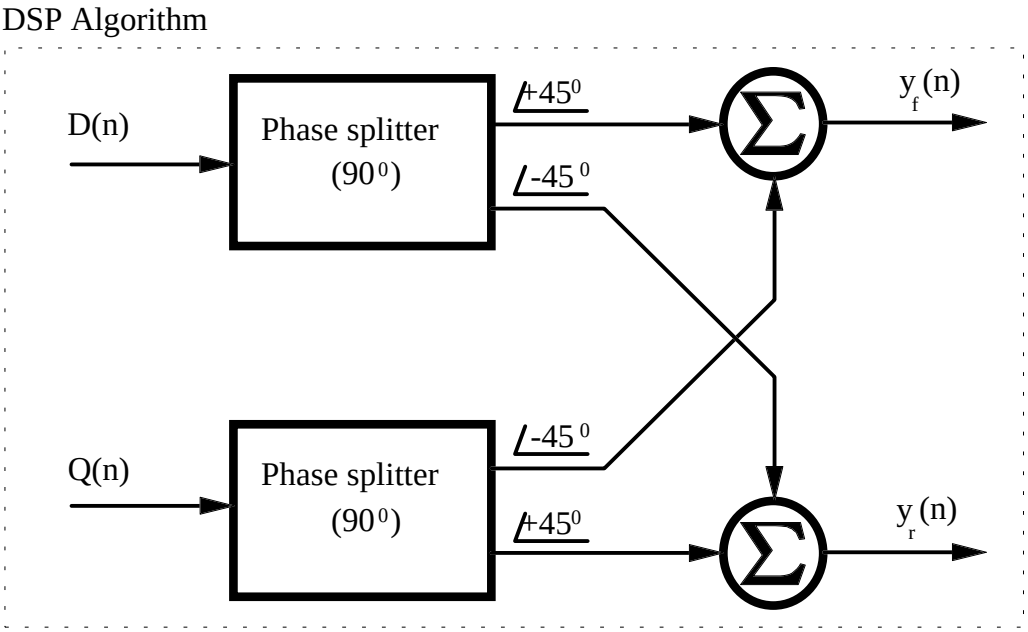

Figure 5.3 Symmetrical implementation of the PFT algorithm using phase splitters.

$$\begin{cases} y_f(n) = D(n) - H[Q(n)] = 2s_f(n) \\ y_r(n) = Q(n) - H[D(n)] = 2s_r(n) \end{cases} \qquad 5.6$$

An alternative algorithm is to implement the HT using phase splitting networks (Oppenheim 1970, Ansari 1987). A $\mathbf{90^0}$ phase splitter is an all-pass filter which produces a quadrature signal pair from a single input as illustrated in Fig. 5.3. The main advantage of this algorithm over the single filter HT is that the two filters have almost identical pass-band ripple characteristics.

5.3.2. Extended Weaver Receiver Technique (EWRT)

This algorithm which is based on the SSB quadrature signal generation method introduced by Weaver (1956), utilises a digitally implemented quadrature mixer and a sharp low-pass filter (LPF). In fact this technique is an application of the frequency translation or modulation principles.

For a theoretical description of the system consider the quadrature Doppler signal defined by Eq. 5.1 which is band limited to $f_s / 4$, and a pair of quadrature pilot frequency signals given by $p_d(n) = \sin \omega_c n$, $p_q(n) = \cos \omega_c n$ where $\omega_C/2\pi=f_S/4$. The LPF is assumed to be an ideal LPF having a cut-off frequency of $f_s / 4$.

5.3.1.1. Asymmetrical implementation of the EWRT.

The block diagram of this algorithm is shown in Fig. 5.4. It employs four digital mixers and four LPFs which eliminate unwanted frequency components.

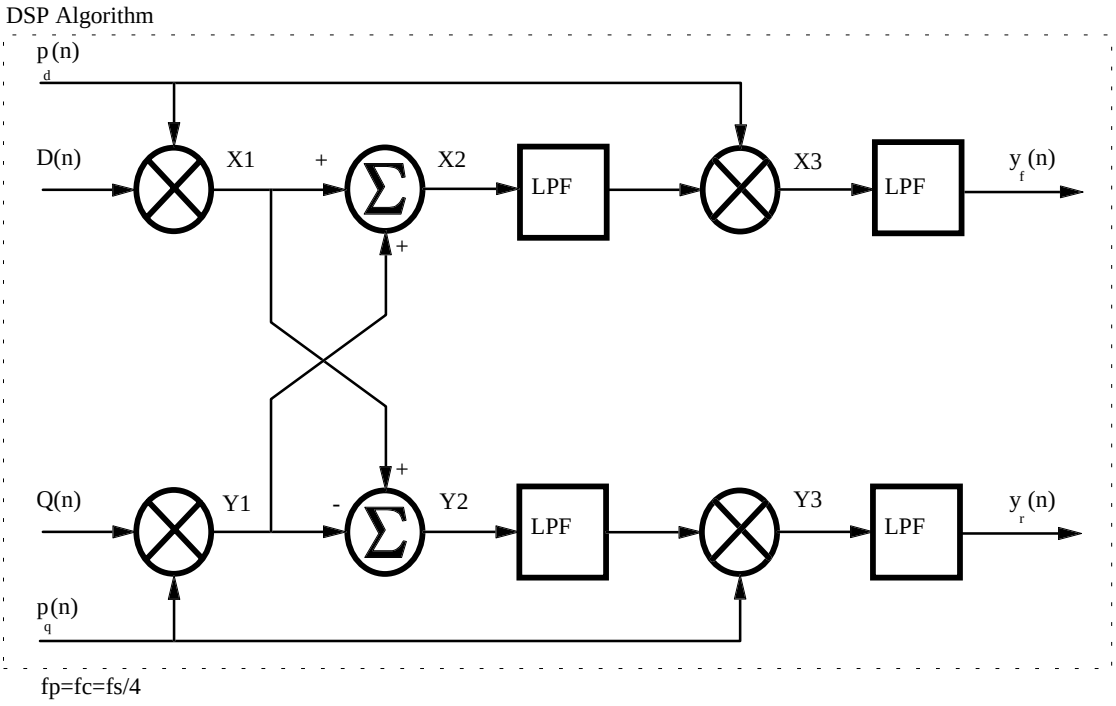

Figure 5.4 Asymmetrical implementation of the EWRT algorithm.

Since the first stage is basically a single side-band (SSB) signal generator, the general expression for this stage (Gibson 1989) is:

$$\boldsymbol{X2, Y2 = D(n).\, p_d(n) \pm Q(n).\, p_q(n)} \quad 5.7a$$

$$\boldsymbol{= \{s_f(n).\sin\omega_c n + H[s_r(n)].\sin\omega_c n\} \pm \{H[s_f(n)].\cos\omega_c n + s_r(n)\cos\omega_c n\}} \quad 5.7b$$

If we define the Fourier transform of $\boldsymbol{s_f(n)}$ and $\boldsymbol{s_r(n)}$ as

$$\boldsymbol{F\{s_f(n)\} = S_f(\omega) \;\; and \;\; F\{s_r(n)\} = S_r(\omega)} \quad 5.8$$

then given that

$$F\{H[s_f(n)]\} = H[S_f(\omega)] = \begin{cases} -jS_f(\omega), & 0 \le \omega < \pi \\ +jS_f(\omega), & -\pi \le \omega < 0 \end{cases} \quad 5.9$$

and

$$F\{H[s_r(n)]\} = H[S_r(\omega)] = \begin{cases} -jS_r(\omega), & 0 \le \omega < \pi \\ +jS_r(\omega), & -\pi \le \omega < 0 \end{cases} \quad 5.10$$

Defining

$$\begin{cases} S_f^+(\omega) = S_f(\omega), 0 \le \omega < \pi \\ S_f^-(\omega) = S_f(\omega), -\pi \le \omega < 0 \end{cases} \quad 5.11$$

$$\begin{cases} S_r^+(\omega) = S_r(\omega), 0 \le \omega < \pi \\ S_r^-(\omega) = S_r(\omega), -\pi \le \omega < 0 \end{cases} \quad 5.12$$

we can write

$$\begin{cases} S_f(\omega) = S_f^+(\omega) + S_f^-(\omega) \\ S_r(\omega) = S_r^+(\omega) + S_r^-(\omega) \end{cases} \quad 5.13$$

$$\begin{cases} H[S_f(\omega)] = -jS_f^+(\omega) + jS_f^-(\omega) \\ H[S_r(\omega)] = -jS_r^+(\omega) + jS_r^-(\omega) \end{cases} \quad 5.14$$

Taking the Fourier transform of Eq. 5.7, we have

$$\begin{aligned}F\{X2,Y2\} = &-\frac{j}{2}S_f^+(\omega-\omega_c)+\frac{j}{2}S_f^+(\omega+\omega_c)-\frac{j}{2}S_f^-(\omega-\omega_c)+\frac{j}{2}S_f^-(\omega+\omega_c)\\ &-\frac{1}{2}S_r^+(\omega-\omega_c)+\frac{1}{2}S_r^+(\omega+\omega_c)+\frac{1}{2}S_r^-(\omega-\omega_c)-\frac{1}{2}S_r^-(\omega+\omega_c)\\ &\mp\frac{j}{2}S_f^+(\omega-\omega_c)\mp\frac{j}{2}S_f^+(\omega+\omega_c)\pm\frac{j}{2}S_f^-(\omega-\omega_c)\pm\frac{j}{2}S_f^-(\omega+\omega_c)\\ &\pm\frac{1}{2}S_r^+(\omega-\omega_c)\pm\frac{1}{2}S_r^+(\omega+\omega_c)\pm\frac{1}{2}S_r^-(\omega-\omega_c)\pm\frac{1}{2}S_r^-(\omega+\omega_c)\end{aligned}$$

$$F\{X2\} = \{-jS_f^+(\omega-\omega_c)+jS_f^-(\omega+\omega_c)\}+\{S_r^+(\omega+\omega_c)+S_r^-(\omega-\omega_c)\} \quad 5.15a$$

$$= H[S_f(\omega_c-\omega)]+S_r(\omega_c+\omega) \quad 5.15b$$

$$F\{Y2\} = \{jS_f^+(\omega+\omega_c)-jS_f^-(\omega-\omega_c)\}+\{-S_r^+(\omega-\omega_c)-S_r^-(\omega+\omega_c)\} \quad 5.16a$$

$$= -H[S_f(\omega_c+\omega)]-S_r(\omega_c-\omega). \quad 5.16b$$

If we pass the signals defined by Eq. 5.15 and Eq. 5.16 through the LPF that retains only the lower side-band, the remaining signals are

$$F\{X2\} = H[S_f(\omega_c-\omega)] = -jS_f^+(\omega-\omega_c)+jS_f^-(\omega+\omega_c) \quad 5.17$$

$$F\{Y2\} = -S_r(\omega_c-\omega) = -S_r^+(\omega-\omega_c)-S_r^-(\omega+\omega_c). \quad 5.18$$

Similarly, the outputs of the second mixing stage are

$$F\{X3\} = \frac{1}{2}S_f^+(\omega)+\frac{1}{2}S_f^-(\omega)-\frac{1}{2}S_f^+(\omega-2\omega_c)-\frac{1}{2}S_f^-(\omega+2\omega_c) \quad 5.19a$$

$$= \frac{1}{2}S_f(\omega)-\frac{1}{2}S_f(2\omega_c-\omega) \quad 5.19b$$

$$F\{Y3\} = -\frac{1}{2}S_r^+(\omega)-\frac{1}{2}S_r^-(\omega)-\frac{1}{2}S_r^+(\omega-2\omega_c)-\frac{1}{2}S_r^-(\omega+2\omega_c) \quad 5.20a$$

$$= -\frac{1}{2}S_r(\omega)-\frac{1}{2}S_r(2\omega_c-\omega). \quad 5.20b$$

Applying the LPF, the frequency components greater than f_c are removed, so the separated outputs are

$$\begin{cases} F\{y_f(n)\} = \frac{1}{2} S_f(\omega), \\ F\{y_r(n)\} = -\frac{1}{2} S_r(\omega). \end{cases} \quad 5.21$$

Taking the inverse Fourier transform of these results, we have

$$\begin{cases} y_f(n) = F^{-1}\{\frac{1}{2} S_f(\omega)\} = \frac{1}{2} s_f(n), \\ y_r(n) = F^{-1}\{-\frac{1}{2} S_r(\omega)\} = -\frac{1}{2} s_r(n). \end{cases} \quad 5.22$$

In order to clarify this method a graphical explanation of the same process is sketched in Fig. 5.5 using a perfect quadrature signal given by

$$\boldsymbol{x(t) = D(t) + jQ(t) = (\cos \omega_f t + \sin \omega_r t) + j(\sin \omega_f t + \cos \omega_r t)}.$$

Here, the spectra of the signals produced at each processing stage in Fig. 5.4 are plotted sequentially. In fact, this constitutes a frequency domain description of the frequency shifting and modulation process.

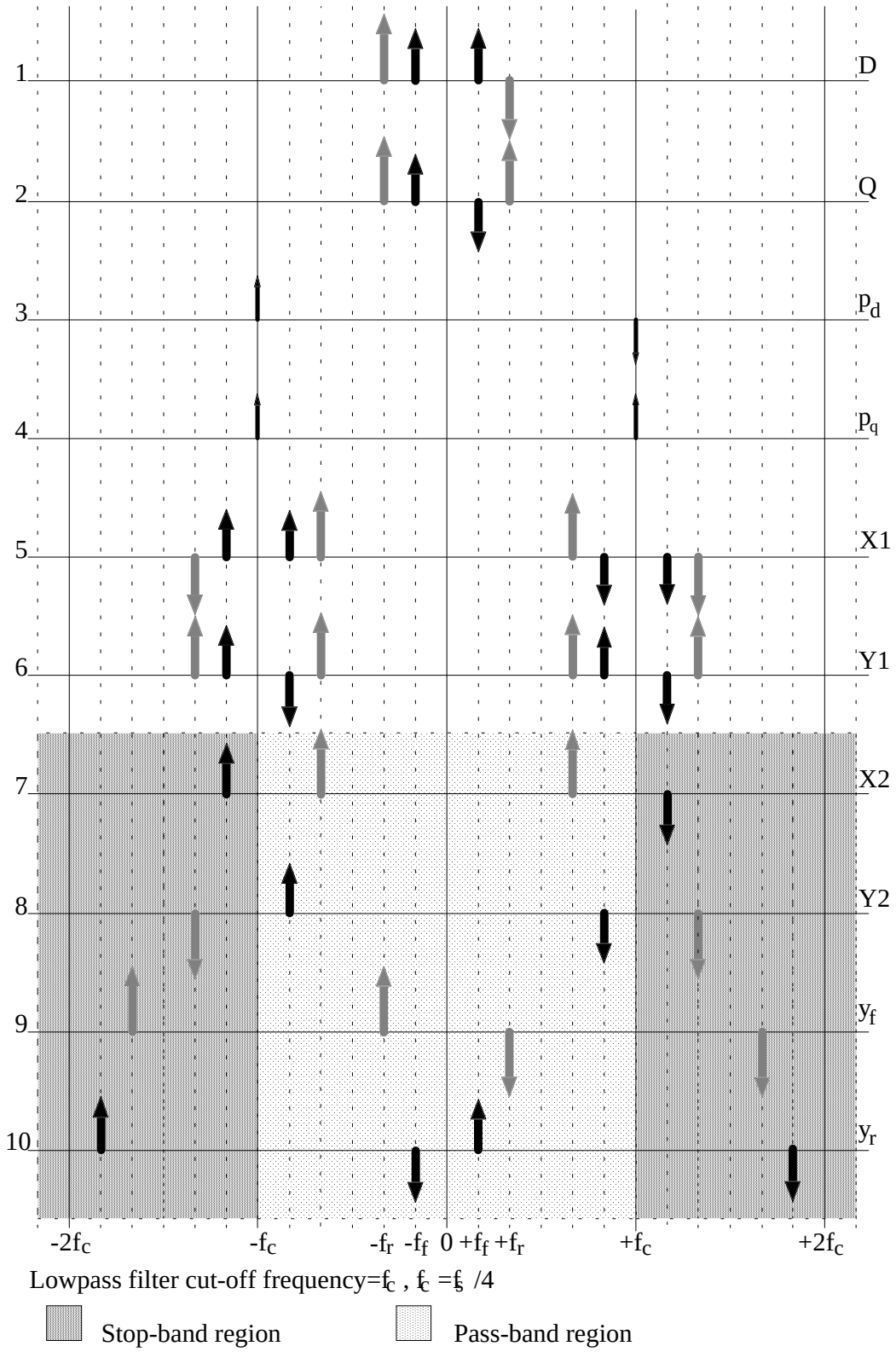

Figure 5.5 Spectra at each processing stages of the EWRT (Fig. 5.4). Input signal to be considered $\sin\omega_f t + \cos\omega_r t + j\cos\omega_f t + j\sin\omega_r t$. Spectra indexed by letters on the right hand side correspond to the results at each processing stage indexed by the same letters in Fig. 5.4.

5.3.1.2. Symmetrical implementation of the EWRT.

An alternative algorithm utilising two quadrature mixers instead of one is given in Fig. 5.6. The advantage of this algorithm is that both channels have exactly the same characteristics.

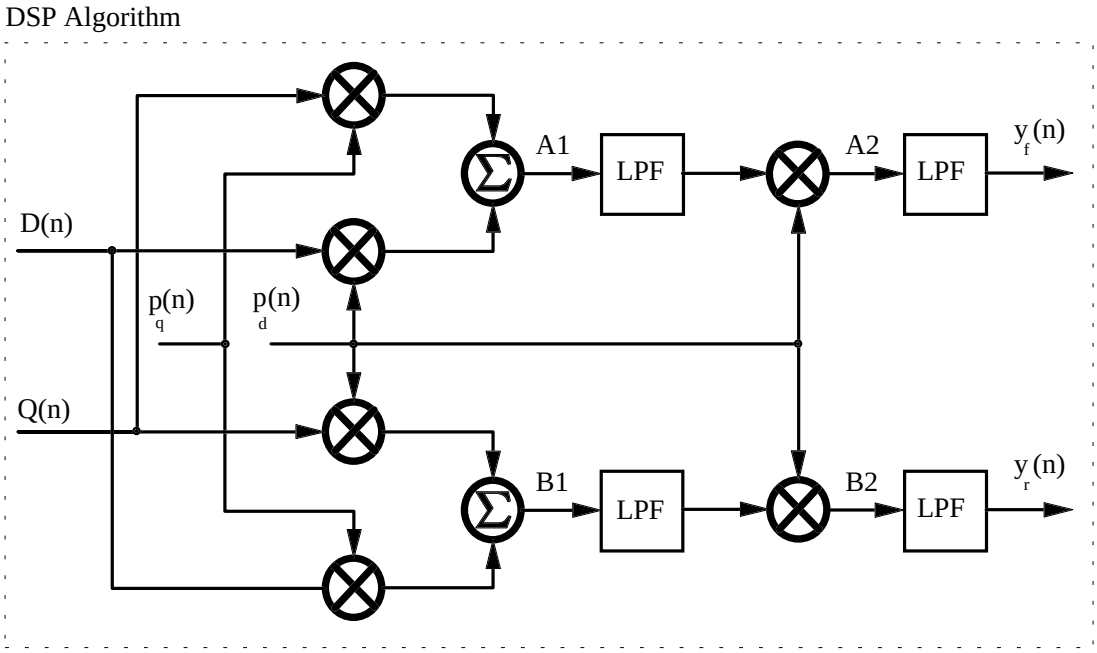

Figure 5.6 Symmetrical implementation of the EWRT algorithm.

From Fig. 5.6, A1 can be written as

$$\boldsymbol{A1 = D(n).\, p_d\,(n) + Q(n).\, P_q\,(n)} \qquad 5.23$$

which is equal to 52 given by equation 5.7a. So we can directly write that

$$\boldsymbol{y_f\,(n) = \frac{1}{2} s_f\,(n).} \qquad 5.24$$

By considering the same definitions given by equations 5.8, 5.9, 5.10, 5.11, and 5.12 and following the same procedure, ***B1*** can be worked out:

$$B1 = D(n).\,p_q(n) + Q(n).P_d(n) \qquad 5.25$$
$$= \{s_f(n).\cos\omega_c n + H[s_r(n)].\cos\omega_c n\} + \{H[s_f(n)].\sin\omega_c n + s_r(n)\sin\omega_c n\}$$

Taking the Fourier transform, we have

$$\begin{aligned} F\{B1\} = {} & \frac{1}{2}S_f^+(\omega-\omega_c) + \frac{1}{2}S_f^+(\omega+\omega_c) + \frac{1}{2}S_f^-(\omega-\omega_c) + \frac{1}{2}S_f^-(\omega+\omega_c) \\ & - \frac{j}{2}S_r^+(\omega-\omega_c) - \frac{j}{2}S_r^+(\omega+\omega_c) + \frac{j}{2}S_r^-(\omega-\omega_c) + \frac{j}{2}S_r^-(\omega+\omega_c) \\ & - \frac{1}{2}S_f^+(\omega-\omega_c) + \frac{1}{2}S_f^+(\omega+\omega_c) + \frac{1}{2}S_f^-(\omega-\omega_c) - \frac{1}{2}S_f^-(\omega+\omega_c) \\ & - \frac{j}{2}S_r^+(\omega-\omega_c) + \frac{j}{2}S_r^+(\omega+\omega_c) - \frac{j}{2}S_r^-(\omega-\omega_c) + \frac{j}{2}S_r^-(\omega+\omega_c) \end{aligned}$$

$$F\{B1\} = \{S_f^+(\omega+\omega_c) + S_f^-(\omega-\omega_c)\} + \{-jS_r^+(\omega-\omega_c) + jS_r^-(\omega+\omega_c)\} \qquad 5.26a$$
$$= S_f(\omega_c+\omega) + H[S_r(\omega_c-\omega)]. \qquad 5.26b$$

After LPF, lower side-band signal is retained:

$$F\{B1\} = H[S_r(\omega_c-\omega)] = -jS^+{}_r(\omega_c-\omega) + jS^-{}_r(\omega_c-\omega) \qquad 5.27$$

The output of the second mixing stage is:

$$F\{B2\} = \frac{1}{2}S_r^+(\omega) + \frac{1}{2}S_r^-(\omega) - \frac{1}{2}S_r^+(\omega-2\omega_c) - \frac{1}{2}S_r^-(\omega+2\omega_c) \qquad 5.28a$$
$$= \frac{1}{2}S_r(\omega) - \frac{1}{2}S_r(2\omega_c-\omega). \qquad 5.28b$$

Applying the LPF, the frequency components greater than f_c are removed, so the separated output is

$$\boldsymbol{F\{y_r(n)\} = \frac{1}{2} S_r(\omega)} \tag{5.29}$$

Taking the inverse Fourier transform of this result, we have

$$\boldsymbol{y_r(n) = F^{-1}\{\frac{1}{2} S_r(\omega)\} = \frac{1}{2} s_r(n)}. \tag{5.30}$$

The final separated signal pair is:

$$\begin{cases} y_f(n) = \frac{1}{2} s_f(n), \\ y_r(n) = \frac{1}{2} s_r(n). \end{cases} \tag{5.31}$$

5.3.1.3. Implementation of the EWRT algorithm using low-pass/high-pass filter pair.

Unlike the other two implementations of the EWRT, this method uses both the upper side-band (USB) and the lower side-band (LSB) to recover directional signals as depicted in Fig 5.7. The high-pass filter (HPF) is assumed to be an ideal HPF having a cut-off frequency of $\boldsymbol{f_s / 4}$.

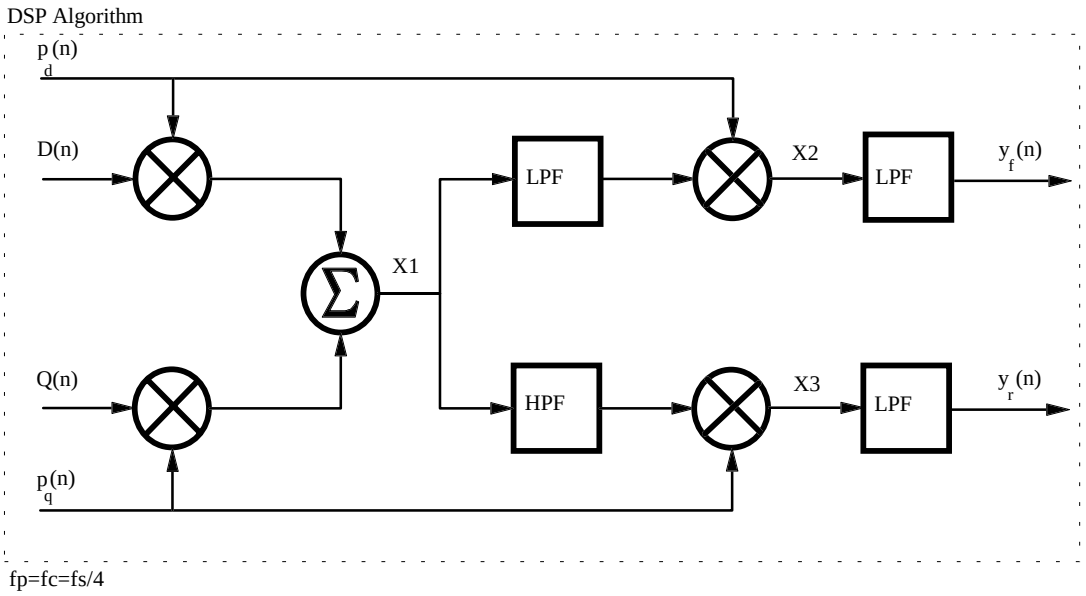

Figure 5.7 Implementation of the EWRT algorithm using low-pass/high-pass filter pair.

From Fig. 5.7, ***X*1** is:

$$\boldsymbol{X1 = D(n).\, p_d(n) + Q(n).\, P_q(n)} \qquad 5.32$$

It can be seen that the output $\boldsymbol{y_f(n)}$ is the same as for the other two implementations.

Using the same definitions (from Eq. 5.8 to 5.12) $\boldsymbol{y_r(n)}$ can be found. If we pass ***X*1** (given by Eq. 5.15 in frequency domain) through the HPF that retains only the USB, the remaining signal is

$$\boldsymbol{F\{X1\} = S_r(\omega_c + \omega) = S_r^+(\omega + \omega_c) + S_r^-(\omega - \omega_c)} \qquad 5.33$$

Similarly, the output of the second mixing stage is

$$\boldsymbol{F\{X3\} = \frac{1}{2}S_r^+(\omega) + \frac{1}{2}S_r^-(\omega) + \frac{1}{2}S_r^+(\omega + 2\omega_c) + \frac{1}{2}S_r^-(\omega - 2\omega_c)} \qquad 5.34a$$

$$= \frac{1}{2} S_r(\omega) + \frac{1}{2} S_r(2\omega_c + \omega). \qquad 5.34b$$

Applying the LPF, the frequency components greater than f_c are removed, so the separated output is

$$F\{y_r(n)\} = \frac{1}{2} S_r(\omega) \qquad 5.35$$

The final directional time domain outputs are:

$$\begin{cases} y_f(n) = F^{-1}\{\frac{1}{2} S_f(\omega)\} = \frac{1}{2} s_f(n), \\ y_r(n) = F^{-1}\{\frac{1}{2} S_r(\omega)\} = \frac{1}{2} s_r(n). \end{cases} \qquad 5.36$$

5.4. FREQUENCY DOMAIN PROCESSING

Because the algorithms in this section are almost entirely implemented in the frequency domain (after fast Fourier transform), they are based on the complex FFT process. The common steps for the all these implementations are the complex FFT, the inverse FFT and overlapping techniques to avoid Gibbs phenomena (Harris 1982). Three types of frequency domain algorithm will be described: the Hilbert transform method, the complex FFT method, and the spectral translocation method.

5.4.1. Frequency Domain Hilbert Transform Method (HTM)

Unlike the phasing filter technique this method utilises a complex HT in the frequency domain. As outlined in Fig. 5.8 the method requires a complex FFT

(CFFT) and an inverse FFT (IFFT). The ideal frequency response of the HT (Gold *at al* 1970; Oppenheim 1975) is given by:

$$H(\omega) = \begin{cases} -j, 0 \le \omega < \pi \\ +j, -\pi \le \omega < 0 \end{cases} \qquad 5.37$$

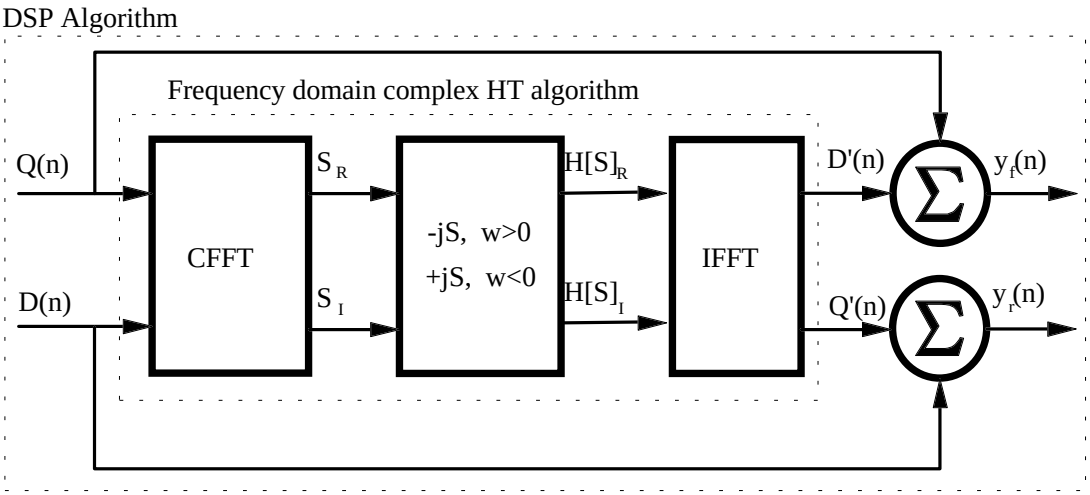

Figure 5.8 Block diagram of the frequency domain Hilbert transform algorithm.

To describe the method theoretically, let us consider the general Doppler signal defined by Eq. 5.1 as a complex signal:

$$\begin{aligned} \boldsymbol{s(n) &= D(n) + jQ(n)} \\ &\boldsymbol{= \{s_f(n) + H[s_r(n)]\} + j\{H[s_f(n)] + s_r(n)\}.} \end{aligned} \qquad 5.38$$

Applying the Fourier transform to $\boldsymbol{s(n)}$, we have

$$\boldsymbol{F\{s(n)\} = \{S_f(\omega) + H[S_r(\omega)]\} + j\{H[S_f(\omega)] + S_r(\omega)\}} \qquad 5.39$$

This expression can be rewritten using the definitions given by Eq. 5.9, 5.10, 5.13 and 5.14.

$$\boldsymbol{F\{s(n)\} = S(\omega) = \{S_f^+(\omega) + S_f^-(\omega) - jS_r^+(\omega) + jS_r^-(\omega)\} + j\{-jS_f^+(\omega) + jS_f^-(\omega) + S_r^+(\omega) + S_r^-(\omega)\}} \quad 5.40$$

Using Eq. 5.37, the HT of Eq. 5. 40 can be given as

$$H[S(\omega)] = \begin{cases} -jS(\omega), 0 \le \omega < \pi \\ +jS(\omega), -\pi \le \omega < 0 \end{cases} \quad 5.41$$

$$\begin{aligned} H[S(\omega)] &= \{-jS_f^+(\omega) + jS_f^-(\omega) - S_r^+(\omega) - S_r^-(\omega)\} + \\ & j\{-S_f^+(\omega) - S_f^-(\omega) - jS_r^+(\omega) + jS_r^-(\omega)\} \\ &= \{H[S_f(\omega)] - S_r(\omega)\} + j\{-S_f(\omega) + H[S_r(\omega)]\} \end{aligned} \quad 5.42$$

After taking inverse Fourier transform, the HT of the input signal is obtained.

$$\boldsymbol{F^{-1}\{H[S(\omega)]\} = \{H[S_f(n)] - S_r(n)\} + j\{-S_f(n) + H[S_r(n)]\} = D'(n) + jQ'(n) = H[s(n)]} \quad 5.43$$

The final step is to add the complex input signal and its HT as depicted in Fig. 5.8:

$$\begin{cases} y_f(n) = D'(n) + Q(n) = 2H[s_f(n)], \\ y_r(n) = D(n) + Q'(n) = 2H[s_r(n)]. \end{cases} \quad 5.44$$

5.4.2. Complex FFT Method (CFFT)

The complex FFT has been used to separate the directional signal information from quadrature signals so that the spectra of the directional signals can be estimated and displayed as sonograms (Aydin and Evans 1994). It can be shown that the phase information of the directional signals is well preserved and can be used to recover these signals. The method is sketched in Fig. 5.9.

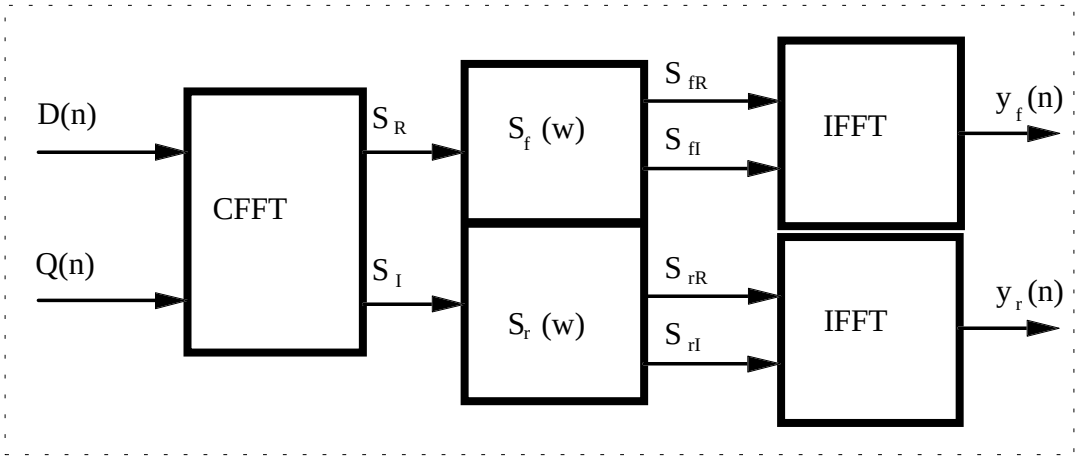

Figure 5.9 Block diagram of the complex FFT method.

For a discrete Doppler quadrature signal pair given by Eq. 5.1, it can be shown that

$$\begin{aligned} \boldsymbol{s(n) = D(n) + jQ(n) = \{s_f(n) + H[s_r(n)]\} + j\{H[s_f(n)] + s_r(n)\}} \\ \boldsymbol{= \{s_f(n) + jH[s_f(n)]\} + j\{s_r(n) - jH[s_r(n)]\}} \end{aligned} \quad 5.45$$

Using the frequency response of the HT given by Eq. 5.37, it is easy to obtain the Fourier transform of $\boldsymbol{s(n)}$:

$$F\{[s(n)\} = \begin{cases} \{S_f(\omega) + S_f(\omega)\} + j\{S_r(\omega) - S_r(\omega)\}, 0 \le \omega < \pi \\ \{S_f(\omega) - S_f(\omega)\} + j\{S_r(\omega) + S_r(\omega)\}, -\pi \le \omega < 0 \end{cases} \quad 5.46a$$

$$F\{s(n)\} = S(\omega) = \begin{cases} 2S_f(\omega), 0 \le \omega < \pi \\ j2S_r(\omega), -\pi \le \omega < 0 \end{cases} \quad 5.46b$$

It is clear that the positive frequencies of $\boldsymbol{S(\omega)}$ contain only the spectrum of the forward channel signal $\boldsymbol{s_f(n)}$, and its negative frequencies contain only the $\mathbf{90^0}$ shifted spectrum of the reverse channel signal $\boldsymbol{s_r(n)}$.

If the following spectra are defined

$$S^{+}(\omega)=\begin{cases}S(\omega),0\le\omega<\pi\\0,-\pi\le\omega<0\end{cases} \quad 5.47a$$

$$S^{-}(\omega)=\begin{cases}0,0\le\omega<\pi\\S(\omega),-\pi\le\omega<0\end{cases} \quad 5.47b$$

using the properties of the Fourier transform, i.e., for a real signal, the real part of its spectrum is an even function, and the imaginary part is an odd one, it is easy to recover the spectra of the two real directional signals. The real part of $\boldsymbol{S_f(\omega)}$ is

$$\Re\{S_f(\omega)\}=\begin{cases}\Re\{S^{+}(\omega)\},0\le\omega<\pi\\\Re\{S^{+}(-\omega)\},-\pi\le\omega<0\end{cases} \quad 5.48$$

and its imaginary part is

$$\Im\{S_f(\omega)\}=\begin{cases}\Im\{S^{+}(\omega)\},0\le\omega<\pi\\-\Im\{S^{+}(-\omega)\},-\pi\le\omega<0\end{cases} \quad 5.49$$

The real part of $\boldsymbol{S_r(\omega)}$ is

$$\Re\{S_r(\omega)\}=\begin{cases}\Im\{S^{-}(-\omega)\},0\le\omega<\pi\\\Im\{S^{-}(\omega)\},-\pi\le\omega<0\end{cases} \quad 5.50$$

and its imaginary part is

$$\Im\{S_r(\omega)\}=\begin{cases}\Re\{S^{-}(-\omega)\},0\le\omega<\pi\\-\Re\{S^{-}(\omega)\},-\pi\le\omega<0\end{cases} \quad 5.51$$

The directional time domain outputs can then be obtained by taking inverse Fourier transform of the spectra of the directional signals.

5.4.3. Spectral Translocation Method (STM)

This method is similar to the CFFT but it requires only one inverse Fourier transform to recover directional time domain signals. The phase information is manipulated in the frequency domain in such a way that the real output of the inverse Fourier transform gives one direction, the imaginary output gives the other direction.

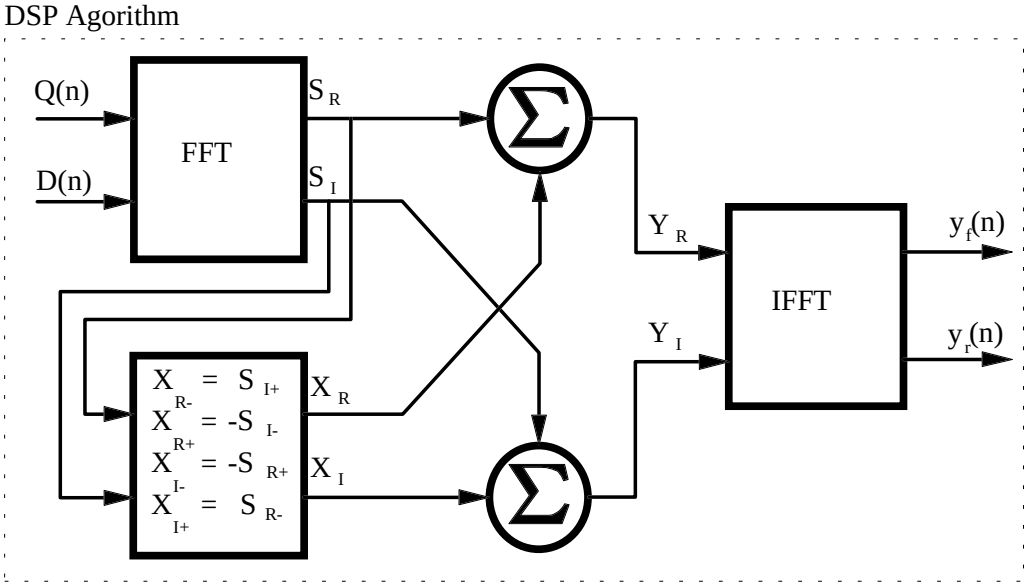

Figure 5.10 Block diagram of the spectral translocation algorithm.

In Fig. 5.10, the Fourier transform of the input signal is the same as that obtained in Eq. 5.46b. We can rewrite this equation in terms of the positive and negative frequencies.

$$\boldsymbol{S(\omega) = 2S_f^+(\omega) + j2S_r^-(\omega) = \Re\{S^+(\omega) + S^-(\omega)\} + j\Im\{S^+(\omega) + S^-(\omega)\}} \qquad 5.52$$

Defining

$$\boldsymbol{S^-(-\omega) = S^+(\omega), \quad S^+(-\omega) = S^-(\omega)} \qquad 5.53$$

we can create a new complex frequency domain signal:

$$\begin{aligned} \boldsymbol{X(\omega) &= \Re\{S^{+}(-\omega) - S^{-}(-\omega)\} + j\Im\{-S^{+}(-\omega) + S^{-}(-\omega)\}} \\ &= \Re\{-S^{+}(\omega) + S^{-}(\omega)\} + j\Im\{S^{+}(\omega) - S^{-}(\omega)\} \end{aligned} \quad 5.53$$

If this is applied to Eq. 5.52, we have

$$\boldsymbol{X(\omega) = 2S_f^{+}(-\omega) + j2S_r^{-}(-\omega) = 2S_f^{-}(\omega) + j2S_r^{+}(\omega).} \quad 5.54$$

By adding Eq. 5.52 and 5.54, we can obtain another complex frequency domain signal where the directional signals are ready for separation by the use of a single inverse FFT process:

$$\begin{aligned} \boldsymbol{(\omega) &= S(\omega) + X(\omega)} \\ &= \{\Re\{S(\omega)\} + \Re\{X(\omega)\}\} + j\{\Im\{S(\omega)\} + \Im\{X(\omega)\}\} \\ &= 2S_f^{+}(\omega) + j2S_r^{-}(\omega) + 2S_f^{-}(\omega) + j2S_r^{+}(\omega) \end{aligned} \quad 5.55a$$

$$\begin{aligned} &= 2\{S_f^{+}(\omega) + S_f^{-}(\omega)\} + j2\{S_r^{+}(\omega) + S_r^{-}(\omega)\} \\ &= 2S_f(\omega) + j2S_r(\omega) \end{aligned} \quad 5.55b$$

Inverse Fourier transform of Eq. 5.55b yields the complex time domain signal

$$\boldsymbol{y(n) = 2s_f(n) + j2s_r(n)} \quad 5.56$$

where the real part of it gives one direction and the imaginary part gives the other direction.

$$\begin{cases} y_f(n) = 2s_f(n), \\ y_r(n) = 2s_r(n). \end{cases} \quad 5.57$$

5.5. SIMULATION STUDY

The five method described above (the PFT, the EWRT, the HTM, the CFFT, and the STM) were simulated in order to compare their relative performances. The simulations were implemented using commercially available digital signal processing software (*Hypersignal*) and C language code when a required function was not available in *Hypersignal*. All the algorithms were applied to the same data set which was a band limited signal derived from pre-recorded white noise. The record length was 100 frames where each frame consisted of 512 data points. The recorded white noise was filtered by a band-pass filter having 70 dB stop-band attenuation and a reference band limited quadrature signal was derived from this filtered signal. The complex FFT spectrum of this quadrature signal is shown in Fig. 5.11a. Since the separation level is better than 60 dB, the signal can be assumed to be an ideal quadrature signal.

After obtaining separated signals using each of the five algorithms, a 512 point real FFT preceded by a Hanning window was applied to each of the signals. 50 frames of the FFT results were averaged. The averaged logarithmic power spectra of each signal were then plotted side by side , as if they were a result of the complex FFT (Figs. 5.11b to 5.11e)

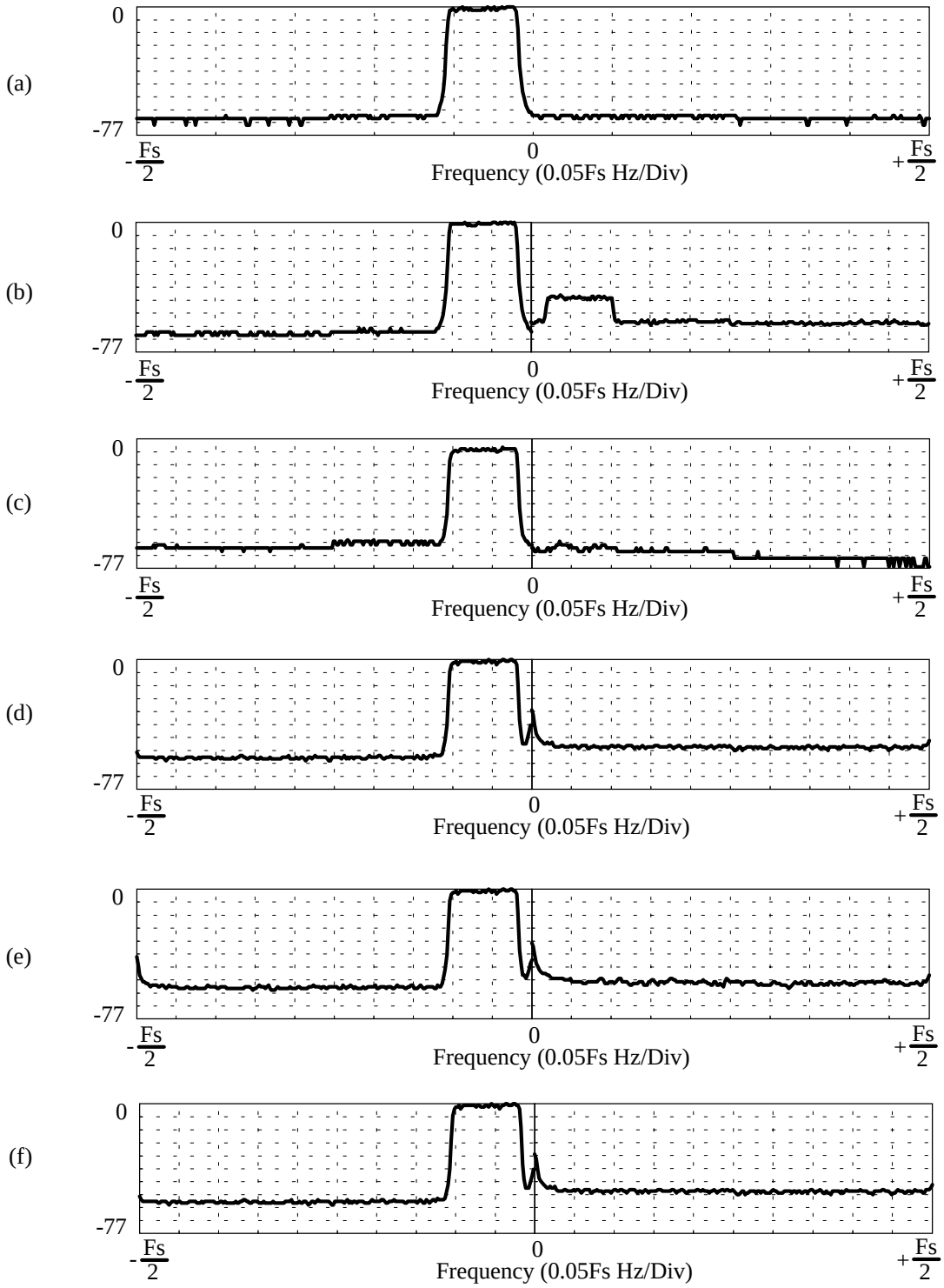

Figure 5.11 The averaged output power spectra of the simulations for; (a) the reference quadrature signal, (b) the PFT, (c) the EWRT, (d) the HTM, (e) the CFFT and (f) the STM. Magnitude scale is 7.7 dB/Div.

5.6. RESULTS AND CONCLUSION

The simulation results are shown in Fig. 5.11. Fig. 5.11a is the reference quadrature signal spectrum. Fig. 5.11b are the averaged power spectra of the separated channels plotted side by side for the PFT. Here, the crosstalk level is approximately -45 dB. The level of the crosstalk depends on the HT filter characteristics. A reduction in pass-band ripple and an increase in stop-band attenuation result in a decrease in the crosstalk. However, this will increase the length of the filter , i.e. its execution time. This problem is associated with FIR type Hilbert transform implementations. If a 90^0 phase splitter is used this problem can be avoided.

The result of the EWRT is illustrated in Fig. 5.11c, where the separation level is approximately -55 dB. In the EWRT the separation level is a function of the quadrature pilot frequency signal. The best performance is obtained for a quadrature pilot signal frequency of $\boldsymbol{f_S/4}$ when the look-up table method is used.

The frequency domain methods (Figs. 5.11d and 5.11e) produce almost the same separation levels (≈-50 dB). The main drawback of these methods is the discontinuities caused by the data segmentation. Although this effect is minimised by using an overlapping technique, these methods corrupt the output signal with a very low frequency signal. However, since the level of this signal and its harmonics are usually less than -30 dB, this effect is negligible.

The results of the simulations show that the crosstalk rejection for all the methods is greater than 40 dB and this is summarised in Table 5.1. The EWRT provided the best crosstalk rejection. In this chapter, the digital algorithms to obtain directional time domain Doppler signals from the quadarture Doppler signal have been described. The real-time implementations of these algorithms will be discussed in next chapter.

method	**EWRT**	**PFT**	**CFFT**	**HTM**	**STM**
separation level	-55 dB	-45 dB#	-52 dB	-50 dB	-50 dB

depends on the HT filter specifications

Table 5.1 The approximate crosstalk rejection levels of the algorithms. PFT: Phasing filter technique; EWRT: Extended Weaver receiver technique; CFFT: Complex FFT; HTM: Hilbert transform method; STM: Spectral translocation method.

6. IMPLEMENTATION OF THE SIGNAL PROCESSING ALGORITHMS

6.1. INTRODUCTION

In this chapter, the implementation of the signal processing algorithms described in previous chapters will be presented. In order to clarify these implementations the processing environment must be identified. Fig. 6.1 depicts a general block diagram of the system used. It is based on a DSP board equipped with the AT&T DSP32C (a powerful 32 bit floating point processor), two A/D and D/A converters, and an on-board memory. As is necessary for all signal processing systems involving data conversion, the system includes anti-aliasing and reconstruction filters. Since the heart of the system is a floating point processor these devices will be described with refrence to the DSP32C.

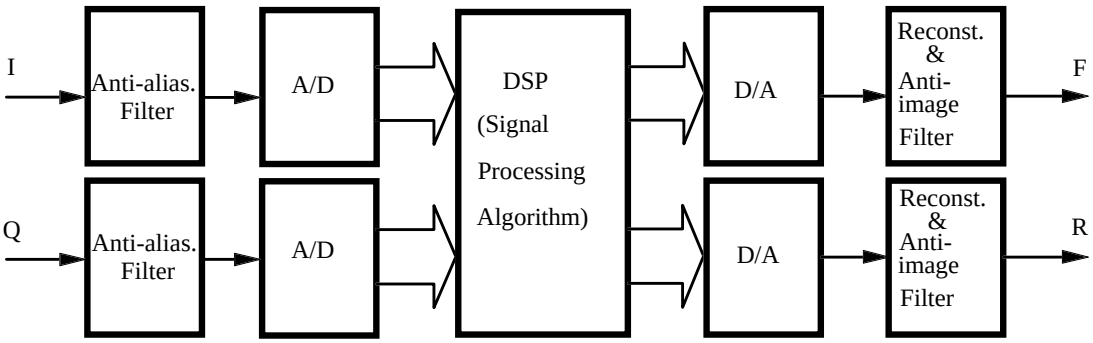

Figure 6.1 General block diagram of the system.

6.2. FLOATING POINT DSP SYSTEMS

The one key element that virtually all DSP application algorithms share is a large number of repetitive mathematical operations. To perform these operations,

conventional microprocessors and co-processors use software simulation and microcode that tends to be slow. To execute floating-point maths and logic operations, the modern DSP devices use a hardware multiplier and an arithmetic logic unit. This approach enables designers to utilise the DSP systems in applications where real time processing is necessary. Floating point arithmetic also allows designers to easily port existing algorithms developed on mainframe computers. The move is simplified because the designer need not to be concerned with the effects of scaling, normalization, and overflow that greatly complicates the port when fixed-point devices are used.

One of the design parameters that must be resolved early in the design phase is the dynamic range (DR) and precision required for a particular application. The DR of a floating-point processor is determined by the size of the exponent and the precision is determined by the size of the mantissa.

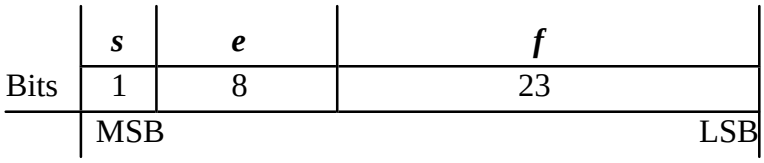

Figure 6.2 IEEE standard 32-bit floating-point format.

Fig. 6.2 shows IEEE floating-point format where:

s = the sign bit (0 for positive, 1 for negative)

f = fractional part of the mantissa

s,f = the mantissa

e = the exponent

For the representation of the number ***z***, five different cases can be considered:

1. If ***e*=255** and ***f*≠0**, then ***z*** is NaN (not a number) regardless of ***s***.

2. If ***e*=255** and ***f*=0**, then $z = (-1)^s * \infty$.
3. If **0<*e*<255** , then $z = (-1)^s * 2^{(e-127)} * (1.f)$.
4. If ***e*=0** and ***f*≠0**, then $z = (-1)^s * 2^{(-126)} * (0.f)$ (denormalized number).
5. If ***e*=0** and ***f*=0**, then $z = (-1)^s * 0$ (zero).

6.2.1. A Dedicated Floating-point Digital Signal Processor: DSP32C

The AT&T WE™-DSP32C Digital Signal Processor is a 32-bit floating point processor designed for real time processing, interfacing to analogue I/O and other external devices, and efficient execution of typical DSP operations. It has been used in applications including audio signal processing, video compression, speech recognition, neural networks, sonar and radar implementations. Its high speed, large memory capacity, and ease of programming make it a cost effective means to implement DSP systems. The fastest processing speed is 25 Mflops (25 million floating-point operations per second) for a 50 MHz clock. This speed is achieved using a built in hardware floating point unit with some parallel pipeline processing.

Concurrent operation of the host computer and DSP32C processor is possible because the DSP32C processor runs independently of the host computer and data can be transferred between the host and the DSP's memory without interrupting the DSP's execution. Data can also be acquired from, and sent to, analogue I/O or other devices in the background, concurrently with real time processing. This means that the DSP can at the same time be acquiring a new set of data; outputting results; carrying on with processing; and exchanging data with the host computer.

The DSP32C floating-point format shown in Fig. 6.3 is different from the IEEE standard floating-point format.

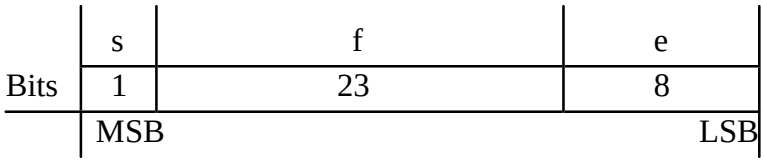

Figure 6.3 DSP32C 32-bit floating-point format.

There are actually two floating-point formats used inside the Data Arithmetic Unit (DAU): a 32-bit format (no guard bits), and a 40-bit format (32 bits, plus 8 mantissa guard bits). The latter format is used only inside the DAU and is not recognised by the rest of the device.

The floating-point quantity shown in Fig. 6.3 is represented in decimal as follows:

$$N = M * 2^{(e-128)}$$

where:

N = the decimal value

e = exponent, the unsigned quantity "eeeeeeee" expressed in base 10.

M = mantissa, the 2's complement quantity "$\overline{s}s$.ffff – – – fff " equivalent to "(-2)^{s}+0.ffff---fff" expressed in base 10.

***** = multiplication

The magnitude of the mantissa is always normalized to lie between 1 and 2. So, the leading "1" (or leading "0" if a negative mantissa) does not appear explicitly in the floating-point word. This implicit bit is the s bar that appears above. A floating-point value with ***e***=0 is reserved to represent the number zero.

This data format provides over 1500 dB of dynamic range. The range of nonzero positive floating-point numbers is:

$N = [1 * 2^{-127}, [2 - 2^{-23}] * 2^{127}]$ inclusive.

The range of nonzero negative floating-point numbers is:

$N = [-[1 + 2^{-23}] * 2^{-127}, -2 * 2^{127}]$ inclusive.

The corresponding range for the magnitude of a floating point number N, in decimal, is approximately:

$$|N| = [5.87747E-39, 3.40282E38]$$

Fig. 6.4 shows the DR for DSP32C floating-point numbers as compared with the DR of 16- and 24-bit fixed-point devices.

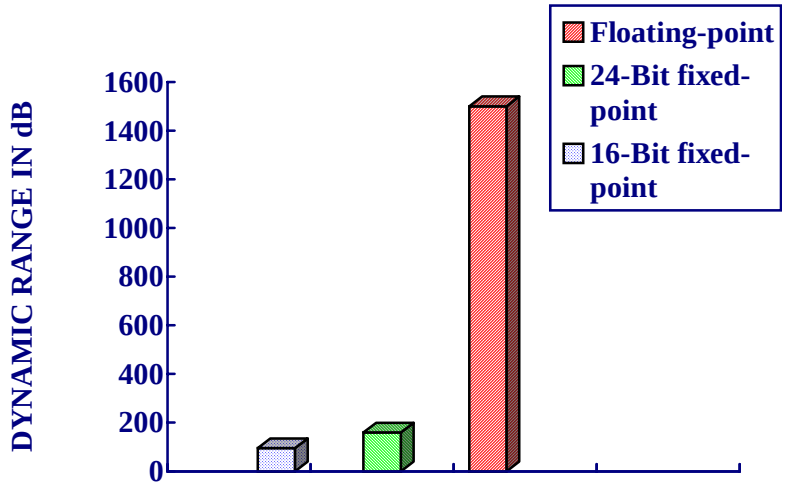

Figure 6.4 Dynamic range of fixed- and floating-point DSPs.

The DSP32C floating-point format provides 24 bits of precision at all magnitudes within the range of numbers represented by 24-bit mantissa and 8-bit exponent. The precision of a fixed-point number is a function of the word size and the magnitude of the number. Fig. 6.5 shows the bits of precision versus magnitude of a number for the DSP32C floating-point format, as well as 16- and 24-bit fixed-point devices.

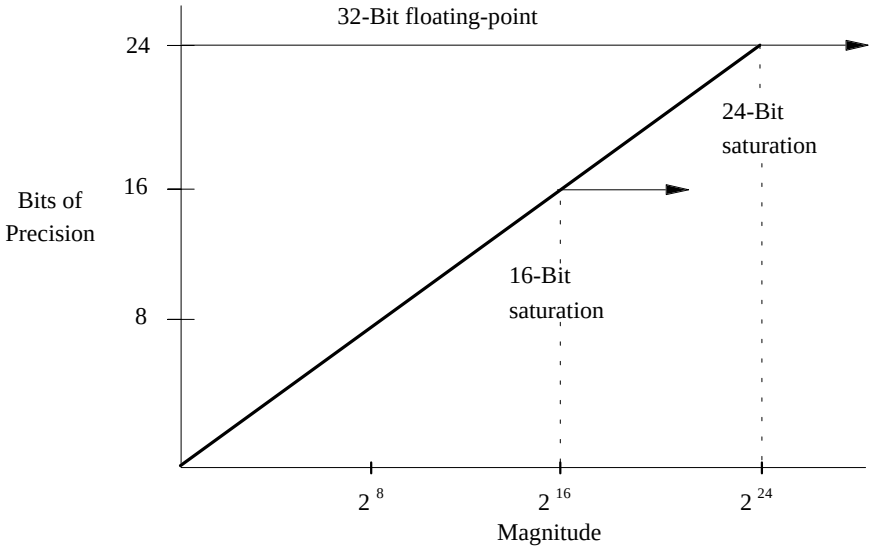

Figure 6.5 Precision of fixed- and floating-point DSPs.

Following this brief introduction to the processing environment, the test conditions for verification of the algorithms are described. For this purpose, two kind of test signals were used: one is a single frequency quadrature signal containing only one direction and the other is a narrow-band quadrature signal containing both directions. Two methods for generation of the quadrature test signals are described below.

6.3. GENERATION OF THE QUADRATURE TEST SIGNALS

In order to verify the algorithms described in Chapter 5, a continuous narrow band quadrature signal pair containing components corresponding to both directions was used. For this purpose the output of a wide-band analogue white noise generator was digitised and digitally processed to produce a quadrature pair. Then the digital quadrature signals were converted to analogue form via the D/A converters. The block diagram of the system is shown in Fig. 6.6.

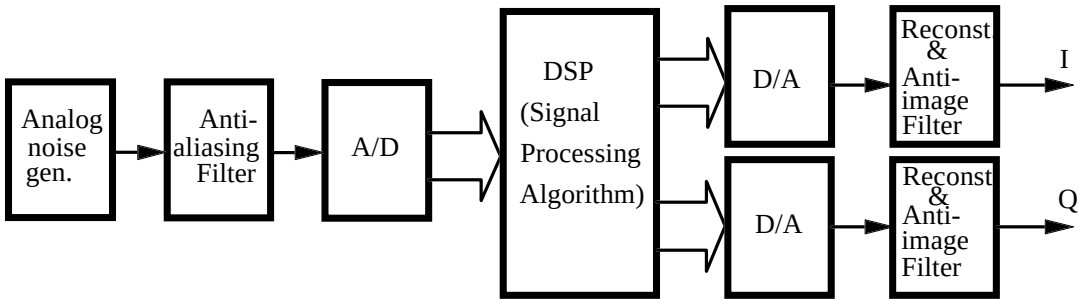

Figure 6.6 Block diagram for generation of the quadrature test signals.

The complex FFT spectrum of this quadrature pair is illustrated in Fig. 6.7 where the narrow-band signals occupy different frequency ranges and correspond to opposite directions of flow. This quadrature signal was processed using the methods described and the separated channels were recorded on digital audio tape. These results were monitored on a dual channel spectrum analyser by replaying the recordings.

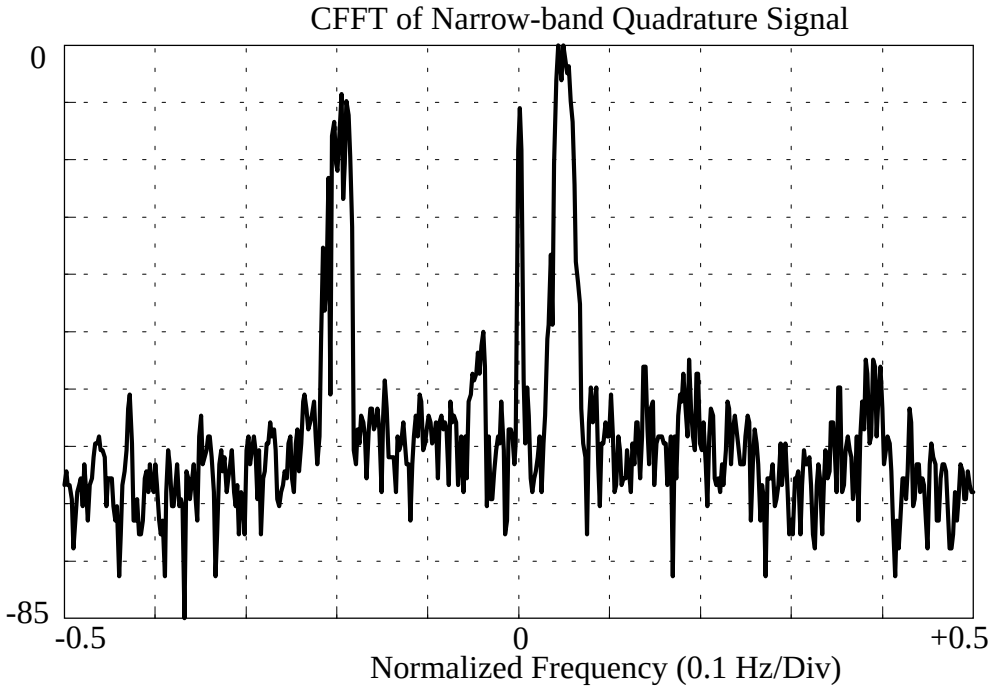

Figure 6.7 Complex FFT spectrum of the narrow-band quadrature test signal (8.5 dB/Div).

The DSP algorithms described in chapter 5 can be modified in order to generate narrow-band quadrature test signals. In this case, the spectral translocation method was modified to generate the quadrature test signal. Two other methods to generate a narrow-band quadrature test signal using DSP techniques are described in Appendix C. For the generation of the single frequency quadrature test signal, a low-pass/high-pass filter pair was used.

6.3.1. Quadrature test signal generation using the spectral translocation method

A block diagram of the algorithm is shown in Fig. 6.8. In this method, two narrow-band signals are obtained using a single arbitrary FIR filter and the phase relationship is manipulated in the frequency domain. The inverse FFT outputs are complex and quadrature.

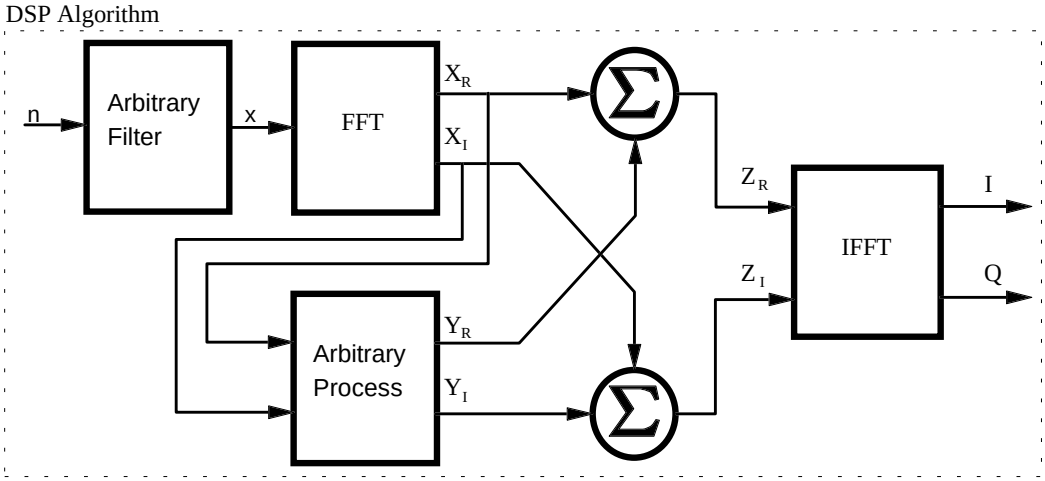

Figure 6.8 Narrow-band quadrature test signal generation using the STM.

The arbitrary filter is implemented using the FIR type design. A typical frequency response of the FIR type arbitrary filter is illustrated in Fig. 6.9.

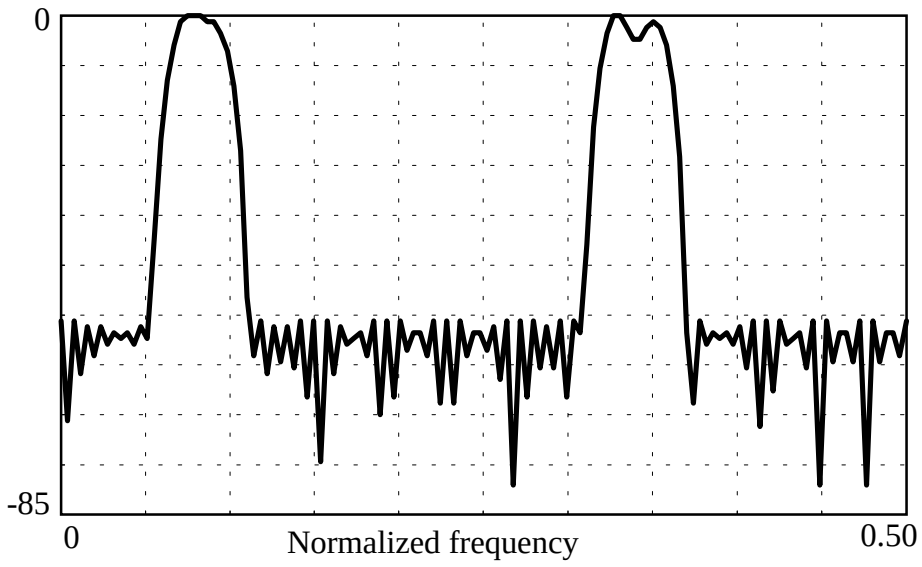

Figure 6.9 Frequency response of the arbitrary FIR filter (8.5 dB/Div).

In order to explain this method graphically, let the arbitrary filter output be

$$x(t) = A\cos\omega_1 t + B\sin\omega_2 t + C\cos\omega_3 t + D\sin\omega_4 t. \qquad 6.1$$

These components have been chosen to demonstrate how the phase information which is preserved in the signal spectra is manipulated to generate the desired quadrature test signal.

If the FFT is applied, the real and imaginary parts of Eq. 6.1 and subsequent arbitrary processes are depicted in Fig. 6.10. For both real and imaginary parts of the complex FFT result, the left hand side of the axis corresponds to negative frequencies and the right hand side to positive frequencies. In order to obtain the spectra given in Fig 6.10b from the spectra given in Fig. 6.10a, the magnitudes of the spectral lines in the less negative half of the negative frequencies and the more positive half of the positive frequencies of the real part, and the magnitudes of the spectral lines in the more negative half of the negative frequencies and the less positive half of the positive frequencies of the imaginary part are multiplied by **-1**.

Then the spectra given in Fig. 6.10c is obtained by adding the spectra given in Fig. 6.10a and 6.10b.

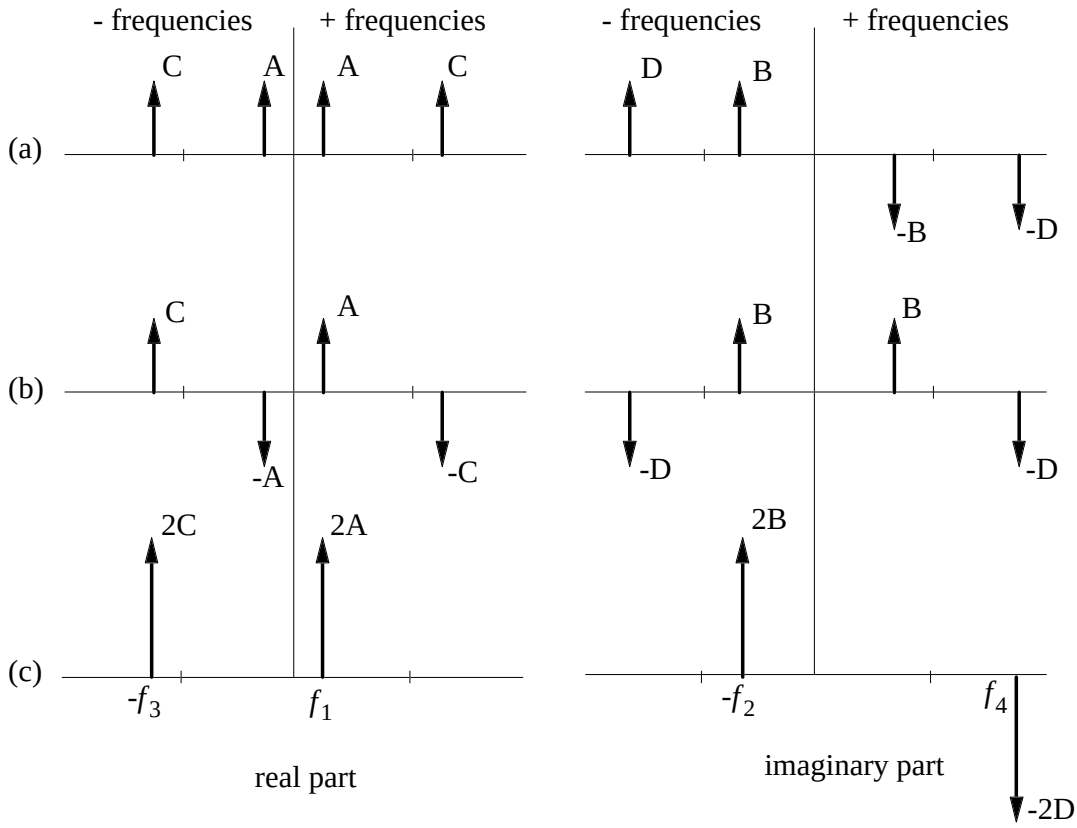

Figure 6.10 Graphical explanation of the narrow-band quadrature test signal generation using the STM: (a) X(f), (b) Y(f), (c) Z(f).

According to the properties of the complex Fourier transform, Fig. 6.10c represents the spectrum of the complex quadrature signal (Appendix B). We can conclude that the signals with frequency components f_1 and f_4 form one direction, the signals with frequency components f_2 and f_3 the other. So the time domain outputs are

$$I(t) = 2A\cos\omega_1 t + 2B\sin\omega_2 t + 2C\cos\omega_3 t + 2D\sin\omega_4 t$$
$$Q(t) = 2A\sin\omega_1 t + 2B\cos\omega_2 t - 2C\sin\omega_3 t - 2D\cos\omega_4 t \qquad 6.2$$

It is possible to produce very precise quadrature test signals using the DSP techniques to test quadrature Doppler systems but it requires an expensive DSP system.

6.3.2. Quadrature test signal generation using the high-pass/low-pass filter combination.

This method was mainly used to test the algorithms developed for spectral analysis (chapter 3).

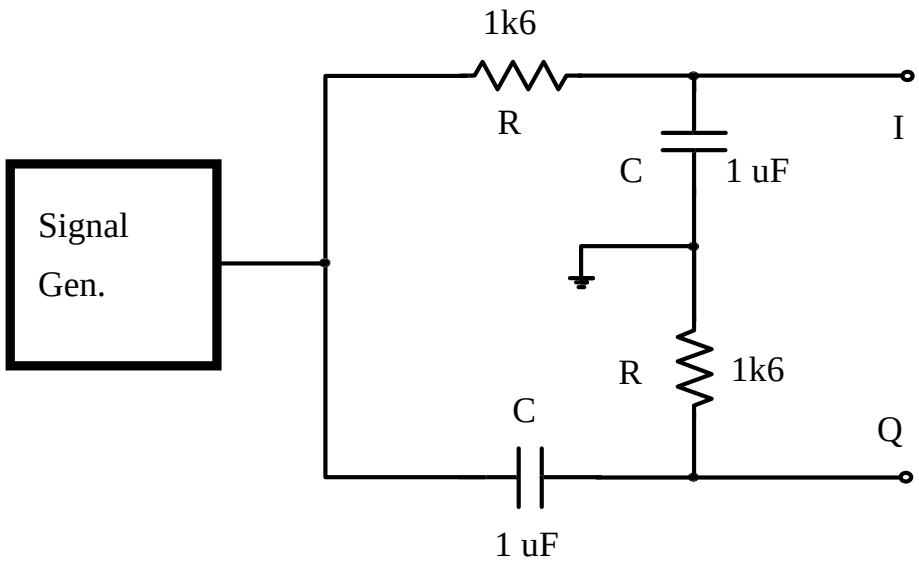

Figure 6.11 Single frequency quadrature test signal generation.

Fig. 6.11 shows a very simple single frequency quadrature test signal generator. A simple filter pair formed by RC high-pass and low-pass filters generates a quadrature signal pair for a certain frequency. At the cut-off frequency (3 dB point) the high-pass filter introduces $\mathbf{+45^{o}}$ and the low-pass filter $\mathbf{-45^{o}}$. The total phase difference is $\mathbf{90^{o}}$. It has the advantage of being very simple. But in practice, it is difficult to match the resistors and capacitors for the desired frequency. For a better

performance, the tolerances of the components must be as small as possible. Although we used it to test some of the algorithms, it is better to avoid using it.

Algorithms to obtain directional signals from a quadrature Doppler signal for spectral analysis and time domain outputs (which are suitable for tape recording) have been given in chapter 3 and 5 respectively. In the following sections, practical implementations will be presented with practical results. They will also be classified as time domain and frequency domain processing.

6.4. IMPLEMENTATION OF TIME DOMAIN PROCESSING FOR SPECTRAL ANALYSIS AND SEPARATED TIME DOMAIN OUTPUTS

Although a data length of $\mathbf{2^n}$ points was used in the implementations described here, this is not obligatory for time domain processing, and any data length satisfying real-time processing conditions can be used for the separated time domain outputs. Since the FFT routine is applied for spectral analysis, a data length of $\mathbf{2^n}$ points should be used or overlapping techniques (Oppenheim, 1975; Harris, 1982) employed.

6.4.1. Implementation of the phasing filter technique

The phasing filter technique (PFT) is based on a digital Hilbert transform (HT). The HT of a band limited signal can be obtained by convolving this signal with the impulse response of the HT. Digital implementation of the HT can be achieved most readily using FIR techniques (Rabiner and Schafer, 1974; Bateman and Yates, 1988). Details of the design of HT have been given by Gold et al., 1970; Oppenhaim and Schafer, 1975; Rabiner and Schafer, 1974 and Taylor, 1983.

A digital HT introduces a time delay. For the correct operation of the quadrature system, the delays in both channels must be equalised and thus a delay filter (DF) was implemented. The HT and DF were implemented using the filter design option of the Hypersignal DSP software package.

In this algorithm, improved specifications of the HT leads to an improved separation level. However this improvement is limited by the DSP microprocessor speed. The normalized impulse, frequency and phase responses and group delay of the HT and DF are shown in Fig. 6.12a. Fig. 6.12b illustrates the responses of another HT and DF pair showing better specifications with 100 dB stop-band attenuation and 0.5 dB pass-band ripple, but using more taps (93). In practice, no more than 70 to 75 dB is usually achievable. Our experiments indicate that the HT designed using the specifications listed in Table 6.1 is sufficient to provide a reasonable separation level, which is around 40 dB between two channels. Also in real time applications, it is important to keep computation time as short as possible.

Parameter	**Units**	**Hilbert T.**	**Delay F.**
Sampling freq.	Hz	16000	16000
Centre freq.	Hz	4000	4000
Bandwidth	Hz	7500	8000
Transition BW1	Hz	250	0
Transition BW2	Hz	250	0
Stop-band attn.	dB	40	40
Filter length	# of taps	37	37
Pass-band ripple	dB	1.5	1.5

Table 6.1 Specifications of the HT and DF used in the practical implementation.

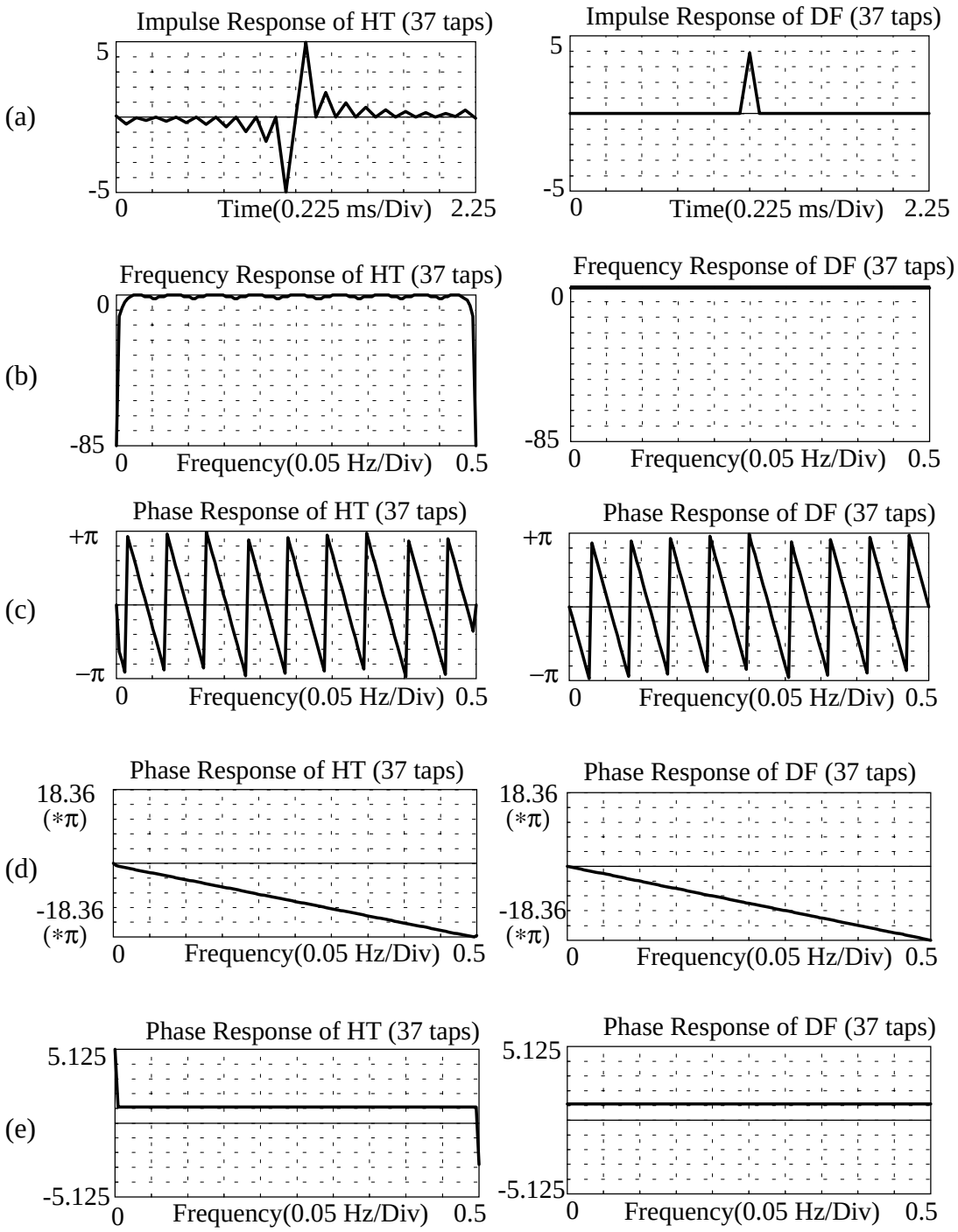

Figure 6.12a (a) Impulse (1 V/Div); (b) frequency (8.5 dB/Div); (c) phase (wrapped); (d) phase (unwrapped) responses and (e) group delay (1.025 ms/Div) of the Hilbert transform and delay filter with 37 taps.

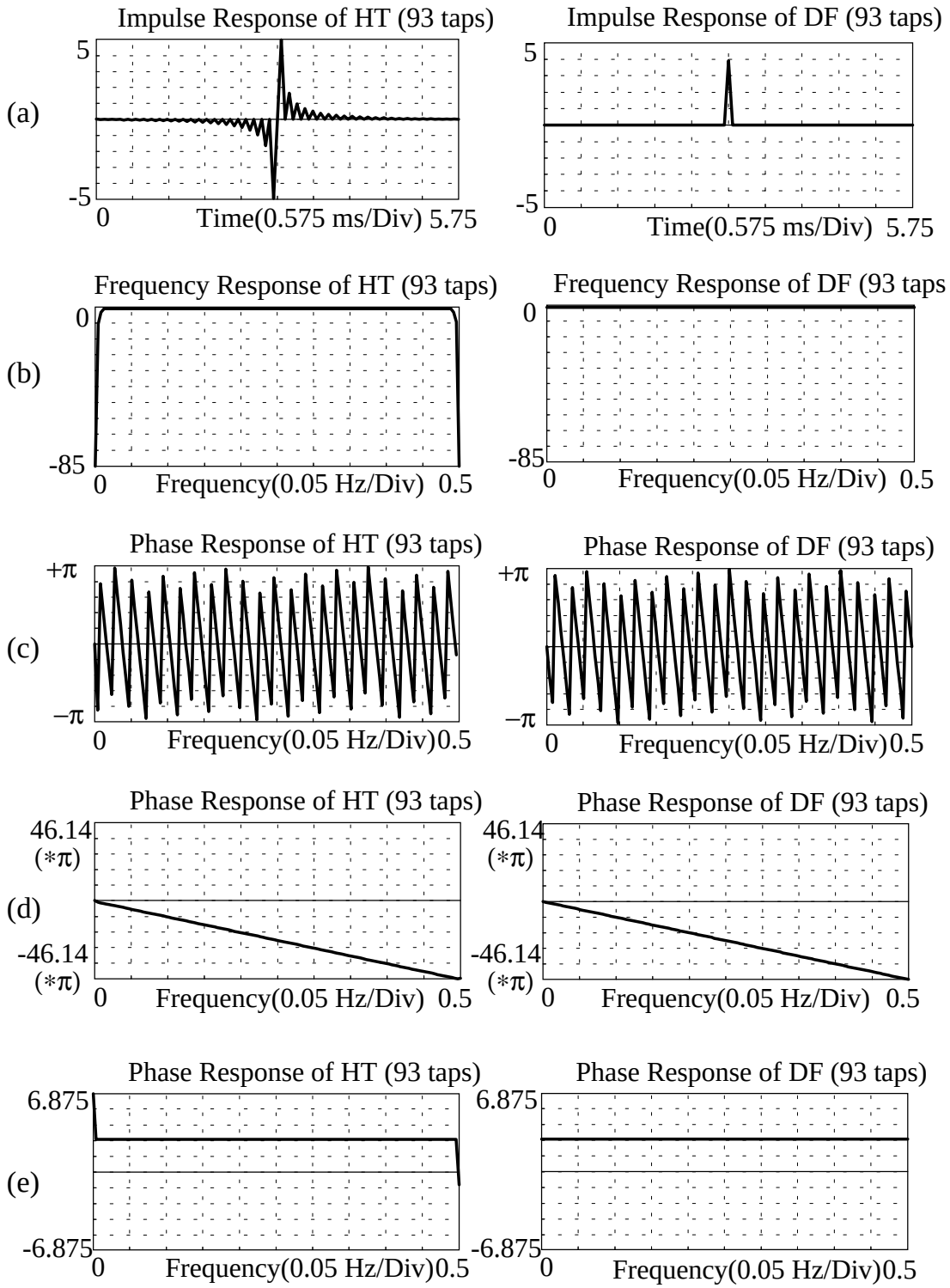

Figure 6.12b (a) Impulse (1 V/Div); (b) frequency (8.5 dB/Div); (c) phase (wrapped); (d) phase (unwrapped) responses and (e) group delay (1.025 ms/Div) of the Hilbert transform and delay filter with 93 taps.

Fig. 6.13 shows the actual output of the asymmetrical PFT implemented using the HT filter with 37 taps when a single frequency quadrature test signal (1 kHz signal with a magnitude of 1 V) is applied. This is an output of a 6 channel real time digital oscilloscope implemented in software on a personal computer. ***D*** and ***Q*** are sinusoidal quadrature signals digitised by the on-board A/D converters. The data length is 512 points for each channel. ***D_H*** and ***Q_D*** stand for the outputs of the HT and DF respectively. It can be clearly seen that the phase difference between ***D_H*** and ***Q_D*** is $\mathbf{180^0}$ because the HT filter introduces $\mathbf{90^0}$ phase shift into the in-phase component ***D***. The last two traces show the separated outputs in the time domain. Output y_r is almost twice the input magnitude and y_f is very small (at least 40 dB down). This practical result confirms the mathematical and simulation results presented in earlier chapters. The output spectra of the system plotted on a logarithmic scale are shown in Fig. 6.16a.

Fig. 6.17a shows the results of the same system but with more taps (93) when the narrow-band quadrature signal whose spectra given in Fig. 6.7 is applied to the inputs.

6.4.2. Implementation of the Weaver receiver technique and extended Weaver receiver technique

The Weaver receiver technique (WRT) has been implemented to produce a frequency domain display for spectral analysis rather than time domain outputs. The extended Weaver receiver technique (EWRT) is an extension of this method to produce totally separated time domain outputs.

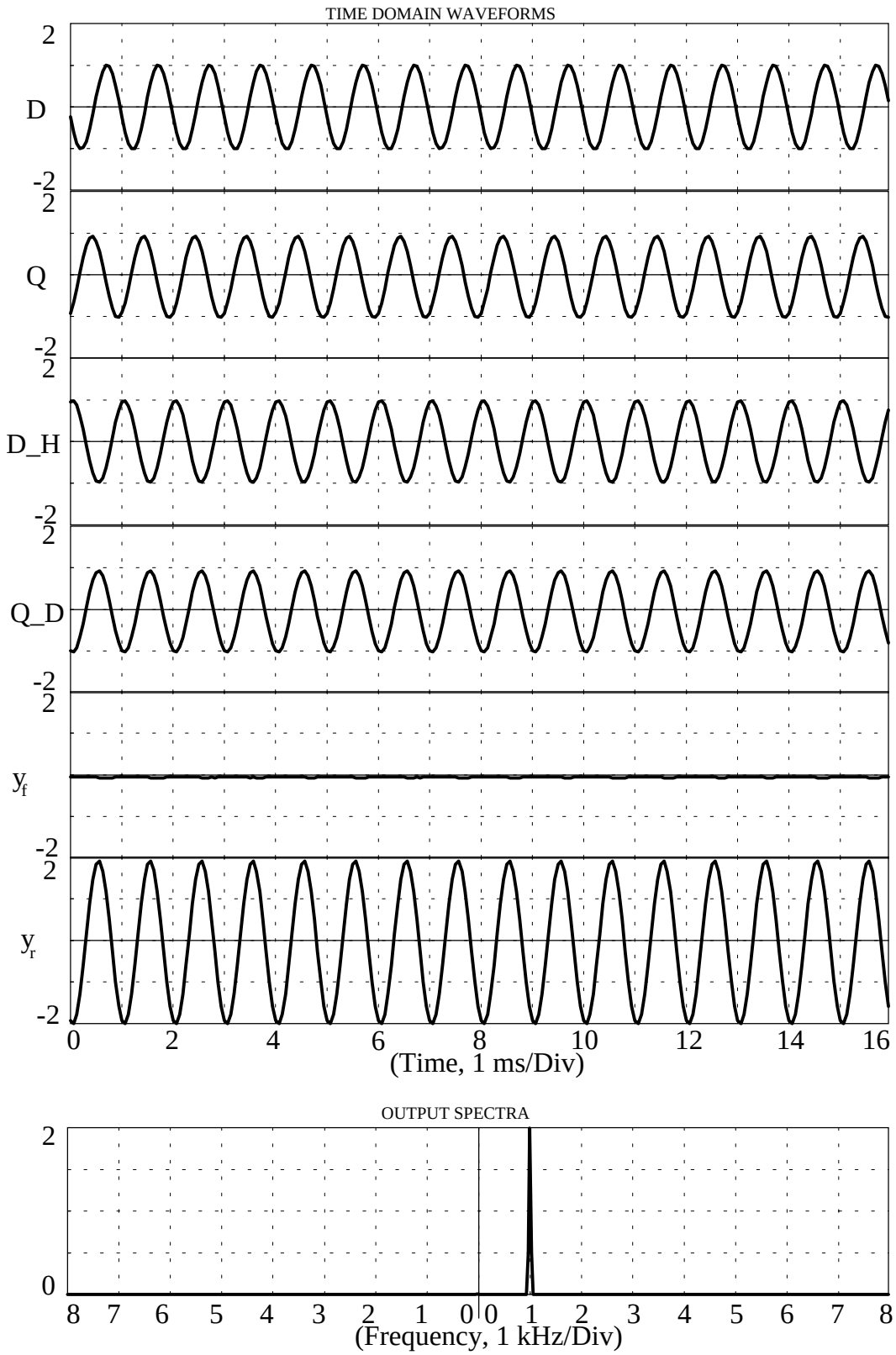

Figure 6.13 Time domain display of each processing stage and output spectra of the asymmetrical PFT implemented practically (magnitude scale is 1 V/Div).

For implementation of the WRT, 1024 data points were used for each channel instead of 512 in order to use the full screen width of the computer display after performing the real FFT. The frequency of the input quadrature signal was set to 1 kHz and the magnitude to 1 V. The quadrature data were captured by the DSP board and mixed with the digitally generated 4 kHz quadrature pilot frequency signal. The outputs of the digital mixers ***X*1** and ***Y*1** were than summed. The output (***X*2**) is directional around the 4 kHz pilot frequency signal. Here the process is similar to SSB modulation. The waveforms at all processing stages are illustrated in Fig. 6.14, where ***D*** and ***Q*** stand for the quadrature input signals, ***P*1** and ***P*2** for the quadrature pilot frequency signals, ***X*1** and ***Y*1** for the modulated signals and ***X*2** for the SSB (directional) output signal.

The number of samples for the pilot frequency signal should be equal to that of the input quadrature signal. For example if 256 data points are sampled by the A/D converter, then 256 complex data samples must be generated for the pilot frequency signal. In order to minimise cross-talk and avoid possible aliasing, the pilot frequency signal should ideally be set to $\boldsymbol{F_s / 4}$, however, it is perfectly valid to use other frequencies provided that they do not cause aliasing which results in misinterpretation of the signal spectra.

Digital quadrature sinusoidal signal generators are more precise than their analogue counterparts, but their word length is finite which produces rounding errors which change both the amplitude and frequency of the generated signal. Improving the performance of digital sinusoidal oscillators has been investigated by Abu-El-Haija and Al-Ibrahim (1986). More discussion of digital sinusoidal oscillators can be found in (Furuno *et. al* 1975) and (Fliege and Wintermantel 1992). The resultant output spectrum of this method is shown in Fig. 6.16b.

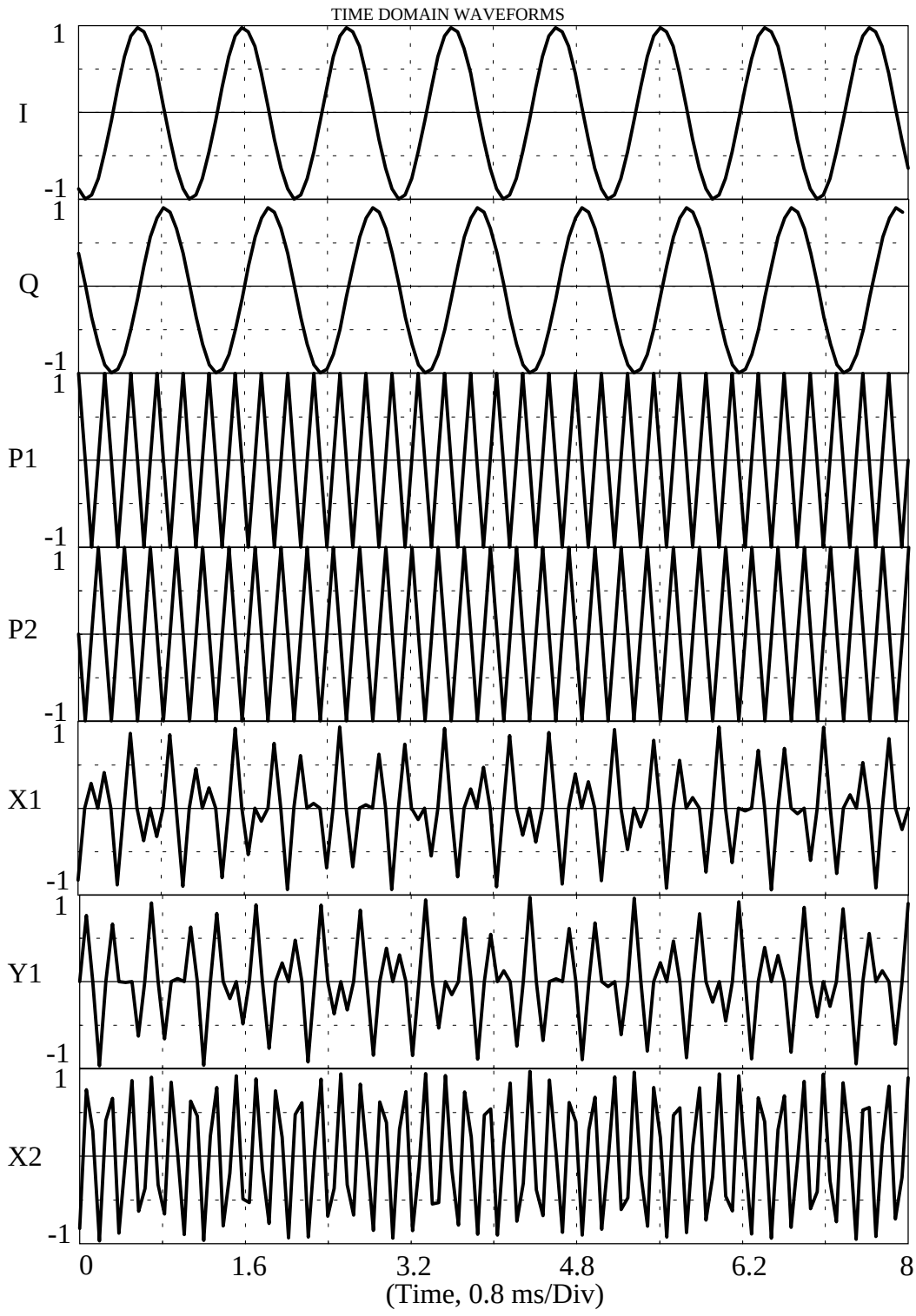

Figure 6.14 Time domain display of each processing stage of the WRT implemented practically (magnitude scale is 0.5 V/Div).

For implementation of the EWRT, some extra processes must be performed. As an example, the asymmetrical EWRT produces two SSB signals after the first mixing stage. The upper side-bands are removed by the low-pass filters. After filtering, the forward and reverse signals are separated, but are still modulated with the pilot frequency and so they must be translated down to the base-band. The second mixing stage implements this translation as explained in chapter 5. The outputs of the mixers contain higher frequency signals as well as base-band signals, so the higher frequency components are filtered out by the last filtering stage.

Since a linear phase response is not required, the filters were implemented using an IIR structure which enabled the design of faster filters. The cut-off frequency of the filters must be equal to the pilot frequency signal. The transition bandwidth should be kept as narrow as possible. As an example, in our implementation the low-pass filters provide at least 40 dB attenuation at a frequency of $(f_s/4)+(f_s/400)$

In this particular application the sampling frequency was set to be 40.96 kHz and the frequency of the pilot frequency signal and filter cut-off frequencies were 10.24 kHz. The normalized frequency response of a 12th order elliptical low-pass filter which is used in the implementation is shown in Fig. 6.15. Notice that the decline of the frequency response is extremely sharp. This would not have been possible with analogue processing.

The spectra of the directional signals produced by the EWRT are illustrated in Fig 6.17b when the narrow-band quadrature signal described above is applied to it.

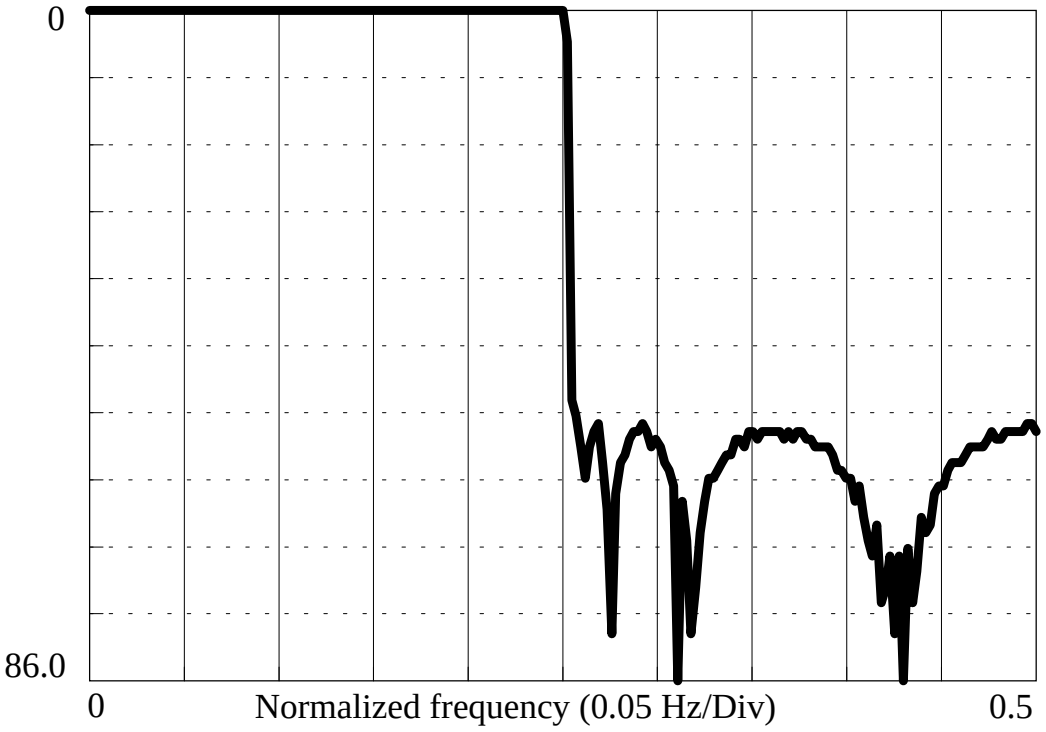

Figure 6.15 Normalized frequency response of 12th order IIR filter used in the implementation of the EWRT (frequency scale is 8.6 dB/Div).

6.5. IMPLEMENTATION OF FREQUENCY DOMAIN PROCESSING FOR SPECTRAL ANALYSIS AND SEPARATED TIME DOMAIN OUTPUTS

As their name implies, these signal processing functions are performed in the frequency domain. The common step for all such frequency domain processing methods is the FFT which uses a data length defined by 2^{n}, where n is the FFT order. It should be pointed out that overlap techniques should be used for time domain outputs to avoid discontinuities caused by the edge effects (Oppenheim and Schafer 1975, Harris 1982).

For the directional frequency domain output (i.e., the sonogram) one complex FFT is sufficient when the input signal is in quadrature. However, at least one extra process such as inverse FFT is necessary for the time domain outputs.

6.5.1. Implementation of Hilbert transform method

The implementation of the Hilbert transfer method (HTM) is based on Eq. 5.37 which is the ideal frequency response of the HT. An ***M*** element complex discrete time domain signal must be converted into the frequency domain using an ***N*** point complex FFT, where ***N*** must be greater than ***M*** to use overlap techniques as mentioned above.

The complex FFT result is a complex frequency domain signal containing real and imaginary parts where the phase information is preserved. Applying Eq. 5.37 to this frequency domain signal produces a complex frequency domain signal which is equal to the complex FFT of the HT of the original input signal. The inverse FFT of the new frequency domain signal gives the HT of the input complex discrete time domain signal. After scaling, simple additions give the separated outputs. Because of the scaling problems after the inverse FFT, two inverse FFTs may be necessary for fixed point DSPs. Since floating point DSPs have a huge dynamic range (over 1500 dB) one inverse FFT is sufficient.

The response of the system when the narrow-band quadrature signal is applied to it is shown in Fig. 6.17c.

An alternative implementation of the HT in the frequency domain is to use multiplication in the frequency domain instead of the time domain convolution employed in the PFT realisation. This is performed by taking the FFT of the FIR HT filter impulse response once and storing the result. Then this result and the complex FFT of the input signal are multiplied to produce the complex FFT of the HT of the input signal. The same process as described above is then performed.

6.5.2. Implementation of complex FFT

For the frequency domain display, a 512 point complex quadrature signal was digitised by the DSP board and placed in the on-board memory. These data were then windowed using a complex Hanning window routine. Finally the 512 point complex FFT was implemented using a complex FFT routine. The result is complex and directional as explained in chapter 3. The resultant data are rearranged for display on the screen and sent to the PC. The output of this system in the frequency domain is illustrated in Fig. 6.16c. when a single frequency quadrature signal (1 kHz, 1 V) is applied to it.

In this method the separation is in the frequency domain and therefore there are no direct separated time domain outputs. However, the separated time domain signals can be derived as described in chapter 5. The implementation of the further processing is based on the properties of the complex FFT which is straightforward, but again overlapping is necessary in practice to overcome the discontinuity problem caused by data segmentation. The real-time implementation steps can be summarised as follows:

1. ***N*/4** points of data are captured from each channel (D&Q) by the DSP board;
2. These data are added to **3*N*/4** points of the most recent data to obtain an overlapped ***N*** point data block for each channel;
3. The two ***N*** point data blocks are taken as the real and imaginary input parts to calculate the complex FFT;
4. With the complex FFT results (Eq. 5.46), the necessary processing (Eq. 5.47-Eq. 5.51) is done to separate the information of forward and reverse channels;
5. The two N point inverse FFTs are calculated using Eq. 5.48, 5.50 and Eq. 5.49, 5.51 as the real and imaginary parts respectively.
6. The middle N/2 point data of each of the inverse FFTs are output to a D/A converter so that there is no discontinuity in the output signal;

7. The processing from step one is repeated until an interruption is received.

The steps 1-7 do not represent the time sequence of the implementation. For example, the capturing of the quadrature signals, the outputting of the directional signals and the calculation of the FFTs are carried out simultaneously in practice.

The output spectra of the system for the quadrature narrow-band signal described above are shown in Fig. 6.17d.

6.5.3. Implementation of the spectral translocation method

The implementation of the spectral translocation method (STM) is an application of the properties of the complex FFT. The process is depicted in Fig. 5.10. In order to apply this process correctly, the complex FFT output format for a particular DSP microprocessor must be considered. The output format of a ***N*** point complex FFT (real and imaginary) routine performed on the DSP32C is given in Table 6.2.

	zero frq.(dc)	positive frqs.	nyquist frq.	negative frqs.
real	R(0)	R(1),...,R($\frac{N}{2}-1$)	R($\frac{N}{2}$)	R($\frac{N}{2}+1$),...,R(N-1)
imag.	I(0)	I(1),...,I($\frac{N}{2}-1$)ı	I($\frac{N}{2}$)	I($\frac{N}{2}+1$),...,I(N-1)

Table 6.2 ***N*** point complex FFT output format for the DSP32C.

Since the process is discrete, the output of a ***N*** point complex FFT routine done on the DSP32C can be defined as:

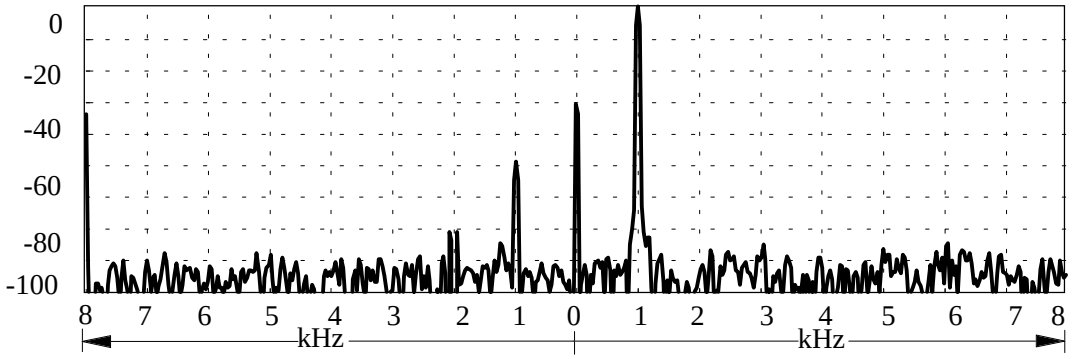

(a) Output spectra of Phasing-Filter Technique

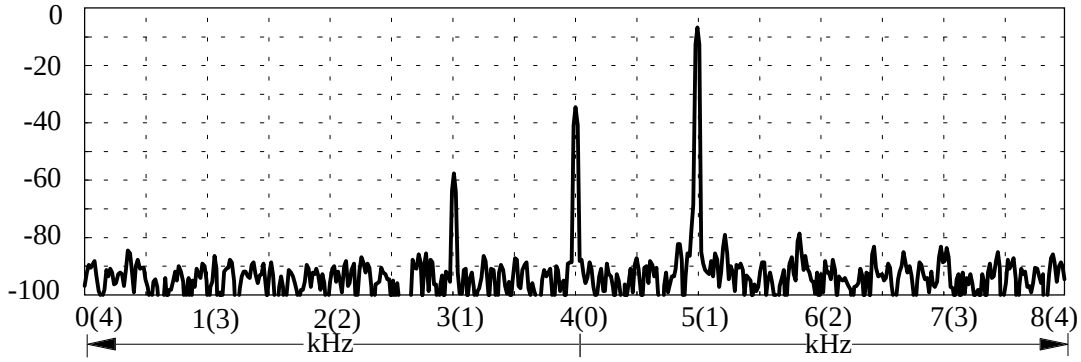

(b) Output spectrum of Weaver Receiver Technique

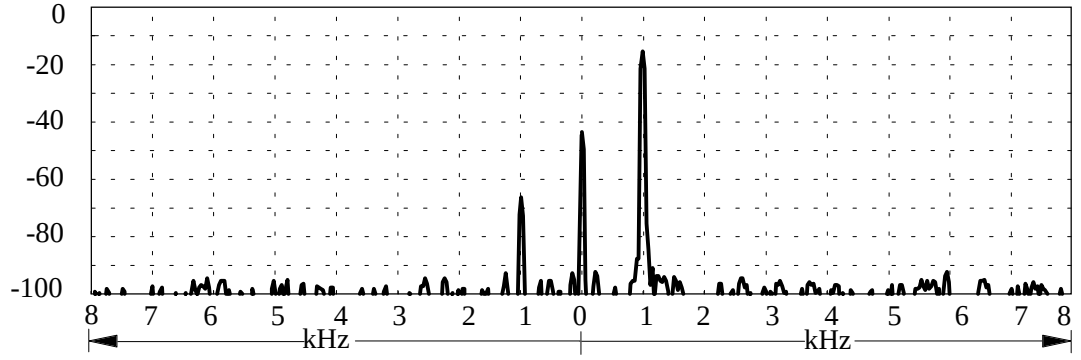

(c) Output spectrum of Complex FFT

Figure 6.16 Results for frequency domain separation techniques. Comparative logarithmic scale output spectra of practical implementations for; (a) the PFT; (b) the WRT; (c) the complex FFT (magnitude scale is 10 dB/Div).

$$S_R(k)=\begin{cases} S_R^+(k), & k=0 to \frac{N}{2}-1 \\ S_R^-(k), & k=\frac{N}{2} to N-1 \end{cases} \text{ and} \qquad 6.3a$$

$$S_I(k)=\begin{cases} S_I^+(k), & k=0 to \frac{N}{2}-1 \\ S_I^-(k), & k=\frac{N}{2} to N-1 \end{cases} \qquad 6.3b$$

This is a complex data array and the first bin of the array corresponds to the zero frequency, the bin number of **N/2** to the Nyquist frequency , the bin numbers up to **N/2** correspond to the positive and the rest of the bins to the negative frequencies. Applying the spectral translocation process to the data array given by Eq. 6.3 will result in:

$$X_R(k)=\begin{cases} -S_R^-(N-k), & k=1 to \frac{N}{2}-1 \\ +S_R^+(N-k), & k=\frac{N}{2}+1 to N-1 \end{cases} \text{ and} \qquad 6.4a$$

$$X_I(k)=\begin{cases} +S_I^-(N-k), & k=1 to \frac{N}{2}-1 \\ -S_I^+(N-k), & k=\frac{N}{2}+1 to N-1 \end{cases} \qquad 6.4b$$

Implementing additions as described in chapter 5 gives a new data array:

$$\begin{aligned} \boldsymbol{_R(k) = S_R(k) + X_R(k), \quad k = 0 \ \ to \ \ N-1} \\ \boldsymbol{_I(k) = S_I(k) + X_I(k), \quad k = 0 \ \ to \ \ N-1} \end{aligned} \qquad 6.5$$

The final step is to take the inverse FFT whose output is time domain complex signal. The real part of it is one direction and the imaginary part the other. The output spectra of the system for the quadrature narrow-band signal described above are shown in Fig. 6.17e.

6.6. SUMMARY AND COMMENTS

6.6.1. Separation for spectral analysis (frequency domain output)

The implementation of three different method for the separation of forward and reverse flow signals in an ultrasonic Doppler system have been described. The processing platform was a powerful 32-bit floating point digital signal processor capable of processing signals at up to 150 kHz in real time.

The PFT is based on a HT and the forward and reverse outputs are totally separated. Because the output consists of two separated channels, a dual channel spectrum analyser is required, i.e., two real FFT routines must be implemented to obtain the output spectra. The output signal bandwidth is limited by the HT frequency response. In our case, the bandwidth is 7500 Hz for each channel. Output spectra of this system have been illustrated in Fig. 6.16a. Here, two channels were displayed side by side as one display. The execution time for the real FFT (including the routine call) is 0.976 ms for 512 data points. The total processing time required by the DSP chip to perform all processing tasks (2 filters, 2 Hanning windows and two FFTs) is 13.25 ms.

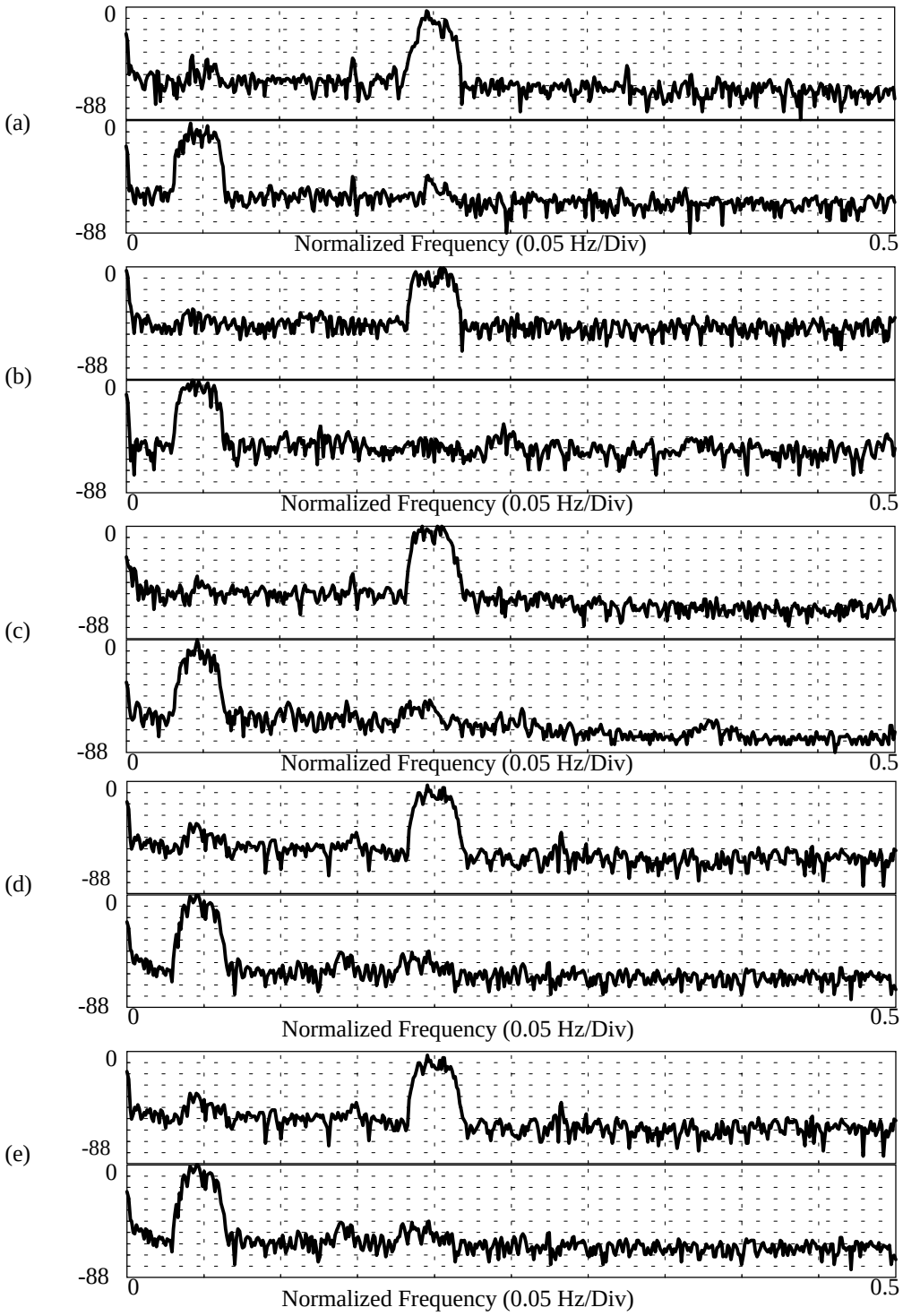

Figure 6.17 Results for time domain separation techniques. Logarithmic scale output spectra of practical implementations for; (a) PFT; (b) EWRT; (c) HTM; (d) complex FFT; (e) STM when the input is a narrow band quadrature signal containing the forward and reverse flow components (magnitude scale is 8.8 dB/Div).

The WRT is based on the SSB modulation method described by Weaver (1956). The output is a LSB or an USB around a fixed quadrature pilot signal frequency, depending on the combination of the real and imaginary parts of the quadrature input signal. The output is one channel and requires only one real FFT routine to obtain the output spectrum, but the bandwidth for forward and reverse flow signals is half of the full range ($\boldsymbol{f_s/4}$). Fig. 6.16b illustrates output spectrum for this system when the input is a 1 kHz complex quadrature signal and the pilot signal frequency is 4 kHz. The execution time for the real FFT (including the routine call) is 2.085 ms for 1024 data points. The total processing time (including the signal generation, the mixing, the windowing and the FFT) is 10.3125 ms. Notice that 1024 data samples were used to obtain this result. When 512 samples were used, the total processing time was 5 ms.

Fig. 6.16c shows the output spectrum of the complex FFT when the input is a 1 kHz complex quadrature signal. Separation is totally in the frequency domain and so no direct separated time domain output can be obtained using this method. However, further processing may be applied in order to obtain totally separated time domain outputs. The execution time for the complex FFT routine (including the routine call) is 1.778 ms for 512 data points. The total processing time is 5.0625 ms.

The processing speeds of these techniques can be increased by decreasing the data length and optimising the DSP32C source code. When 512 data samples were used for these implementations, the WRT was the fastest. Table 6.3 shows the total processing times required by the AT&T DSP32C processor to perform all real-time processing tasks for several data lengths.

Data length	1024	512	256	128	64	
Total	26.6875	13.25	6.5625	3.25	1.5625	**PFT**
processing	10.3125	5.001	2.4375	1.1875	0.5625	**WRT**
time (ms)	10.50	5.0625	2.4375	1.1875	0.5625	**CFFT**

Table 6.3 Total processing times required by the DSP chip for the separation in frequency domain. PFT: Phasing filter technique; WRT: Weaver receiver technique; CFFT: Complex FFT.

6.6.2. Separation for time domain output

The implementations of the derivation of the separated time domain signals from a band limited quadrature signal have been described. It has been shown that DSP methods make it possible to implement techniques such as EWRT and complex FFT to obtain the separated time domain outputs. All the methods described are able to process Doppler signals with frequencies of upto 15 kHz in real time when a DSP board based on the AT&T DSP32C DSP chip is used as the processing platform. Although the execution times may be decreased by optimizing the DSP code, the real-time execution speeds of our implementations are summarised in Table 6.4.

A narrow-band quadrature noise signal containing components representing both flow directions was used to test the methods by first recording the separated outputs on stereo tape, then playing them back and observing them on a dual channel spectrum analyser. The spectra of the signals produced by the five systems are illustrated in Fig. 6.17. The performances of all the methods are very similar. In fact, since floating point DSPs offer the implementation of near ideal systems, the limitations on the performances of digital techniques are defined by external conditions such as the anti-aliasing and reconstruction filters.

method	**data length**	**sampling frq.**	**execution time**
EWRT	512	40.96 kHz	7.5 ms
PFT	256	20.48 kHz	8.9 ms
CFFT	256	20.48 kHz	8.5 ms
HTM	256	20.48 kHz	9.5 ms
STM	256	20.48 kHz	9.3 ms

Table 6.4 Total processing times required by the DSP chip for the separation in time domain. PFT: Phasing filter technique; EWRT: Extended Weaver receiver technique; CFFT: Complex FFT; HTM: Hilbert transform method; STM: Spectral translocation method.

The PFT is more suitable for fixed point processors since it employs FIR type filters. It also requires less memory to record the quadrature Doppler signal. The main limitation of the PFT is the bandwidth of the HT filter response. The separation level can be increased by increasing the filter specifications, but this will cause an increase in the execution time of the algorithm. Since this method implements a time domain convolution, the input data length does not have to be fixed to $\mathbf{2^n}$.

The EWRT utilises modulation techniques and very sharp digital filters. It gave the fastest execution time. However, the Doppler signal must be band-limited to $\boldsymbol{f_s/4}$. This implies that the required memory space to record a digitized quadrature Doppler signal is twice that required by the other methods. The performance of the algorithm also depends on the accuracy of the quadrature pilot frequency signal generated digitally. Only one real FFT is required to display the separated frequency domain signal while it outputs totally separated time domain signals. When a floating point processor is used this appears to be the best method. Again,

since the process is done in the time domain, the input data length does not have to be fixed.

Since the performances of the frequency domain processing methods based on the applications of the FFT properties (complex FFT, HTM and STM) rely entirely on the FFT resolution, it is better to use them with faster processors to implement higher resolution complex FFTs. Using larger FFT sizes leads to finer resolution results. However, the discontinuities caused by the Gibbs phenomenon must be avoided by applying overlapping or zero padding techniques. This implies that the FFT length must be longer than the input data length.

Although there are minor differences between the performances of the five algorithms, the simulated and practical results show that all the methods give satisfactory results, so the method of choice will depend on the details of the implementation platform.

7. THE EXTRACTION OF MAXIMUM AND MEAN FREQUENCY ENVELOPES FROM THE SONOGRAMS AND CALCULATION OF INDICES

7.1. INTRODUCTION

Doppler shift signals obtained using one of the methods described previously have no quantitative meaning without further interpretation. An experienced observer can identify the nature of blood flow qualitatively by listening to Doppler shift signals or looking at the sonogram of the signal. Since qualitative interpretation relies on the expertise of the user and is subject to observer bias, considerable previous work has been carried out to develop objective methods to interpret Doppler shift signals. Most of these objective (quantitative) methods concentrate on detecting an envelope of the sonogram and developing some frequency indices which are independent of the angle between the Doppler probe and blood vessel.

Two such envelopes are the maximum frequency envelope, which is directly proportional to the maximum velocity of the red blood cells in the ultrasonic beam path and the mean frequency envelope which is proportional to the mean flow velocity. Both waveforms have found important applications in the quantitative diagnosis of vascular disease, since both are affected by stenoses. Extraction of these envelopes is described below.

7.2. THE EXTRACTION OF THE MEAN FREQUENCY ENVELOPE

Since the mean frequency envelope is proportional to the mean velocity of flow in the target blood vessel, it has been found useful in the assessment of vascular

disease. The intensity weighted mean frequency envelope (IWMFE) is the most widely used and is defined by:

$$\bar{f}(t) = \int_f P(f)\, f df \Big/ \int_f P(f) df \qquad 7.1$$

where ***P(f)*** is the Doppler power spectrum.

The IWMFE can be derived using continuous time analogue techniques (Arts and Roevros 1972, Roevros 1974, DeJong *et al* 1975, Gerzberg and Meindl 1977, 1980a, 1980b, Evans *et al* 1987) or discrete time domain equivalents of analogue techniques (Angelsen and Kristoffersen 1983, Kristoffersen and Angelsen 1985, Barber *et al* 1985). However the widespread use of real time digital spectrum analysers has given rise to a numerical frequency domain evaluation of equation 7.1 (Prytherch *et al* 1985, Kontis 1987, Schlindwein *et al* 1988) given by:

$$\bar{f} = \sum_{f=1}^{N} A_f^2\, f \Big/ \sum_{f=1}^{N} A_f^2 \qquad 7.2$$

where ***N*** is the number of frequency intervals used in the spectral analysis of the Doppler signal and $\boldsymbol{A_f}$ is the amplitude of the signal with Doppler frequency ***f***. More detailed discussion on this subject can be found in Evans *et al* (1989a) and a numerical comparison of performance for five mean frequency estimators is given by Sirmans and Bumgarner (1975).

7.3. THE EXTRACTION OF THE MAXIMUM FREQUENCY ENVELOPE

Interest in obtaining the maximum frequency envelope (MFE) from the Doppler sonogram first appeared in the work of Gosling *et al* (1969, 1971) as a means of improving the estimation of pulsatility index. The output of the MFE follower is not

significantly influenced by ultrasonic beam shape, not affected by the wall thump filters, and has higher noise immunity than the mean frequency follower (Evans *et al* 1989a). For these reasons the maximum frequency follower has gained widespread clinical acceptance.

7.3.1. Description of the maximum frequency envelope detection methods

Although hardware implementations have been reported (Sainz *et al* 1976, Skidmore and Follet 1978, Johnston *et al* 1978, Nowicki *et al* 1985) nowadays almost all implementations are based on fast Fourier transform analysis of Doppler shift signals (Gibbons *et al* 1981, Prytherch and Evans 1985, D'Alessio 1985, Nowicki and Marasek 1991). There are several methods used to extract the MFE from Doppler sonograms numerically (Mo *et al* 1988). Amongst them are the percentile method, the simple threshold method, the modified threshold method, and the modified geometric method.

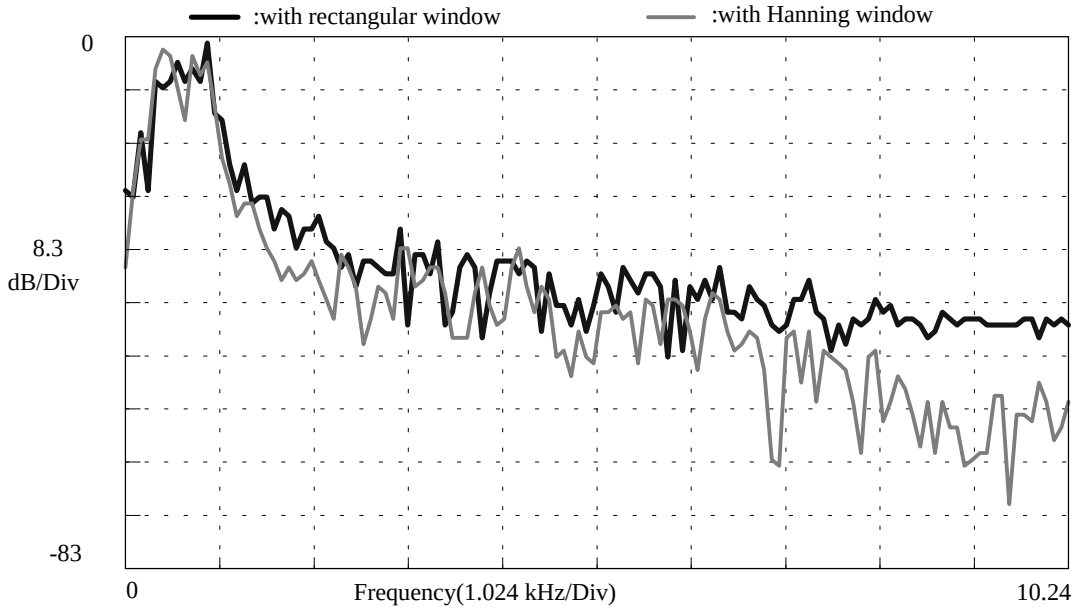

Figure 7.1 Doppler signal spectra obtained from the carotid artery using rectangular and Hannig window.

Fig 7.1 illustrates typical spectra of a short Doppler signal segment obtained from the carotid artery using both a rectangular window and a Hanning window. They give information about the intensity of the combined signal and noise components. MFE detectors have to find the transition level between the signal and noise regions. This corresponds to the highest frequency present in the signal.

7.3.1.1. Percentile method

This method depends on the integrated Doppler signal spectrum and is given as

$$\Phi(f_{max}) = \frac{(100-\alpha)}{100}\Phi_T \qquad 7.3$$

where Φ_T is the total signal-plus-noise power and α is a chosen parameter whose optimum value depends on the signal to noise ratio (SNR) and signal bandwidth, and between 2 and 5% provides a reliable estimate of the MFE for high SNR (Mo *et al* 1988).

7.3.1.2. Simple threshold method (STM)

Gibbons *et al* (1981) proposed the use of an arbitrary threshold to detect the transition mentioned above. This threshold is increased or decreased by the user through the computer keyboard according to his/her evaluation of the quality of the resulting MFE. Having found the threshold that produces the best performance this is kept constant within a particular segment of signal. An algorithm which seeks to automate the threshold selection has been described by Evans *et al* (1989b).

7.3.1.3. Modified threshold method (MTM)

This method is based on D'Alessio's algorithm (1985). The method considers that the tail of the Doppler spectra gives information on the level of the noise present in the signal since white noise is equally spread over all frequencies. An estimation of the noise level is made in the tail of the spectrum and then used for setting a threshold. The magnitude of each of bin of the spectra (scanning from the upper to the lower frequency bins) is compared with the threshold and when the magnitudes of two successive bins are larger than the threshold, the first bin is labelled as the maximum frequency bin. The application of this method for each column of the sonogram allows the determination of a threshold that dynamically adapts to the SNR.

This method assumes that a rectangular window is applied to the Doppler signal. However this window introduces large side-lobes (Harris 1987) and therefore it is not frequently used. When other windows are applied to the sampled Doppler signal, there is a smoothing of the noise present in the tail of spectra (Fig. 7.1 - Hanning window) and based on its level, a higher threshold needs to be set for the MFE detection. To determine this threshold, the noise estimation is multiplied by a constant that is empirically chosen for the system in use (Mo *et al* 1988). It should be noted that in either situation, the noise estimation is also affected by the anti-aliasing filter characteristics.

With the MTM the signal must not be present in the tail of spectra where the noise magnitude is estimated. This can cause difficulties with fixed length FFT systems because the Doppler spectrum must be confined to the lower part of the spectrum, requiring the use of a higher sampling frequency. This implies a poorer resolution which will give less accuracy in the maximum velocity estimation.

7.3.1.4. Modified geometric method (MGM)

Nowicki and Marasek (1991) proposed a method in which the maximum frequency for each column of the sonogram is estimated on the basis of the shape of its integrated spectrum curve (ISC). Fig. 7.2 shows a typical Doppler spectra and its ISC given by the curve GED. The maximum frequency of the spectra is assumed to correspond to the point where the perpendicular distance between the ISC and a reference line is maximum ('f_B'- Fig. 7.2). The reference line (|CD| - Fig. 7.2) is drawn from the end of the ISC to the point corresponding to the frequency which has the maximum magnitude of the spectra ('f_{MC}'- Fig. 7.2). According to these authors, this method gives better results than the MTM for narrow band signals and similar results for wide band signals, though a detailed evaluation of this method was not given.

We have implemented this algorithm in real-time and made three modifications. When the blood flow is changing direction, it is possible to have some columns of the spectra in which no flow is detected. In this case, the ISC will be formed only by the noise power. Application of the geometric method in this case will produce a spike. To prevent this, we have introduced a minimum threshold to be compared to the total power of the spectrum. If the power is smaller than the threshold, it is assumed that no flow is present. This threshold is made adaptable to the SNR by weighting its value with the power of the last two spectra columns of the signal. The results of this proved to be quite satisfactory.

A second problem with the method is that it depends on the position of the absolute maximum magnitude in the spectrum which can fluctuate quite markedly due to the variance of the spectral estimator and may also be influenced by noise spikes. The modified implementation uses a reference line which links the first to the last point of the ISC (|GD| - Fig. 7.2) and therefore is unaffected by the variation of the estimator.

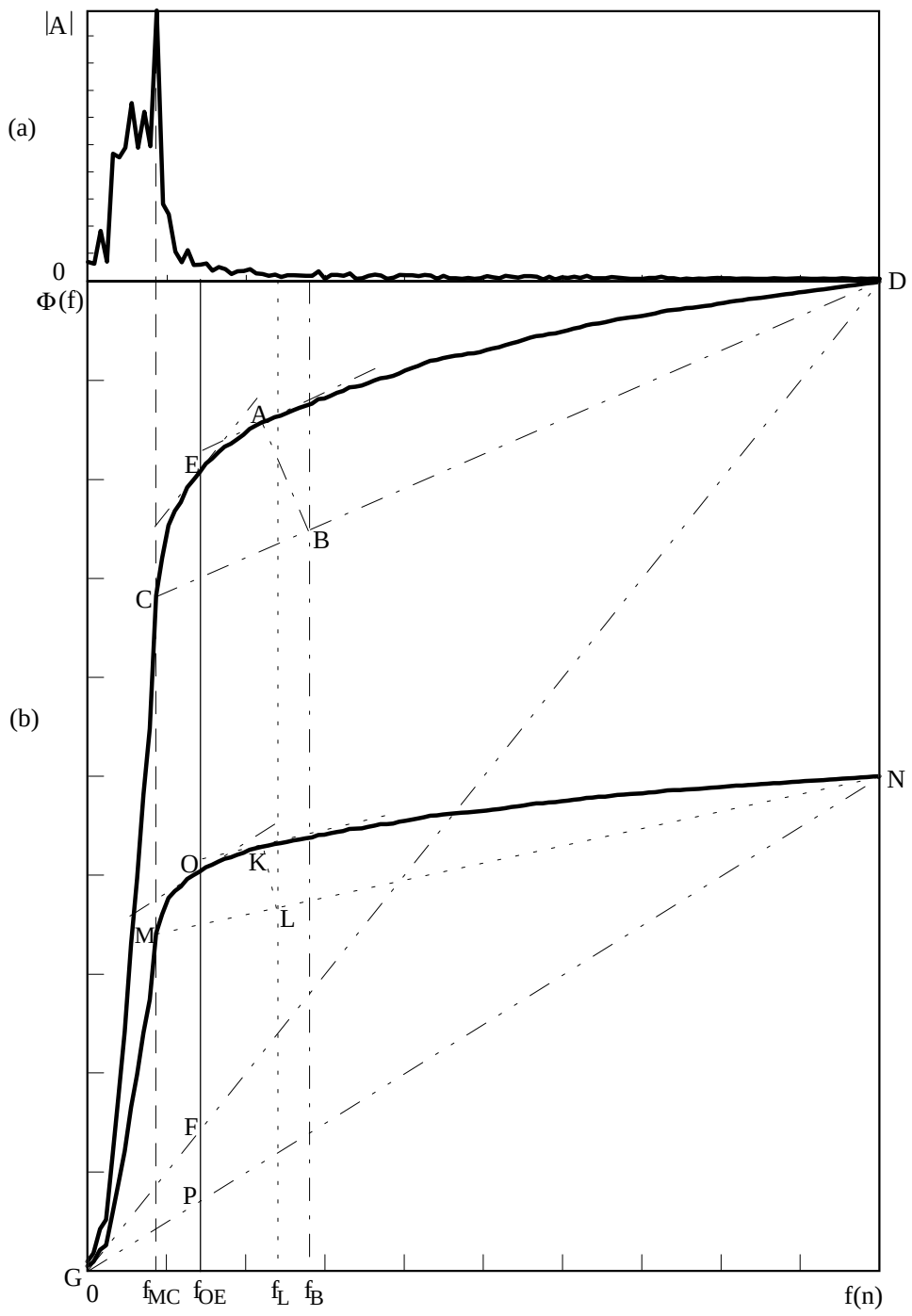

Figure 7.2 Doppler signal spectra (a) and its integrated spectrum curve at two different gains (b).

Nowicki and Marasek (1991) used the projection of the maximum distance between the reference line and the ISC on the frequency axis, making the maximum frequency detection susceptible to amplifier gain. If the power of the signal is

halved (curve GON - Fig. 7.2), there obviously is no change in the maximum frequency, but the projection given by |KL| is different from that given by |AB| (Appendix D). In order to provide maximum frequency detection independent of gain, the position of the peak was associated with the point that corresponds to the maximum distance between the ISC and the line from the origin to the end of the ISC rather than using its projection ('f_{OE}' for both curves - Fig. 7.2). With these modifications, it is possible to see that this method produces a reasonable detection of the 'knee' of the ISC which has been shown to correspond to the maximum frequency (Mo *et al* 1988).

7.3.2. Real-time implementations and simulations of the algorithms

The methods described above were implemented in real-time and some simulations were evaluated. The percentile method was excluded from simulations since its behaviour for different SNRs has been reported to be worse than the others (Mo *et al* 1988).

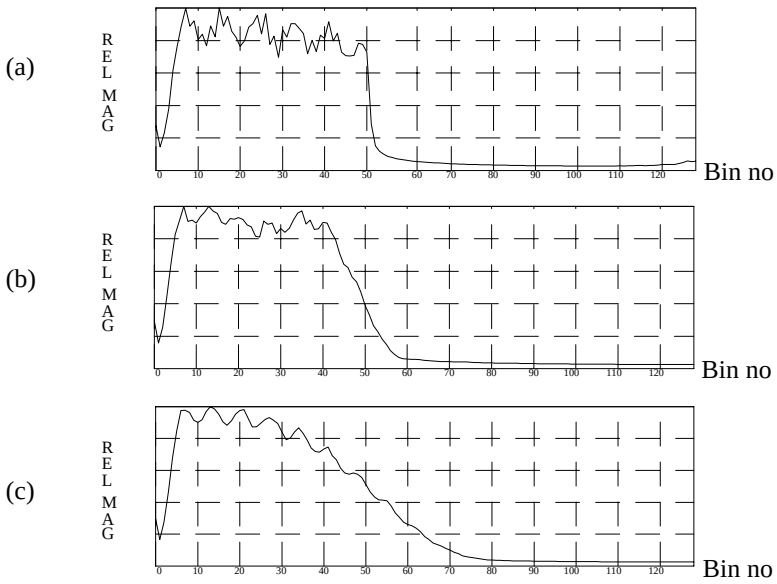

Figure 7.3 Spectra of the test signals used to compare the performances of the MFE detectors (the horizontal scale is 80 Hz/bin, each graduation represents 10 bins).

7.3.2.1. Methodology

For a quantitative evaluation, analogue narrow-band quadrature signals were derived from an analogue white noise generator using DSP techniques. Their frequency content was determined by digital band-pass filters. The spectra of the signals used in this study are illustrated in Fig. 7.3.

The spectrum shown in Fig. 7.3a has a very well defined maximum frequency (4 kHz) and provides a good basis for an objective comparison of the methods. However this spectra does not correspond to those obtained in clinical practice since these are subject to the intrinsic spectral broadening (ISB) effect (Evans *et al* 1989a). The other simulated Doppler signals (Fig. 7.3b and c) were designed to incorporate this effect. These signals were designed to have their 4 kHz frequency components lying in fall-off region thus being attenuated by half of the stop-band attenuation. This was done to provide a reference value for the detections. For all three signals, the high-pass cut-off frequency was set to 0.4 kHz to include a wall-thump filtering effect.

The MFEs obtained with simulated Doppler signals were digitally stored for statistical evaluation. For further analysis, sampled white noise (therefore incorporating the effect of anti-aliasing filters) was digitally added to the simulated Doppler signals to produce different SNRs and the behaviour of the MFE detection algorithms for these signals was observed. The waveforms used in these experiments were sampled at a frequency of 20.48 kHz. The DSP board anti-aliasing filters were 4th order Butterworth, having a cut-off frequency of 6 kHz. The software applies a Hanning window to the data and calculates a 256 point complex FFT before performing the MFE detections.

7.3.2.2. Results and comments

500 detections were used to estimate each of the averaged values and their standard deviation (SD). The bin detection mean and SD of the detected maximum bin obtained with each of the three methods for the signals at different SNRs are shown in Figs. 7.4 and 7.5 respectively. The reference value for all the methods is set at bin 50 which corresponds to the maximum frequency of 4 kHz as explained previously.

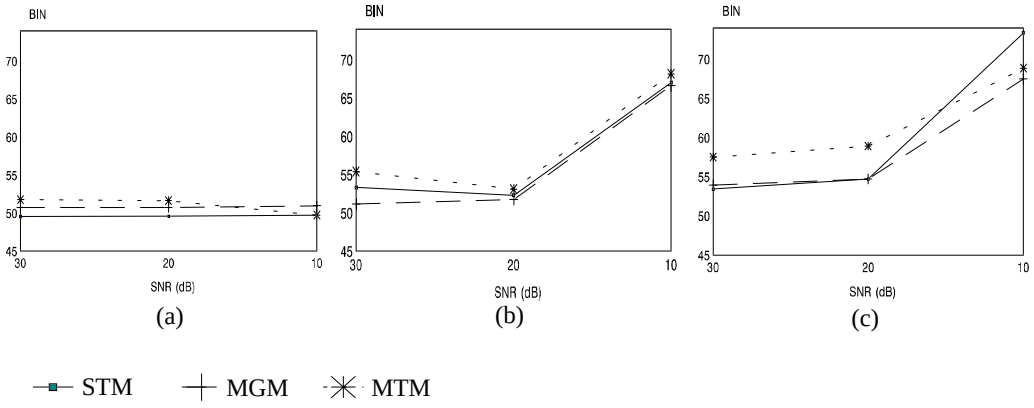

Figure 7.4 Bin detections for each of the signals whose spectra is presented in Fig 7.3 at different SNR values. The reference value is 50.

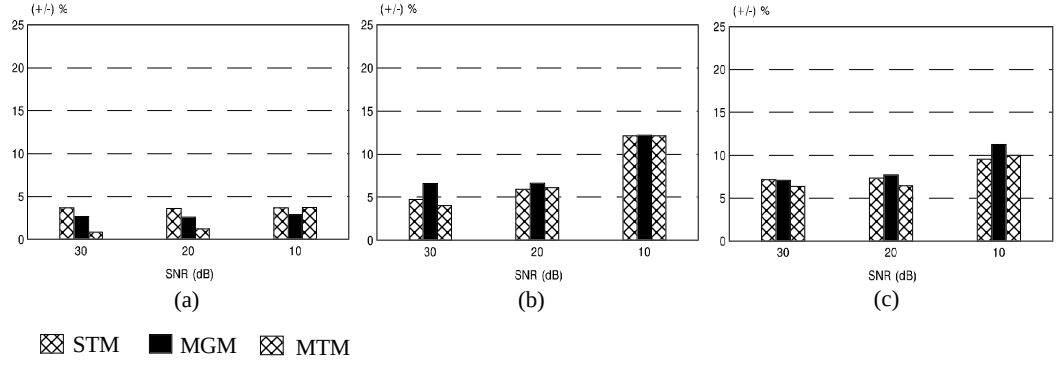

Figure 7.5 Standard deviation for the bin detections presented in Fig. 7.4

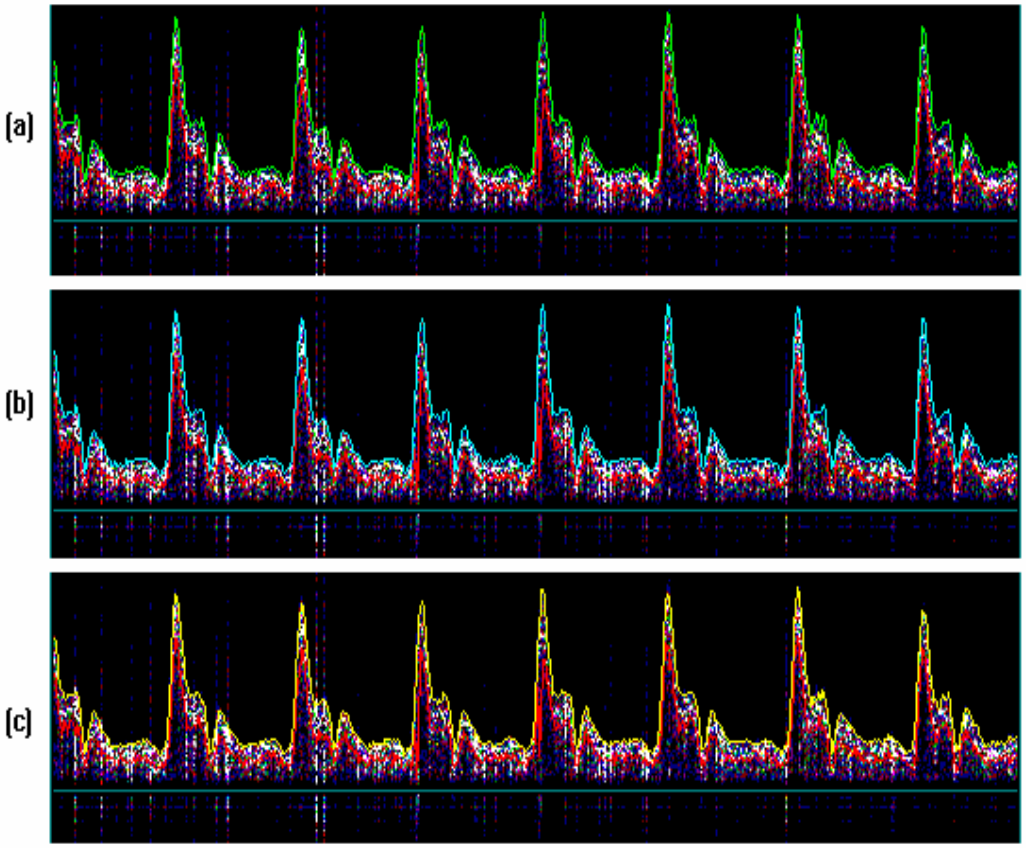

Figure 7.6 Maximum frequency envelopes obtained from a Doppler signal recorded from a carotid artery; (a) Modified geometric method, (b) Modifed threshold method, (c) Simple threshold method.

Fig 7.6 shows the MFE obtained using each of the methods for a Doppler signal recorded from the carotid artery. The results show a similar performance for all three methods. The STM is more useful for off-line applications where several values might be tried in order to achieve the best MFE fitting.

The MTM has a simpler and faster algorithm than the MGM and may be used where a loss of resolution is acceptable. However, since the constant chosen for a certain SNR may not be adequate for another SNR, care should be taken to determine it in order to achieve the best results. It has an advantage over the STM that it can adapt to small SNR changes.

Software may be written to sample, at different frequencies, Doppler signals interrogated by any Doppler system. The MGM is more suitable for such general purpose software since an evaluation of the level of noise produced by the interaction between a computer and a particular Doppler system is not necessary. However it uses a more complex algorithm when compared to the other methods. For our application, the MTM was the most appropriate method because the system uses a high sampling frequency and a fixed Doppler unit.

7.4. CALCULATION OF FREQUENCY INDICES

There are a number of indices based on the MFE of the Doppler sonogram which are independent of the angle between the Doppler probe and the blood vessel. A detailed description of these indices can be found in the literature (see for example Evans *et al* 1989a).

7.4.1. Calculation of pulsatility index (PI)

Pulsatility index (PI) (Gosling *et al* 1971) is the most widely used index and has been shown to be of value in preliminary studies of graft monitoring (Thrush and Evans 1990). Therefore we preferred to use this index as well as intensity weighted mean velocity in our monitoring system. PI was originally defined as the total oscillatory energy in the flow-velocity waveform divided by the energy in the mean flow-velocity over the cardiac cycle (Fitzgerald *et al* 1971, Woodcock *et al* 1972) but later it was superseded and simplified (Gosling and King 1974). It is currently calculated by dividing the maximum excursion of the waveform by its mean height (Fig. 7.7).

$$PI = \frac{\textit{peak to peak frequency}}{\textit{mean frequency over one cardiac cycle}} = \frac{S - D}{M} \qquad 7.4$$

Several studies have confirmed that the PI yields good diagnostic accuracy for significant peripheral occlusive disease when applied to the MFE (Harris *et al* 1974, Johnston *et al* 1983).

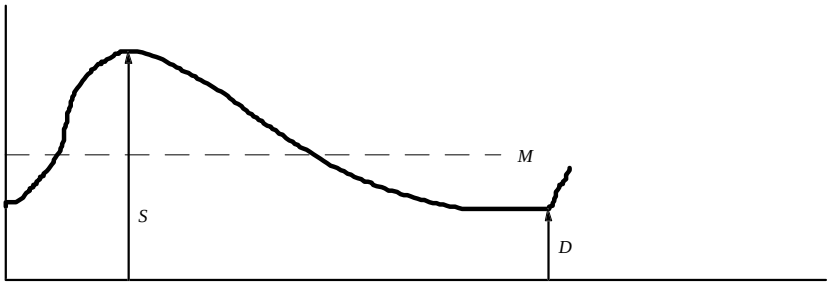

Figure 7.7 Diagram illustrating the variables involved in the definition of pulsatility index.

7.4.2. Waveform identification for calculation of the PI

A MFE waveform must be partitioned into individual cardiac cycles to automatically derive the desired indices. Various strategies have been used for this purpose (Gibbons *et al* 1981, Johnston *et al* 1982, Fulton *et al* 1983, Prytherch and Evans 1985, Evans 1988). One of these methods or a combination of them can be used to determine the start of the systolic upstroke (or waveform foot).

Before applying these algorithms, the raw MFE waveform must be pre-processed. The main pre-processing task is the smoothing of the waveform. Although *linear smoothers* (moving average, polynomial regression, spline regression) can smooth the waveform considerably sometimes this is not desirable since it removes simple trends from the waveform. These methods are also unable to remove the effect of single unusually large observations such as spikes in the MFE waveform. In this case *non-linear smoothers* (Tukey 1977, Cleveland 1979, Mallows 1980, Velleman

1980) must be applied. These smoothers can successfully remove artefactual abnormalities such as spikes in a waveform which are not a part of the general trend. Differencing is a process that provides a simple approach to removing, rather than highlighting, trends in a waveform. A more detailed description of these and other processes can be found elsewhere (see for example Velleman and Hoaglin 1981, Diggle 1990).

The pulse foot seeking algorithm used in this study is summarised below. In Fig. 7.8, the performance of the algorithm is demonstrated for three different waveforms.

Method:

1. Find the MFE by applying one of the MFE detection algorithms described above to the FFT result. In this application, we used the MTM since the system uses a high sampling frequency (20.48 kHz) and a fixed Doppler unit.
2. Eliminate spikes using non-linear smoothers.
3. Determine direction by comparing the total positive and the total negative magnitudes. A "**sign**" flag is set to be -1 or +1 as a result of the comparison. This process ensures the algorithm to work for both directions.
4. Smooth the waveform using the following linear smoother (moving average of order 3):

   $s_t=(x_{t-2}+2x_{t-1}+3x_t+2x_{t+1}+x_{t+2})/9$.
5. Apply second order differentiation to the waveform using the equation

   $D^2s_t=x_{t-4}+2x_{t-3}-x_{t-2}-4x_{t-1}-3x_t+3x_{t+2}+2x_{t+3}+x_{t+4}$.
6. Apply the following equation to the differentiated array in order to reject the negative magnitudes:

   $s_t=(s_t+|s_t|)/2$.
7. Find the maximum magnitude of the differentiated array and set a threshold level using this magnitude. The threshold is determined by taking a percentage of the maximum magnitude.

8. Eliminate all magnitudes less than this threshold level.
9. The aim is to determine the bins with maximum magnitude for each beat. To do this, find non-zero bins, then find the bin with the maximum magnitude within the next ten bins and eliminate the magnitudes less than this bin by replacing them with zero. This will leave only one bin for each beat. This corresponds to the steepest point in the MFE. These points are marked by magenta lines in Fig. 7.8.
10. The beat interval for this waveform is estimated first by measuring distances between the magenta lines and then by taking the median of this measurement, and the waveform is equally divided using estimated intervals (red lines in Fig. 7.8).
11. Correct waveform partitioning if wrong and reject incomplete beats.
12. Find starting point (green lines in Fig. 7.8), maximum point (cyan markers in Fig. 7.8) and minimum point (red markers in Fig. 7.8) of individual beats.

7.5. CONCLUSION

The basis of the need for waveform identification and practical implementations for computerised calculation of the desired indices have been briefly given. The algorithms described are able to cope with different Doppler signals obtained from different grafts. Since a monitoring system must be reliable the robustness of the algorithms must be proved and must be improved if necessary. Therefore, the system needs extensive evaluation on a variety of grafts. Some early monitoring results will be given in the next chapter.

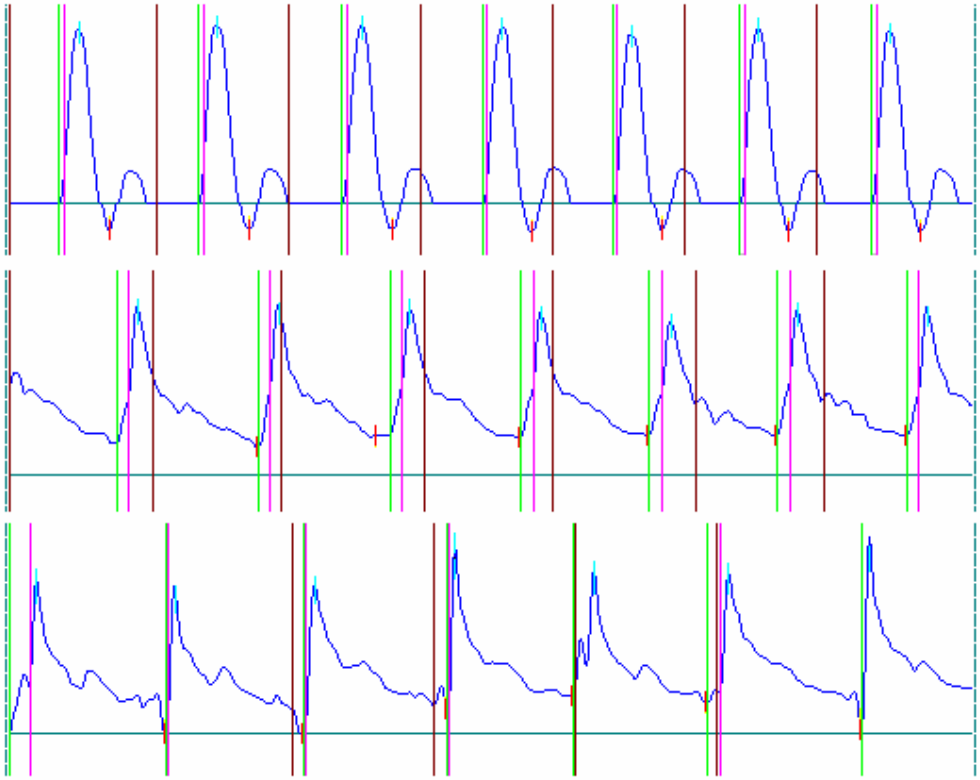

Figure 7.8 Illustration of the pulse foot seeking algorithm.

8. COMPUTERISED GRAFT MONITORING SYSTEM AND PRELIMINARY RESULTS.

8.1. INTRODUCTION

In previous chapters, a computerised graft monitoring system has been introduced and the basic elements of this system have already been described in detail. In this chapter, the organisation of the graft monitoring system, based on the hardware and software implementations given in Chapters 3, 4 ,5 and 6, will be described and some preliminary results will be presented.

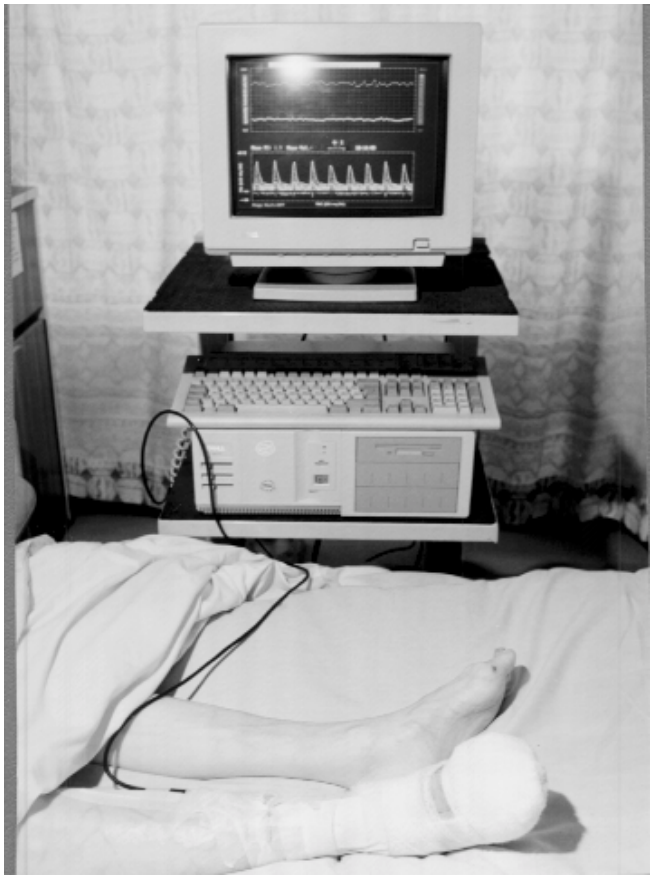

Figure 8.1 The computerised graft monitoring system attached to a patient.

As previously mentioned the graft monitoring system comprises a transducer, a CW Doppler board, a DSP board and an IBM compatible personal computer. The CW Doppler board has been described in Chapter 3. The Doppler board and the DSP board are normally installed in the PC which performs all control and data handling tasks. A photograph of the complete monitoring system attached to a patient is shown in Fig. 8.1.

8.2. ARRANGEMENT OF THE GRAFT MONITORING SYSTEM

The only interface between the patient and the monitoring equipment is an acoustical coupling via a transducer. This is constructed from two identical pieces of piezoelectric material (PZT) as described by Dahnoun *et al* (1990). The operating frequency was 4 MHz. A photograph of the ultrasonic CW Doppler probe attached to a patient is shown in Fig. 8.2. Since there is no direct contact between the probe and the stitched skin, the possibility of any infection is eliminated.

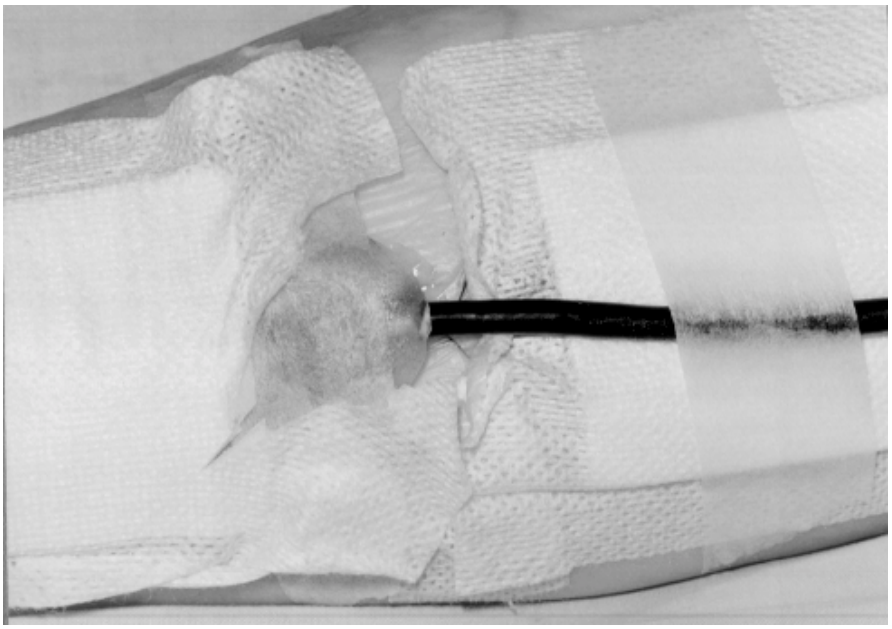

Figure 8.2 Purpose built ultrasonic CW doppler probe attached to a patient.

The quadrature outputs of the CW Doppler board are digitised by the DSP board and processed for the time domain and frequency domain flow direction determination as described in Chapters 4, 5 and 6. For the frequency domain display the complex FFT method preceded by a complex Hanning window was used. The in-phase and the quadrature-phase Doppler signals were considered as the complex input signal for the FFT. This then gives a directional Doppler frequency spectrum as explained in Chapter 4. This result is rearranged and displayed as a color-coded sonogram as shown in the lower part of Fig. 8.3. For the directional time domain outputs the PFT was used. This process is independent of the frequency domain separation. The separated Doppler signals are sent out via the DSP board's DAC outputs.

The CW Doppler board can be programmed for continuous monitoring or intermittent recording. In the latter case, the duration of recording can be programmed through the computer keyboard. The system gain and the lowpass filter cut-off frequency can be similarly programmed. Although the system sampling frequency is entirely programmable, a sampling frequency of 20.48 kHz is used in monitoring mode. The Doppler sonogram and two variables (mean PI and mean IWMV) are displayed on the PC screen. A typical monitoring display is shown in Fig. 8.3.

8.2.1. Software organisation

The software organisation, which is summarised in Fig. 8.4, can be divided into three main parts: processing software, control software and analysis software.

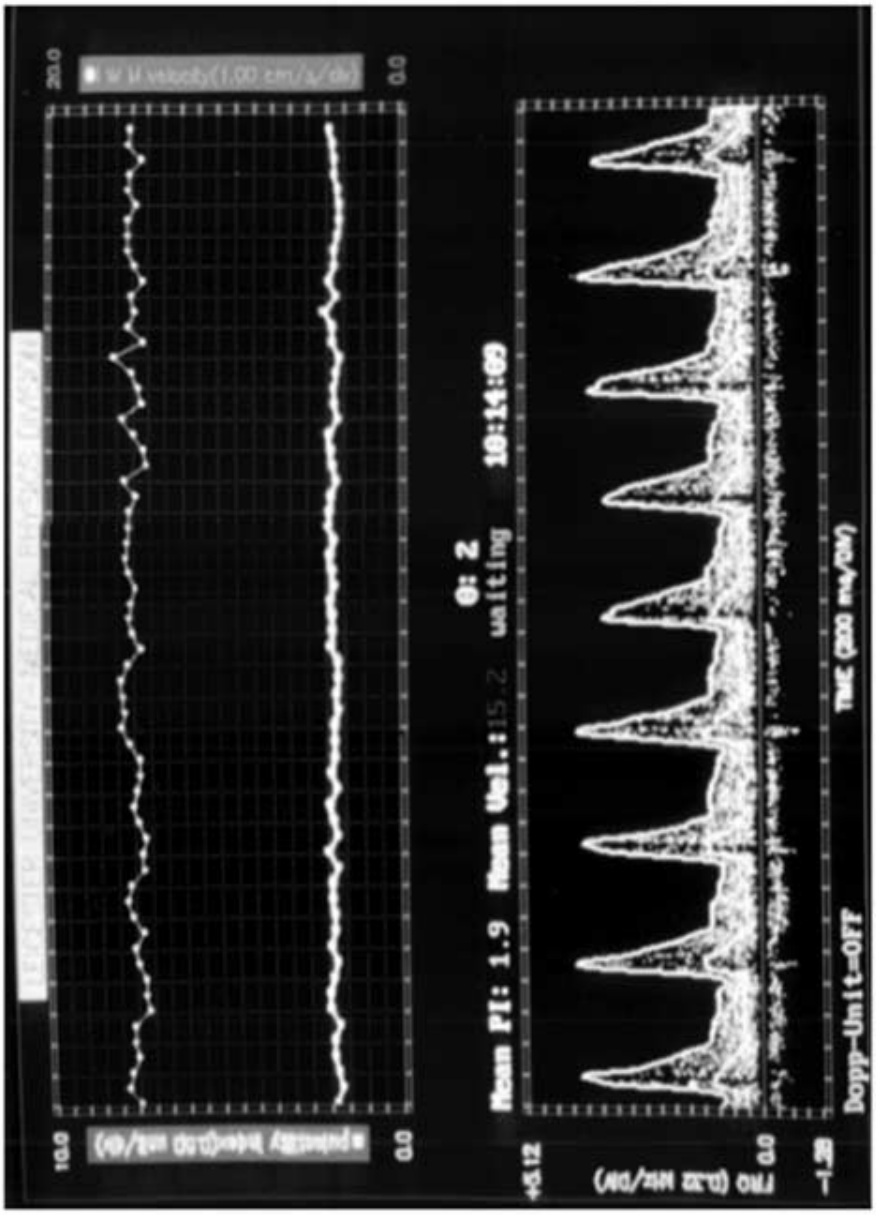

Figure 8.3 A typical graft monitoring display.

The processing software is the program running on the DSP board. This runs independently and is responsible for: acquisition of the quadrature data digitised by the on-board ADCs; separation of flow direction; execution of the complex FFT and finding the maximum and IWMF bins in real-time. This software was written in the DSP32C assembler language (refer to Chapter 6). The digitised quadrature data are also stored in a ram-disk for off-line analysis.

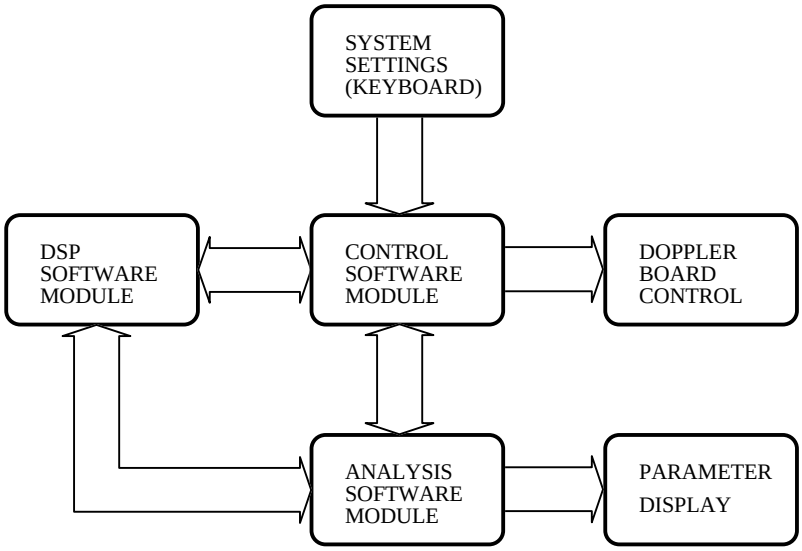

Figure 8.4 The general software organisation for graft monitoring system.

The control software is menu driven and written in the C language. It performs data handling between the DSP board and the PC; controls the Doppler board settings and allows interaction between the monitoring system and the operator. The latter is done by selecting related options from the menu (Appendix E). Some parameters related to the DSP software can also be set.

Although the majority of the analysis software runs on the PC some tasks such as the complex FFT and extraction of the frequency envelopes are performed on the DSP board. This first processes the stored quadrature data to generate a Doppler sonogram while it acts as a coprocessor to the PC. It then analyses this sonogram, and calculates the desired parameters as explained in Chapter 7.

8.2.2. Operation of the graft monitoring system

The software developed for the system offers several options (Appendix E). To operate the system in monitoring mode the following steps should be performed:

1. The position where the probe is attached to the patient is determined by selecting the "system setup" option from the main menu. This option provides basic Doppler spectrum analysis functions based on the FFT. The Doppler spectral magnitude (linear or logarithmic) and the separated time domain Doppler signals can be displayed as well as the Doppler sonogram. Figs 8.5 and 8.6 respectively illustrate these displays.

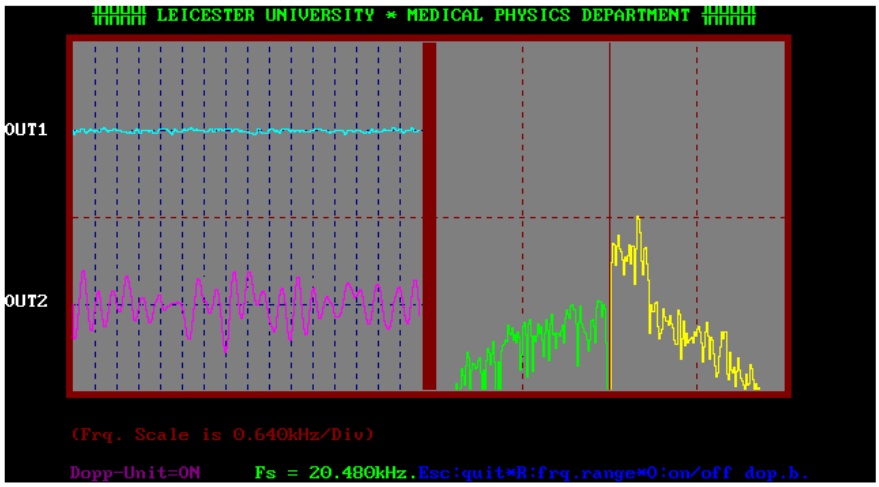

Figure 8.5 An example of the separated time domain Doppler signals and logarithmic spectral display.

   This option also allows the operator to change the sampling frequency. The probe position is adjusted by looking at the quality of the Doppler sonogram and listening to the audio Doppler signal. After selecting the best signal the probe is then fixed to this position using a double-sided adhesive ring.
2. Patient data is entered by choosing a related option. Unless this option is chosen, parameters will not be stored.

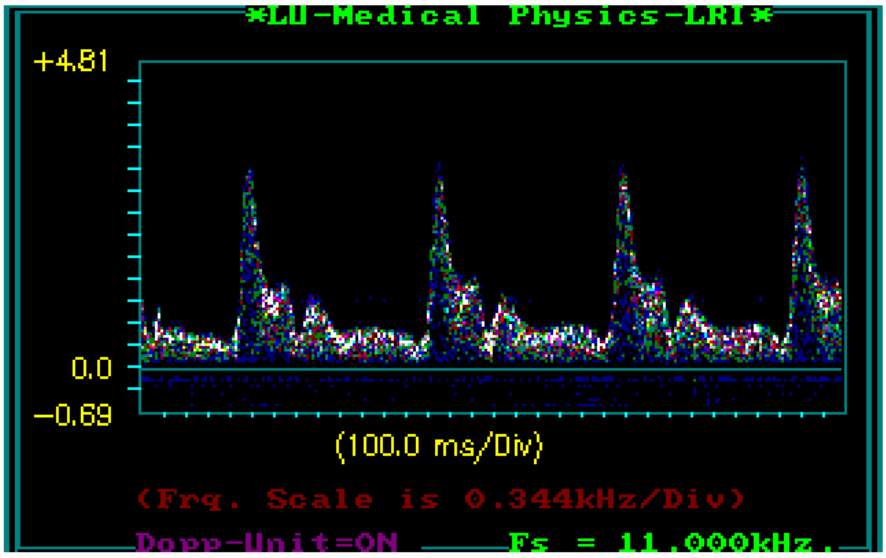

Figure 8.6 An example of the Doppler sonogram display.

3. The graft monitoring option is chosen and the related parameters such as the Doppler board "On-time", the FFT size, the "Cycle-time", etc., are set. After starting the monitoring process, the computer screen is set up as illustrated in Fig. 8.3. The system first switches the Doppler board on and displays the Doppler sonogram. It also stores the quadrature data in ram-disk in real-time. This process is the recording stage determined by "On-time" setting. At the end of the recording stage, the Doppler board is switched off, the Doppler signal processing is performed on the DSP board, the results are analysed by the PC and they are then plotted on the PC screen. This is the processing stage. The mean and maximum frequency envelopes and calculated parameters are stored in a file and the system waits for the next cycle. The waiting stage is determined by the "Cycle-time" option.
4. The operation can be interrupted any time by pressing "Esc" on the computer keyboard if any parameter modification or process termination is required.

The real-time process sequence for the monitoring option can be summarised as following:

1. 256 complex data points (512 total) are captured. Since the sampling frequency is 20.48 kHz all processes including capturing quadrature data, processing it for spectral analysis and time domain separation and displaying the results have to be completed within 12.4 ms.
2. Time domain separation is performed by applying the phasing filter technique (see Chapter 5) to the input data and the results are stored in the output array.
3. The input data are overlapped (50%) to obtain a 512 point complex data array. A 512 point complex FFT, preceded by complex Hanning windowing, is then applied.
4. The squared magnitude of the FFT output values are calculated, rearranged by shuffling the positive and negative frequencies, then scaled for the sonogram display. These results are stored in the output array.
5. The maximum frequency bin is determined by applying the modified threshold method and the IWMF is calculated.
6. The separated time domain signals are sent out via the DAC. The spectrum analysis results and the calculated frequency parameters are read by the PC and at the same time a new complex data array is captured by the DSP board.
7. After performing all these processes in real-time (within 12.4 ms) they are repeated for the new data array.

Since the DSP32C has a pipelined processor architecture, the processes described above do not represent sequential execution. The major tasks such as outputting the separated Doppler signal and capturing the new quadrature Doppler signal are performed simultaneously. Table 8.1 summarises the processes performed by the DSP board and the PC.

A "Utilities" option is supplied to perform off-line operations (after monitoring a graft) such as displaying the maximum and the mean frequency envelopes and trends, binary to ASCII file conversion, etc. (see Appendix E).

Processes performed in the DSP board	**Processes performed in the PC**
• Capture of Doppler signals. • Spectral analysis (Hanning windowing, complex FFT, etc.). • Extraction of the MFE and IWMFE. • Time domain directional signal separation. • Output of directional signals.	• Setting system parameters. • Non-linear smoothing of the MFE and IWMFE. • Waveform identification. • Calculation of the indices. • Control of the Doppler board. • Display of the results.

Table 8.1 Summary of the processes performed by the DSP board and the PC.

8.3. CLINICAL STUDY - PRELIMINARY RESULTS

The computerised graft monitoring system has been tested clinically by monitoring a number of patients. Two parameters, the mean pulsatility index and the mean IWMV, were calculated monitored and stored instantly. Apart from the initial settings all these processes were automatically done by the monitoring system.

8.3.1. Method

The site, where the purpose built probe is attached, is covered with an *op-site*, a sterile sticky plastic dressing. This eliminates any possibility of infection. The best location is determined by continuously monitoring blood flow as described in section 8.2.2 ("system setting" option). This location is marked and the probe is attached using a double-sided adhesive ring. This ensures the stability of the probe. The program parameters are set and then the automatic intermittent monitoring

process is initialised by choosing the "go" option from the menu. No intervention is required during the monitoring process.

8.3.2. Results

Seven patients out of total ten have been successfully monitored. In three patients the grafts were too deep. Therefore they were excluded from this study. Overall monitoring times and patient details for each case included in this study are summarised in Table 8.2.

Unless otherwise stated the following settings were used for all the recordings.

- On-time: 19.2 second, which is equal to three screenfulls of data.
- Cycle-time: 3 minutes (Case 1: 5 minutes; Case 6b:2 minutes).
- Threshold scale factor: 2.
- FFT size: 512 points (Cases 6c, 6d, 6e, and 7: 1024 points).
- Amplifier gain: 0 dB.
- Low-pass filter cut-off frequency: 9.2 kHz.
- Mean PI scale: 10.
- Mean IWMV scale: 20 cm/sec.

The maximum frequency envelope, the mean frequency envelope, the mean PI, and the mean IWMV were stored in the hard-disk as binary files during the monitoring process. The following graphs (Figs. 8.7 to 8.13) were printed using the "utilities" option of the monitoring software. In the Case 1 (Fig. 8.7) one page (screen) corresponds to 320 minutes monitoring time. In the Case 6b (Fig. 8.12b) one page (screen) corresponds to 128 minutes monitoring time. In the Cases 3b (Fig. 8.9b) and 6d (Fig. 8.12d), one page (screen) corresponds to 3.2 hours monitoring time. In the other cases one page (screen) corresponds to 6.4 hours monitoring time.

	Case 1	**Case 2**	**Case 3**	**Case 4**	**Case 5**	**Case 6**	**Case 7**
Age	64	54	78	76	75	93	68
Sex	male	female	male	female	male	male	male
Diabetic	no	no	no	no	oral	oral	insulin
Hyperten.	no	no	no	yes	no	yes	no
Smoker	yes	past	past	no	past	no	no
Angina	no	no	no	no	no	no	no
Indication	critical ischemia	critical ischemia	critical ischemia	critical ischemia	critical ischemia	critical ischemia	critical ischemia
Symptom	rest pain	rest pain	ulcer & rest pain	ulcer & rest pain	rest pain	gangrene	gangrene
Operation	FDB	FDB	FDB	FDB	FDB	PDB	FDB
Op. side	right	right	right	right	left	right	left
Graft	ISVG	RVG (arm)	ISVG1	ISVG + arm vein	ISVG	RVG	ISVG
Result	*	Failed	Patent	Patent	Patent	Patent	Patent
Op. Date	22.12.93	18.01.94	23.02.94	02.03.94	09.03.94	21.03.94	04.04.94
Mon. Date	04.01.94	20.01.94	24.02.94	03.03.94	10.03.94	21.03.94	05.04.94
Overall mon. tim. (hours)	14.4	19.2	19	34.1	19.2	69	64

* Proximal graft was patent, distal graft was occluded.

FDB: Femoro-Distal Bypass; ISVG: In-Situ Vein Graft; RVG: Reversed Vein Graft

PDP: Popliteal-Distal Bypass

Table 8.2 Patient details and overall monitoring times for each case.

A total of 13 studies have been performed on 7 patients. These studies are summarised below:

Case 1. The graft was monitored 13 days after the operation. The results are plotted in Fig. 8.7. It appears that the mean PI and the mean IWMV follow a similar but reciprocal pattern. However, the mean IWMV was very low. This was due to the fact that the distal graft was occluded and the

proximal graft was patent. However the blood flow was maintained between the blocked artery and patent half of the graft via collaterals. The gaps in the graphs represent rejected measurements. The monitoring process was terminated normally.

Case 2. This graft was monitored 2 days after the operation. The results are plotted in Fig. 8.8. The mean PI and the mean IWMV follow a reciprocal pattern. Unfortunately, the monitoring process had to be stopped because the probe cable was broken by nurses. This graft failed 4 days after this study and the patient's limb was amputated.

Case 3. Two studies were performed on this graft. The first monitoring was performed 24 hours after the operation for 12.8 hours. The results are plotted in Fig. 8.9a. The mean PI and the mean IWMV follow a similar pattern as observed in the Cases 1 and 2. The first monitoring was terminated because of a software failure. In the second study (Fig. 8.9b), the graft was monitored for 6.2 hours. An apparent sudden change in the first page was due to an overflow that occurred during integer calculations. This process was terminated normally.

Case 4. Two studies were performed on this graft. The first monitoring was performed 24 hours after the operation for 16.2 hours. The results are plotted in Fig. 8.10a. No abnormal patterns were observed. The first monitoring was terminated because the patient was moved. In the second study, the graft was monitored for 17.9 hours. As shown in Fig. 8.10b, initially the graphs were normal. But later (second and third pages) the patient changed her position and blocked the graft temporarily. This resulted in an unstable trend. However the trends were recovered later as seen from the graphs. The monitor was disconnected by nurses because the patient did not want to be monitored any longer.

Case 5. This graft was monitored 24 hours after the operation. The results are plotted in Fig. 8.11. Although it is difficult to see that the mean PI and the mean IWMV follow a similar pattern, the mean PI increases whenever

there is a decrease in the mean IWMV. Note once again the transient graft blockage due to patient position. The monitoring process was terminated normally because the patient did not want to be monitored any longer.

Case 6. Five studies were performed on this graft. The first monitoring was performed several hours after the operation for 25.6 hours. The results are plotted in Fig. 8.12a. In this study a very strong reverse flow component was observed. As a result, the MFE detection failed frequently. This was attributed to misplacement of the Doppler probe. This process was terminated because of a software failure. The second study was performed the next day for 6.4 hours while the patient was sitting. The probe position was adjusted. The result is shown in Fig. 8.12b. This was terminated because the patient moved back to the bed. The third monitoring was performed half an hour later. The fluctuations were caused by movements of the patient. Probe displacement was also suspected. This process was terminated. After readjusting the position of the probe the fourth monitoring was performed for 3.9 hours. This was terminated because the patient had a bath. The last monitoring was then performed for 17 hours. In the last two pages, the fluctuations were possibly caused by the patient's position. This process was terminated normally.

Case 7. This graft was monitored 24 hours after the operation for 64 hours without any intervention. The results are plotted in Fig. 8.13. Apart from several individual fluctuations the general trend was quite stable. These fluctuations were due to the position of the patient. In page (screen) 8 one particular change in the trends was caused by the nurse, who unplugged the probe and than plugged it back incorrectly The monitoring process was terminated normally.

Case 1.

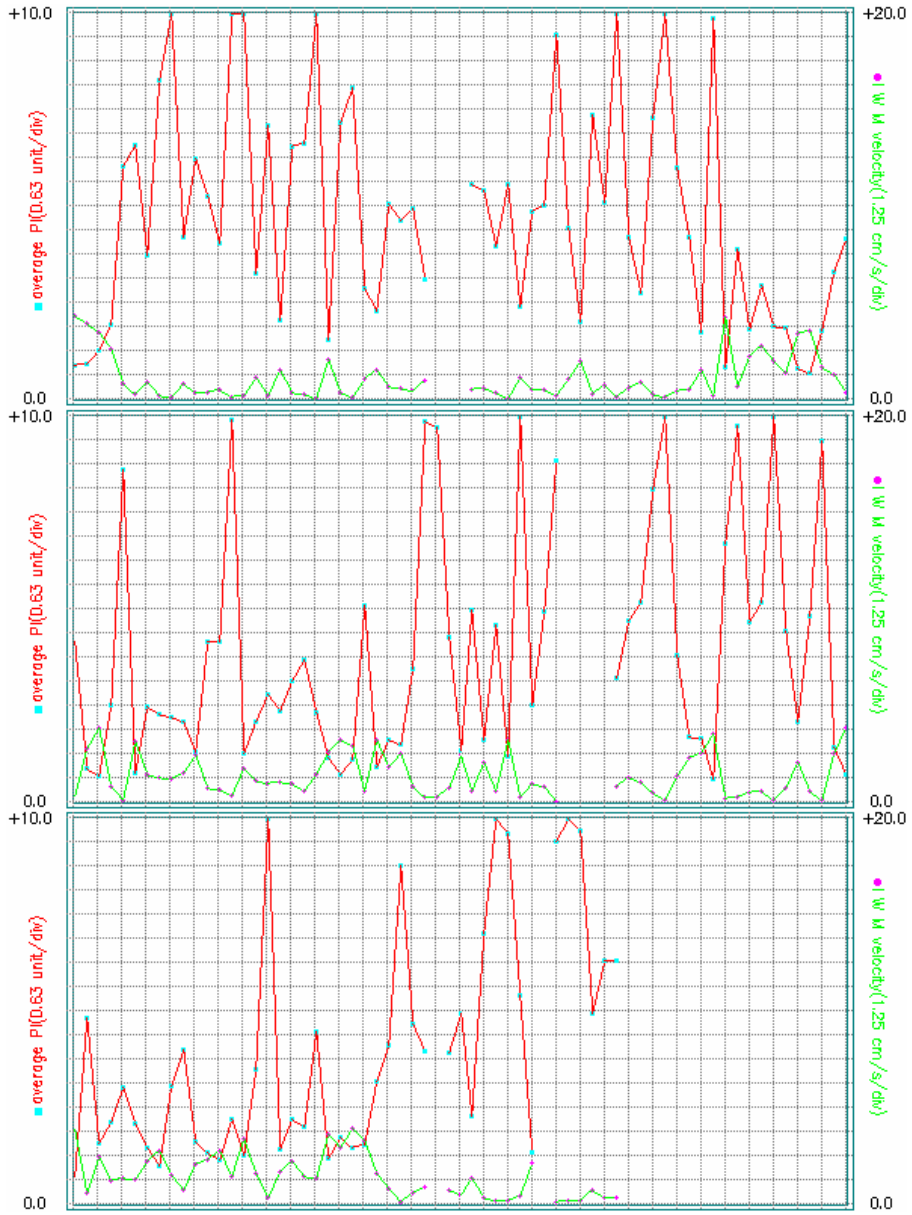

Figure 8.7 Graphs of the mean PI and the mean IWMV for Case 1. Cycle-time is 5 minutes (10 min/div, 64 points per display).

Case 2.

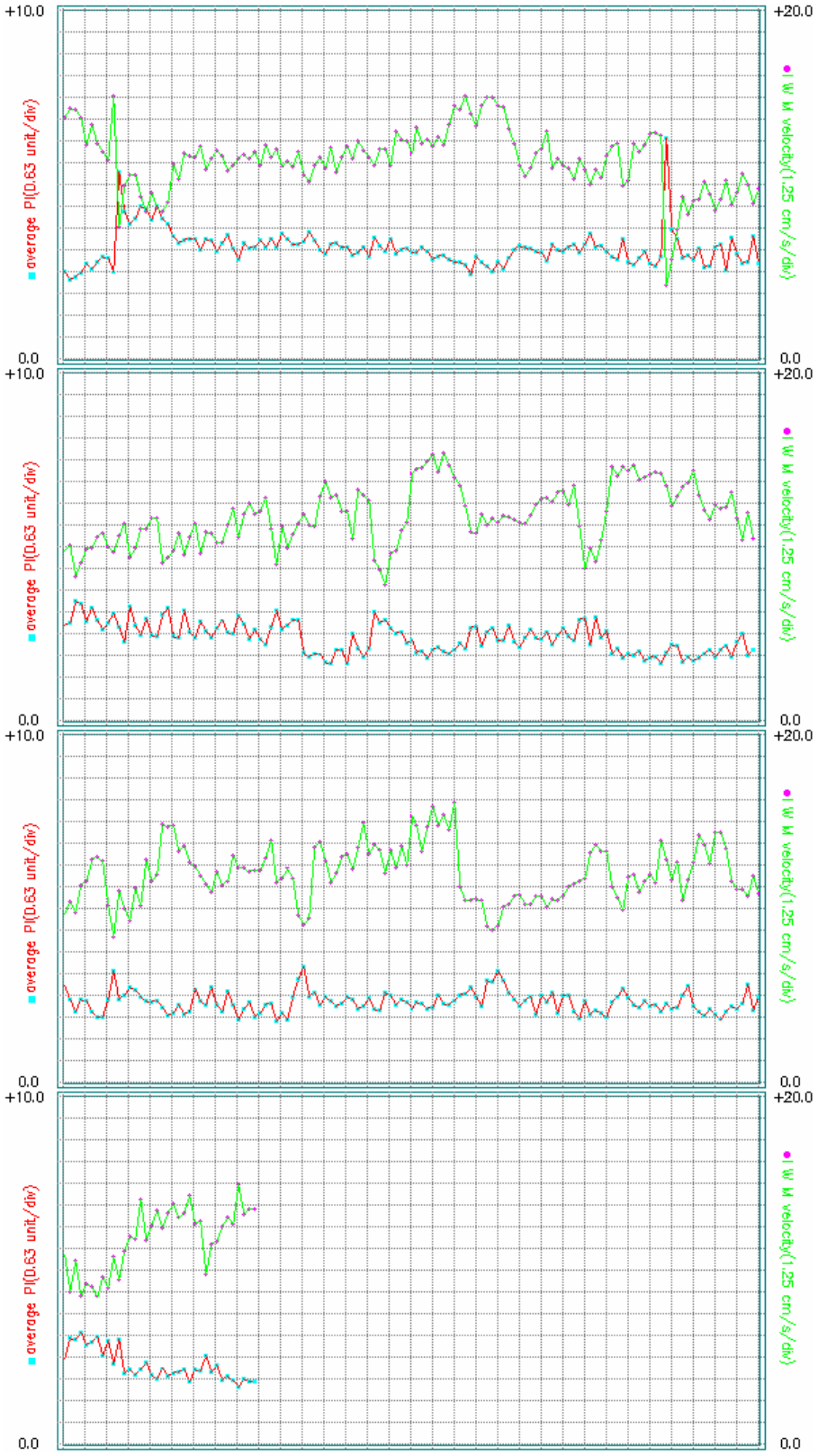

Figure 8.8 Graphs of the mean PI and the mean IWMV for Case 2. Cycle-time is 3 minutes (12 min/div, 128 points per display).

Case 3a.

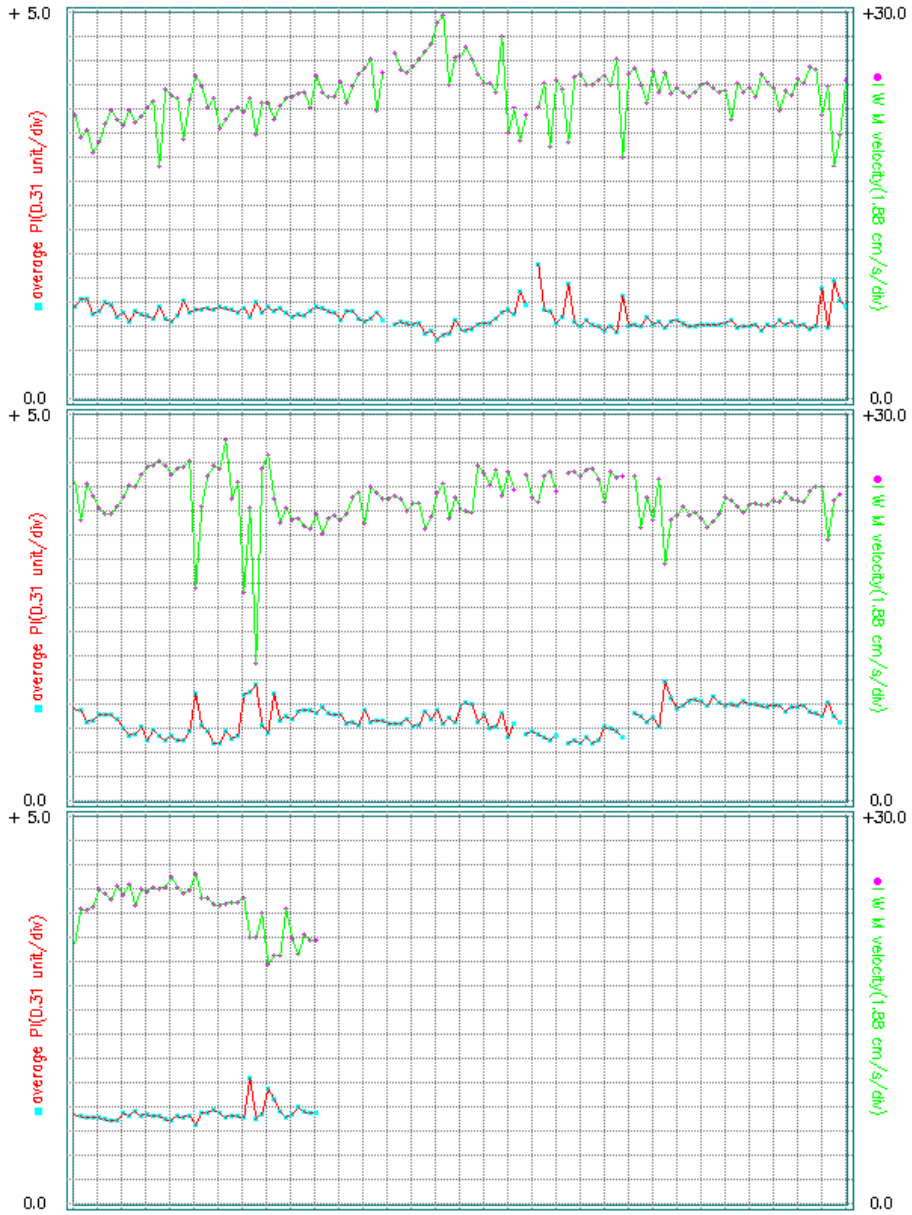

Figure 8.9a Graphs of the mean PI and the mean IWMV for Case 3. Cycle-time is 3 minutes (12 min/div, 128 points per display).

Case 3b.

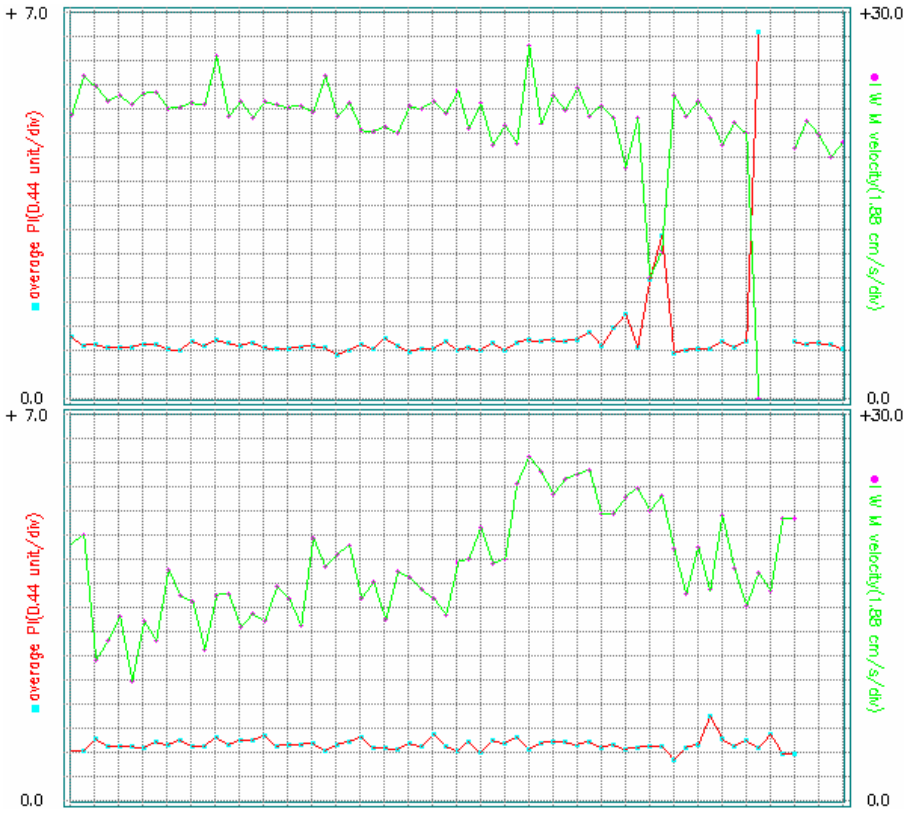

Figure 8.9b Graphs of the mean PI and the mean IWMV for Case 3. Cycle-time is 3 minutes (6 min/div, 64 points per display).

Case 4a.

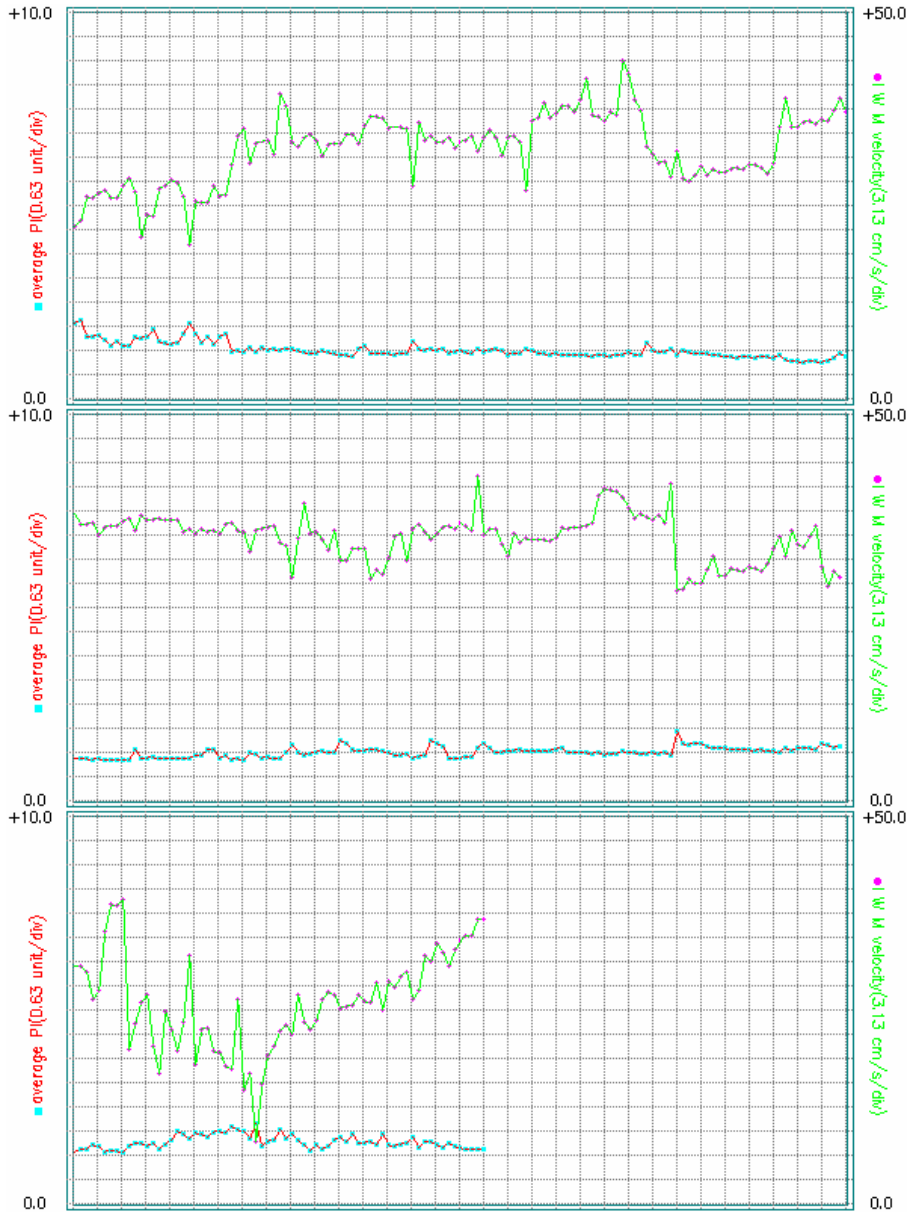

Figure 8.10a Graphs of the mean PI and the mean IWMV for Case 4a. Cycle-time is 3 minutes (12 min/div, 128 points per display).

Case 4b.

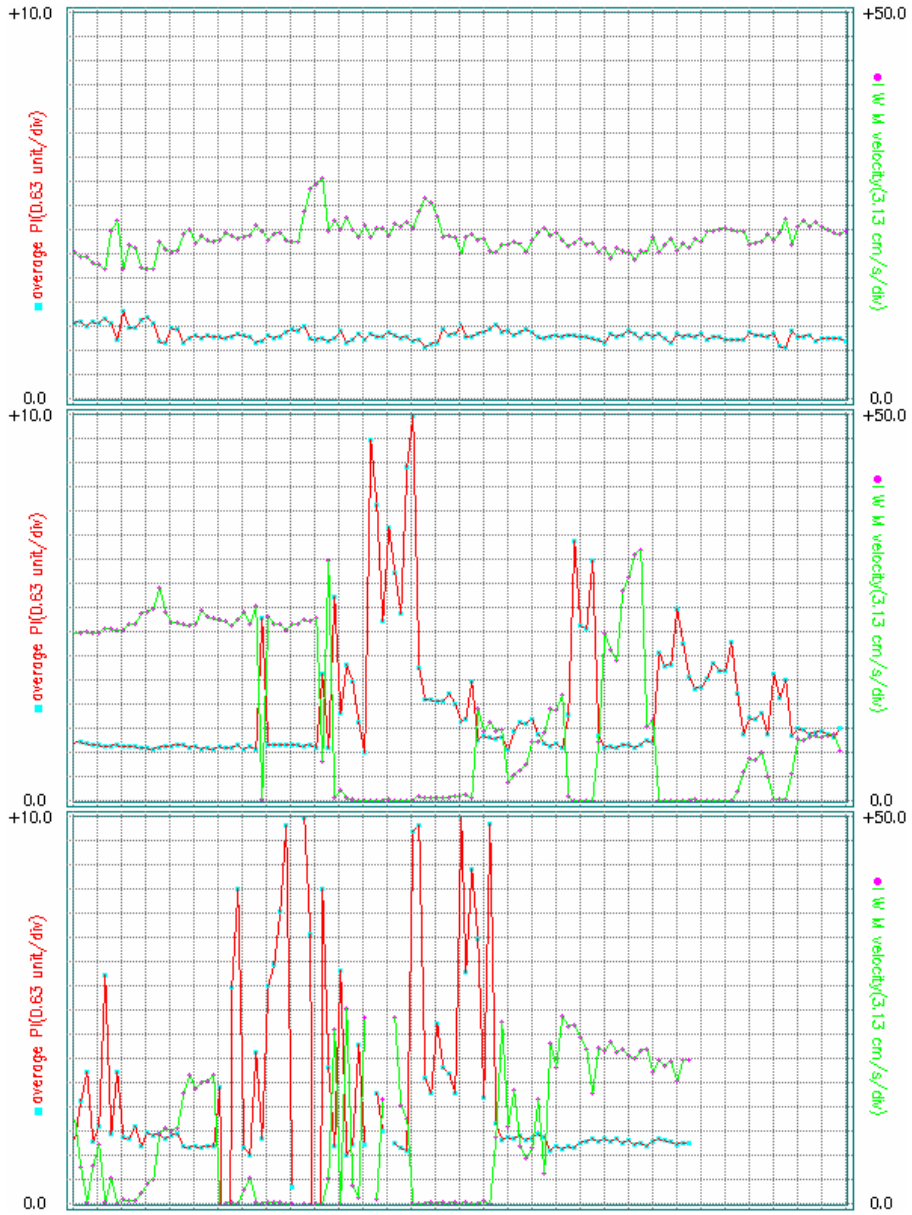

Figure 8.10b Graphs of the mean PI and the mean IWMV for Case 4b. Cycle-time is 3 minutes (12 min/div, 128 points per display).

Case 5.

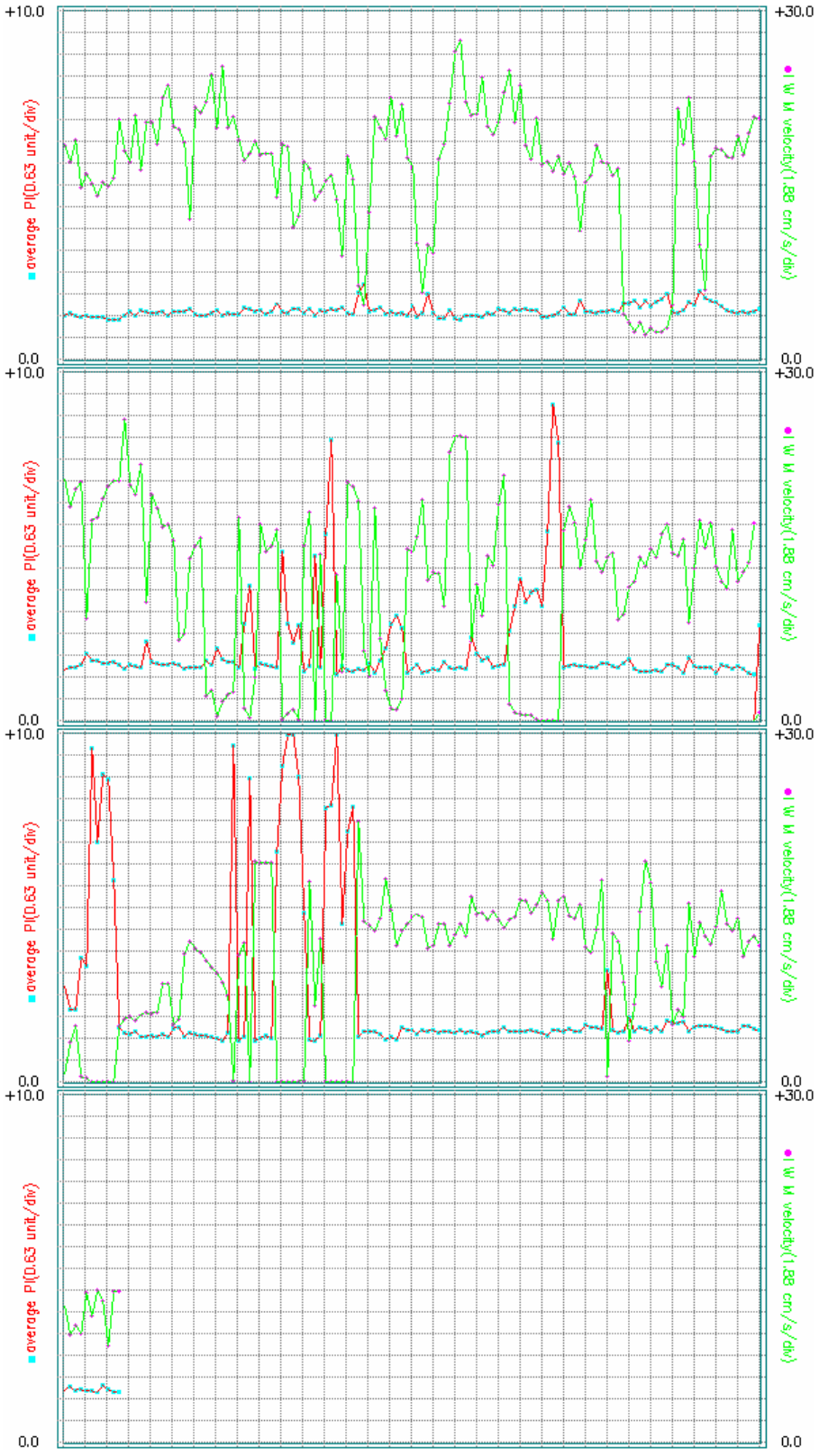

Figure 8.11 Graphs of the mean PI and the mean IWMV for Case 5. Cycle-time is 3 minutes (12 min/div, 128 points per display).

Case 5.

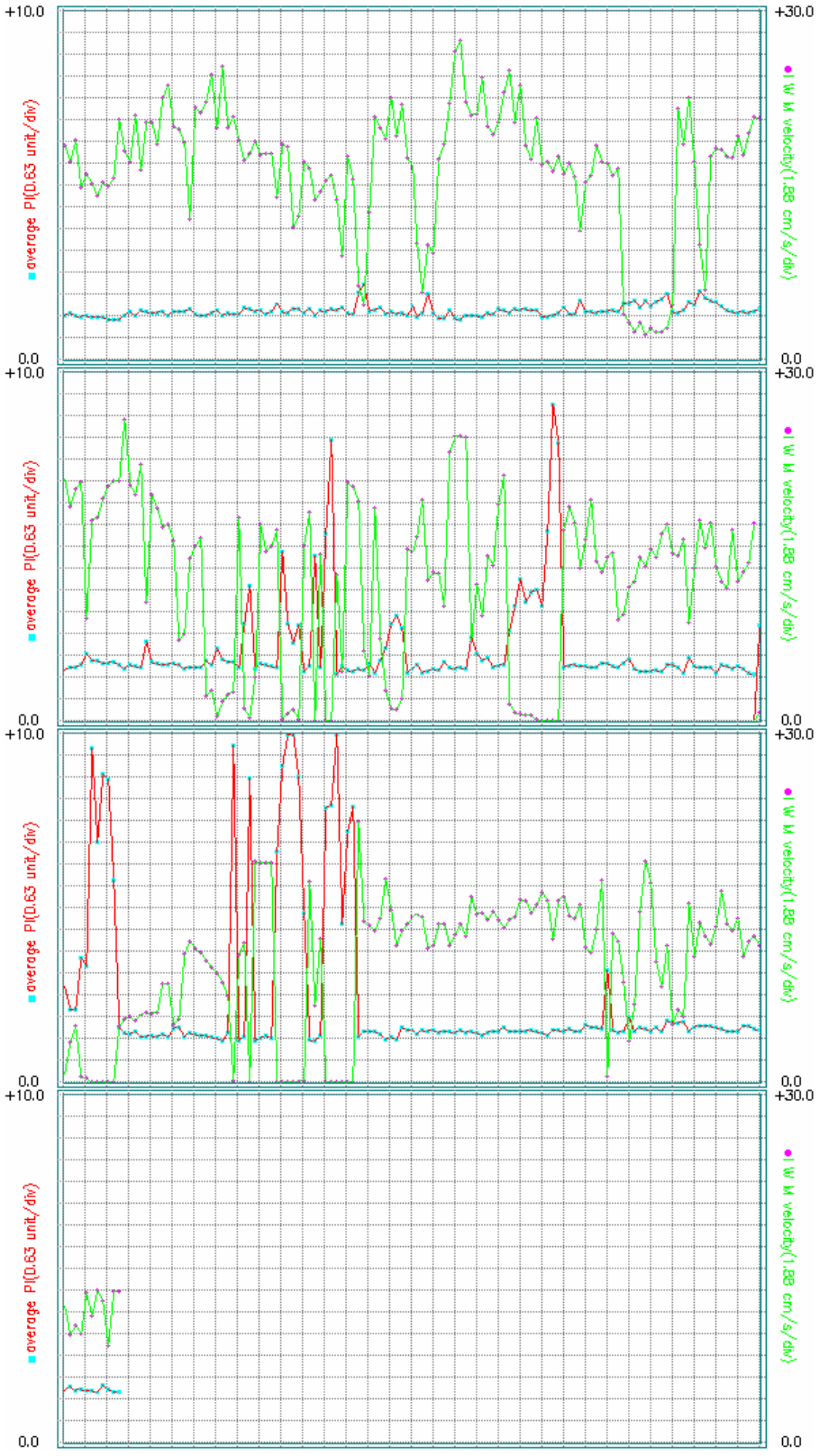

Figure 8.11 Graphs of the mean PI and the mean IWMV for Case 5. Cycle-time is 3 minutes (12 min/div, 128 points per display).

Case 6b.

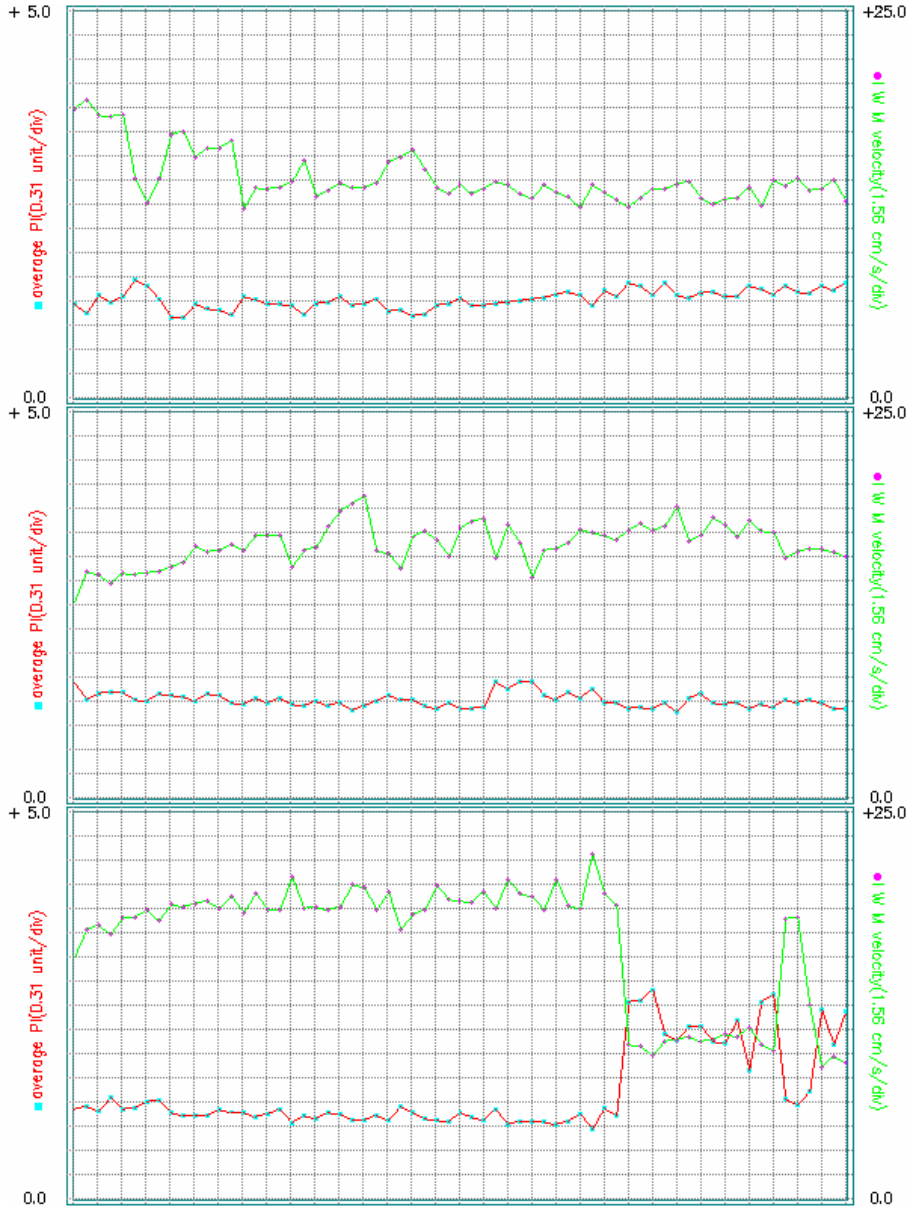

Figure 8.12b Graphs of the mean PI and the mean IWMV for Case 6b. Cycle-time is 2 minutes (4 min/div, 64 points per display).

Case 6c.

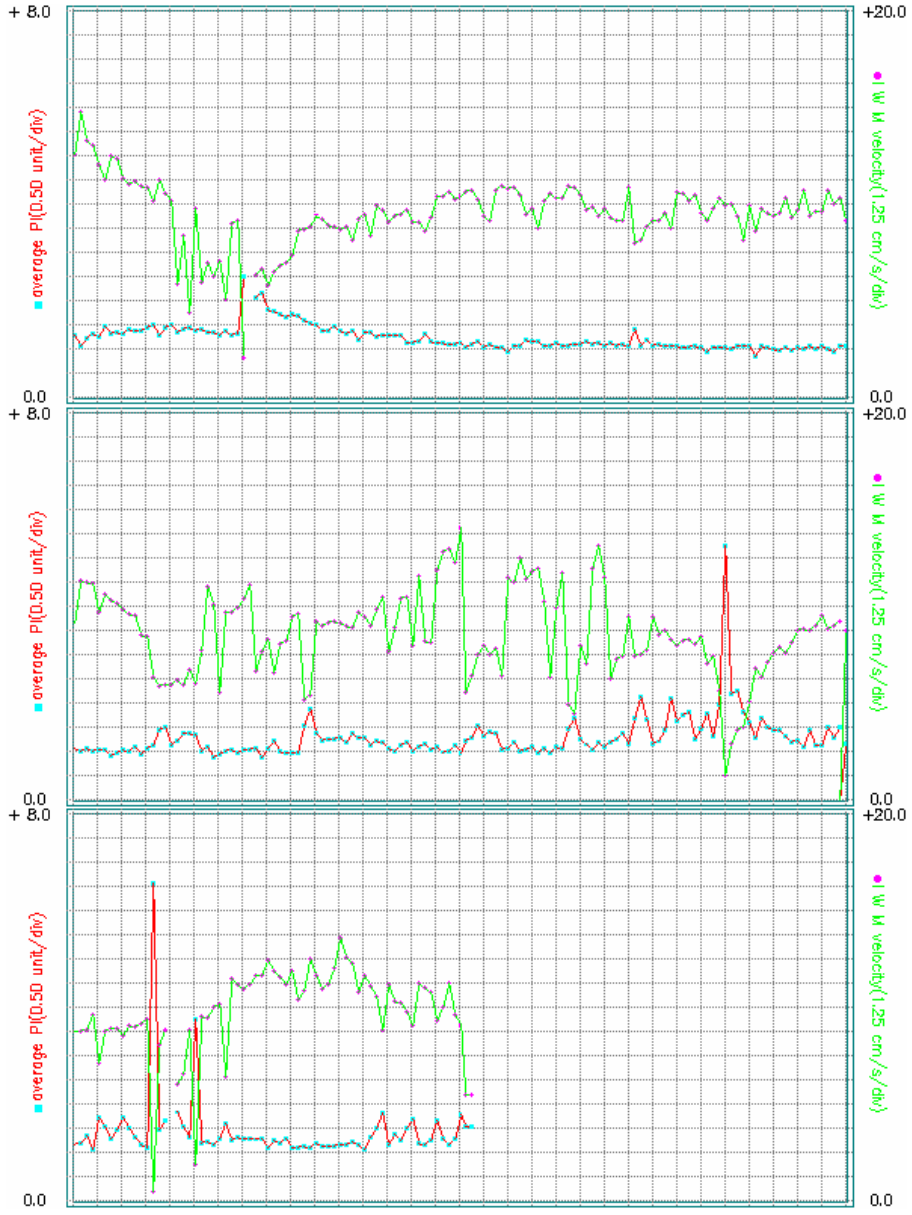

Figure 8.12c Graphs of the mean PI and the mean IWMV for Case 6c. Cycle-time is 3 minutes (12 min/div, 128 points per display).

Case 6d.

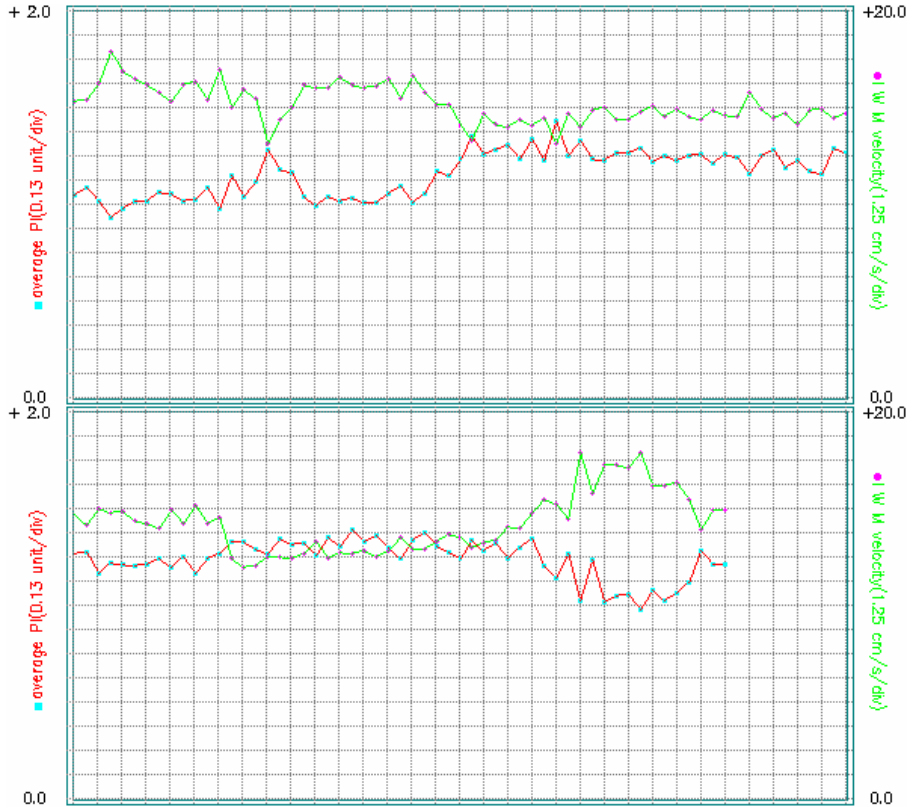

Figure 8.12d Graphs of the mean PI and the mean IWMV for Case 6d. Cycle-time is 2 minutes (4 min/div, 64 points per display).

Case 6e.

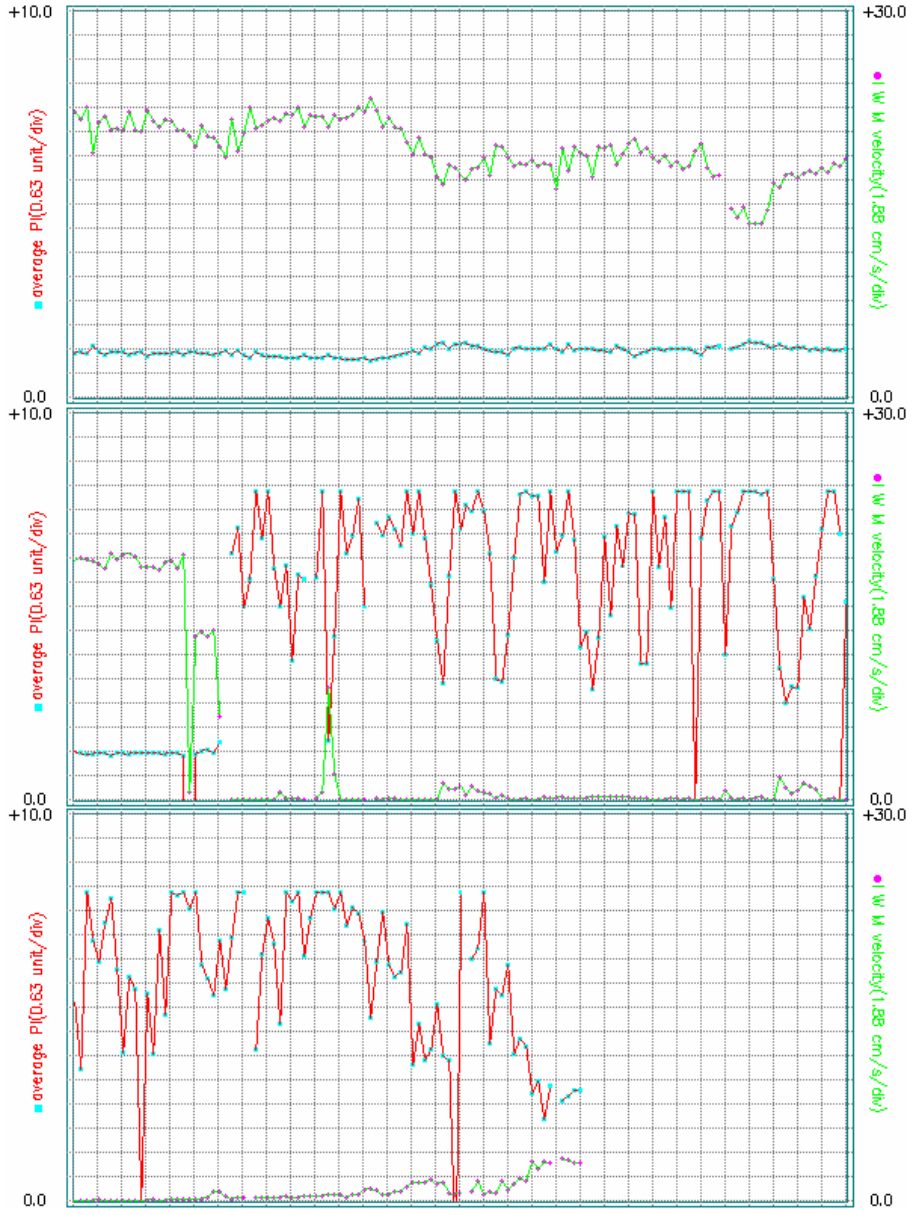

Figure 8.12e Graphs of the mean PI and the mean IWMV for Case 6e. Cycle-time is 3 minutes (12 min/div, 128 points per display).

Case 7.

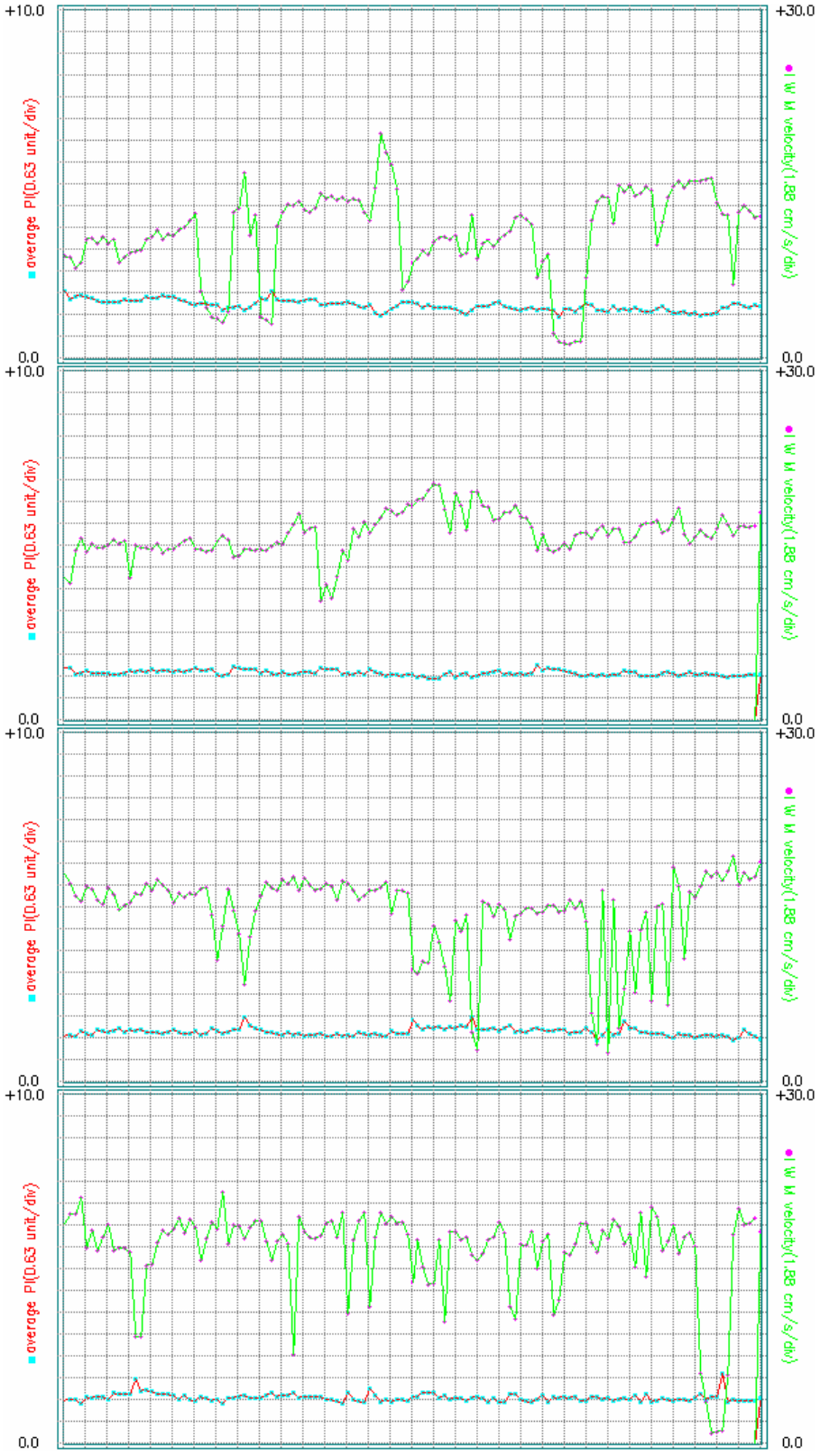

See page 28 for figure caption.

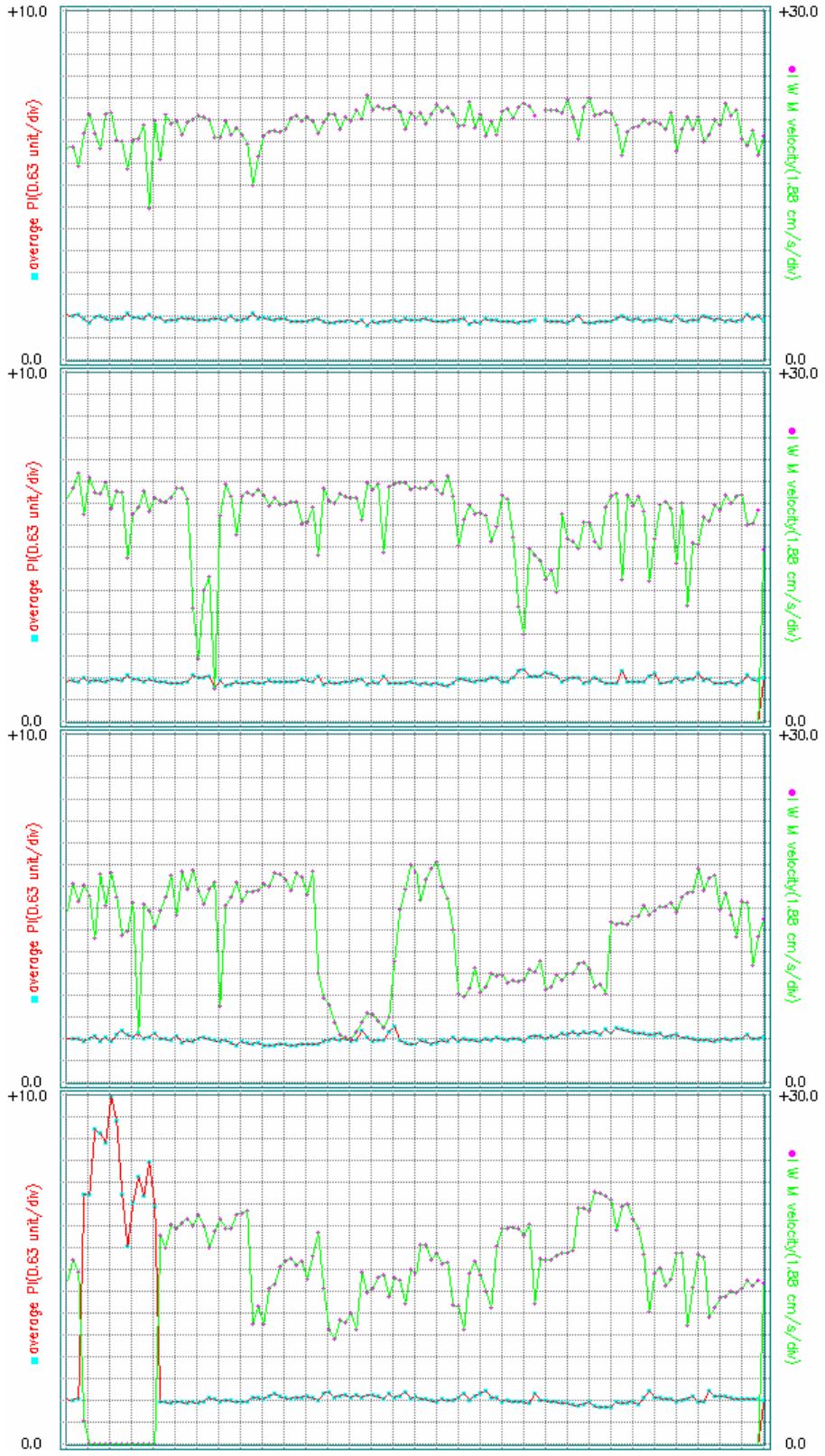

See page 28 for figure caption.

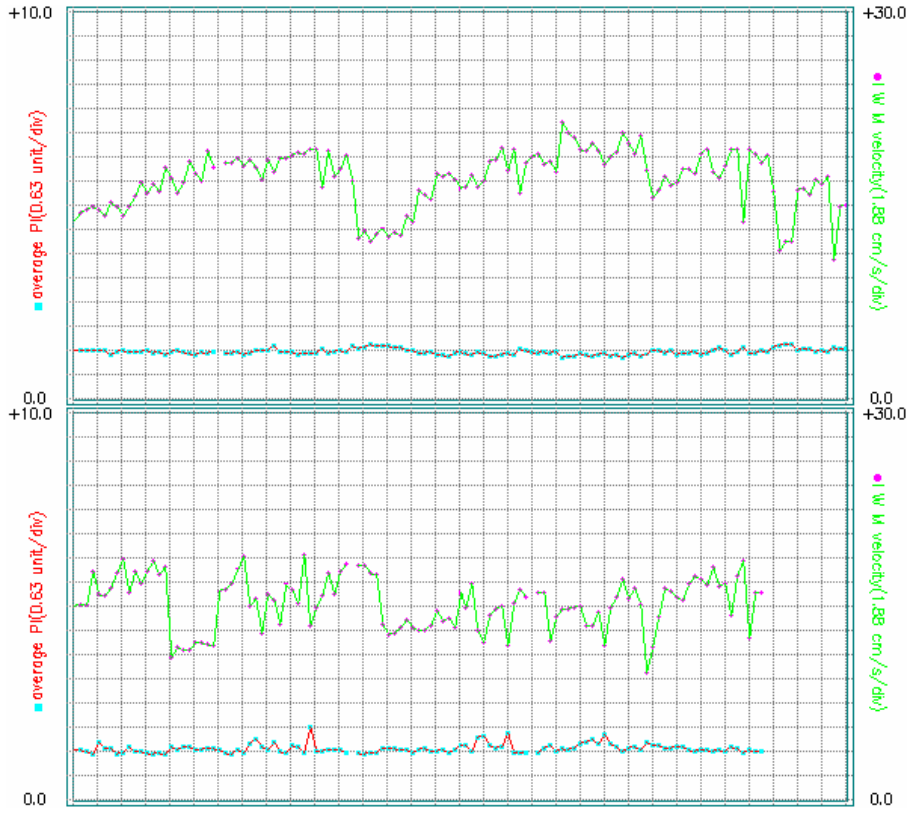

Figure 8.13 Graphs of the mean PI and the mean IWMV for Case 7. Cycle-time is 3 minutes (12 min/div, 128 points per display).

8.3.3 Discussion

For all plots different scales were used. Although this hides an apparent pattern in some cases, the mean PI and the mean IWMV curves exhibit an opposite movement in almost all cases. This pattern disappears when there is no proper signal but these cases were few. As is noted in an earlier study (Thrush and Evans 1990) the PI increases while the IWMV decreases. If such a pattern continues this may indicate a failing graft. However this requires numerous clinical evaluations

8.3.4. Some practical problems related to the graft monitoring system

The graft monitoring system has been used to monitor a number of patients. During these studies some practical difficulties have been encountered. The monitoring system has failed in some cases due to technical problems which had not been detected in the development stage or problems in management such as misuse of the system by nurses.

One apparent technical failure was caused by the MS-DOS operating system caching utility "SMARTDRV.EXE" which was supposed to improve the performance of the computer. This utility interfered with the real-time quadrature signal recording when the calculated parameters were being written to the hard-disk during the program execution. This was solved by simply disabling this utility. Another failure was due to the use of limited dynamic range numbers (integers) to calculate desired parameters during the analysis stage. This was corrected by converting each value to floating point format before performing the calculations.

The problems in management include unfamiliarity of the nurses with the system, patient resistance to continued monitoring, misplacement of the probe and

unsuitable grafts (deep grafts). Although the nurses were cooperative, they caused a system failure on one occasion by breaking a cable. The whole probe was later replaced. On another occasion, the probe was unplugged by the nurse to move the patient, then plugged back incorrectly. However this was detected and corrected immediately. All the patients monitored were extremely cooperative, but most of them did not want to be monitored for long periods. This was probably due to the impression given that the patient would be immobilised. In two cases the monitoring system was almost useless because the grafts were too deep. In another case, despite having a good signal, the system was failing because of an artefact produced by misplacement of the probe. This was corrected by relocating the probe.

Despite having these difficulties, the system has monitored a number of grafts successfully. Whenever a problem was detected it was corrected and the system was updated. It appears that the system is now relatively bug free but will need further clinical evaluation before its utility can be determined.

9. SUMMARY AND CONCLUSION

9.1. SUMMARY AND CONCLUSION

Since the medical treatment of vascular disorders, which sometimes cause loss of limb or even death, is unsatisfactory, surgical procedures to overcome failing blood supply in certain specific sites are common. Deficient arteries are replaced by prosthetic or vein bypass grafts to recover normal blood flow. A successful graft will relieve the symptoms at the affected site and result in limb salvage. However, some grafts fail after the operation due to various reasons. Intermediate and late failures can be prevented by applying graft surveillance programs. However, the methods used for graft surveillance are not practical for early continuous monitoring of the grafts. Therefore it is necessary to develop a graft monitoring system which may detect early failures which account for 20% of the total. Ideally, it must be noninvasive, cheap, reliable and versatile.

To fulfil these requirements a computerised graft monitoring system comprising an IBM-PC compatible computer, a floating point DSP board and a custom built CW Doppler board has been developed. The system can be used as a real-time Doppler signal analyser as well as the continuous or intermittent graft monitor.

The CW Doppler board, described in Chapter 3, was specifically designed to be installed in an IBM-PC compatible computer. Therefore, some of the conventional Doppler signal processing stages such as derivation of the directional Doppler signals implemented using analogue techniques were eliminated. Instead digital signal processing algorithms were introduced to implement these processes. These algorithms have been extensively discussed in Chapters 4, 5 and 6. It can be concluded that digital signal processing techniques have several advantages compared to analogue systems, for example they are easier to set up, less

susceptible to noise, and in general more flexible. These have already been demonstrated by simulation and practical results. Since a monitor should be reliable, decreasing hardware dependency in the Doppler systems will also increase reliability.

Using a floating point processor to perform DSP algorithms tremendously increases system dynamic range and accuracy. As the results obtained in Chapters 4, 5 and 6 have demonstrated floating-point DSP chips have made it possible to implement precision numerical computation in real-time.

Maximum frequency envelope detection is one of the most important intermediate processing stage in Doppler signal analysis. In Chapter 7 a new technique called the modified geometric method has been described as well as some other well known methods. Evaluation of these methods has revealed that none of the MFE detection methods are superior to all others in all situations. The choice of the method should be determined by the type of application. For example the simple threshold method is more appropriate for off-line applications, where several values might be tried for achieving the best MFE estimation. The modified threshold method can be used in systems in which the SNR slightly changes and a loss of resolution is acceptable. The modified geometric method is capable of adapting to large SNR changes, so it can be useful for general purpose software implementations being installed in different systems having different SNRs. A Doppler waveform classification algorithm has also been described.

Implementation and operation of the graft monitoring system have been described in Chapter 8. Several patients have been monitored using this system. It was found useful as it provided surgeons an immediate spectral analysis of Doppler signals and interpretation of the Doppler sonograms. It was possible to see instantly how a patients position was affecting the blood flow in the graft. The results have been presented in Chapter 8. It is as yet too early to make accurate predictions about

impending graft failure. Although it is not immediately apparent, a trend indicating graft failure may be derived from further analysis of these preliminary results. This will require further extensive evaluation of the system.

9.2. THE FUTURE

The computerised graft monitoring system described in this thesis forms a useful basis for future work. There is however much to be done in several directions. Firstly the present system needs extensive clinical evaluation. This will lead to the creation of a waveform database which may help both future monitoring systems and the surgeon to identify grafts at risk.

The Doppler unit can be improved by applying new technologies such as direct digital synthesisers. Basically, these devices are numerically controlled signal generators and may be used to design multi-frequency Doppler units. This approach could also solve the problems associated with quadrature signal generation. Another approach to design high performance Doppler systems is to use total digital design. Since very high speed and high resolution ADCs are now available and reasonably priced, Doppler signals can be digitised directly and digitally processed using dedicated signal processing chips.

Many studies have shown that simple monitoring systems employing an on/off alarm control are not convenient to monitor complex signals. Therefore more intelligent monitoring systems need to be developed. New analysis and pattern recognition tools such as expert systems, neural networks, artificial intelligence, etc., should be applied. Doppler probe design can also be improved for the convenience of the patient and staff.

APPENDIX A

Review of monitoring methods

Statistical monitoring methods are adapted from time series analysis methods and applied to patient monitoring systems to determine the trend of a medical time series which is usually a finite number of physiological data (Lewis 1971, Hope *et al* 1973, Hill and Endresen 1978, Stoodley, Allen 1983). Another approach to the monitoring problem is to use intelligent or knowledge-based (K-B) instrumentation (Shortliffe *et al* 1979, Adlassnig 1986, Papp *et al* 1988, Sztipanovits and Karsai 1988, Schecke *et al* 1991).

Basic statistical monitoring techniques include the patient-alarm-warning-system (PAWS) (Taylor 1971), cumulative sum (CUSUM) (Lewis 1970), Trig's tracking signal (Trigg 1964), patient condition factor (PCF) (Hope *et al* 1973) Box-Jenkins techniques and the Kalman filter (Kalman 1960).

PAWS is a bedside patient monitor. It is a hybrid hard-wired arrangement whose input signals are two DC voltages proportional to the patient's heart rate and mean arterial blood pressure respectively. This technique is valuable in providing warning of long-term changes in the patient, but it misses important short-term information such as brief runs of ectopic beats.

CUSUM is a sequential testing technique commonly employed to monitor industrial processes. It is a plot of the cumulative sum of the difference between the data point and a specified reference or target value for the process (Woodward and Goldsmith 1964). The CUSUM method is useful in patient monitoring to activate alarms when there has been a change in the mean level of a variable that is greater than certain preset limits.

Trig's tracking signal (TTS) is a sequential testing method which has been developed for the monitoring of forecasting systems used in economics. It is defined as the ratio between the sum of the exponentially weighted error and the sum of the exponentially absolute value of the error. The error at any instant is defined as the difference between the actual data value and the figure predicted one sampling period earlier. Although the TTS is simple to implement on a computer it is not suitable for patient monitoring because a slow change in the mean value of the process might not be detected, it is not able to distinguish between different kinds of changes and it cannot quantify a change

The PCF is a modification of the TTS. It is based on a knowledge of the maximum and minimum values which can be defined for a particular physiological variable in that patient and also the clinically normal value for that patient. Movement of the variable away from the normal value is taken as a deterioration and movement towards the normal as an improvement. A weighting factor is introduced to have maximum effect near the maximum and minimum values and little effect near the normal value (Hope and Hill 1976).

Box-Jenkins type models can be used in patient monitoring to forecast future values and to compare with incoming data in order to provide a check on whether there is a change. The idea of this approach is to express the present value of a time-series as a linear combination of past values of the series and present and past values of a random series. The parameters of the model can be estimated using maximum likelihood or least squares estimation techniques.

A powerful, recursive estimator is the Kalman filter algorithm which was suggested by Hill and Endresen (1978) as providing a possible basis for a patient monitoring. In this method, the current output is simply the sum of the past level of the system, the past trend, and a random component. It can be thought of as an efficient

formulation of the least squares method, but its recursive nature provides the means whereby the parameter can vary between data samples. The optimum parameter estimates are given at sample time *t* by the sum of the prediction based at sample time *t*-1, and a correction term. The filter generates the gain of the correction term to utilise new information arriving at time *t* in an attempt to steer the parameter estimates to their true values. A measure of the accuracy of the estimates is provided by the error covariance matrix which is recursively updated along with the parameters.

Monitoring systems incorporating the methods summarised above are termed as "vital sign monitors" by Mora *et al* (1993) and problems such as the high incidence of false alarms inherent to the classical monitoring systems have led to the proposition of intelligent alarm schemes which are based on knowledge-based systems. In K-B systems the computers are used to interpret data about a specific problem, in the light of knowledge represented or contained in the knowledge base, to develop a problem specific model and then strategies for problem solution. However model based monitoring and management systems are in their infancy and no clinical systems yet exist.

APPENDIX B

Interpretation of the complex Fourier transform

If an input of the complex Fourier transform is a complex quadrature time signal (specifically, a quadrature Doppler signal), it is possible to extract directional information by looking at its spectrum. Below, some results are obtained by calculating the complex Fourier transform for several combinations of the real and imaginary parts of the time signal (single frequency sine and cosine for simplicity). These results were confirmed by implementing simulations. The simulations were implemented on the *Hypersignal* DSP software by combining following equations as complex time function:

$$\boldsymbol{c(n) = \cos(2\pi n 7/16)}, \quad \boldsymbol{s(n) = \sin(2\pi n 7/16)} \ . \qquad \text{B.1}$$

If the complex time function is $\boldsymbol{x(t) = x_r(t) + jx_i(t)}$, where $\boldsymbol{x_r(t)}$ is the real and $\boldsymbol{x_i(t)}$ is the imaginary part, the complex Fourier transform of $\boldsymbol{x(t)}$ is

$$F\{x(t)\} = X(\omega) = \int_{-\infty}^{+\infty} x(t)e^{-j\omega t}dt = \int_{-\infty}^{+\infty} (x_r(t) + x_i(t))e^{-j\omega t}dt \ . \qquad \text{B.2}$$

Specifically the Fourier transforms of the sine and cosine are

$$F\{\cos\omega_0 t\} = \pi\{\delta(\omega - \omega_0) + \delta(\omega + \omega_0)\} \qquad \text{B.3}$$

$$F\{\sin\omega_0 t\} = \frac{\pi}{j}\{\delta(\omega - \omega_0) - \delta(\omega + \omega_0)\} \qquad \text{B.4}$$

Case (1).

$$\boldsymbol{x_r(t) = \cos\omega_0 t, \quad x_i(t) = \sin\omega_0 t,}$$
$$\boldsymbol{X(\omega) = F\{\cos\omega_0 t\} + jF\{\sin\omega_0 t\} = 2\pi\delta(\omega - \omega_0)} \qquad \text{B.5}$$

Case (2).

$$x_r(t) = \cos\omega_0 t, \quad x_i(t) = -\sin\omega_0 t,$$
$$X(\omega) = F\{\cos\omega_0 t\} + jF\{-\sin\omega_0 t\} = 2\pi\delta(\omega + \omega_0) \qquad \text{B.6}$$

Case (3).

$$x_r(t) = -\cos\omega_0 t, \quad x_i(t) = \sin\omega_0 t,$$
$$X(\omega) = F\{-\cos\omega_0 t\} + jF\{\sin\omega_0 t\} = -2\pi\delta(\omega + \omega_0) \qquad \text{B.7}$$

Case (4).

$$x_r(t) = -\cos\omega_0 t, \quad x_i(t) = -\sin\omega_0 t,$$
$$X(\omega) = F\{-\cos\omega_0 t\} + jF\{-\sin\omega_0 t\} = -2\pi\delta(\omega - \omega_0) \qquad \text{B.8}$$

Case (5).

$$x_r(t) = \sin\omega_0 t, \quad x_i(t) = \cos\omega_0 t,$$
$$X(\omega) = F\{\sin\omega_0 t\} + jF\{\cos\omega_0 t\} = j2\pi\delta(\omega + \omega_0) \qquad \text{B.9}$$

Case (6).

$$x_r(t) = \sin\omega_0 t, \quad x_i(t) = -\cos\omega_0 t,$$
$$X(\omega) = F\{\sin\omega_0 t\} + jF\{-\cos\omega_0 t\} = -j2\pi\delta(\omega - \omega_0) \qquad \text{B.10}$$

Case (7).

$$x_r(t) = -\sin\omega_0 t, \quad x_i(t) = \cos\omega_0 t,$$
$$X(\omega) = F\{-\sin\omega_0 t\} + jF\{\cos\omega_0 t\} = j2\pi\delta(\omega - \omega_0) \qquad \text{B.11}$$

Case (8).

$$x_r(t) = -\sin\omega_0 t, \quad x_i(t) = -\cos\omega_0 t,$$
$$X(\omega) = F\{-\sin\omega_0 t\} + jF\{-\cos\omega_0 t\} = -j2\pi\delta(\omega + \omega_0) \qquad \text{B.12}$$

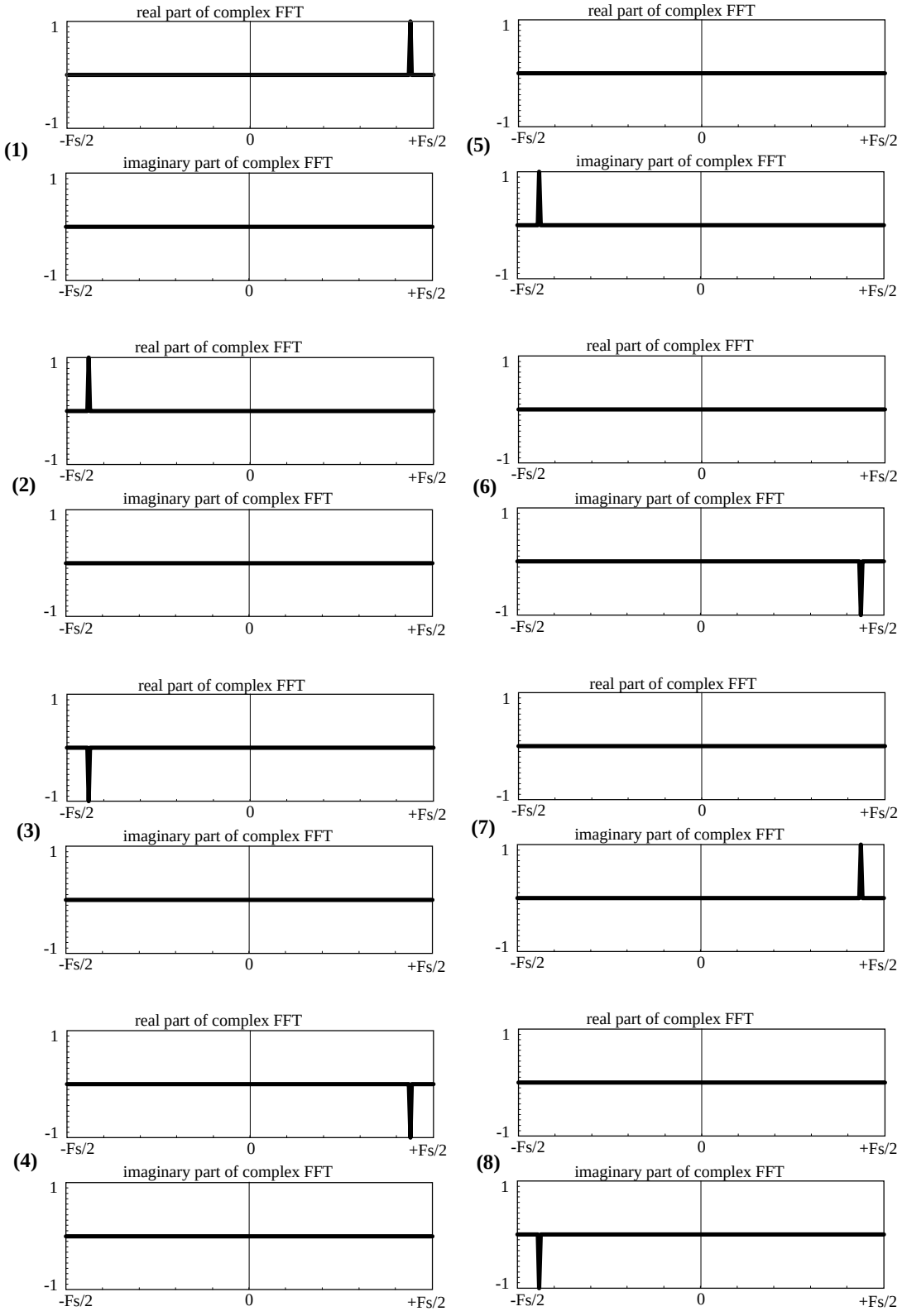

Figure B.1 Real and imaginary parts of the complex FFT of the complex quadrature sinusoidal signals (see text for explanation).

The simulation results are presented in Fig. B.1. The discrete time expressions of the sine and cosine given by B.1 form the real and imaginary inputs of the complex FFT. The following combinations were used to obtain the results illustrated in Fig. B.1.

Case (1).	$x(n)=c(n)+js(n)$	Case (5).	$x(n)=s(n)+jc(n)$
Case (2).	$x(n)=c(n)-js(n)$	Case (6).	$x(n)=s(n)-jc(n)$
Case (3).	$x(n)=-c(n)+js(n)$	Case (7).	$x(n)=-s(n)+jc(n)$
Case (4).	$x(n)=-c(n)-js(n)$	Case (8).	$x(n)=-s(n)-jc(n)$

APPENDIX C

C.1. Quadrature test signal generation using the phasing filter technique (PFT)

Fig. C.1 shows the algorithm obtained by modifying the symmetrical phasing filter technique (PFT).

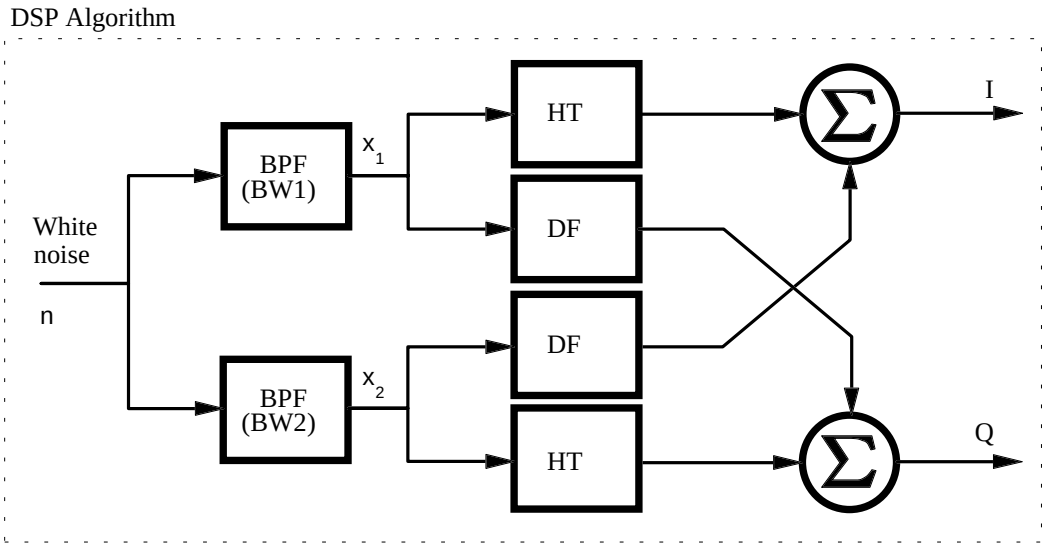

Figure C.1 Narrow-band quadrature test signal generation using the PFT.

In Fig. C.1, BPF stands for the band-pass filter and produces a narrow-band signal from a wide-band noise. Using two BPFs with different band-width gives two narrow-band signals. Processing these signals as depicted in Fig C.1 produces a quadrature pair which includes both directions. For a mathematical justification of this method, let us assume that the BPFs are ideal filters and able to select only one component of the input signal given by Eq. C.1.

$$n(t) = \cos\omega_1 t + \cos\omega_2 t + \ldots + \cos\omega_n t + \qquad \text{C.1}$$

After the BPFs, ignoring the time delays introduced by the filters:

$$x_1(t) = \cos\omega_1 t \text{ and } x_2(t) = \cos\omega_2 t. \quad \text{C.2}$$

The Hilbert transform of these signals are:

$$H[x_1(t)] = \sin\omega_1 t \text{ and } H[x_2(t)] = \sin\omega_2 t. \quad \text{C.3}$$

The final step is to implement two additions:

$$I = H[x_1(t)] + x_2(t) = \sin\omega_1 t + \cos\omega_2 t, \quad \text{C.4a}$$

$$Q = x_1(t) + H[x_2(t)] = \cos\omega_1 t + \sin\omega_2 t \quad \text{C.4b}$$

C.2. Quadrature test signal generation using the extended Weaver receiver technique

This algorithm is obtained by modifying the extended Weaver receiver technique (EWRT) algorithm described in Chapter 5 and shown in Fig. C.2.

Let us assume that input signal is given by Eq. C.1 and the outputs of the BPFs are given by Eq. C.2. The quadrature pilot signals are given as

$$p(t) = \cos\omega_p t \text{ and } q(t) = \sin\omega_p t. \quad \text{C.5}$$

$$\begin{aligned} x_3(t) &= x_1(t).p(t) + x_2(t).q(t) = \cos\omega_1 t.\cos\omega_p t + \cos\omega_2 t.\sin\omega_p t \\ &= \cos(\omega_1 - \omega_p)t + \cos(\omega_1 + \omega_p)t - \sin(\omega_2 - \omega_p)t + \sin(\omega_2 + \omega_p)t \end{aligned} \quad \text{C.6}$$

$$\begin{aligned} x_4(t) &= x_1(t).p(t) - x_2(t).q(t) = \cos\omega_1 t.\cos\omega_p t + \cos\omega_2 t.\sin\omega_p t \\ &= \cos(\omega_1 - \omega_p)t + \cos(\omega_1 + \omega_p)t + \sin(\omega_2 - \omega_p)t - \sin(\omega_2 + \omega_p)t \end{aligned} \quad \text{C.7}$$

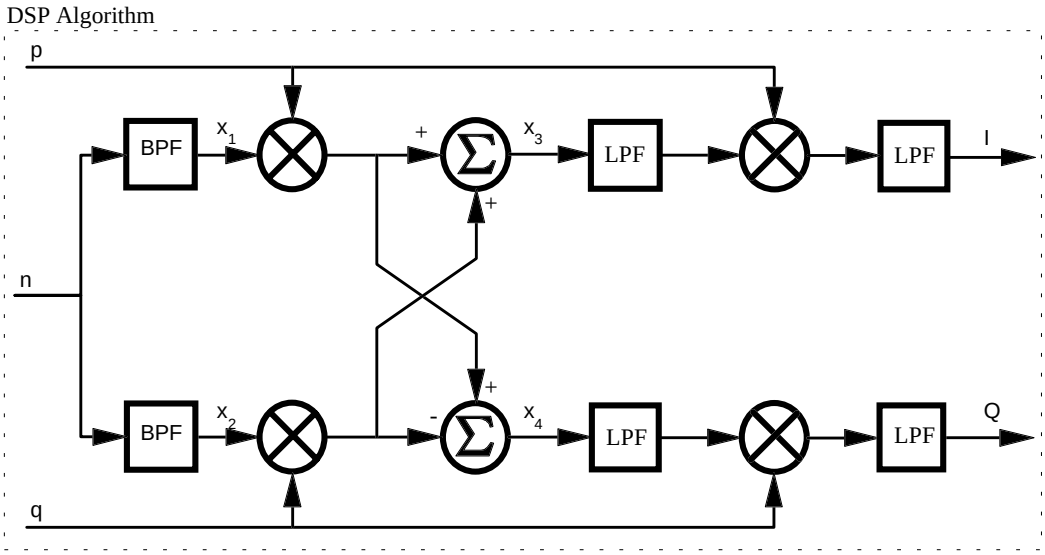

Figure C.2 Narrow-band quadrature test signal generation using the EWRT.

After low-pass filtering:

$$x_3(t) = \cos(\omega_1 - \omega_p)t - \sin(\omega_2 - \omega_p)t$$
$$x_4(t) = \cos(\omega_1 - \omega_p)t + \sin(\omega_2 - \omega_p)t \qquad \text{C.8}$$

The outputs of the final mixing stage are:

$$I(t) = x_3(t).p(t) = \cos(\omega_1 - \omega_p)t.\cos\omega_p t - \sin(\omega_2 - \omega_p)t.\cos\omega_p t$$
$$= \cos(\omega_1 - 2\omega_p)t + \cos\omega_1 t - \sin(\omega_2 - 2\omega_p)t - \sin\omega_2 t \qquad \text{C.9}$$

$$Q(t) = x_3(t).q(t) = \cos(\omega_1 - \omega_p)t.\sin\omega_p t + \sin(\omega_2 - \omega_p)t.\sin\omega_p t$$
$$= -\sin(\omega_1 - 2\omega_p)t + \sin\omega_1 t + \cos(\omega_2 - 2\omega_p)t - \cos\omega_2 t \qquad \text{C.10}$$

After low-pass filtering, the quadrature outputs are:

$$I(t) = \cos\omega_1 t - \sin\omega_2 t$$
$$Q(t) = \sin\omega_1 t - \cos\omega_2 t \qquad \text{C.11}$$

APPENDIX D

Gain dependency in the geometric method

The statement made about the geometric method can be justified by deriving related equations from Fig. D.1.

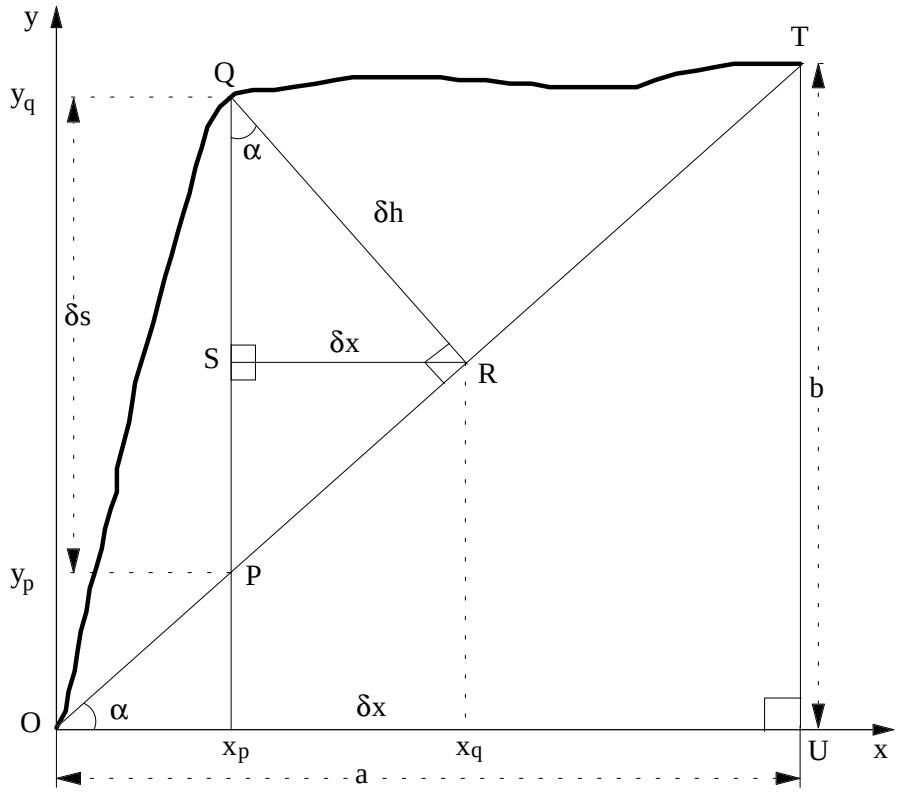

Figure D.1 Integrated spectrum curve.

From similar triangles (ΔQRS, ΔQPR and ΔOTU) we can write that

$$\cos\alpha = \frac{a}{\sqrt{a^2 + b^2}} = \frac{\delta h}{\delta s}, \qquad \text{D.1}$$

$$\sin\alpha = \frac{b}{\sqrt{a^2 + b^2}} = \frac{\delta x}{\delta h}. \qquad \text{D.2}$$

Rearranging these equations, we obtain that

$$\delta h = \frac{a}{\sqrt{a^2 + b^2}} \delta s, \qquad \text{D.3}$$

$$\delta x = \frac{b}{\sqrt{a^2 + b^2}} \delta h. \qquad \text{D.4}$$

By substituting Eq. D.3 into Eq. D.4, δx can be expressed as

$$\delta x = \frac{ab}{a^2 + b^2} \delta s \qquad \text{D.5}$$

where $\delta s = y_q - y_p$.

y_p can be calculated using the line equation defined for line |OT| which is given by y=(b/a)x. So δs can be expressed as

$$\delta s = y_q - y_p = y_q - \frac{b}{a} x_p. \qquad \text{D.6}$$

By substituting Eq. D.6 into Eq. D.5, δx can be found

$$\delta x = \frac{ab}{a^2 + b^2} (y_q - \frac{b}{a} x_p). \qquad \text{D.7}$$

From Eq. D.7 it is possible to conclude that different values of b (controlled by the system) will result in different values for δx which represents the difference between the maximum frequency bin and the knee of the ISC.

APPENDIX E

Graft Monitoring Software User Manual

E.1. Installation

To install the software a sub directory should be created on the hard-disk and the following files related to the graft monitoring system should be copied.

- PRG1.EXE
- GRMNS.OUT
- FINMT.FIN
- MODERN.FON
- MAXZ.OUT

To run the program type **PRG1** and press "↵". A main menu similar to that shown in Fig. E.1 is displayed, the following keys are active immediately:

↑,↓ Change current menu selection in respective direction (up or down)

↵ Invokes currently selected (highlighted) menu function

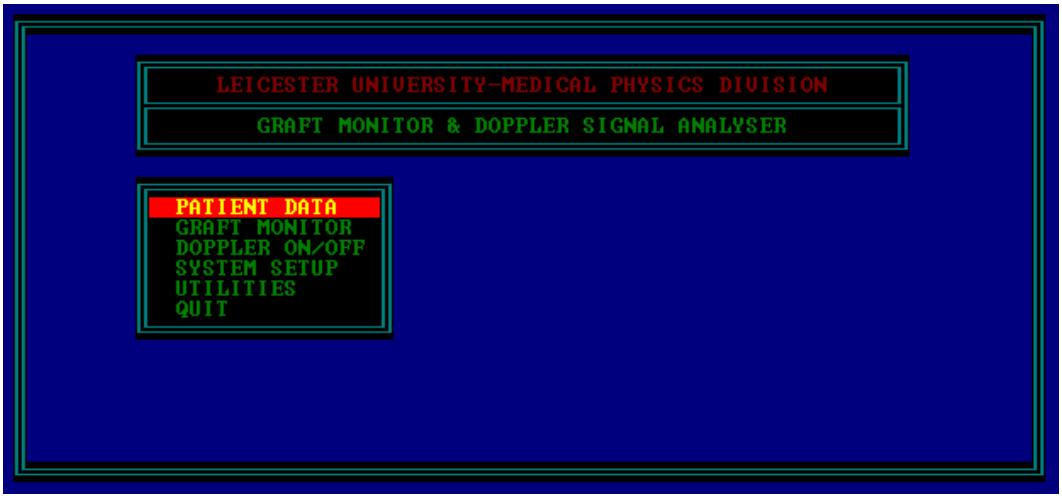

Figure E.1 Graft monitoring software main menu display.

In this area, the arrow keys can be used to highlight a particular function. Then the "↵" key activates the highlighted function.

E.2. "PATIENT DATA" field

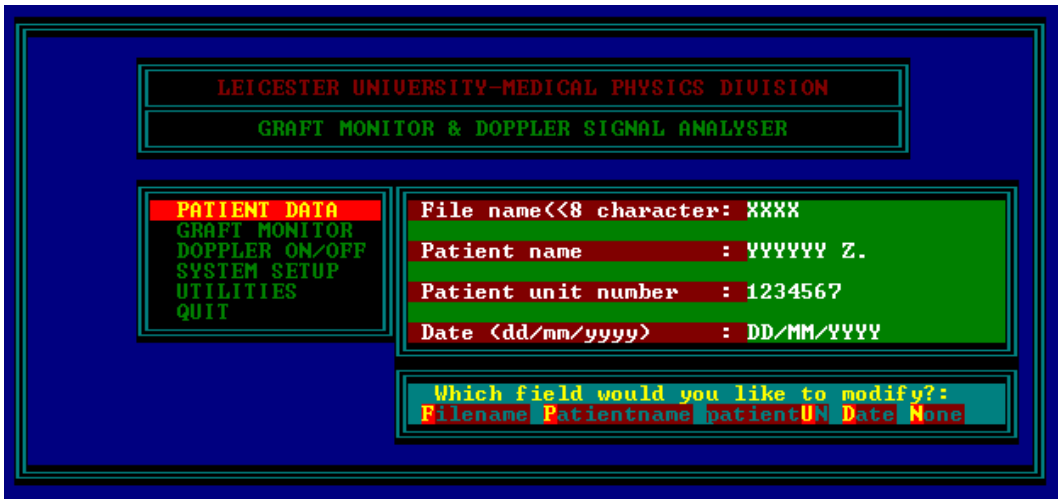

Figure E.2 A typical patient data editor display.

This selection allows basic patient data entry. The following data fields can be entered:

File name Defines the name of the files (with different extensions) used in subsequent data storage. The file name cannot be more than 8 characters.

Patient name This field is used to enter the patient name.

Patient unit number This field is used to enter the patient unit number.

Date This is used to enter the date on which monitoring started.

After entering these fields the operator is asked if data is correct. If the answer is yes (key **Y**) a data file "*.PID" will be created and the patient data will be saved as an ASCII file. Three other files associated with the file name entered will also be created: *.MAX to store the maximum frequency envelope; *.MEN to store the

mean frequency envelope; *.REC to store the mean PI, the mean IWMV, and actual times for each measurement. These are saved as binary files.

If the answer is no (key **N**) then the operator is asked which field to modify as illustrated in Fig. E.2. By pressing one of the highlighted keys the related field can be modified. If key **N** (none) is pressed this process will be cancelled and **no data will be stored**.

E.3. "GRAFT MONITOR" field

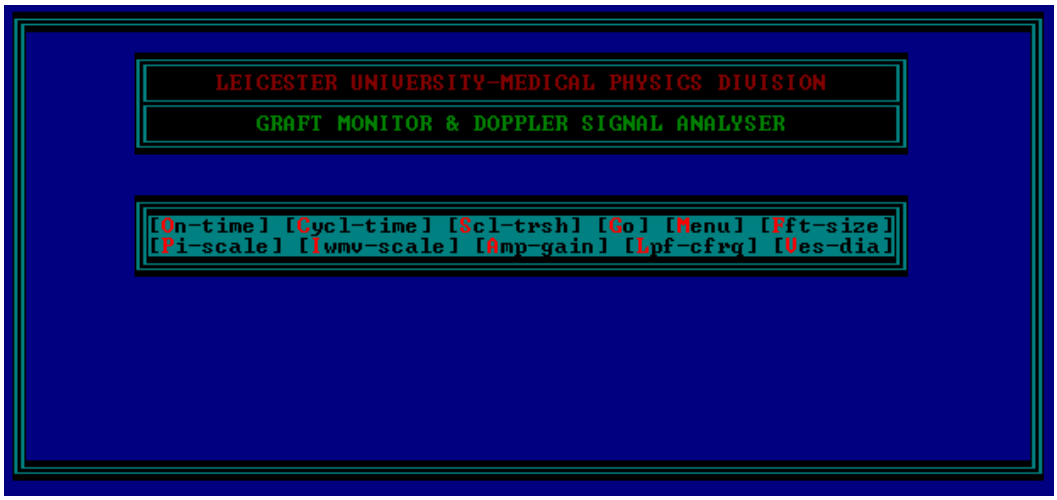

Figure E.3 Graft monitor menu display.

The "GRAFT MONITOR" option, illustrated in Fig. E.3, allows the user to set up the monitoring parameters. The following options are available:

On-time This option is activated by pressing "**O**". This field determines the Doppler board's on time duration., i.e., the data collection period. The default time is 6.4 second which corresponds to one page (screen). The maximum on-time duration is 60

seconds and determined by the available operating system memory acting as RAM disk.

Cycl-time (Cycle time). This option is activated by pressing "**C**". This field determines the duration of one complete process cycle. The default time is 1 minute. There is no upper limit for this parameter.

Scl-trsh (Scale threshold). This option is activated by pressing "**S**". This is an arbitrary constant related to the MFE algorithm (modified threshold method). The default value is 2. It can be modified to obtain the best MFE estimation.

Go This option is activated by pressing "**G**". It starts the monitoring process.

Menu This option is activated by pressing "**M**". It allows a return to the main menu.

Fft-size This option is activated by pressing "**F**". The user is prompted as shown in Fig D.4 to chose the FFT size used for subsequent spectral analysis. Pressing one of the numbers selects the corresponding FFT size. "Esc" will cancel the selection process.

Figure E.4 FFT size selection menu.

Pi-scale This option is activated by pressing "**P**". This option allows the mean PI display scale to be modified for the graft monitoring. The default scale is 10.

Iwmv-scale This option is selected by pressing "**I**". It allows modification of the mean IWMV display scale for graft monitoring. The default scale is 20 cm/sec. If "Ves-dia" (see later explanation) field is entered then the volume flow (ml/min) will be displayed.

Amp-gain (Amplifier gain). This option is activated by pressing "**A**". It allows the gain of the CW Doppler board to be set. Any gain between -25 dB and +25 dB can be selected. The default gain is 0 dB.

Lpf-cfrq (Low-pass filter cut-off frequency). This option is activated by pressing "**L**". It allows the cut-off frequency of the programmable low-pass filter to be set. Any frequency between 1 kHz and 20 kHz can be selected. The default cut-off frequency is 9.2 kHz.

Ves-dia This option is activated by pressing "**V**". Entering this field causes volume flow to be displayed as ml/min instead of IWMV. After the vessel diameter is entered the user will be prompted for confirmation. If "**Y**" is pressed the volume flow will be displayed. If "**N**" is pressed then the mean IWMV will be displayed. A typical data entry dialogue box is illustrated in Fig D.5.

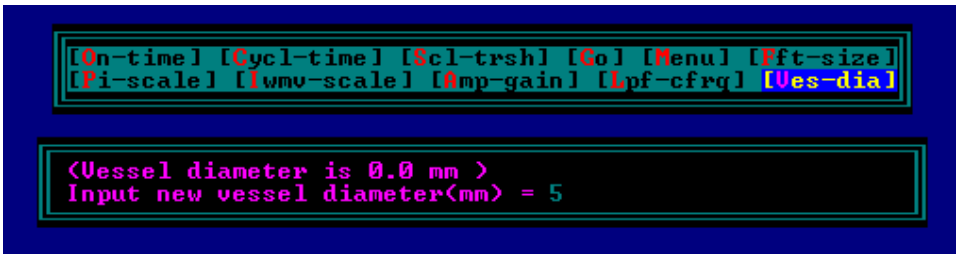

Figure E.5 A typical data entry dialogue box.

E.4. "DOPPLER ON/OFF" field

The "DOPPLER ON/OFF" field allows the user to switch the CW Doppler board on or off. When this field is selected (highlighted) a dialogue box, indicating the condition of the board, appears automatically as shown in Fig. E.6. While this field is highlighted pressing the "↵" key toggles the condition of the Doppler board. This can immediately be observed in the dialogue box. The dialogue box disappears as any other field is selected.

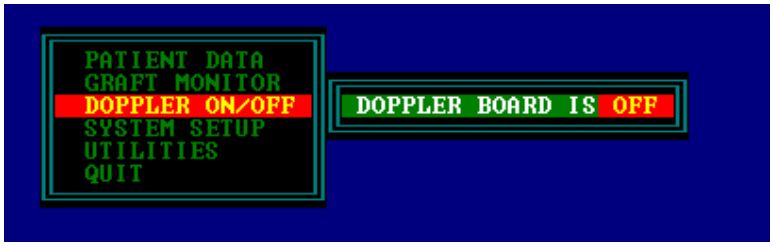

Figure E.6 Appearance of "DOPPLER ON/OFF" menu selection.

E.5. "SYSTEM SETUP" field

Selecting this field by highlighting and pressing "↵" turns the system into a general purpose Doppler signal analyser. The separated time domain signals and their spectra or the Doppler sonogram can be displayed. The following keys are immediately active:

A Enables or disables spectral averaging process (smoothing).

D Stops (freezes) the operation temporarily. The second press of this key reruns the program

E Enables or disables the display of the MF and IWMF envelopes.

F Invokes the system sampling frequency selection menu. It allows the selection of one of the following sampling frequencies by choosing the appropriate option.

<1>1.024, <2>2.048, <3>5.12, <4>10.24, <5>20.48 kHz.

L Sets the spectrum analyser display for linear or logarithmic scale.

O Enables or disables the CW Doppler board.

R Reverses the signal channels, i.e., the Doppler sonogram.

S Switches the screen between the Doppler sonogram display and time domain signal and spectrum analyser display.

T Sets the system output to the quadrature or directional output mode.

+ Decreases the intensity of the Doppler sonogram.

- Increases the intensity of the Doppler sonogram.

→ Increases the system sampling frequency.

← Decreases the system sampling frequency.

PgUp Shifts the Doppler sonogram up.

PgDn Shifts the Doppler sonogram down.

Alt G Allows setting of the system gain.

Alt F Allows setting of the low-pass filter cut-off frequency.

Esc Terminates all the operations and returns to the main menu.

E.6. "UTILITIES" field

Fig E.7 shows a typical menu display when the "UTILITIES" field is activated. This option provides some utilities performed after a monitoring session. The following utilities are available:

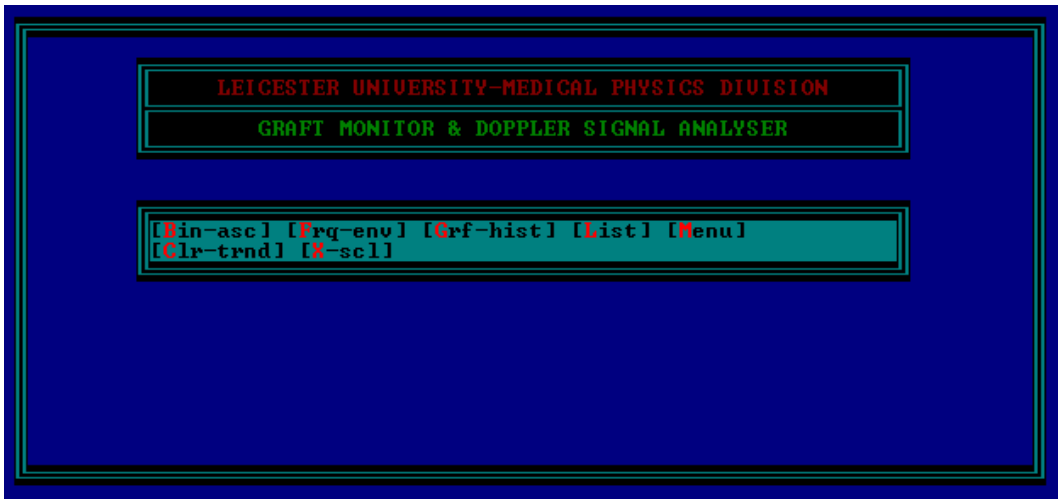

Figure E.7 Utilities menu display.

Bin-asc (Binary-to-ASCII conversion). This option is activated by pressing "**B**". It provides conversion of the binary files stored during the monitoring stage into the ASCII files. It is especially useful when the results are desired to be imported to a graphic package. Only the binary files with extensions IQS, MAX, MEN and REC can be converted. (see description of the files created by the monitoring software). The file conversion is summarised in Table E.1.

Binary file	Resulting ASCII files			
*.IQS	*_I.IQS	*_Q.IQS		
*.REC	*_A.AIM	*_A.API	*_A.TIM	*_A.PRN
*.MAX	*_A.MAX			
*.MEN	*_A.MEN			

Table E.1 Binary-to ASCII file conversion results (see Table E.2 for further details).

Frq-env (Frequency envelopes). This option is activated by pressing "**F**". It allows the display of the MF and IWMF envelopes stored during the on-line monitoring stage. The envelopes are displayed page by page.

Grf-hist (Graft history). This option is activated by pressing "**G**". It allows the display of the mean PI and mean IWMV stored during the on-line monitoring stage. These parameters are displayed point by point.

List (List files). This option is activated by pressing "**L**". It causes all the files related to the monitoring program to be listed. This is done by choosing one of the options illustrated in Fig. E.8.

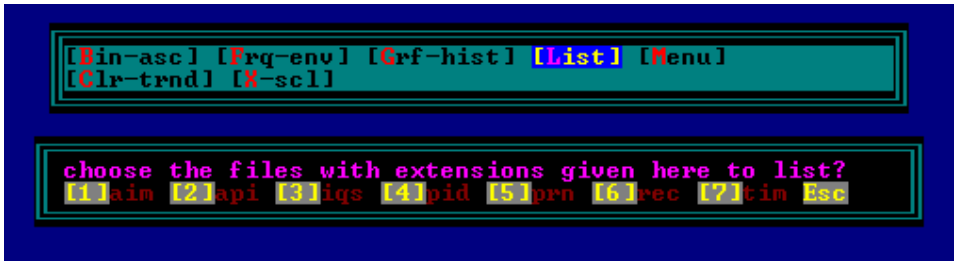

Figure E.8 List menu display.

Menu This option is activated by pressing "**M**". It allows a return to the main menu.

Clr-trnd (Clear trends). This option is activated by pressing "**C**". It is related to the on-line monitoring stage. The monitored parameters existing on the screen can be cleared.

X-scl (X axis scale). This option is activated by pressing "**X**". It allows the x scale used in the "Frq-env" and "Grf-hist" utilities to be changed.

The graft monitoring program can be terminated by choosing the "**QUIT**" field. This is illustrated in Fig. E.9.

Figure E.9 The graft monitoring software "QUIT" display.

E.7. Description of the files created by the monitoring software

The graft monitoring software generates four binary files and the utilities software generates eight ASCII files. Filename extensions are summarised in Table E.2.

Extension	Description of data file
***.PID**	ASCII data file holding basic patient data
***.IQS**	Binary quadrature Doppler signal data stored in the RAM-disk during the recording stage
***.REC**	Binary file in which the mean PI, the mean IWMV and actual measurement times are stored
***.MAX**	Binary file in which the MF envelope is stored
***.MEN**	Binary file in which the IWMF envelope is stored
***_I.IQS**	ASCII data file holding the in-phase component of the quadrature Doppler signal. This file is generated from the binary *.IQS file by the "Bin-asc" utility
***_Q.IQS**	ASCII data file holding the quadrature-phase component of the quadrature Doppler signal. This file is generated from the binary *.IQS file by the "Bin-asc" utility
***_A.API**	ASCII data file holding the mean PI values. This file is generated from the binary *.REC file by the "Bin-asc" utilityı
***_A.AIM**	ASCII data file holding the mean IWMV values. This file is generated from the binary *.REC file by the "Bin-asc" utility
***_A.TIM**	ASCII data file holding the actual measurement times. This file is generated from the binary *.REC file by the "Bin-asc" utilityı
***_A.PRN**	ASCII data file holding the mean PI values, the mean IWMV values and the actual measurement times in form of a table. So it can be printed for off-line inspection. This file is generated from the binary *.REC file by the "Bin-asc" utility
***_A.MAX**	ASCII data file holding the MF envelope. This file is generated from the binary *.MAX file by the "Bin-asc" utility
***_A.MEN**	ASCII data file holding the IWMF envelope. This file is generated from the binary *.MEN file by the "Bin-asc" utility

Table E.2 Description of the files created by the monitoring software.

REFERENCES

Abu-el-Haije AI, Al-Ibrahim MM (1986) Improving performance of digital sinusoidal oscillators by means of error feedback circuits. *IEEE Trans Circuits Syst*, **CAS-33**, 373-380.

Adlassnig KP (1986) Fuzzy set theory in medical diagnosis. *IEEE Eng Med Biol M*, **9**, 38-44.

Ahn YB, Kim YG, Park SB (1988) New multigate pulsed Doppler system using second order sampling. *Electron Lett*, **24**, 1091-1093.

Allen R (1983) Time series methods in the monitoring of intracranial pressure. Part 1: problems, suggestions for a monitoring scheme and review of appropriate techniques. *J Biomed Eng*, **5**, 5-18.

Allen R (1983) Time series methods in the monitoring of intracranial pressure. Part 2: comparative study and initial assesment. *J Biomed Eng*, **5**, 103-109.

Ansari R (1987) IIR discrete-time Hilbert transformers. *IEEE Trans Acoust Speech Signal Processing*, **ASSP-35**, 116-119.

Armytage WHG (1961) A social history of engineering. Faber and Faber, London, pp 310-313.

Arts MGJ, Roevros JMJG (1972) on the instantaneous measurement of blood flow by ultrasonic means. *Med Biol Eng*, **10**, 23-34.

Aydin N, Evans DH (1994) Implementation of directional Doppler techniques using a digital signal processor. *Med Biol Eng Comput*, **32**, S157-S164.

Aydin N, Fan L, Evans DH (1994) Quadrature-to-directional format conversion of Doppler signals using digital methods. *Physiol Meas*, **15**, 181-199.

Baker DW (1970) Pulsed ultrasonic Doppler blood-flow sensing. *IEEE Trans Sonics Ultrasonics* , **SU-17**, 170-185.

Bandyk DF, Seabrook GR, Moldenhauer P *et al* (1988) Hemodynamics of vein graft stenosis. *J Vasc Surg*, **8**, 688-695.

Bandyk DF, Cato RF, Towne JB (1985) A low flow velocity predicts failure of femoro-popliteal and femoro-tibial bypass grafts. *Surgery*, **98**, 799-809.

Barber WD, Eberhard JW, Karr SG (1985) A new time domain technique for velocity measurements using Doppler ultrasound. *IEEE Trans Biomed Eng*, **BME-32**, 213-229.

Barnes RW, Thompson BW, MacDonald CM *et al* (1989) Serial noninvasive studies do not herald postoperative failure of femoropopliteal or femorotibial bypass grafts. *Ann Surg*, **210**, 486-494.

Bateman A, Yates W (1988) Digital signal processing design, Pitman Publishing, London, 279-332.

Berkowitz HD (1985) Postoperative screening in peripheral arterial disease. *in Noninvasive diagnostic techniques in vascular disease, edited by Bernstein EF*, CV Mosby Co, St Luis, 633-638.

Brennan JA, Thrush AJ, Evans DH (1991a) Perioperative monitoring of blood flow in femoroinfragenicular vein grafts with Doppler ultrasonography: A preliminary report. *J Vasc Surg*, **13**, 468-474.

Brennan JA, Walsh AKM,Beard JD, Bolia AA, Bell PRF (1991b) The role of simple non-invasive testing in infrainguinal vein graft surveillance. *Eur J Vasc Surg*, **5**, 13-17.

Broman H (1988) Knowledge-based signal processing in the decomposition of myoelectric signals. *IEEE Eng Med Biol M*, **7(2)**, 24-28.

Bush G, Evans DH (1993) Digital audio tape as a method of storing Doppler ultrasound signals. *Physiol Meas*, **14**, 381-386.

Carrel A, Guthrie CG (1906) Uniterminal and biterminal venous transplantations. *Surg Gynecol Obstet*, **2**, 266.

Chang SH, Park SB, Cho GH (1993) Phase-error-free quadrature sampling technique in the ultrasonic B-scan imaging system and its application to the synthetic focusing system. *IEEE Trans Ultrason Ferroelec Freq Contr*, **40**, 216-223.

Cizek V (1970) Discrete Hilbert transform. *IEEE Trans Audio Electroacoust*, **AU-18**, 340-343.

Cleveland WS (1979) Robust locally weighted regression and smoothing scatterplots. *J Amer Statist Assoc*, **74**, 829-836.

Coghlan BA, Taylor MG (1976) Directional Doppler techniques for detection of blood velocities. *Ultrasound Med Biol*, **2**, 181-188.

Crook J (1970) User needs of patients and nurses in clinical monitoring. *Postgrad Med Journ*, **46**, 374-377.

Crooks LE, Kaufman L (1984) NMR imaging of blood flow. *Br Med Bull*, **40**, 167-169.

Cross G, Light LH (1974) Non-invasive intra-thoracic blood velocity measurement in the assessment of cardio-vascular function. *Biomed Eng*, **9**, 404-471.

Cullen DJ, Teplick DJ (1979) The role of computers in the future of intensive care. *Proc IEEE*, **67**, 1307-1308.

Dahnoun N (1990) Continuous monitoring of blood flow. PhD thesis, Leicester University.

Dahnoun N, Thrush AJ, Fothergill JC, Evans DH (1990) Portable directional ultrasonic Doppler blood velocimeter for ambulatory use. *Med Biol Eng Comput*, **28**, 474-482.

D'Alessio T (1985) 'Objective' algorithm for maximum frequency estimation in Doppler spectral analysers. *Med Biol Eng Comp*, **23**, 63-68.

Davies AH, Magee TR, Wyatt M, Baird R, Horrocs M (1993) Impedance analysis versus colour duplex in femorodistal vein graft surveillance. *Eur J Vasc Surg*, **7**, 14-15.

DeJong DA, Megens PHA, DeVlieger M, Thon H, Holland WPJ (1975) A directional quantifying Doppler system for measurement of transport velocity of blood. *Ultrasonics*, **13-3**, 138-141.

Diggle PJ (1990) Time series-a biostatistical introduction. Oxford University Press, Oxford.

Edward WS, Lyons C (1958) Three years' experience with peripheral arterial grafts of crimped nylon and teflon. *Surg Gynecol Obstet*, **107**, 62.

Edward WS, Tapp JS (1955) Chemically treated naylon tubes as arterial grafts. *Surgery*, **38**, 61.

Evans DH (1988) A pulse-foot-seeking algorithm for Doppler ultrasound waveforms. *Clin Phys Physiol Meas*, **9**, 267-271.

Evans DH, McDicken WN, Skidmore R, Woodcock JP (1989a) Doppler ultrasound: physics, instrumentation and clinical applications. John Wiley & Sons Ltd, Chichester, pp 98-100, 145-149.

Evans DH, Schlindwein FS, Levene MI (1989b) An automatic system for capturing and processing ultrasonic Doppler signals and blood pressure signals. *Clin Phys Physiol Meas*, **10**, 241-251.

Evans JM, Beard JD, Skidmore R, Horrocks M (1987) An analogue mean frequency estimator for the quantitative measurement of blood flow by Doppler ultrasound. *Clin Phys Physiol Meas* , **8**, 309-315.

Eyer MK, Brandestini MA, Phillips (1981) Color digital echo/Doppler image presentation, *Ultrasound Med Biol* , **7**, 21-31.

Fitzgerald DE, Gosling RG, Woodcock JP (1971) Grading dynamic capability of arterial collateral circulation. *Lancet*, **1**, 66-67.

Fliege NJ, Wintermantel J (1992) Complex digital oscillators and FSK modulators. *IEEE Trans Signal Processing*, **40**, 333-342.

Follet DH (1991) Electromagnetic radio frequency interference with Doppler equipment. *Phys Med Biol*, **36**, 1443-1455.

Forsberg F, Jorgensen MO (1989) Sampling technique for an ultrasound Doppler system. *Med Biol Eng Comput*, **27**, 207-210.

Freimen AH, Steinberg CA (1964) The analysis of simultaneously recorded cardiovascular data with the digital computer. *Annals of the New York Academy of Sciences*, **115**, 1091.

Fulton TJ, Hamilton WAP, Graham JC, Roberts VC (1983) On-line analysis of the femoral artery flow velocity waveform and its application in the diagnosis of arterial disease. *J Biomed Eng*, **5**, 151-156.

Furuno K, Mitra SK, Hirano K, Ito Y (1975) Design of digital sinusoidal oscillators with absolute periodicity. *IEEE Trans Aerospace and Electronic Systems*, **AES-11**, 1286-1299.

Geddes LA, Hoff HE, Spencer WA, Vablona C (1962) Acquisition of physiological data at the bedside: a progress report. *American Journal of Medical Electronics*, **1**, 62.

Gerzberg L, Meindl JD (1977) Mean frequency estimator with applications in ultrasonic Doppler flowmeters. *In: Ultrasound in medicine 3B (Eds D White, RE Brown)*, Plenum Press, London, pp 1173-1180.

Gerzberg L, Meindl JD (1980a) Power-spectrum centroid detection for Doppler systems applications. *Ultrasonic Imaging*, **2**, 232-261.

Gerzberg L, Meindl JD (1980b) The root *f* power-spectrum centroid detector: system considerations, implementation and performance. *Ultrasonic Imaging*, **2**, 262-289.

Gibbons DT, Evans DH, Barrie WW, Cosgriff PS (1981) Real time calculation of ultrasonic pulsatility index. *Ultrasound Med Biol*, **19**, 28-34.

Gibson JD (1989) Principles of digital and analog communications, Macmillan Publishing Company, New York, 113-118.

Gold B, Oppenheim AV, Rader CM (1970) Theory and implementation of discrete Hilbert transform. *Proc Symp Comput Process Comm*, Polytechnic Press, 235-250.

Gosling RG, Dunbar G, King DH, Newman DL, Side CS, Woodcock JP, Fitzgerald DE, Keates JS, MacMillan D (1971) The quantitative analysis of occlusive peripheral arterial disease by a non-intrusive ultrasonic technique. *Angiology*, **22**, 52-55.

Gosling RG, King DH, Newman DL, Woodcock JP (1969) Transcutaneous measurement of arterial blood velocity by ultrasound. *In: Ultrasonic for industry 1969 (conference papers)*, 16-23.

Graham H (1956) Surgeons all, Rich and Cowan, London, 357.

Greer JRB (1970) A clinical computer and monitor. *Postgrad Med Journ*, **46**, 369-373.

Gross RE, Hurwitt ES, Bill AH Jr *et al* (1948) Preliminary observations on the use of human arterial grafts in the treatment of certain cardiovascular defects. *N Engl J Med*, **239**, 578.

Halberg LI, Thiele KE (1986) Extraction of blood flow information using Doppler-shifted ultrasound. *Hewlett-Packard Journal*, **37**, 35-40

Hansteen V, Lorentsen E (1974) Vasodilator drugs in the treatment of peripheral arterial insufficiency. *Acta Medica Scandinavica*, **Suppl. 556**, 3-62.

Harris FJ (1978) On the use of windows for harmonic analysis with discrete Fourier transform. *Proc IEEE*, **66**, 51-83.

Harris FJ (1982) The discrete Fourier transform applied to time domain signal processing. *IEEE Communication Magazine,* **20-3**, 13-22.

Harris PL (1992) Vein graft surveillance-all part of the service. *Br J Surg*, **79**, 97-98.

Harris PL, Taylor LA, Cave FD, Charlesworth D (1974) The relationship between Doppler ultrasound assesment and angiography in occlusive arterial disease of the lover limbs. *Surg Gynecol Obstet*, **138**, 911-914.

Harrison R (1978) A review of SSB phasing techniques. *Ham Radio*, **Jan**, 52-63.

Hill DW, Endreswen J (1978) Trend recording and forecasting in intensive therapy. *Brit J Clin Equip*, **3**, 4-14.

Hitchings DJ, Campbell MJ, Taylor DEM (1975) Trend detection of pseudo-random variables using an exponentially mapped past statistical approach: an adjunct to computer assisted monitoring. *Int J Bio-med Computing*, **6**, 73-87.

Hope CE, Hill DW (1976) Computer -assisted blood flow measurement in anaesthesia and intensive care. in *Clinical blood flow measurement* (Ed: Woodcock J), Sector Publishing Ltd, London, 177-180.

Hope CE, Lewis CD, Perry IR, Gamble A (1973) Computed trend analysis in automated patient monitoring systems. *Brit J Anaesth*, **45**, 440-448

Jensen RE, Shubin H, Meager PF, Weil MH (1966) On-line computer monitoring of the seriously ill patient. *Med Biol Eng*, **4**, 265.

Johnston KW, Kassam M, Cobbold RSC (1982) Online identifying and quantifying Doppler ultrasound waveforms. *Med Biol Eng Comp,* **20**, 336-342.

Johnston KW, Kassam M, Cobbold RSC (1983) Relationship between Doppler pulsatility index and direct femoral pressure measurements in the diagnosis of aortoiliac occlusive. *Ultrasound Med Biol*, **9**, 271-281.

Johnston KW, Maruzzo BC, Cobbold RSC (1978) Doppler methods for quantitative measurement and localization of peripheral arterial occlusive disease by analysis of the blood flow velocity waveform. *Ultrasound Med Biol*, **4**, 209-223.

Johnston KW, Zuech P, Kassam MS (1985) Kriteria for selection of Doppler instrumentation. *in Non invasive diagnostic techniques in vascular disease, edited by Berstein EF,* The CV Mosby Company, 33-39.

Kasai T, Iwata M, Oosaki K (1974) Computerized patient monitoring system. *Fujitsu Sci Tech J*, **10-3**, 67-82.

Kempczinski RF (1984) Vascular grafts-an overview. *in Vascular Surgery, edited by Rutherford RB,* W.B. Saunders Company, Philadelphia, 361-366.

Kirsten J, Flemig T (1991) Undersampling reduces data acquisition costs. *Electronic Engineering*, **63-775**, 39-43.

Kirsten J, Flemig T (1991) Applications of undersampling techniques. *Electronic Engineering*, **63-776**, 41-47.

Kontis S (1987) Algorithms for fast computation of the intensity weighted mean Doppler frequency. *Med Biol Eng Comp*, **25**, 75-76.

Leather RP, Shah DM, Chang BB, Kaufman JL, (1988) Resurrection of the in situ saphenous vein bypass. *Ann Surg*, **208**, 435-442.

Lewis CD (1971) Statistical monitoring techniques. *Med Biol Eng*, **9**, 315-323.

Lewis FJ, Deller S, Yokochi H, Rosi PS, Quin ML, Kite M, Rabin S (1970) Automatic monitoring in the postoperative recovery room. *Surg Gynecol Obstet*, **130**, 333-341.

MacKenzie J (1925) Diseases of the heart, Oxford University Press, Oxford.

Mallows CL (1980) Some theory of nonlinear smoothers. *Ann Statist*, **8**, 695-715.

Maloney JV (1968) The trouble with patient monitoring. *Ann Surg*, **168**, 605-619.

Mardiguian M (1984) Interference control in computers and microprocessor-based equipment, Don White Consultants, Inc., Virginia.

McClellan JH, Parks TW, Rabiner LR (1973) A computer program for designing optimum FIR linear phase digital filters. *IEEE Trans Audio and Electroacoustics*, **AU-21**, 506-526.

McClure DK, Greenburg AG, Fink RM (1975) Computerized patient monitoring - a critical evaluation. *Proc San Diego Bio-Medical Symp*, **14**, 289-295

McLeod FD (1967) A directional Doppler flowmeter. *Digest 7th Int Conf Med Biol Eng*, p213.

Mo LYL, Yun LC, Cobbold RSC (1988) Comparison of four digital maximum frequency estimators for Doppler ultrasound. *Ultrasound Med Biol*, **14**, 355-363.

Moody AP, Gould DA, Harris PL, (1990) Vein graft surveillance improves patency in femoropoplitel bypass. *Eur J Vasc Surg*, **4**, 117-121.

Mora FA, Passariello G, Carrault G, Le Pichon JP (1993) Intelligent patient monitoring and management systems: a review. *IEEE Eng Med Biol*, **12(4)**, 23-33.

Mozersky DJ, Hokanson DE, Baker DW, Sumner DS, Stradnes DE (1971) Ultrasonic arteriography. *Arch Surg*, **103**, 663-667.

Nowicki A, Karlowcz P, Piechocki M, Secomski W (1985) Method for the measurement of the maximum Doppler frequency. *Ultrasound Med Biol*, **11**, 479-486.

Nowicki A, Marasek K (1991) Comparison of five spectral techniques for estimation of mean and maximum Doppler frequency. *in: EuroDop 92* , 222-223.

Oppenheim AV, Schafer RW (1975) Digital signal processing. Prentice-Hall, Inc., Englewood Cliffs, New Jersey.

Osborn JJ, Beamont JO, Raison JCA, Russel J, Gerbode F (1968) Measurement and monitoring of acutely ill patients by digital computer. *Surgery*, **64**, 1057-1070.

Ott HW (1988) Noise reduction techniques in electronic systems, John Wiley & Sons, Inc., New York.

Papp Z, Péceli G, Bagó B, Pataki B (1988) Intelligent medical instruments. *IEEE Eng Med Biol M*, **7(2)**, 18-23.

Powers JE, Phillips DJ, Brandestini MA, Sigelman RA (1980) Ultrasound phased array delay lines based on quadrature sampling techniques. *IEEE Trans Sonics Ultrasonics* , **SU-27**, 287-294.

Prytherch DR, Evans DH (1985) Versatile microcomputer-based system for the capture, storage and processing of spectrum-analyzed Doppler ultrasound blood flow signals. *Med Biol Eng Comp*, **23**, 445-452.

Rabiner LR (1973) Approximate design relationships for low-pass FIR digital filters. *IEEE Trans Audio and Electroacoustics*, **AU-21**, 456-460.

Rabiner LR, Gold B (1975) Theory and application of digital signal processing. Englewood Cliffs, Piscataway, New Jersey, chapter 3.

Rabiner LR, Rader CM (1972) Digital signal processing. IEEE Press, Piscataway, New Jersey, part 1.

Rabiner LR, Schafer RW (1974) On the behaviour of minimax FIR digital Hilbert transformers. *Bell System Tech J*, **53**, 363-389.

Raison JCA (1970) Patient monitoring: on-line computing. *Postgrad Med Journ*, **46**, 339-343.

Rich A (1982) Understanding interference type noise. How to deal with noise without black magic. *Analog Dialogue*, **16-3**, 16-19.

Rich A (1983) Shielding and guarding. How to exclude interference type noise. *Analog Dialogue*, **17-1**, 8-13.

Roevros JMJG (1974) Analogue processing of CW Doppler flowmeter signals to determine average frequency shift momentaneously without use of a wave analyser. *in: Cardiovascular applications of ultrasound (Ed. RS Reneman)*, North Holland, Amsterdam, pp 43-54.

Rutter P, Wolfe JHN, (1992) Late complications of arterial grafts. *BMJ*, **304**, 246-249.

Sainz A, Roberts VC, Pinardi G (1976) Phase-locked loop techniques applied to Ultrasonic Doppler Signal Processing. *Ultrasonics*, **14**, 128-132.

Satomura S (1959) Study of the flow patterns in peripheral arteries by ultrasonics. *J Acoust Soc Jap*, **15**, 151, 158.

Schecke T, Rau G, Popp HJ, Kasmacher H, Kalff G, Zimmermann HJ (1991) A knowledge-based approach to intelligent alarms in anaesthesia. *IEEE Eng Med Biol M*, **9**, 38-44.

Schlindwein FS, Smith MJ, Evans DH (1988) Spectral analysis of Doppler signals and computation of the normalized first moment in real-time using a digital signal processor. *Med Biol Eng Comput*, **26**, 228-232.

Sheppard LC (1979) The computer in the care of critically ill patients. *Proc IEEE*, **67**, 1300-1306.

Sheppard LC, Kouchoukos NT, Kurts MA, Kirklin JW (1968) Automated treatment of critically ill patients following operation. *Ann Surg*, **168**, 596-604.

Shortliffe EH, Buchanan BG, Feigenbaum EA (1979) Knowledge engineering for medical decision making: A review of computer-based clinical decision aids. *Proc IEEE*, **67**, 1207-1224.

Siregar P, Coatrieux JL, Mabo P (1993) How can deep knowledge be used in CCU monitoring. *IEEE Eng Med Biol*, **12(4)**, 92-99.

Sirmans D, Bumgarner B (1975) Numerical comparison of five mean frequency estimators. *J Appl Meteor*, **14**, 991-1003.

Skidmore R, Follett DH (1978) Maximum frequency follower for the processing of ultrasonic Doppler shift signals. *Ultrasound Med Biol*, **4**, 145-147.

Smallwood RH (1985) Recording Doppler blood flow signals on magnetic tape. *Clin Phys Physiol Meas*, **6**, 357-359.

Stark DD, Bradley WG (1988) Magnetic resonance imaging. CV Mosby Co, St Luis.

Stept LL, Flinn WR, McCarthy WJ, Bartlett ST, Bergan JJ, Yao JST, (1987) Technical defects as a cause of early graft failure after femorodistal bypass. *Arch Surg*, **122**, 599-604.

Stewart JSS (1970) The aim and philosophy of patient monitoring. *Postgrad Med Journ*, **46**, 339-343.

Stoodley KDC, Mirnia M (1979) The automatic detection of transients, step changes and slope changes in the monitoring of time series. *The Statistician*, **28**, 163-170.

Sukuvaara T, Sydänmaa M, Nieminen H, Heikelä A, Koski EMJ (1993) Object-oriented implementation of an architecture for patient monitoring. *IEEE Eng Med Biol*, **12(4)**, 69-81.

Sztipanovits J, Karsai G (1988) Knowledge-based techniques in instrumentation. *IEEE Eng Med Biol M*, **7(2)**, 13-17.

Taylor DEM (1971) Computer-assisted patient monitor systems. *Bio-med Eng*, **6**, 560-566.

Taylor DEM (1976) Probabilistic trend detection: implementation and utility. in *Real-time computing in patient management* (Eds: Payne JP and Hill DW), Chartridge Symposium Series, Peter Peregrinus, Stevenage, 175-187.

Taylor DEM, Whamond JS (1975) Reliability of human and machine measurements in patient monitoring. *Europ J Intensive Care Medicine*, **1**, 53-59.

Taylor FJ (1983) Digital filter design handbook, Marcel Dekker, Inc., New York and Basel, 183-188.

Thrush AJ, Evans DH (1990) Simple system for automatic intermittent recording of blood flow in femoro-distal bypass grafts using Doppler ultrasound. *Med & Biol Eng & Comput*, **28**, 193-195.

Tukey JW (1977) Exploratory data analysis. Addison-Wesley, Reading.

Velleman PF (1980) Definition comparison of robust nonlinear data smoothing algorithms. *J Amer Statist Assoc*, **75**, 609-615.

Velleman PF, Hoaglin DC (1981) Applications, basics, and computing of exploratory data analysis. Duxpury Press, Boston.

Walker MF, Souza SP, Dumoulin CL (1988) Quantitative flow mesurement.in phase contrast MR angiography, *J Comput Assist Tomogr*, **as(2)**, 304-313.

Warner HR, Gardner RM, Toronto AF (1968) Computer based monitoring of cardiovascular function in post-operative patients. *Circulation*, **67, Supplement 2**, 68-74.

Watt RC, Maslana ES, Mylrea KC (1993) Alarms and anasthesia - challenges in the design of intelligent systems for patient monitoring. *IEEE Eng Med Biol*, **12(4)**, 34-41.

WE DSP32C Digital signal processor information manual (1990), AT&T Microelectronics.

Weaver DK Jr (1956) A third method of generation and detection of single-sideband signals. *Proc IRE*, **44**, 1703-1705.

White DRJ, Atkinson K, Osburn DJM (1985) Taming EMI in microprocessor systems. *IEEE Spectrum*, **December**, 30-37.

Whittemore AD, Clowes AW, Couch NP, Mannick JA, (1981) Secondary femoropopliteal reconstruction. *Ann Surg*, **193**, 35-42.

Wolfe JHN, Taylor PR, Cheshire NJ (1991) Graft surveillance-a biased overview. *in The Maintenance of Arterial Reconstruction, edited by Greenhalgh RM and Hollier LH*, WB Saunders Company Ltd, London, 119-127.

Wolfe JHN, Thomas LN, Jamieson CW, Bruwse NL, Burnand KG, Rutt DL (1987) Early diagnosis of femorodistal graft stenoses. *Br J Surg*, **74**, 268-270.

Woodcock JP, Gosling RG, Fitzgerald DE (1972) A new non-invasive technique for assessment of superficial femoral artery obstruction. *Br J Surg*, **59**, 226-231.

Wyatt MG, Tennant WG, Scott DJA, Baird RN, Horrocs M (1991) Impedance analysis to identify the "at risk" femoro-distal graft. *J of Vasc Surg*, **13**, 284-293.

Young SW (1984) Nuclear magnetic resonance imaging: Basic principles. Raven Press, New York.